ORGANIC CHARGE-TRANSPORT MATERIALS BASED ON OLIGOTHIOPHENE AND NAPHTHALENE DIIMIDE: TOWARDS AMBIPOLAR AND AIR-STABLE N-CHANNEL ORGANIC FIELD-EFFECT TRANSISTORS

A Thesis
Presented to
The Academic Faculty

By

Lauren E. Polander

In Partial Fulfillment
Of the Requirements for the Degree
Doctor of Philosophy in Organic Chemistry

Georgia Institute of Technology

December 2011

ORGANIC CHARGE-TRANSPORT MATERIALS BASED ON OLIGOTHIOPHENE AND NAPHTHALENE DIIMIDE: TOWARDS AMBIPOLAR AND AIR-STABLE N-CHANNEL ORGANIC FIELD-EFFECT TRANSISTORS

Approved by:

Dr. Seth R. Marder
School of Chemistry and Biohemistry
Georgia Institute of Technology

Dr. Charles L. Liotta
School of Chemistry and Biochemistry
Georgia Institute of Technology

Dr. Jean-Luc Brédas
School of Chemistry and Biochemistry
Georgia Institute of Technology

Dr. Bernard Kippelen
School of Electrical and Computer Engineering
Georgia Institute of Technology

Dr. Laren M. Tolbert
School of Chemistry and Biochemistry
Georgia Institute of Technology

Date Approved: October 04, 2011

For my future.

ACKNOWLEDGEMENTS

There are so many people who contributed to my work either through mentoring and guidance, or through support, both emotional and financial, that it is difficult deciding where to start! So, we'll go from the beginning…

My mom may not have sparked my interest in science, in particular, but she always taught me to push myself, whether it was in the swimming pool or the classroom. During the 18 years we spent as the two "Pals"-of-the-house, and the last 8 years we spent calling each other anytime something good, bad, or otherwise happened, we have grown into integral parts of each other's support system and I would never have made it to where I am today without her wisdom, guidance, and support over the years.

My interest in chemistry, however, all began at Cherry Creek High School. I would never have checked the "chemistry" box on my undergraduate college application without Dr. Lisa Johnson, my AP Chemistry teacher. She taught me about moles, stoichiometry, and gas laws, but also served as a mentor and counselor during the time I spent as her eighth period teaching assistant. I will always be grateful to her for introducing me to chemistry.

Once at Tech, it took me a little while to get involved in research… and then I met Prof. Seth Marder. It was very intimidating sitting in his office for the first time being quizzed about my physics grades and the concept of refractive index when I thought I was looking for research experience in chemistry, but Seth has taught me that chemistry can be much more than just cooking in the lab. He has served as my advisor, mentor, counselor, and role model over the years, and I am extremely grateful for the role he has played in my life.

I am also indebted to both Dr. Simon Jones and Dr. Steve Barlow, one for getting me into this mess, and the other for helping me get out of it. When I joined the group for the first time as an REU student in 2006, Simon was assigned as my mentor. Over that summer, he taught me the basics of working in the lab, but more importantly, he introduced me to the life of a research chemist. Based on the time I spent working with Simon, I decided to apply for graduate school that next Fall. Not long after I began my graduate school career, Simon left the group for a new job and I started working more and more with Steve. Steve has helped guide me in my research projects, make sense of a mountain of data, learn to write journal articles (even if the grammar still needs work), and even to decode Seth's sometimes cryptic emails. Not to mention, he has proofread and helped to edit all of my thesis chapters! The work he has put into helping me complete and make sense of my research go beyond anything I would have expected; I genuinely appreciate all the time and effort he has spent working with me.

There are many other people that have helped guide and mentor me throughout the last 5 years including Dr. Susan Odom, who helped get me started in my project and served as a graduate student role model, Dr. Yulia Getmanenko, for her seemingly endless knowledge in synthetic methodologies and for her helpful suggestions and discussion throughout my time as a graduate student, and Dr. Reddy Dasari, for his incredible knack at solving problems whether through a literature search or just finding the right glassware fitting. I also appreciate the help I received from the rest of the Marder group, especially Dr. Yadong Zhang, Dr. Tissa Sajoto, Dr. Chun Huang, and Dr. Michal Maliki, along with my undergraduate students, Kristen Brown and Brian Seifried, who helped synthesize products and provided in-lab entertainment!

Additionally, there are many people outside of the Marder group who contributed to the success of my graduate research projects. I would like to mention, in particular, Prof. Bernard Kippelen and his postdoctoral researchers, Dr. Shree Tiwari and Dr. Do

Kyung (DK) Hwang, for screening all of my compounds in transistor devices; Prof. Jean-Luc Brédas and his graduate student Laxman Pandey and research scientist Dr. Chad Risko, for their help describing and predicting phenomena using computational methods; and Dr. Tatiana Timofeeva and her graduate students Alexander Romanov and Alexandr Fonari, for analyzing what single crystals I could grow through X-ray diffraction studies. Each of these people not only contributed scientifically to my projects, but also helped by adding their perspective on my work as a whole. Without their input and guidance, this thesis would be a list of synthetic methodologies strung together with UV-vis. spectra and cyclic voltammograms with little explanation of phenomena or results!

Last, but certainly not least, I want to acknowledge my husband Brandon for his love and support throughout this whole process! He has been there for me literally every step of my way through this program and I can't thank him enough for his understanding and encouragement. The only way we made it through this last year being "newly weds", dealing with our SGA duties, going to job interviews, passing data reviews, and writing a thesis shows what a great team we make and I look forward to seeing what we can achieve together in the future.

TABLE OF CONTENTS

LIST OF TABLES

LIST OF FIGURES

LIST OF SCHEMES

LIST OF ABBREVIATIONS

D	Donor
A	Acceptor
HOMO	Highest occupied molecular orbital
LUMO	Lowest unoccupied molecular orbital
vis.	Visible
NIR	Near-infrared
OPV	Organic photovoltaic
OFET	Organic field effect transistor
CPBT	4,4-Dialkyl-4*H*-cyclopenta[2,1-*b*:3,4-*b'*]bithiophene
DTS	4,4-Dialkyl-4*H*-silolo[3,2-*b*:4,5-*b'*]bithiophene
DTP	4-Alkyl-4*H*-dithieno[3,2-*b*:2',3'-*d*]pyrrole
BTD	[2,1,3]-Benzothiadiazole
THF	Tetrahydrofuran
TGA	Thermogravimetric analysis
DSC	Differential scanning calorimetry
DFT	Density functional theory
LCAO	Linear combination of atomic orbitals
HF	Hartree-Fock
TD-DFT	Time-dependent density functional theory
CT	Charge transfer
UV	Ultra violet
soln	Solution
calc	Calculated
CV	Cyclic voltammetry
IP	Ionization potential
EA	Electron affinity
IP(s)	Solid-state ionization potential
EA(s)	Solid-state electron affinity
IP_{adi}	Adiabatic ionization potential
EA_{adi}	Adiabatic electron affinity
IP_{vert}	Vertical ionization potential
EA_{vert}	Vertical electron affinity
DMF	Dimethylformamide
eV	Electron volts
V	Volts
nm	Nanometers
cm	Centimeters
M	Molar concentration (moles / liter)
4T	2,2':5',2'':5'',2'''-quaterthiophene
3T	3',4'-dimethyl-5,5''-bis(trimethylsilyl)-terthiophene
3TPh	3',4'-dibutyl-5,5''-diphenyl-terthiophene
K	Kelvin
MO	Molecular orbital
SOMO	Singly occupied molecular orbital
s	Seconds
min	Minutes

d	Days
W	Width
L	Length
NMR	Nuclear magnetic resonance
PL	Photoluminescence
ET	Electron transport
NDI	Naphthalene diimide
PDI	Perylene diimide
NDA	naphthalene tetracarboxylic dianhydride
et al.	Et alia
DBI	Dibromoisocyanuric acid
cmpd	Compound
kcal	Kilocalorie
mol	Mole
TT	thieno[3,2-*b*]thiophene
DTT	dithieno[3,2-*b*:2',3'-*d*]thiophene
SCF	Self consistent field

Other abbreviations are explained in the text.

LIST OF SYMBOLS

ε	Dielectric constant
ε_{max}	Extinction coefficient at maximum absorption
λ_{max}	Wavelength at maximum absorption
μ	Mobility
μ_h	Hole mobility
μ_e	Electron Mobility
σ	Hammett parameter
v	Energy / cm^{-1}
f	Oscillator strength
E_{ox}	Oxidation potential
$E_{1/2}$	Half-wave potential
$E_{1/2}^{+/0}$	First half-wave oxidation potential
$E_{1/2}^{2+/+}$	Second half-wave oxidation potential
$E_{1/2}^{0/-}$	First half-wave reduction potential
$E_{1/2}^{-/2-}$	Second half-wave reduction potential
E_{op}	Optical gap
E_{echem}	Electrochemical gap
λ_h	Internal hole reorganization energy
λ_e	Internal electron reorganization energy
V_{TH}	Threshold voltage
I_{on} / I_{off}	Current on / off ratio
T_d	Decomposition temperature
T_g	Glass transition temperature
T_m	Melting point temperature
z_L	Long axis of the molecule
z_R	Short axis of the molecule
P	Pitch angle, molecular slipping along the long axis
R	Roll angle, molecular slipping along the short axis
d	π-π Distance between two stacked molecular planes
d_P	Slip distance along the long axis of the molecule
d_R	Slip distance along the short axis of the molecule
d_{tot}	Total slip distance
t	Electronic coupling

Other symbols are explained in the text.

SUMMARY

To better understand the physical and electronic properties of donor and acceptor-based structures used in organic electronic applications, a variety of oligothiophene and naphthalene diimide-based small conjugated molecules were designed, synthesized, and characterized. The materials were initially synthesized using oxidative copper-chloride coupling reactions, palladium-catalyzed amination reactions, Friedal-Crafts acylations, Negishi coupling reactions, and Stille coupling reactions. Once isolated, the physical properties of the compounds were characterized through a combination of X-ray crystal structure, thermogravimetric analysis, differential scanning calorimetry, UV-vis. absorption spectroscopy, cyclic voltammetry, and differential pulse voltammetry, along with comparison to quantum-chemical calculations. In some cases, the radical cations or radical anions were generated by chemical oxidation and analyzed by vis-NIR spectroscopy. Furthermore, the electronic properties of the materials were investigated through incorporation as solution-processed active layers in organic field-effect transistors. Multiple examples exhibited hole- and / or electron-transport properties with electron mobility values of up to 1.5 $cm^2V^{-1}s^{-1}$, which is among the highest yet reported for an n-channel OFET based on a solution-processed small molecule.

CHAPTER 1

INTRODUCTION

1.1 Organic Electronics

Our daily life involves the use of electronic devices such as televisions, cell phones, portable readers, credit cards and computer screens. Since the invention of the first transistor in 1947 by John Bardeen, William Shockley and Walter Brattain,[1,2] the vast majority of these devices have mainly been based on inorganic semiconductors and, in particular, on silicon. However, due to processing limitations associated with the use of silicon, many scientists, physicists and engineers are working to develop new technology in the field of organic electronics.

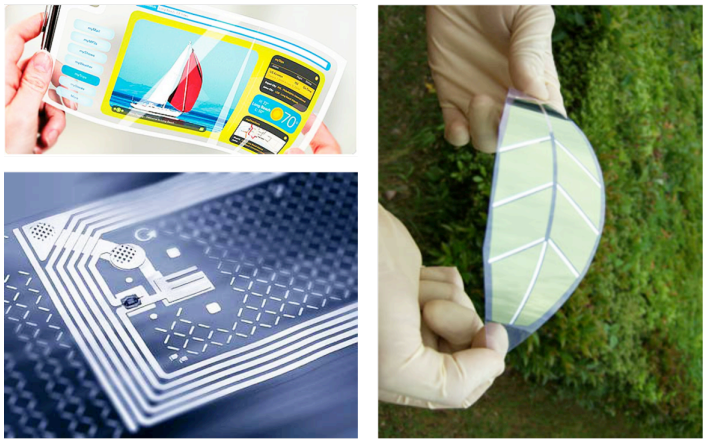

Figure 1.1. Examples of flexible organic electronic devices. (top) Organic light emitting diode (Universal Display); (bottom) organic field-effect transistor; (right) organic photovoltaic (AIST, Mitsubishi Corp., Tokki Corp.).

The processing characteristics of organic materials make them potentially useful for electronic applications where low-cost, large area coverage and structural flexibility

are required. Fabrication of devices using amorphous or polycrystalline silicon, which are widely used in solar cells and flat screen displays, often requires high-temperature vacuum deposition and sophisticated lithography techniques. Organic materials offer the benefits of low-temperature solution deposition onto plastic substrates involving more convenient and potentially less expensive fabrication techniques such as spin coating, stamping, and inkjet printing.[3-5]

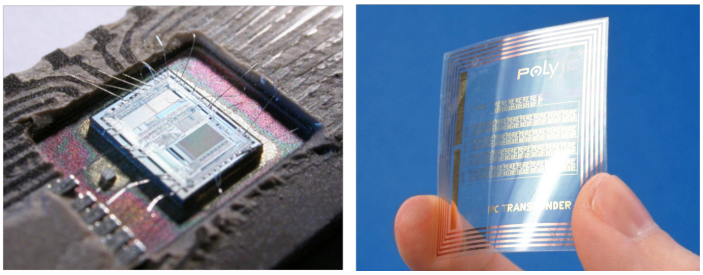

Figure 1.2. Example of silicon-based electronics (left, Intel) vs. organic-based electronic devices (right, PolyIC).

Organic electronic materials may not replace silicon in high-density, high-speed circuits, but they could open the door for integration into large-area flexible electronic devices such as light-emitting diodes (OLEDs),[6-8] photovoltaic cells (OPVs),[9-11] field-effect transistors (OFETs),[12,13] radio frequency identification tags,[14] electronic paper[15,16] and sensors,[17,18] and may prove advantageous in a variety of new uses and applications.

1.1.1 Conductivity and Charge-Carrier Mobility

In order for an electronic device to function, the device must contain a material that allows for the movement of charge or electricity. An electronic material can be classified as a metal, semiconductor, or insulator depending on the ability of the material to conduct an electric current, which can be quantified by the electrical conductivity (σ) of

the material. The electrical conductivity in a semiconductor is proportional to the product of the charge-carrier concentration and the mobility (μ) of those charge carriers, or how quickly the charge carriers move through a material when pulled by an electric field. The conductivity of a semiconductor can then be expressed as:

$$\sigma = \frac{J}{E} = ne\mu \tag{1.1}$$

where J is the current density in Acm^{-1}, E is the magnitude of the electric field in Vcm^{-1}, n is the number density of charge carriers in cm^{-3}, e is the elementary charge in C, and μ is the mobility in $cm^2V^{-1}s^{-1}$. Based on this relationship, it is not surprising that one of the key parameters used to characterize charge-transport materials in electronic devices is the charge-carrier mobility associated with that material in a device.

1.1.2 Factors Effecting the Mobility in Organic Semiconductors

The mobility of charge carriers in organic semiconductors is not an inherent property of the material and many factors, including charge-transport mechanisms, molecular disorder, and the presence of charge-carrier traps, influence the mobility as measured in a device.

1.1.2.1 Electron-Transfer Theory

Typical inorganic semiconductors, such as silicon, are composed of an array of atoms that are held together with strong covalent bonds forming a highly crystalline solid, which permits charge transport to take place through delocalized bands. The speed of charge carriers in this type of band transport regime is mainly limited by defects in the lattice or lattice vibrations.[3,5,13,19]

In contrast, organic semiconductors are composed of individual molecules that are weakly bound together through van der Waals, hydrogen-bonding, and π-π

interactions. These systems, although well-ordered single-crystals can be used, typically produce disordered, polycrystalline films and charge transport mainly occurs along the conjugated backbone of a single molecule or between the π-orbitals of adjacent molecules. Therefore, charge transport between π-systems of neighboring molecules rarely occurs through band-like transport and carriers move instead by hopping from these localized states (Figure 1.3).[3,5,13,19,20]

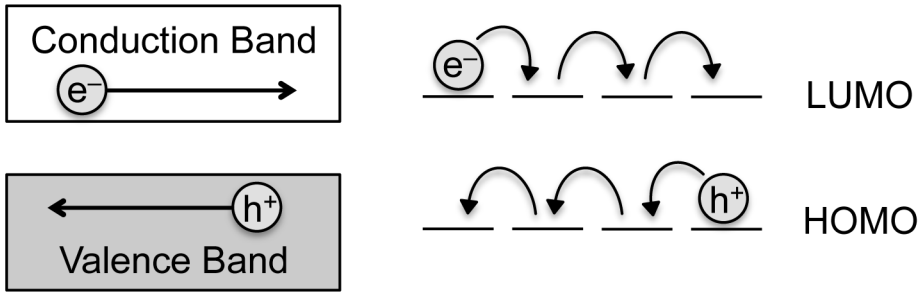

Figure 1.3. Schematic representation of band (left) versus hopping (right) transport regimes. Note: Directionality of arrows as depicted is arbitrary.

Charge transport in organic semiconductors has been reviewed by many groups[13,19,21-25] and is often related to the theory of electron-transfer reactions originally formulated by Marcus for the description of redox reactions in solution.[26,27] Based on this model, the two major parameters affecting the charge transfer rate (k_{ET}) between two states are the transfer integral (t), which needs to be large, and the reorganization energy (λ), which needs to be small for efficient charge transport (Equation 1.2) [5,21,26-28]

$$k_{ET} = \frac{4\pi^2}{h}\frac{1}{\sqrt{4\pi k_B T}} t^2 e^{\left(-\frac{\lambda}{4k_B T}\right)} \qquad (1.2)$$

Electronic Coupling. The transfer integral reflects the strength of the electronic coupling between two adjacent molecules, which depends on the extent of intermolecular overlap of the orbitals involved in the charge transfer process. The

transfer integral can be influenced by two main parameters: 1) the intermolecular separation and 2) lateral displacements (deviation from cofacial arrangement) and is highly sensitive to the molecular packing in the films.[21,25]

As an example, consider a dimer made of two superimposed ethylene molecules. The HOMO and LUMO wavefunctions for an isolated ethylene molecule are shown in Figure 1.4. In the HOMO, the lobes of the two π-orbitals with the same sign interact (bonding, zero nodes), whereas in the LUMO, two lobes of opposite sign interact (antibonding, one node). In a cofacial ethylene dimer, the interaction between the two molecules leads to a splitting of the HOMO / LUMO energy levels; the degree of the splitting correlates to the degree of the electronic coupling between the molecules. The HOMO splitting is much larger than the LUMO splitting due to the nature of the interaction between the HOMO wavefunctions of the superimposed ethylene molecules; the interaction is either fully bonding (highly stabilized dimer HOMO–1 level) or fully antibonding (highly destabilized dimer HOMO level). The LUMO splitting is much less pronounced due to the diagonal antibonding / bonding interactions present in the dimer LUMO / LUMO+1 wavefunctions that partially compensate for the direct bonding / antibonding interactions (Figure 1.4).[21,25]

If the intermolecular distance between these two ethylene molecules was increased, the degree of orbital overlap between the two molecules would decrease, resulting in a decreased interaction between the HOMO / LUMO wavefunctions and a smaller HOMO / LUMO splitting observed for the dimer (decreased electronic coupling). In fact, the electronic coupling between two stacked sexithiophene molecules was calculated to decay exponentially when the interplanar distance was increased.[21]

Additionally, a lateral displacement between the two ethylene molecules would cause a change in the electronic coupling associated with the interaction. In a perfectly cofacial arrangement, the π-orbital coefficients interact in a particular way (as described

for ethylene above); however, if one of the molecules was shifted relative to the other, the interaction between coefficients would change resulting in a different HOMO / LUMO splitting for the resulting dimer (different level of electronic coupling).

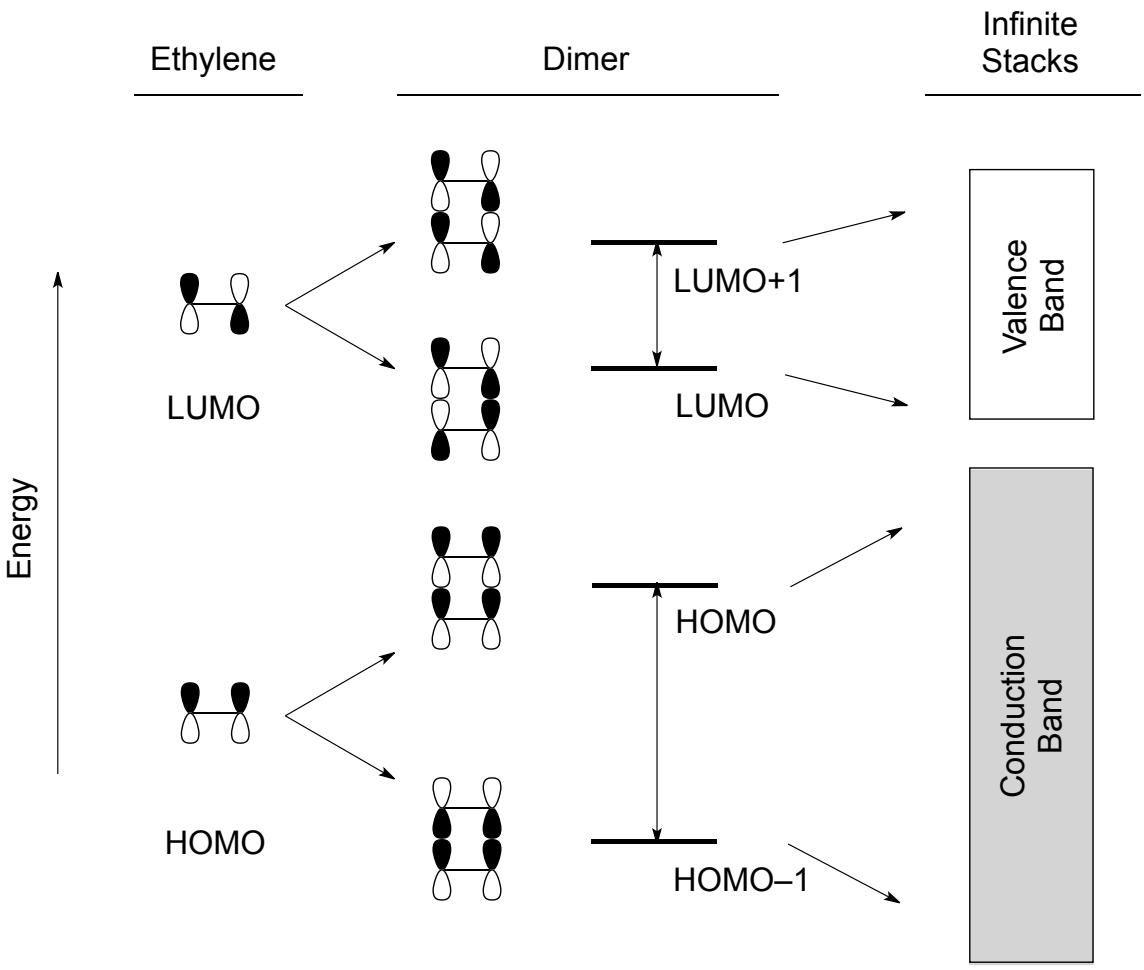

Figure 1.4. Illustration of the interactions between the HOMO / LUMO levels of two ethylene molecules in a cofacial configuration to form an ethylene dimer and, in the ideal case, an infinite stack of ethylene molecules. Adapted from Ref. 21.

In the ideal case, an infinite stack of ethylene molecules would lead to the formation of a conduction band and a valence band allowing for band transport (Figure 1.4); however, due to the disorder present in typical organic solids, this regime is only observed in some very high-purity, highly ordered organic single crystals that exhibit

excellent orbital overlap (observed in pentacene, tetracene, and other acene derivatives[19,29,30]).

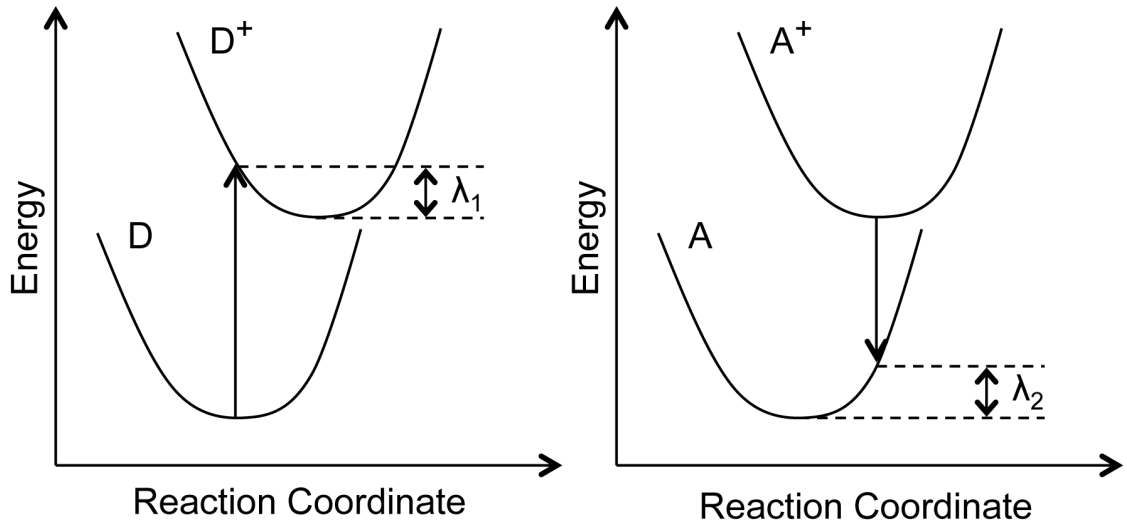

Figure 1.5. Schematic representation of potential energy surfaces, in the monomer coordinate representation, related to electron transfer. The vertical transitions are shown along with the components involved in the intermolecular reorganization energy.

Reorganization Energy. The reorganization energy reflects the energy involved to "reorganize" the system structure from the initial to final coordinates and has both an inner and outer contribution, which arise from the change in equilibrium geometry as a result of the intermolecular electron transfer reaction and the polarization / relaxation of the surrounding medium, respectively. For example, in the case of a donor (D) and acceptor (A) electron transfer reaction of the type $D + A^+ \rightarrow D^+ + A$, the intermolecular reorganization energy is defined as the sum of the geometrical relaxation energies of one molecule upon going from the neutral-state geometry (D) to the charged-state geometry (D^+) and the neighboring molecule upon going from the charged-state geometry (A^+) to the neutral-state geometry (A, Figure 1.5).[5,25] In the same case, the outer reorganization energy is defined as the sum of the geometrical relaxation energies

of the solvent molecules surrounding both D and A^+ upon going to D^+ and A, respectively. The outer reorganization energy cannot be easily accessed from quantum-chemical calculations, though estimations can be obtained from models based on a dielectric continuum.[25]

Mobility. The mobility of a material can be expressed as a function of the electronic coupling and reorganization energy by

$$\mu = \frac{d}{\tau E} \tag{1.3}$$

where E is the magnitude of the applied electric field, d is the total distance traveled by the charge, and τ is the total time calculated as the sum of the inverse of the transfer rates (k_{ET}, Equation 1.2).[25] High charge-carrier mobility values are required for many device applications, which makes the intrinsic charge-transport properties of a material crucial to its use in organic electronics.

1.1.2.2 Borsenberger-Bässler Disorder Model

The disorder formalism of Borsenberger, Bässler, and co-workers[31-33] attempts to account for the effects of energetic and positional disorder within an organic semiconductor on the mobility of the charge carriers while not explicitly considering electron-transfer theory. In particular, the effect of the disorder of organic semiconductors compared to their inorganic counterparts is evaluated and predictions are made concerning the functional dependence of the mobility, μ, on the temperature, T, and applied field, E. This relationship can be expressed by:

$$\mu = \mu_{00} e^{-\left(\frac{2\sigma}{3k_B T}\right)^2} e^{\beta E^{1/2}} \tag{1.5}$$

where μ_{00} is the mobility at infinite absolute temperature and zero-field; k_B is the Boltzman constant; T is the temperature; $\beta = C[(\sigma/k_B T)^2 - \Sigma^2]$ and is typically positive for

amorphous organic semiconductors; σ and Σ characterizes the energetic and positional disorder, respectively; and E is the magnitude of the field.[31-33] From this relationship, it is predicted that the mobility in organic materials will increase with increasing temperature and increasing electric field. It also indicates that increasing disorder in the organic semiconductor leads to decreased mobility values.

1.1.2.3 Charge-Carrier Traps

It is also important to consider charge-carrier trapping mechanisms when discussing the mobility in organic charge-transport materials. Charge carriers can be trapped through many mechanisms, including the presence of chemical impurities, ambient species, and structural defects, leading to a decrease in the mobility measured for a particular material.

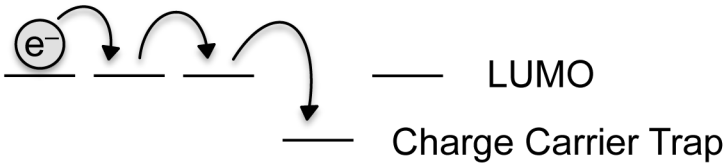

Figure 1.6. Schematic representation of trapping of an electron by a chemical impurity in an organic semiconductor.

Chemical impurities in organic charge-transport materials can very efficiently capture charge carriers as they move through the material. Due to relatively wide HOMO / LUMO energy gaps, which are typical for this material class, a wide energy range exists in which impurity states can act as traps (Figure 1.6).[19,30] Ambient species are a particular type of chemical impurity that can inhibit charge mobility. Mobile electrons present in the charge-transport material can be trapped by reduction of water and / or oxygen present in the air. In general, increasing the electron affinity of the charge-

transport material can prevent this type of trapping by energetically stabilizing the electrons during charge transport, which occurs primarily by hopping through LUMO levels.[22]

In addition, the concentration of physical defects in the solid-state packing of the material disrupts the orbital overlap of adjacent molecules providing yet another mode for charge-carrier trapping. Structural defects within the organic semiconductor due to poor molecular self-assembly are one of the most important origins of charge-carrier traps.[34]

1.1.3 Types of Organic Charge-Transport Materials

In order to fabricate fully all-organic electronic devices, the development of a number of new materials is needed including conducting electrodes, organic semiconductors, insulating dielectric materials, and plastic substrates. While there is a significant amount of ongoing research in each of these areas, this thesis will focus on the development of organic charge-transport materials.

Most organic charge-transport materials fall into one of three classes: 1) molecular single crystals, 2) molecular polycrystalline materials, or 3) polymers. The degree of molecular organization in the semiconductor largely affects the charge transport through overlapping π-orbitals of adjacent conjugated molecules.[3,5,19-21] For this reason, devices made using highly ordered single-crystal semiconductors often show significantly higher performance than those using polycrystalline films;[3,35] however, single-crystal devices are not easily applicable to large-area processing techniques and alternatives are required. Conjugated polymers, on the other hand, often possess good film forming properties when deposited from solution; however, the increased disorder in the polymer film compared to devices based on single crystals limits charge transport resulting in lower mobility values.[5] Due to the drawbacks associated with single-crystal

and polymer charge-transport materials, small-molecule semiconductors have increased in popularity in the recent literature. Small-molecule materials can be obtained with high chemical purity using techniques such as vacuum sublimation and, although typically processed *in vacuo*, they have the potential to be processed from solution through the incorporation of solubilizing alkyl substituents.

In general, regardless of the specific class of material, charge-transport materials that form quality, well-ordered films when processed from solution are desired in order to take advantage of more convenient and potentially less expensive fabrication techniques such as spin coating, stamping, and inkjet printing.[3-5] These solution-based processing techniques offer the potential for low-temperature deposition enabling the use of flexible plastic substrates, which are not as readily applicable to silicon-based electronics.

1.2 Organic Field-Effect Transistors

Combining the processability benefits of organic materials with the function of a traditional transistor – the main logic unit in modern electronic devices where they act to amplify or switch electronic signals – organic field-effect transistors (OFETs) hold promise for use in lightweight, foldable products.[5,12,23]

The first OFET device was reported in 1986 by Tsumura *et al.* and was based on a film of electrochemically grown polythiophene; the devices exhibited mobility values of up to 10^{-5} $cm^2V^{-1}s^{-1}$.[36] Four years later, the first OFET employing a conjugated small molecule (sexithiophene) was fabricated and improved mobility values of up to 10^{-3} $cm^2V^{-1}s^{-1}$ were reported.[37] The performance of OFETs in the last 25 years has improved significantly and device characteristics that reach and surpass amorphous silicon (0.1-1 $cm^2V^{-1}s^{-1}$)[38] have been achieved.

Figure 1.7. (left) Full-color top-emission active-matrix organic light emitting diode driven by OFETs fabricated on a flexible substrate (Sony). (right) E-ink flexible paper (Plastic Logic). (bottom) Printed radio-frequency identification tags on flexible substrate (PolyIC).

1.2.1 Components and Structure of an Organic Field-Effect Transistor

An organic transistor is analogous to the conventional silicon-based metal oxide semiconductor field-effect transistor (MOSFET) with a basic structure consisting of a semiconducting layer, an insulating layer (dielectric) and three terminals (source, drain and gate). In the traditional inorganic device, the semiconducting layer is commonly comprised of silicon, whereas in an OFET, the semiconducting layer is an organic charge-transport material, which is usually vacuum sublimed, spin coated, or drop cast depending on the properties of the material.

The most widely used gate dielectrics include inorganic oxides (e.g.; SiO_2, Al_2O_3), but polymeric insulators (e.g.; poly(methylmethacrylate)) have also been used.[19,20] The dielectric material plays a major role in the device characteristics due to its influence on the electric field in the device and on the morphology of the organic semiconductor. In particular, inorganic oxides typically have rough surfaces – roughness can lead to valleys in the channel region, which may act as carrier traps – and are characterized by having terminal hydroxyl groups – reduction of the hydroxyl groups by the charge

carriers can serve as a trapping mechanism. Organic silanes are often used to modify the interface between the dielectric and the semiconductor; it has been demonstrated that these treatments often have strong effects on the film structure and on the resulting electrical characteristics. Common surface modifiers include *n*-octyltriethoxysilane (OTS), hexamethyldisiloxane (HMDS), and poly(alpha-methoxysilane) (PαMS).[13,19]

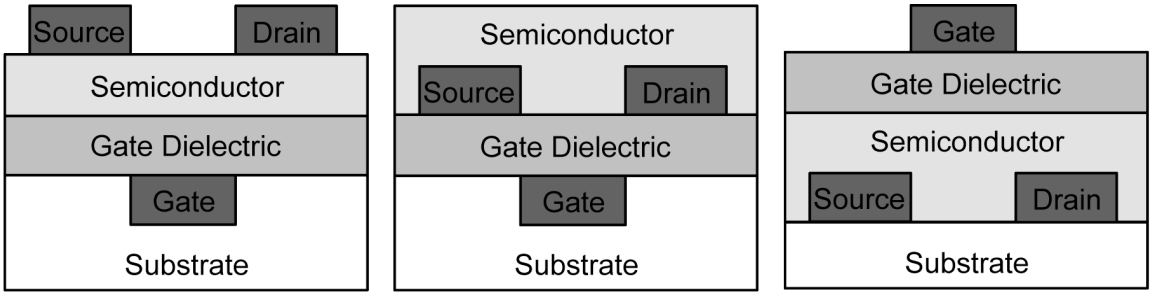

Figure 1.8. Common field-effect transistor configurations: (left) top contact, bottom gate (TC/BG); (middle) bottom contact, bottom gate (BC/BG); (right) bottom contact, top gate (BC/TG).

The source and drain electrodes, which inject charges into the semiconductor, are often high work function metals (e.g.; gold), but some lower work function metals (e.g.; aluminum, calcium) and conducting polymers (e.g.; PDOT:PSS) are also used.[39]

The three most commonly used device architectures are shown in Figure 1.8. The major difference between these device geometries arises from the position of the source and drain electrodes relative to the gate electrode and the dielectric / semiconductor and electrode / semiconductor interfaces.[5,13,19,40]

1.2.2 Types of Organic Field-Effect Transistors

Depending on the type of doping in silicon, devices in which the majority of carriers are holes (p-channel) or electrons (n-channel) can be fabricated.[5,12] Similarly, an OFET can be either a p- or n-channel device depending on the IP and EA of the organic

semiconductor relative to the work function of the metal electrodes. In contrast to traditional silicon, organic materials have the inherent ability to transport both electrons and holes without the need for doping; therefore, the preference of the organic semiconductor for either charge carrier is dependent on the energy difference between the IP (holes) / EA (electrons) of the material and the work function (φ) of the electrodes (injection barrier). Additionally, it is possible to have an organic semiconductor with a moderate charge injection barrier for either charge carrier allowing the transport of both electrons and holes in one device. This type of material can be used to fabricate so-called ambipolar devices (Figure 1.9).[12,20]

In order to build an electronic circuit comparable to the current silicon-based technology, logic elements such as inverters are required. Silicon-based inverters often consist of complementary p-channel and n-channel metal oxide semiconductor field-effect transistors (CMOS) that share gate and drain electrodes. Complementary technology has led to the fabrication of digital circuits with high robustness, low power dissipation, and wide noise margins.[20,41] In order to fabricate organic complementary inverters for application in organic electronics, OFETs with p- and n-channel capabilities are required.

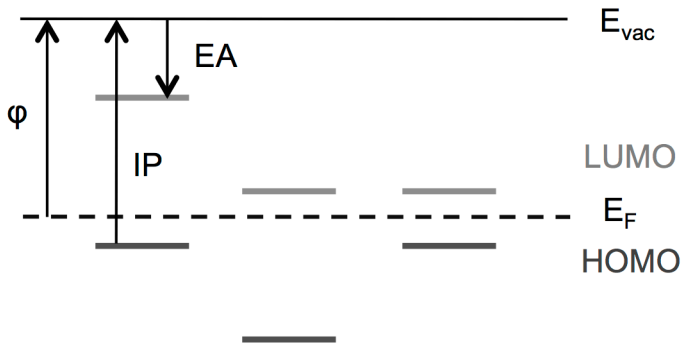

Figure 1.9. Representations of the energy levels for hole-transport (left), electron-transport (middle), and ambipolar (right) materials for p-channel, n-channel, and ambipolar OFETs, respectively. E_F = Fermi energy of the electrodes.

1.2.3 Organic Field-Effect Transistor Device Function and Characterization

Device Function. The key steps of OFET operation involve 1) the formation of a conducting channel at the organic semiconductor / dielectric interface due to the application of a gate voltage (V_G) and 2) charge migration across the organic semiconductor due to the application of a voltage between the source and the drain electrodes ("drain voltage", V_D). When a voltage is applied to the gate, an electric field is produced at the semiconductor / dielectric interface and this field causes a shift in the energy levels of the organic semiconductor (Figure 1.10). Depending on the Fermi energy of the electrodes relative to the HOMO / LUMO levels of the semiconductor, either holes can be injected into the HOMO (hole accumulation, Figure 1.10) or electrons can be injected into the LUMO (electron accumulation, Figure 1.10) of the organic semiconductor forming a conducting channel between the source and drain. Current can then be driven through the device by applying a drain voltage (hole / electron transport, Figure 1.10).

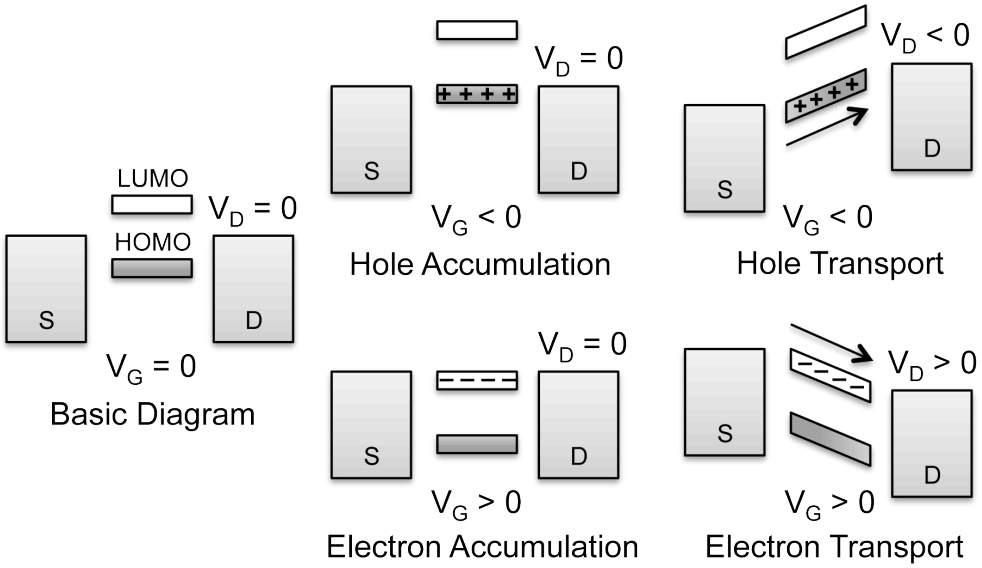

Figure 1.10. Simplistic depiction of the energy levels of the source and drain electrodes and the HOMO and LUMO of the organic semiconductor in an OFET device upon application of either a positive or negative gate and drain voltage. Adapted from Ref. 22.

Figure 1.10 depicts a simplistic model of the energetics behind charge transport and many limitations must be considered including the effect of traps and energy level misalignments. Not all of the charges accumulated in the active material by the applied gate voltage will contribute to the current and deep traps first have to be filled before the charges can be mobile. That is, a gate voltage has to be applied that is higher than a threshold voltage (V_{TH}), which is defined as the gate voltage required for a conduction channel to form in the semiconductor. The effective gate voltage in the device can then be defined as the difference between the gate voltage applied and the threshold voltage ($V_{G,eff.} = V_G - V_{TH}$). Additionally, large energy barriers can, and often do, lead to limitations in semiconductor performance. For example, a large energy barrier between the EA (IP) of the semiconductor and work function of the electrodes can prohibit electron (hole) injection resulting in a device in which only holes (electrons) can be injected and, therefore, transported. This type of device is referred to as unipolar and most of the organic transistors that have been fabricated to date exhibit this type of performance.

The fabrication of devices exhibiting ambipolar transport, although rare, has been reported. One of the major challenges associated with ambipolar transport materials lies in the efficient injection of both charge carriers. Most organic semiconductors have an energy difference between the IP and EA of the material (energy gap) of ca. 2-3 eV, which often results in large injection barriers for at least one charge carrier. In materials that do exhibit very low energy gaps (< 2 eV), the opposite is true; It is often difficult to turn these devices “off” resulting in a small ratio between the current in the “on” and “off” states (current on / off ratio, I_{ON}/I_{OFF}).

Characterization. OFET device function is typically characterized by what are referred to as output and transfer curves (Figure 1.11). An output curve is obtained by holding the gate at a constant voltage while sweeping the drain voltage and the transfer

curve is obtained by holding the drain voltage constant while sweeping the gate voltage. These plots are used to describe the two regimes that are typically observed in normal OFET device operation: the linear regime and the saturation regime, which are dependent on the behavior of the drain current with respect to the drain voltage. When no drain voltage is applied, the charge-carrier concentration in the transistor channel is uniform. When a drain voltage is increased to a voltage level smaller than the effective gate voltage ($V_D < V_{G,eff.}$), the device operates in the linear regime, which is characterized by a current flowing through the channel that is directly proportional to the drain voltage applied. In the linear regime, the drain current (I_D) can be expressed as:

$$I_D = \frac{W}{L} \mu C_i \left(V_G - V_{TH} \right) V_D \tag{1.6}$$

where W is the width of the channel, L is the length of the channel, μ is the mobility of the charge carriers, and C_i is the capacitance of the dielectric per unit area. Due to the linear correlation of the drain current and gate voltage in this regime, the mobility of the charge carriers can be determined from the slope of the linear portion of the I_D-V_D curve (Figure 1.11). Increasing the drain voltage above the effective gate voltage ($V_D \geq V_{G,eff.}$) will not substantially increase the current (Figure 1.11). This is referred to as the saturation region and is a result of a local potential within the channel that is below the effective gate voltage of the device. In the saturation regime, the drain current (I_D) can be expressed as:

$$I_D = \frac{W}{2L} \mu C_i \left(V_G - V_{TH} \right)^2 \tag{1.7}$$

The quality of an organic semiconductor in an OFET device is mainly characterized by the charge-carrier mobility (μ), current on / off ratio (I_{ON}/I_{OFF}), and threshold voltage (V_{TH}). While these properties can, in part, be optimized through the design and manipulation of the molecular structure, it is important to realize that these

properties are also dependent on the particular device configuration and processing. As defined in section 1.1.1, the mobility of a material is a measure of how easily charge carriers can move within the semiconductor under the influence of an electric field (velocity per unit field) and can be directly related to the switching speed of the device. Typical mobility values for polycrystalline silicon (> 100 $cm^2V^{-1}s^{-1}$)[42] are much higher than those of organic materials; however, as mentioned earlier, some organic semiconductors currently have mobility values comparable to and surpassing that of amorphous silicon (0.1-1 $cm^2V^{-1}s^{-1}$)[38]. The current on / off ratio is defined as the ratio of the current in the "on" and "off" states. It is desirable to have little to no current in the "off" state to eliminate leakage and ratios on the order of 10^6 are generally suitable for most applications. Finally, the threshold voltage is the gate voltage required for the conduction channel to form in the semiconductor and low values are desired (< ± 2.5 V) for low power consumption.

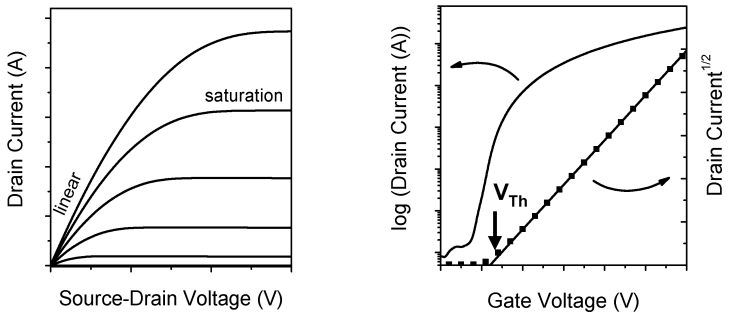

Figure 1.11. Representative current-voltage characteristics of an n-channel organic field-effect transistor: (left) output characteristics; (right) transfer characteristics in the saturation regime. Adapted from Ref. 20.

1.3 Charge-Transport Materials for Organic Field-Effect Transistors

The development of new materials for p-channel transistors continues to be a major area of research; however, many high performance materials have been identified

including small molecules, processed either *in vacuo* or from solution, and solution-processed polymers. Very recently Minemawari *et al.* also reported the ability to use printed single crystals to yield thin-film transistors with average p-channel mobility values as high as 16.4 $cm^2V^{-1}s^{-1}$.[43] The majority of efficient hole-transporting materials, however, require vacuum deposition including a variety of promising oligothiophenes and acene derivatives. The highest p-channel mobility values reported to date for single crystalline, vacuum-deposited small molecule, polymeric, and solution-processed small-molecule hole-transport materials are measured for rubrene (15-20 $cm^2V^{-1}s^{-1}$),[44,45] pentacene (> 5.0 $cm^2V^{-1}s^{-1}$),[3] TIPS-pentacene (1.5 $cm^2V^{-1}s^{-1}$),[46] and a copolymer based on cyclopentadithiophene and benzothiadiazole (3.3 $cm^2V^{-1}s^{-1}$),[47] respectively.

For brevity, a review of materials for p-channel OFETs will not be included here, but many articles discussing a variety of hole-transporting materials can be found in the literature.[3,48-50]

1.3.1 Materials for n-Channel Transistors

While p-channel OFETs have been reported extensively in the literature, development of organic charge-transport materials for n-channel and ambipolar OFETs has proven more difficult. Two of the major challenges observed with materials for n-channel transistors are 1) efficient charge injection from a suitable electrode,[41] and 2) the operating stability of charge carriers under ambient conditions.

For p-channel transistors, the energy barrier for injection of holes is usually moderate when using gold electrodes; the IPs of many organic semiconductors are in the range of 4.8 to 5.3 eV, which aligns well with the work function of gold (~ 5 eV). The EA of many organic semiconductors, on the other hand, is often often much smaller (2-3 eV) and large injection barriers usually prevent the observation of electron transport. Low work function metals, such as calcium or aluminum, can be used to achieve

electron injection in some cases, however these low work function metals are not environmentally stable and gold electrodes are preferred.

Additionally, organic radical anions present in the active layer during device operation can be oxidized by water or oxygen in the air, reducing the number of charge carriers in the film. Using the assumption that ambient degradation is mainly due to the reduction of O_2 and H_2O present in the air by the charge-carrying electrons, de Leeuw *et al.* estimated reduction potential limits for air-stable electron-transport materials of ≥ –0.658 V vs. SCE with respect to H_2O oxidation, and ≥ +0.571 V vs. SCE with respect to O_2 oxidation.[51] However, experimentally, materials with first reduction potentials ≥ –0.4 V (EA ≥ ca. 4.0 eV) exhibit air-stable OFET device characteristics without severe device degradation. Based on these results, an estimated overpotential of 0.5-1.0 V is generally accepted, which is consistent with overpotential values estimated by de Leeuw *et al*.[51] Many n-channel transistors can thus only operate when tested under inert conditions, which makes them technologically unattractive.

Electron mobility has been measured in a variety of small-molecule and polymeric materials and the highest performing electron-transport and ambipolar materials are outlined below (Table 1.1).

1.3.1.1 Oligothiophene

Oligothiophenes and alkyl-oligothiophenes are well known for their use as hole-transport materials, but a few oligothiophene derivatives have shown n-channel OFET properties through functionalization with perfluoroalkyl chains and carbonyl moieties. The introduction of perfluoroalkyl chains in quarterthiophenes was found to increase the EA of the molecules leading to measureable electron mobility values up to 0.2 $cm^2V^{-1}s^{-1}$ with an on / off ratio of 10^6 in devices with gold electrodes and HMDS treated Si / SiO_2 gate dielectric for 5,5'''-bis(perfluorohexyl)-quarterthiophene (EA = –3.31 eV; EA of 2,2'-

hexyl-quarterthiophene = –2.89 eV);[52] however, the mobility values for this class of oligomers greatly decreased in the presence of air. In order to increase the air stability, ketone-functionalized 5,5'''-bis(perfluoroalkan-1-one)-quarterthiophenes (Figure 1.12) were designed and found to exhibit increased electron affinity values (EA of **1.1** = –3.96 eV). The highest electron mobility reported for **1.1** is 0.6 $cm^2V^{-1}s^{-1}$ with an on / off ratio greater than 10^7 in devices with gold contacts and HMDS treated Si / SiO_2 gate dielectric. This oligomer also exhibited electron mobility values of up to 0.02 $cm^2V^{-1}s^{-1}$ when tested in air.[52]

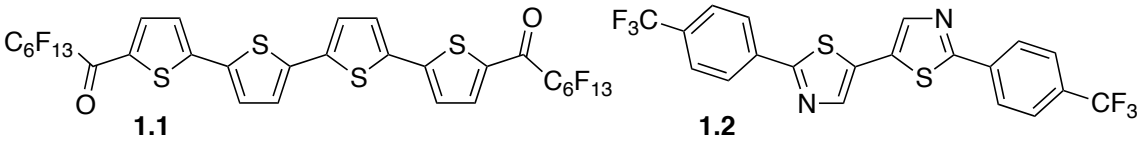

Figure 1.12. Examples of oligothiophene-based electron-transport materials.

Substitution of thiophene by thiazole, which has a higher electron affinity, has also been successful in the development of electron-transport materials. For example, 2,2'-bis(4-(trifluoromethyl)phenyl)-5,5'-bithiazole **1.2** (Figure 1.12) exhibited very high electron mobility values of up to 1.8 $cm^2V^{-1}s^{-1}$ under vacuum (EA of **1.2** = –3.17 eV; EA of 5,5'-bis(4-(trifluoromethyl)phenyl)-2,2'-bithiophene = –2.99 eV).[53]

1.3.1.2 Acene

As an alternative to adding fluorinated substituents to semiconducting oligomers, direct fluorination of the conjugated cores of oligothiophenes, pentacene, and tetracene has also led to electron transport. Perfluoropentacene (EA = –3.67 eV) exhibits an increased electron affinity relative to pentacene (EA = –2.93 eV) and electron mobility values of 0.11-0.22 $cm^2V^{-1}s^{-1}$ with current on / off ratios of 10^5 have been measured.[54]

1.3.1.3 Rylene Diimides

The highest electron mobility values are reported for materials based on naphthalene and perylene diimides (NDIs and PDIs, respectively; Figure 1.13).[55-57] These materials exhibit high electron affinities (> 3.5 eV) due to the substitution of an aromatic core with two sets of π-accepting, conjugated imide groups. Ambient stability in devices has been achieved through the introduction of fluoroalkyl substituents at the *N,N′* positions, which create a kinetic barrier to ambient water and oxygen,[58-60] and through introduction of electron-withdrawing core substituents such as CN and F, which increase the EA of the material.[58,61,62]

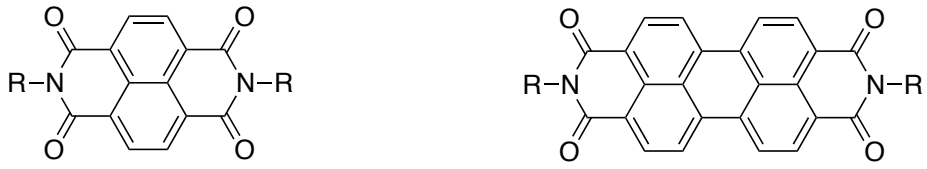

NDI PDI

Figure 1.13. Naphthalene diimide (left) and perylene diimide (right) cores.

The earliest attempt to fabricate OFETs from NDIs yielded an electron mobility of 10^{-4} $cm^2V^{-1}s^{-1}$ for *N*-H NDI.[63] Later, Katz *et al*. demonstrated that the performance and air stability of the OFETs could be greatly improved by varying the NDI imide substituents. Replacing *N*-hydrogen with an *N*-(*n*-hexyl) or *N*-cyclohexyl group led to an enhancement in electron mobility to 0.7 and 6.2 $cm^2V^{-1}s^{-1}$ for **1.3a** and **1.3b**, respectively, in vacuum, although no FET activity was measurable in air for **1.3a** and a large reduction in the mobility was observed for **1.3b** (0.41 $cm^2V^{-1}s^{-1}$) in air.[64] It was found that a *N*-fluoroalkyl substituent significantly improved device air stability,[65-67] with mobility values of 0.57 $cm^2V^{-1}s^{-1}$ measured in air for **1.3c**.[67] Although advances had been made towards air stable electron transport, all NDI-based materials mentioned

above were fabricated by vacuum deposition. Facchetti, *et al.* reported the first solution processed, air-stable NDI derivative with moderate electron mobility through the introduction of cyano groups in the NDI core. Devices based on **1.3d** exhibit a mobility of 0.11 $cm^2V^{-1}s^{-1}$ in air when processed from solution.[61] Following suit, Gao *et al.* developed a series of core expanded NDI derivatives using branched alkyl chains to improve solution processability and achieved average mobility values of 0.43 $cm^2V^{-1}s^{-1}$ with values as high as 1.2 $cm^2V^{-1}s^{-1}$ in air for solution processed **1.3e**.[68,69] In addition to these small-molecule examples of NDI derivatives, a few polymer examples were designed in order to combine the charge-transport properties of NDIs with the improved solution processability often associated with polymeric materials. Babel *et al.* reported field-effect electron mobility as high as 0.1 $cm^2V^{-1}s^{-1}$ in a spin-coated film of a conjugated ladder polymer, poly(benzobisimidazobenzophenanthroline) (BBL),[70] and, more recently, Facchetti *et al.* reported a NDI-bithiophene polymer with branched *N*-alkyl substituents (**1.3f**), which exhibited air-stable electron mobility values of up to 0.85 $cm^2V^{-1}s^{-1}$.[71]

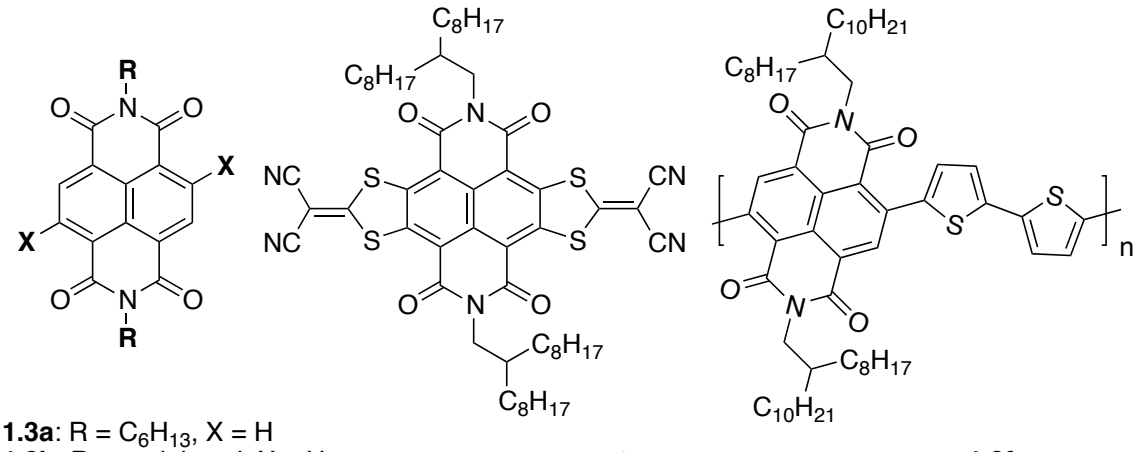

1.3a: R = C_6H_{13}, X = H
1.3b: R = cyclohexyl, X = H
1.3c: R = $C_6H_4CH_2CH_2C_8F_{17}$, X = H
1.3d: R = C_8H_{17}, X = CN

1.3e **1.3f**

Figure 1.14. Examples of naphthalene diimide-based electron-transport materials.

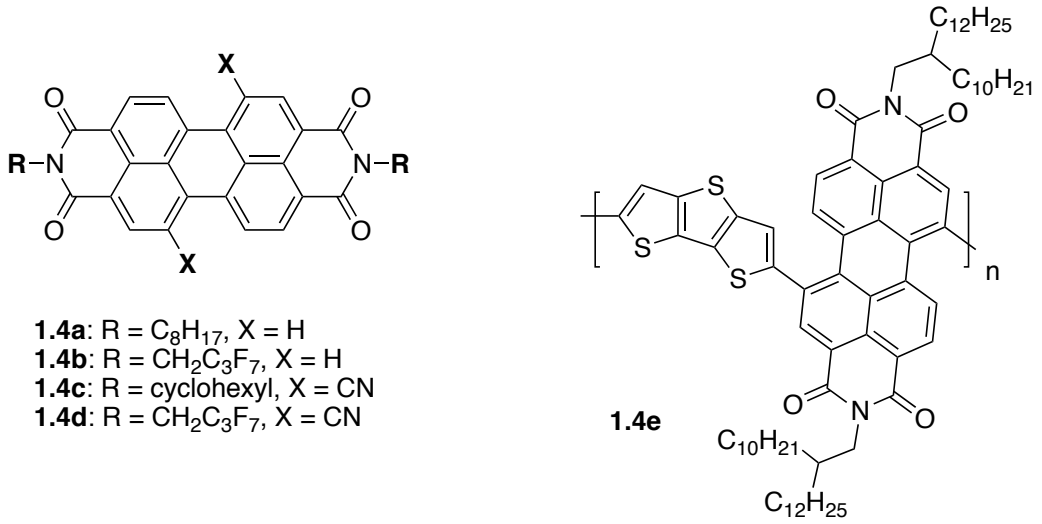

Figure 1.15. Examples of perylene diimide-based electron-transport materials.

In 2001, Malenfant *et al*. reported n-channel OFETs based on *N*-C_8H_{17} PDI **1.4a** with a substantial mobility of 0.6 $cm^2V^{-1}s^{-1}$ under nitrogen.[72] Later, Chesterfield *et al.* demonstrated that devices with a maximum mobility of 1.7 $cm^2V^{-1}s^{-1}$, an on / off ratio of 10^7 can be obtained using **1.4a** by coating the SiO_2 gate dielectric with poly(α-methylstyrene).[73] However, mobility values reported in air for this *N*-(n-alkyl) PDI are significantly lower (0.11 $cm^2V^{-1}s^{-1}$).[74] Bao, Würthner and coworkers reported that OFETs based on *N*-$CH_2C_3F_7$ PDI **1.4b** could exhibit mobility values as high as 0.72 $cm^2V^{-1}s^{-1}$, which decrease only slightly after air exposure and remain stable for more than 50 days.[75] Alternatively, 1,7-dicyano PDIs, first synthesized by Wasielewski *et al*., are significantly more readily reduced than their unsubstituted analogues (by ca. 0.36 V); the associated high electron affinity (EA = –4.3 eV; EA of PDI = –4.0 eV) is believed to be a factor contributing to the high electron mobility (0.10 $cm^2V^{-1}s^{-1}$) achieved in air for OFETs based on **1.4c**.[76] Combining partial fluorination of the imide position and 1,7-dicyano substitution in **1.4d** (EA = –4.4 eV) electron mobility values in air have been measured for devices processed by single crystal (3 $cm^2V^{-1}s^{-1}$)[77], vacuum deposition

(0.67 $cm^2V^{-1}s^{-1}$)[74], and solution spin-coating methods (0.08 $cm^2V^{-1}s^{-1}$)[78]. As with NDIs, solubility improvements were sought through incorporating PDI into polymer structures. Marder *et al.* reported a PDI-dithienothiophene co-polymer (**1.4e**) with solution processed mobility values of 0.013 $cm^2V^{-1}s^{-1}$.[79,80]

Table 1.1. Electron Mobility Values (μ_e) and Current On / Off Ratios for the Highest Performing Electron-Transport Materials in n-Channel OFETs.

cmpd	Processing	Atmosph.	μ_e / $cm^2V^{-1}s^{-1}$	I_{ON}/I_{OFF}	EA / eV	Reference
1.1	v	v	0.6	10^7	–4.0	52
1.2	v	v	1.83	10^4	–3.2	53
1.3a	v	Ar	0.7	10^6	–3.8	64
1.3b	v	Ar	6.2	10^8	–3.8	64
		air	0.41	10^5		
1.3c	v	air	0.57	10^7	–4.0	67
1.3d	s	air	0.11	10^3	–4.3	61
1.3e	s	air	0.43	10^6-10^7	–4.3	68
1.3f	s	air	0.85	10^7	–3.9	71
1.4a	v	N_2	1.7	10^7	–3.7	73
		air	0.11	10^5		74
1.4b	v	v	0.72	10^5	–3.9	75
		air	0.51	10^6		
1.4c	v	air	0.1	10^5	–4.2	76
1.4d	sc	v	6	10^3	–4.3	77
		air	3	10^4		
	v	air	0.64	10^4		76
	s	v	0.15	10^3		76
		air	0.08	10^3		
1.4e	s	v	0.013	10^4	–3.9	80

v = vacuum. s = solution. sc = single crystal. EA = $E^{0/-}$ vs. SCE + 4.44 eV.

1.3.2 Materials for Ambipolar Transistors

Ambipolar transistors are associated with a fair number of synthetic design challenges and performance drawbacks when incorporated into OFET devices; however, they are still interesting for use in organic complementary circuits where both p- and n-channel device function is required. Although independent p- and n-channel materials tend to exhibit better device performance, the controlled deposition of two different organic materials on a single substrate increases the complexity and cost of manufacturing. As an alternative, semiconductors that can provide both p- and n-channel OFET performance in a single material (ambipolar material) could potentially eliminate the need for complicated patterning techniques.

Ambipolar OFETs require efficient injection of both holes, as in well studied p-channel transistors, and electrons, as in n-channel transistors, into the metal electrodes of the device. One method by which this can be achieved is through combining an electron-transport material with a hole-transport material to create a heterostructured semiconducting layer.[81,82] Devices based on bilayers of vacuum deposited pentacene / C_{60}[83,84] and quarterthiophene / PDI[85] have been reported with hole / electron mobility values of 0.14 / 0.23 $cm^2V^{-1}s^{-1}$ and 0.04 / 0.03 $cm^2V^{-1}s^{-1}$, respectively. Another method used to achieve ambipolar OFET device function uses source and drain electrodes with unequal work functions. Schmechel *et al.* reports using a gold electrode for hole injection and a calcium electrode for electron injection in a device with pentacene as the charge-transport material leading to both hole and electron mobility values on the order of 0.1 $cm^2V^{-1}s^{-1}$.[86]

However, it is important to fabricate ambipolar devices employing a single transport material and ambient-stable electrodes to simplify the device fabrication process. Meijer *et al.* first reported that ambipolar devices could be fabricated using semiconductors with a very narrow energy gap (less than 1.8 eV), which could lead to

low injection barriers for both charge carriers if the IP and EA values align well with the electrode work function.[87] Only a few materials with low energy gaps have been shown to behave as ambipolar charge-transport materials; one example is a carbonyl-functionalized quaterthiophene, which exhibited hole / electron mobility values of 0.01 / 0.1 $cm^2V^{-1}s^{-1}$.[52]

1.3.3 Guidelines for the Development of New Materials

There are certain desirable characteristics that apply across the spectrum of electron-transport materials. These include high mobility, ease of synthesis, material stability under both processing and operational conditions and the ability to effectively inject and collect charges in a device.[57] While these properties can, in part, be optimized through the design and manipulation of the molecular structure, it is important to realize that some of these properties are dependent on the particular device configuration and processing. However, there are a few key properties that should be considered when designing new electron-transport materials including high EA values for efficient injection of electrons from suitable electrodes and planar aromatic cores to facilitate overlap between the π-systems of adjacent molecules in the solid state.

1.4 Thesis Overview

The bulk of the thesis will describe the synthesis and characterization of a variety of oligothiophene and naphthalene diimide-based materials aiming to develop new charge-transport materials for n-channel and ambipolar OFETs.

Specifically, Chapter 2 describes the properties of a series of small-molecule D-A-D and A-D-A triads with benzo[*c*][1,2,5]thiadiazole BTD as the acceptor and 4*H*-dithieno[3,2-*b*:2',3'-*d*]pyrrole DTP as the donor. The results of a joint experimental and

theoretical investigation of the optical, electrochemical, and charge-transport properties are presented and compared to current literature in the field of organic electronics.

The syntheses of a similarly structured series of A-D-A triads containing fused oligothiophene derivatives as the donor and NDI as the acceptor are described in Chapter 3. The optical, electrochemical, and charge-transport properties are presented along with a comparison to quantum-chemical calculations. Ambipolar and n-channel charge transport was achieved in OFET devices demonstrating one of the highest electron mobility values reported to date.

In Chapter 4, a new method for functionalizing NDI is presented and the utility of the new precursor is demonstrated through the synthesis of bi- and ter-NDI. The benefit of the synthetic method over other methods reported in the literature is addressed and the optical, electrochemical, and charge-transport properties of the oligomeric products are presented. The second part of Chapter 4 describes the use of this precursor to synthesize two NDI-A-NDI derivatives containing electron-deficient oligothiophene bridge units. The optical, electrochemical, and charge-transport properties are presented.

Chapter 5 describes the synthesis and properties of a variety of A-NDI-A structured triads containing alkyl and aryl ketone derivatives as the acceptor units to yield 2,6-diacyl-NDIs. The crystal structure, optical, electrochemical, and charge-transport properties of the diacyl-NDIs are presented along with comparison to quantum-chemical calculations. The second part of Chapter 5 describes the synthesis of a new planar, fused-ring core based on the diacyl-NDIs. The crystal structures of two products are presented along with DFT estimated electronic coupling values. The optical, electrochemical, and charge-transport properties of the compounds are also described.

1.5 References

(1) Bardeen, J.; Brattain, W. H. *Phys. Rev.* **1948**.

(2) Shockley, W. *IEEE T. Electron. Dev.* **1976**, *ED-23*, 597.

(3) Murphy, A. R.; Fréchet, J. M. J. *Chem. Rev.* **2007**, *107*, 1066.

(4) Voss, D. *Nature* **2000**, *407*, 442.

(5) Mas-Torrent, M.; Rovira, C. *Chem. Soc. Rev.* **2008**, *37*, 827.

(6) Burroughes, J. H.; Bradley, D. D. C.; Brown, A. R.; Marks, R. N.; Mackay, K.; Friend, R. H.; Burns, P. L.; Holmes, A. B. *Nature* **1990**, *347*, 539.

(7) Kulkarni, A. P.; Tonzola, C. J.; Babel, A.; Jenekhe, S. A. *Chem. Mater.* **2004**, *16*, 4556.

(8) Tang, C. W.; Vanslyke, S. A. *Appl. Phys. Lett.* **1987**, *51*, 913.

(9) Thompson, B. C. *Angew. Chem.* **2008**, *47*, 58.

(10) Bundgaard, E. *Sol. Energy Mater. Sol. Cells* **2007**, *91*, 954.

(11) Blom, P. W. M. *Adv. Mater.* **2007**, *19*, 1551.

(12) Dimitrakopoulos, C. D.; Malenfant, P. R. L. *Adv. Mater.* **2002**, *14*, 99.

(13) Horowitz, G. *Adv. Mater.* **1998**, *10*, 365.

(14) Crone, B.; Dodabalapur, A.; Lin, Y. Y.; Filas, R. W.; Bao, Z.; LaDuca, A.; Sarpeshkar, R.; Katz, H. E.; Li, W. *Nature* **2000**, *403*, 521.

(15) Rogers, J. A.; Bao, Z.; Baldwin, K.; Dodabalapur, A.; Crone, B.; Raju, V. R.; Kuck, V.; Katz, H.; Amundson, K.; Ewing, J.; Drzaic, P. *P. Natl. Acad. Sci. USA* **2001**, *98*, 4835.

(16) Sheraw, C. D.; Zhou, L.; Huang, J. R.; Gundlach, D. J.; Jackson, T. N.; Kane, M. G.; Hill, I. G.; Hammond, M. S.; Campi, J.; Greening, B. K.; Francl, J.; West, J. *Appl. Phys. Lett.* **2002**, *80*, 1088.

(17) Zhu, Z. T.; Mason, J. T.; Dieckmann, R.; Malliaras, G. G. *Appl. Phys. Lett.* **2002**, *81*, 4643.

(18) Crone, B.; Dodabalapur, A.; Gelperin, A.; Torsi, L.; Katz, H. E.; Lovinger, A. J.; Bao, Z. *Appl. Phys. Lett.* **2001**, *78*, 2229.

(19) Dimitrakopoulos, C.; Malenfant, P. *Adv. Mater.* **2002**, *14*, 99.

(20) Zaumseil, J.; Sirringhaus, H. *Chem. Rev.* **2007**, *107*, 1296.

(21) Brédas, J.-L.; Calbert, J. P.; da Silva Filho, D. A.; Cornil, J. *P. Natl. Acad. Sci. USA* **2002**, *99*, 5804.

(22) Newman, C. R.; Frisbie, C. D.; da Silva Filho, D. A.; Brédas, J.-L.; Ewbank, P. C.; Mann, K. R. *Chem. Mater.* **2004**, *16*, 4436.

(23) Sirringhaus, H. *Adv. Mater.* **2005**, *17*, 2411.

(24) Katz, H.; Bao, Z. *J. Phys. Chem. B* **2000**, *104*, 671.

(25) Bao, Z.; Locklin, J. *Organic Field-Effect Transistors*, 2007.

(26) Marcus, R. *Rev. Mod. Phys.* **1993**.

(27) Marcus, R. *J. Chem. Phys.* **1956**.

(28) Newton, M. *Chem. Rev.* **1991**, *91*, 767.

(29) Karl, N.; Marktanner, J. r.; Stehle, R.; Warta, W. *Synth. Met.* **1991**, *42*, 2473.

(30) Warta, W.; Stehle, R.; Karl, N. *Appl. Phys. A-Mater.* **1985**, *36*, 163.

(31) van der Auweraer, M.; de Schryver, F. C.; Borsenberger, P. M.; Bässler, H. *Adv. Mater.* **1994**, *6*, 199.

(32) Borsenberger, P.; Magin, E.; van der Auweraer, M.; de Schryver, F. C. *Phys. Status Solidi A* **1993**, *140*, 9.

(33) Bässler, H. *Phys. Status Solidi B* **1993**, *175*, 15.

(34) Pisula, W.; Menon, A.; Stepputat, M.; Lieberwirth, I.; Kolb, U.; Tracz, A.; Sirringhaus, H.; Pakula, T.; Müllen, K. *Adv. Mater.* **2005**, *17*, 684.

(35) Mas-Torrent, M.; Rovira, C. *Chem. Rev.* **2011**, *111*, 4833.

(36) Tsumura, A.; Koezuka, H.; Ando, T. *Appl. Phys. Lett.* **1986**, *49*, 1210.

(37) Horowitz, G.; Fichou, D.; Peng, X.; Xu, Z.; Garnier, F. *Solid State Commun.* **1989**, *72*, 381.

(38) Wong, W. S.; Ready, S. E.; Lu, J. P.; Street, R. A. *IEEE Electr. Dev. L.* **2003**, *24*, 577.

(39) Sirringhaus, H.; Kawase, T.; Friend, R. H.; Shimoda, T.; Inbasekara, M.; Wu, W.; Woo, E. P. *Science* **2000**, *290*, 2123.

(40) Murphy, A.; Fréchet, J. *Chem. Rev.* **2007**, *107*, 1066.

(41) Meijer, E. J.; de Leeuw, D. M.; Setayesh, S.; van Veenendaal, E.; Huisman, B. H.; Blom, P. W. M.; Hummelen, J. C.; Scherf, U.; Kadam, J.; Klapwijk, T. M. *Nature Mater.* **2003**, *2*, 834.

(42) Brotherton, S. *Semicond. Sci. Tech.* **1995**, *10*, 721.

(43) Minemawari, H.; Yamada, T.; Matsui, H.; Tsutsumi, J.; Haas, S.; Chiba, R.; Kumai, R.; Hasegawa, T. *Nature* **2011**, *475*, 364.

(44) Sundar, V. C. *Science* **2004**, *303*, 1644.

(45) Podzorov, V.; Menard, E.; Borissov, A.; Kiryukhin, V.; Rogers, J. A.; Gershenson, M. E. *Phys. Rev. Lett.* **2004**, *93*, 086602.

(46) Park, S. K.; Mourey, D. A.; Han, J.-I.; Anthony, J. E.; Jackson, T. N. *Org. Electron.* **2009**, *10*, 486.

(47) Tsao, H. N.; Cho, D. M.; Park, I.; Hansen, M. R.; Mavrinskiy, A.; Yoon, D. Y.; Graf, R.; Pisula, W.; Spiess, H. W.; Müllen, K. *J. Am. Chem. Soc.* **2011**, *133*, 2605.

(48) Facchetti, A. *Mater. Today* **2007**, *10*, 28.

(49) Allard, S.; Forster, M.; Souharce, B.; Thiem, H.; Scherf, U. *Angew. Chem. Int. Ed.* **2008**, *47*, 4070.

(50) Singh, T. B.; Sariciftci, N. S. *Ann. Rev. Mater. Res.* **2006**, *36*, 199.

(51) deLeeuw, D.; Simenon, M.; Brown, A.; Einerhand, R. *Synth. Met.* **1997**, *87*, 53.

(52) Yoon, M.; DiBenedetto, S.; Facchetti, A.; Marks, T. *J. Am. Chem. Soc.* **2005**, *127*, 1348.

(53) Ando, S.; Murakami, R.; Nishida, J.-i.; Tada, H.; Inoue, Y.; Tokito, S.; Yamashita, Y. *J. Am. Chem. Soc.* **2005**, *127*, 14996.

(54) Sakamoto, Y.; Suzuki, T.; Kobayashi, M.; Gao, Y.; Fukai, Y.; Inoue, Y.; Sato, F.; Tokito, S. *J. Am. Chem. Soc.* **2004**, *126*, 8138.

(55) Jones, B. A.; Facchetti, A.; Wasielewski, M. R.; Marks, T. J. *J. Am. Chem. Soc.* **2007**, *129*, 15259.

(56) Zhan, X.; Facchetti, A.; Barlow, S.; Marks, T. J.; Ratner, M. A.; Wasielewski, M. R.; Marder, S. R. *Adv. Mater.* **2010**, *23*, 268.

(57) Anthony, J. E.; Facchetti, A.; Heeney, M.; Marder, S. R.; Zhan, X. *Adv. Mater.* **2010**, *22*, 3876.

(58) Jones, B.; Ahrens, M.; Yoon, M.; Facchetti, A.; Marks, T.; Wasielewski, M. *Angew. Chem. Int. Ed.* **2004**, *43*, 6363.

(59) Oh, J.; Liu, S.; Bao, Z.; Schmidt, R.; Würthner, F. *Appl. Phys. Lett.* **2007**, *91*.

(60) Chen, H.; Ling, M.; Mo, X.; Shi, M.; Wang, M.; Bao, Z. *Chem. Mater.* **2007**, *19*, 816.

(61) Jones, B. A.; Facchetti, A.; Marks, T. J.; Wasielewski, M. R. *Chem. Mater.* **2007**, *19*, 2703.

(62) Ahrens, M.; Fuller, M.; Wasielewski, M. *Chem. Mater.* **2003**, *15*, 2684.

(63) Laquindanum, J.; Katz, H.; Dodabalapur, A.; Lovinger, A. *J. Am. Chem. Soc.* **1996**, *118*, 11331.

(64) Shukla, D.; Nelson, S. F.; Freeman, D. C.; Rajeswaran, M.; Ahearn, W. G.; Meyer, D. M.; Carey, J. T. *Chem. Mater.* **2008**, *20*, 7486.

(65) Katz, H.; Johnson, J.; Lovinger, A.; Li, W. *J. Am. Chem. Soc.* **2000**, *122*, 7787.

(66) Katz, H.; Lovinger, A.; Johnson, J.; Kloc, C.; Siegrist, T.; Li, W.; Lin, Y.; Dodabalapur, A. *Nature* **2000**, *404*, 478.

(67) See, K. C.; Landis, C.; Sarjeant, A.; Katz, H. E. *Chem. Mater.* **2008**, *20*, 3609.

(68) Gao, X.; Di, C.-A.; Hu, Y.; Yang, X.; Fan, H.; Zhang, F.; Liu, Y.; Li, H.; Zhu, D. *J. Am. Chem. Soc.* **2010**, *132*, 3697.

(69) Hu, Y.; Gao, X.; Di, C.-A.; Yang, X.; Zhang, F.; Liu, Y.; Li, H.; Zhu, D. *Chem. Mater.* **2011**, *23*, 1204.

(70) Babel, A.; Jenekhe, S. *J. Am. Chem. Soc.* **2003**, *125*, 13656.

(71) Yan, H.; Chen, Z.; Zheng, Y.; Newman, C.; Quinn, J. R.; Dötz, F.; Kastler, M.; Facchetti, A. *Nature* **2009**, *457*, 679.

(72) Malenfant, P.; Dimitrakopoulos, C.; Gelorme, J.; Kosbar, L.; Graham, T.; Curioni, A.; Andreoni, W. *Appl. Phys. Lett.* **2002**, *80*, 2517.

(73) Chesterfield, R.; McKeen, J.; Newman, C.; Ewbank, P.; da Silva, D.; Brédas, J.; Miller, L.; Mann, K.; Frisbie, C. *J. Phys. Chem. B* **2004**, *108*, 19281.

(74) Chen, F.-C.; Liao, C.-H. *Appl. Phys. Lett.* **2008**, *93*, 103310.

(75) Oh, J.; Liu, S.; Bao, Z.; Schmidt, R.; Wurthner, F. *Appl. Phys. Lett.* **2007**, *91*, 212107.

(76) Jones, B.; Ahrens, M.; Yoon, M.; Facchetti, A.; Marks, T.; Wasielewski, M. *Angew. Chem. Int. Ed.* **2004**, *43*, 6363.

(77) Molinari, A.; Alves, H.; Chen, Z.; Facchetti, A.; Morpurgo, A. *J. Am. Chem. Soc.* **2009**, *131*, 2462.

(78) Piliego, C.; Jarzab, D.; Gigli, G.; Chen, Z.; Facchetti, A.; Loi, M. A. *Adv. Mater.* **2009**, *21*, 1573.

(79) Zhan, X.; Tan, Z. a. a.; Domercq, B.; An, Z.; Zhang, X.; Barlow, S.; Li, Y.; Zhu, D.; Kippelen, B.; Marder, S. R. *J. Am. Chem. Soc.* **2007**, *129*, 7246.

(80) Zhan, X.; Tan, Z. a. a.; Zhou, E.; Li, Y.; Misra, R.; Grant, A.; Domercq, B.; Zhang, X.-H.; An, Z.; Zhang, X.; Barlow, S.; Kippelen, B.; Marder, S. R. *J. Mater. Chem.* **2009**, *19*, 5794.

(81) Dodabalapur, A.; Katz, H. E.; Torsi, L.; Haddon, R. C. *Science* **1995**, *269*, 1560.

(82) Dodabalapur, A.; Katz, H.; Torsi, L. *Appl. Phys. Lett.* **1996**.

(83) Kang, S. J.; Yi, Y.; Kim, C. Y.; Cho, K.; Seo, J. H.; Noh, M.; Jeong, K.; Yoo, K. H.; Whang, C. N. *Appl. Phys. Lett.* **2005**, *87*, 233502.

(84) Kuwahara, E.; Kusai, H.; Nagano, T.; Takayanagi, T.; Kubozono, Y. *Chem. Phys. Lett.* **2005**, *413*, 379.

(85) Dinelli, F.; Capelli, R.; Loi, M. A.; Murgia, M.; Muccini, M.; Facchetti, A.; Marks, T. J. *Adv. Mater.* **2006**, *18*, 1416.

(86) Schmechel, R.; Ahles, M.; von Seggern, H. *J. Appl. Phys.* **2005**, *98*, 084511.

(87) Meijer, E.; de Leeuw, D.; Setayesh, S.; van Veenendaal, E.; Huisman, B.; Blom, P.; Hummelen, J.; Scherf, U.; Klapwijk, T. *Nature Mater.* **2003**, *2*, 678.

CHAPTER 2

BENZOTHIADIAZOLE-DITHIENOPYRROLE TRIADS: SYNTHESIS AND OPTICAL, ELECTROCHEMICAL, AND CHARGE-TRANSPORT PROPERTIES

2.1 Introduction

Conjugated species composed of linked donor (D) and acceptor (A) moieties have attracted considerable recent attention for organic electronics applications. In particular, the use of donors (possessing small ionization potentials) and acceptors (with large electron affinities) leads to: (i) the possibility of D-to-A charge-transfer-type absorptions in the visible and/or in the near-infrared (NIR) portions of the solar spectrum that can be exploited in photovoltaic cells,[1-25] and (ii) the possibility of both hole and electron injection from appropriate electrode materials and, therefore, of ambipolar OFET behavior.[26-37] While much of the work on D/A materials for OPV and OFET applications has focused on conjugated polymers composed of alternating D and A monomers, there is also increasing interest in D/A small-molecules. As well as serving as models for understanding the fundamental nature of specific D/A interactions in analogous polymers,[38] there are some advantages of directly using small molecules over polymers in device applications. In contrast to polymers, which are typically polydisperse, can be hard to rigorously purify, may contain end groups that interfere with the electronic properties, and which, in some cases, can show considerable batch-to-batch variation in properties, small molecules can be obtained as much purer single-component materials following chromatography, crystallization, and / or sublimation. This potential for purification, coupled with the possibility of obtaining more ordered crystalline structures, can lead to higher charge-carrier mobility values.[39-41]

Fluorene and carbazole have been largely used as donors in D/A materials, but oligothiophene units, and more recently bridged derivatives, (i.e. fused ring such as 4,4-dialkyl-4*H*-cyclopenta[2,1-*b*:3,4-*b*']bithiophene (CPBT)) have perhaps been the most widely employed. The alkyl substituents of bridged bithiophene derivatives such as CPBT, 4,4-dialkyl-4*H*-silolo[3,2-*b*:4,5-*b*']bithiophene (also known as dithieno[3,2-*b*:2',3'-*d*]silole, DTS), and 4-alkyl-4*H*-dithieno[3,2-*b*:2',3'-*d*]pyrrole (DTP) can be varied to modify solubility and intermolecular packing without introducing large torsions between these units and their neighbors in the conjugated backbone. The planarity of these bridged bithiophenes also leads to lower oxidation potentials than those of unbridged bithiophenes[42-44] and, therefore, they behave as stronger donors when incorporated into D/A materials.[45]

Many different acceptor units have been exploited in D/A materials, among which [2,1,3]-benzothiadiazole (BTD) has been among the most widely used. Copolymers of BTD with fluorene,[9,17] silafluorene,[10,11] carbazole,[4,18-20] oligothiophene,[21,22,46] CPDT,[8,38,47] DTS,[23,36,38] and DTP[21,24,25] groups have been reported; photovoltaic devices made from blends with soluble fullerenes show power conversion efficiencies of up to 6.1%[7] and at least one BTD-based material has been shown to be ambipolar.[37] Small-molecule D-A-D and A-D-A molecules with BTD acceptors and various oligothiophene and planarized oligothiophene donors, including CPDT and DTS have also been investigated;[38,48,49] OFET hole mobility values of 0.17 $cm^2V^{-1}s^{-1}$ and 0.006 $cm^2V^{-1}s^{-1}$ have been reported for vacuum and solution-processed films, respectively, of a bithiophene/BTD D-A-D triad[50,51] and power conversion efficiencies of up to 3.15% have been observed for OPV cells based on use of a terthiophene/BTD A-D-A triad.[52] However, the DTP analogues of these small molecules have not been reported. Here we describe the results of a joint experimental and theoretical investigation of the optical, electrochemical, and charge-

transport properties of a series of D-A-D and A-D-A small-molecule triads with BTD as the acceptor and DTP as the donor (Figure 2.1).

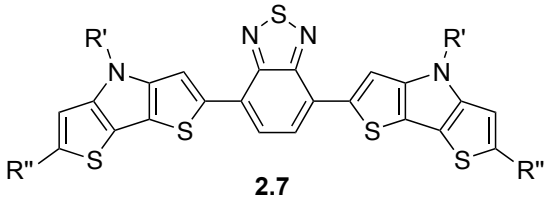

2.7

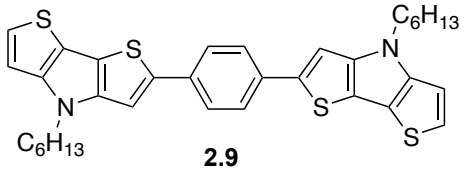

2.9

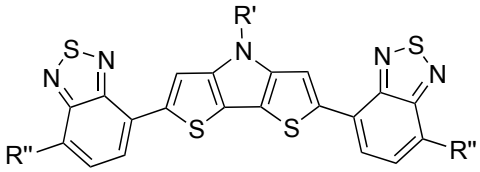

2.8

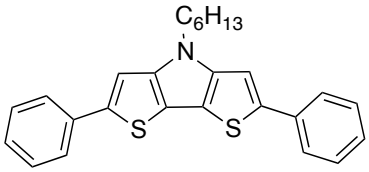

2.10

a: R' = C_6H_{13}, R'' = H
b: R' = $C_{12}H_{25}$, R'' = H
c: R' = C_6H_{13}, R'' = C_6H_{13}
d: R' = $C_{12}H_{25}$, R'' = C_6H_{13}

Figure 2.1. Structures of the D-A-D (**2.7**) and A-D-A (**2.8**) triads discussed in this paper, along with two model compounds (**2.9** and **2.10**).

2.2 Results and Discussion

2.2.1 Synthesis

The syntheses of compounds of type **2.7** and **2.8** are shown in Scheme 2.1 and 2.2. Commercially available BTD, **2.1**, was converted to its 4-bromo and 4,7-dibromo derivatives, **2.2** and **2.3**, respectively, according to literature procedures.[53] Compound **2.3** was converted to **2.4** by Negishi coupling with hexylzinc chloride (Scheme 2.1). The DTP precursors **2.6a** and **2.6b** were prepared from commercially available 3-bromothiophene via base-catalyzed oxidative homo-coupling followed by Buchwald-Hartwig ring closure with the appropriate alkylamine as previously reported.[54-57] The 2-

hexyl substituent of **2.6c** and **2.6d** was installed through Friedel-Crafts acylation of 3,3'-dibromo-2,2'-bithiophene, **2.5**, with hexanoyl chloride and aluminum trichloride in dichloromethane, followed by reduction of the resulting ketone using sodium borohydride / aluminum trichloride in refluxing THF to yield the 5-alkylated bithiophene **2.5'**. Palladium-catalyzed ring closure with the appropriate alkylamine gave the 2-hexyl-DTP precursors, **2.6c** and **2.6d** (Scheme 2.2).[57]

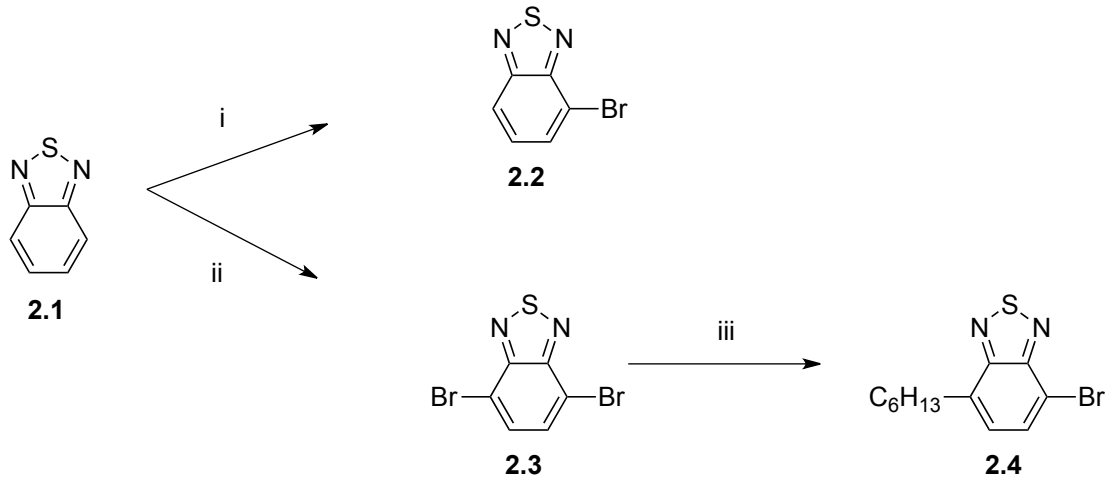

Scheme 2.1. Preparation of BTD precursors. (i) HBr, Br_2 (1 eq.); (ii) HBr, Br_2 (2 eq.); (iii) hexylzinc chloride, $Pd(PPh_3)_4$, THF.

Triads **2.7** and **2.8** were prepared from **2.6** via *in situ* lithiation and stannylation, followed by palladium-catalyzed cross-coupling. The lithiations were performed using either one or two equivalents of *tert*-butyllithium in THF at –78 ºC and the lithiated species was converted to mono or distannyl derivatives by the addition of tributylchlorostannane at room temperature. The freshly prepared stannane intermediate was transferred to a flask containing $Pd(PPh_3)_4$ and the appropriate (di)bromo-BTD, **2.2**-**2.4**, where they were then stirred at reflux for 18 h. The triads were isolated and purified by silica gel chromatography. The 2,6-diphenyl-substituted DTP model compound, **2.9**,

and the 1,4-phenylene-bridged bis(DTP) derivative, **2.10**, were synthesized from Stille coupling of the appropriate (di)stannyl DTP derivative with 1-bromobenzene and 1,4-dibromobenzene, respectively, under similar conditions to those used to obtain triads **2.7** and **2.8**.

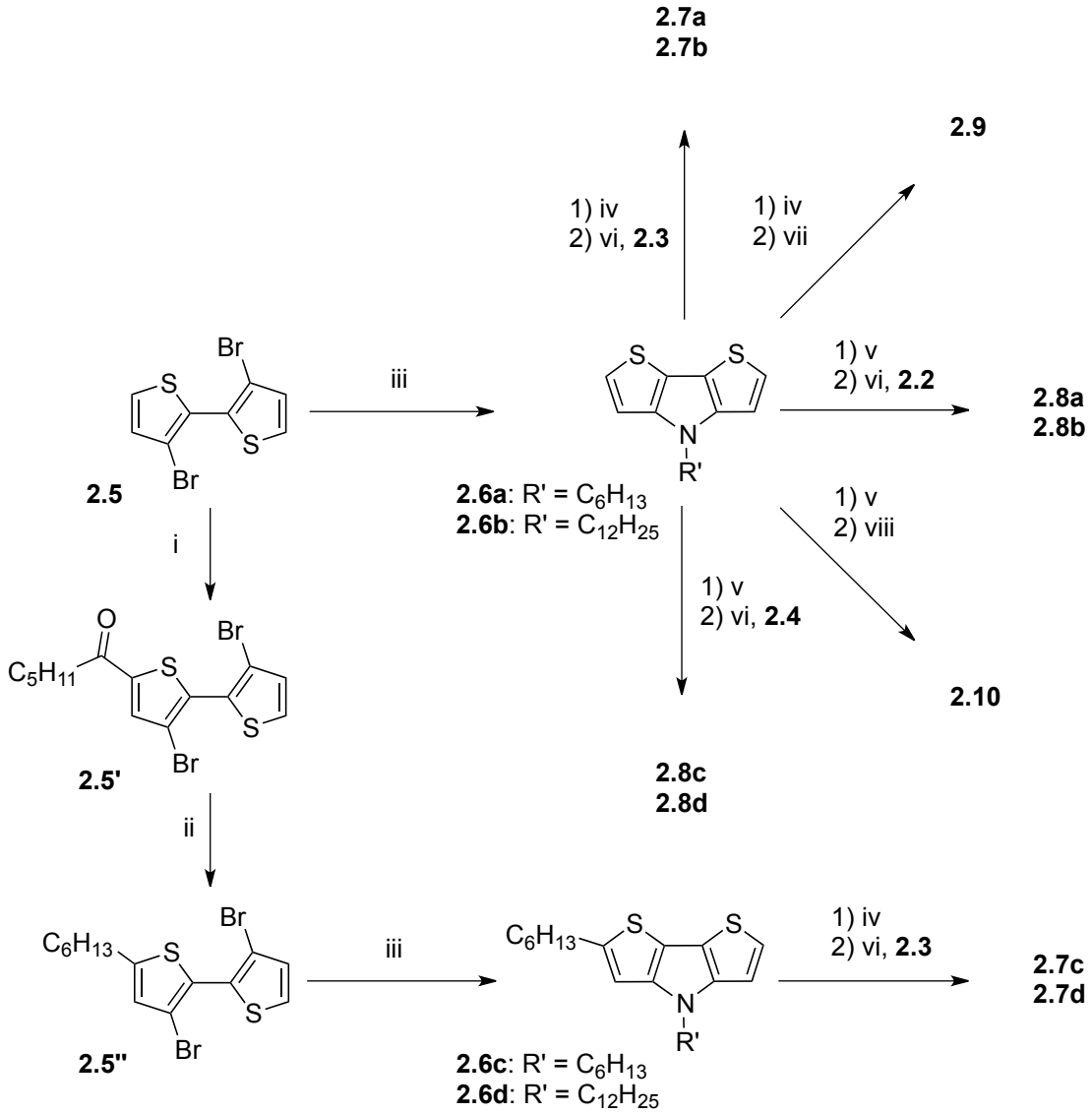

Scheme 2.2. Preparation of BTD-DTP triads. (i) hexanoyl chloride, $AlCl_3$, CH_2Cl_2; (ii) $NaBH_4$, $AlCl_3$; (iii) $R'NH_2$, $Pd_2(dba)_3$, BINAP, NaO^tBu, toluene; (iv) 1) ^{t}BuLi (1 eq.), THF, 2) Bu_3SnCl; (v) 1) ^{t}BuLi (2 eq.), THF, 2) Bu_3SnCl; (vi) $Pd(PPh_3)_2Cl_2$, THF; (vii) $Pd(PPh_3)_2Cl_2$, 1,4-dibromobenzene, THF; (viii) $Pd(PPh_3)_2Cl_2$, 1-bromobenzene, THF.

Triads **2.7** and **2.8** were prepared from **2.6** via *in situ* lithiation and stannylation, followed by palladium-catalyzed cross-coupling. The lithiations were performed using either one or two equivalents of *tert*-butyllithium in THF at –78 ºC and the lithiated species was converted to mono or distannyl derivatives by the addition of tributylchlorostannane at room temperature. The freshly prepared stannane intermediate was transferred to a flask containing $Pd(PPh_3)_4$ and the appropriate (di)bromo-BTD, **2.2**-**2.4**, where they were then stirred at reflux for 18 h. The triads were isolated and purified by silica gel chromatography. The 2,6-diphenyl-substituted DTP model compound, **2.9**, and the 1,4-phenylene-bridged bis(DTP) derivative, **2.10**, were synthesized from Stille coupling of the appropriate (di)stannyl DTP derivative with 1-bromobenzene and 1,4-dibromobenzene, respectively, under similar conditions to those used to obtain triads **2.7** and **2.8**.

All of the compounds were characterized by ^{1}H and $^{13}C\{^{1}H\}$ NMR spectroscopy, high-resolution mass spectrometry, and elemental analysis. In each case, the compounds with 4-(*n*-$C_{12}H_{25}$) substitution on the DTP moiety exhibited increased solubility in $CHCl_3$, CH_2Cl_2, toluene, and THF compared to those with 4-(*n*-C_6H_{13}) substitution. The use of terminal *n*-hexyl chains also increased the solubility of the materials; however, this solubility improvement was more pronounced in the A-D-A triads, **2.8**.

The thermal properties of the compounds were investigated by thermogravimetric analysis (TGA, 5 ºC min^{-1}, Figure 2.2, Table 2.1) and differential scanning calorimetry (DSC, 5 ºC min^{-1}, two heating-cooling cycles, Figure 2.3, 2.4 and 2.5). TGA showed decomposition temperatures (defined as that at which 5 wt% loss is observed) above 350 ºC for all triads. **2.7c** and **2.7d** exhibited two endothermic transitions on heating (and two corresponding exothermic transitions on cooling), perhaps suggesting the formation of liquid-crystalline phases similar to those previously reported for analogous

BTD/bithiophene triads:[58] Those of **2.7c** are seen at 141 and 150 ºC on heating and those of **2.7d** at 53 and 135 ºC. The second heating cycle for the **Ia** and **2.7b** triads exhibited only features attributed to glass transitions at temperatures, T_g, of 55 and 14 ºC, respectively, suggesting films of these compounds can be readily rendered amorphous. Triads **2.8** each showed single endothermic processes, presumably attributable to melting, at 202 ºC, 107 ºC, 160 ºC, and 154 ºC on heating **2.8a**, **2.8b**, **2.8c**, and **2.8d**, respectively (and corresponding single exothermic events on cooling).

Table 2.1. Decomposition (T_d), Glass Transition (T_g) and Melting (T_m) Temperatures Obtained Using TGA and DSC for the BTD-DTP Triads and Model Compounds.

cmpd	T_d / ºC[a]	T_g / ºC[b]	T_m / ºC[b]
2.7a	355	55	173
2.7b	360	14	116
2.7c	362	–	141, 150
2.7d	367	–	53, 135
2.8a	389	–	202
2.8b	384	–	107
2.8c	378	–	160
2.8d	382	–	154
2.9	368	36	203
2.10	315	56	180

[a]Temperature at which 5% weight loss observed using TGA at a heating rate of 5 °C min^{-1}. [b]Glass transition and melting temperatures observed using DSC (second heating, heating rate of 10 ºC min^{-1}).

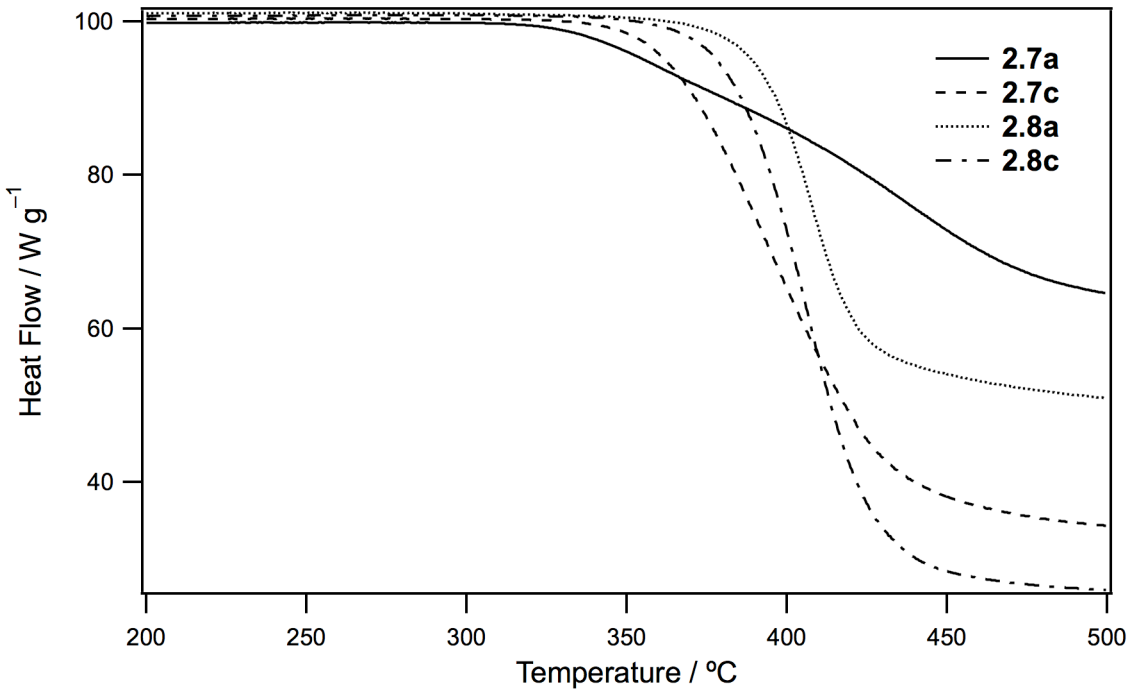

Figure 2.2. Thermogravimetric analysis of **2.7a**, **2.7c**, **2.8a**, and **2.8c** (5 °C min^{-1}).

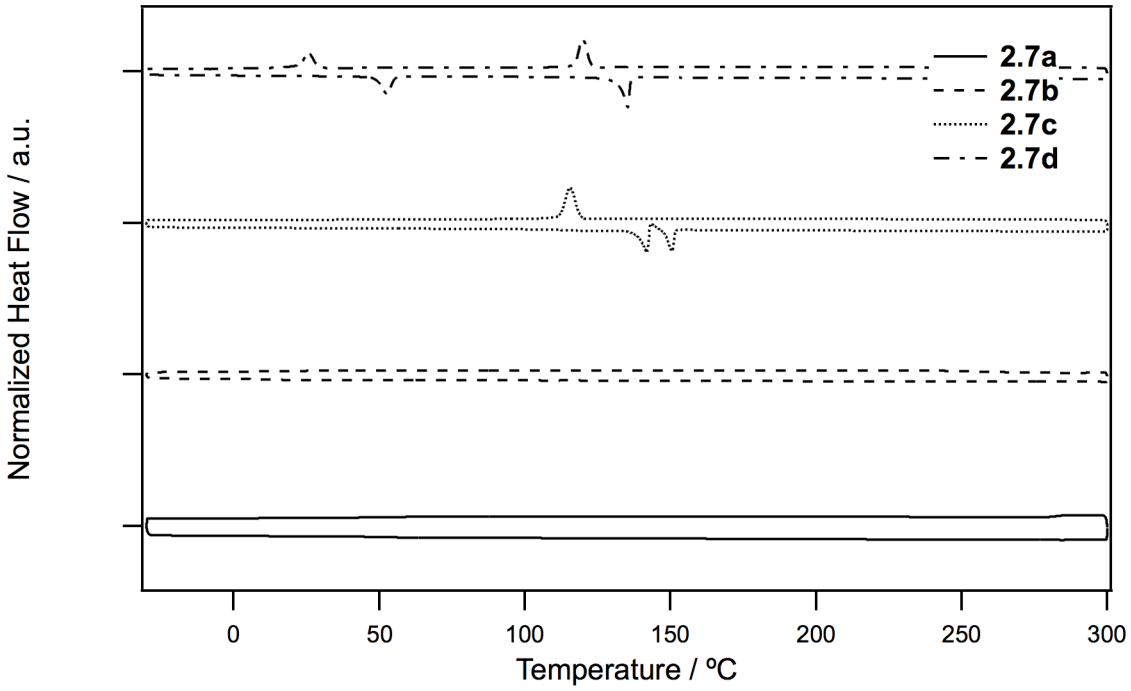

Figure 2.3. Differential scanning calorimetry (second heating and cooling scans) for **2.7a**-**d**. Negative heat flow corresponds to endothermic processes (10 °C min^{-1}).

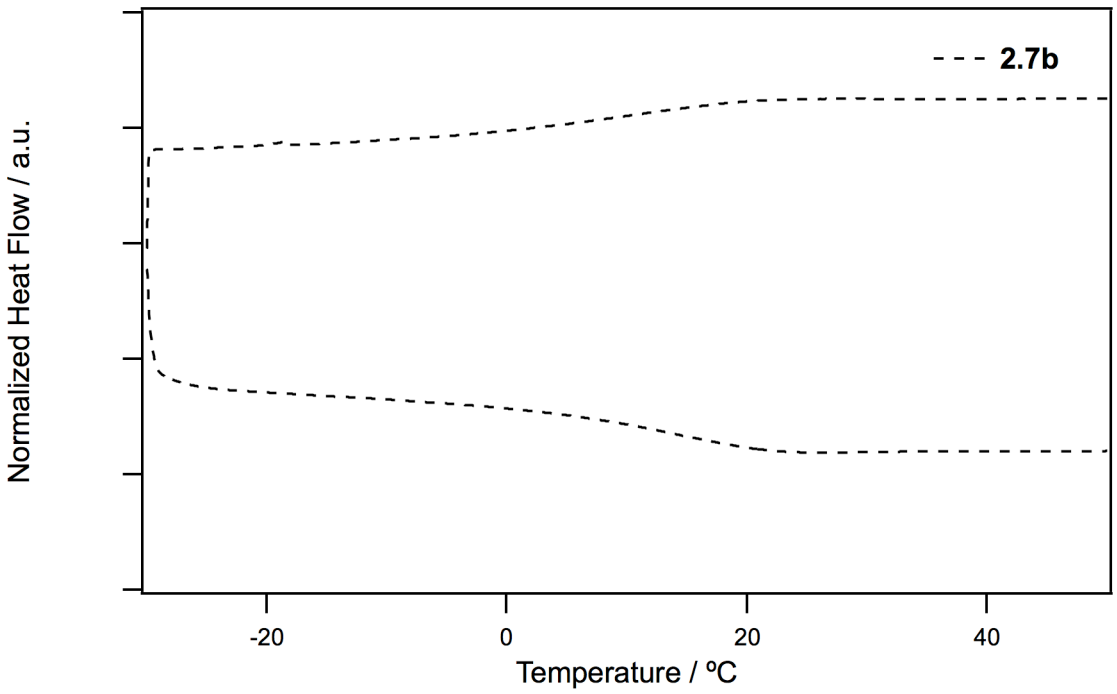

Figure 2.4. Differential scanning calorimetry (second heating and cooling scan) for **2.7b**. Negative heat flow corresponds to endothermic processes (10 °C min^{-1}).

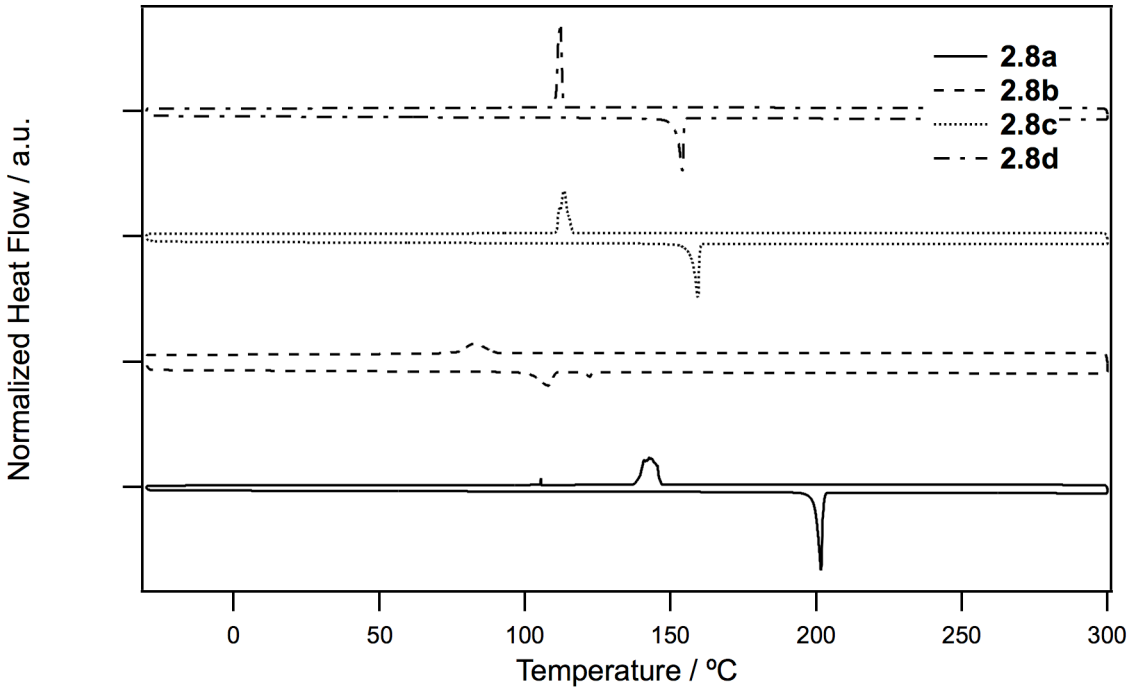

Figure 2.5. Differential scanning calorimetry (second heating and cooling scans) for **2.8a**-**d**. Negative heat flow corresponds to endothermic processes (10 °C min^{-1}).

2.2.2 Molecular Geometry and Frontier Orbitals

The neutral ground-state electronic structures obtained at the DFT (B3LYP/6-31G**) level for triads **2.7** and **2.8** (with all alkyl groups replaced by methyl groups) are characterized by coplanar DTP and BTD units, whereas torsion angles of 24° and 26° are found between the DTP and benzene rings of the diphenyl-DTP, **2.9**, and phenylene-bridged bis(DTP), **2.10**, model compounds.[59] This is consistent with the effects of steric interactions between hydrogen atoms in the 3 / 5 positions of the DTP with hydrogen atoms on the benzene rings.

The HOMO and LUMO wavefunctions (B3LYP/6-31G**) are illustrated for selected compounds in Figure 2.6.[60] The HOMOs of the triads are delocalized over the DTP rings and the hydrocarbon portion of the BTD rings and can be described as out-of-phase combinations of the HOMOs of the DTP[42] and BTD fragments. The LUMOs of **2.7** and **2.8**, on the other hand, are rather strongly localized on the BTD unit(s) with similar energies to that of an isolated BTD molecule (see Table 2.2 and Figure 2.7); this can be attributed to the larger mismatch in the energies of the BTD and DTP LUMOs than for the HOMOs and to the concentration of the BTD LUMO within its heterocyclic ring, leading to lower coefficients at the point(s) of attachment to DTP. Accordingly, the difference in the HOMO energies of, for example, **2.7a** and **2.8a** (0.35 eV) is larger than that in the LUMO energies (0.13 eV). The introduction of inductively electron-donating terminal alkyl groups in **2.7c/d** and **2.8c/d** leads to little difference in the overall shape of the orbitals; however, it destabilizes both HOMO (0.14 and 0.15 eV for **2.7** and **2.8** series, respectively) and LUMO (0.08 vs. 0.11 eV), the smallest effect being on the **2.7** LUMO, which is in accord with the localization of that orbital in the center of the molecule, away from the site of alkylation.

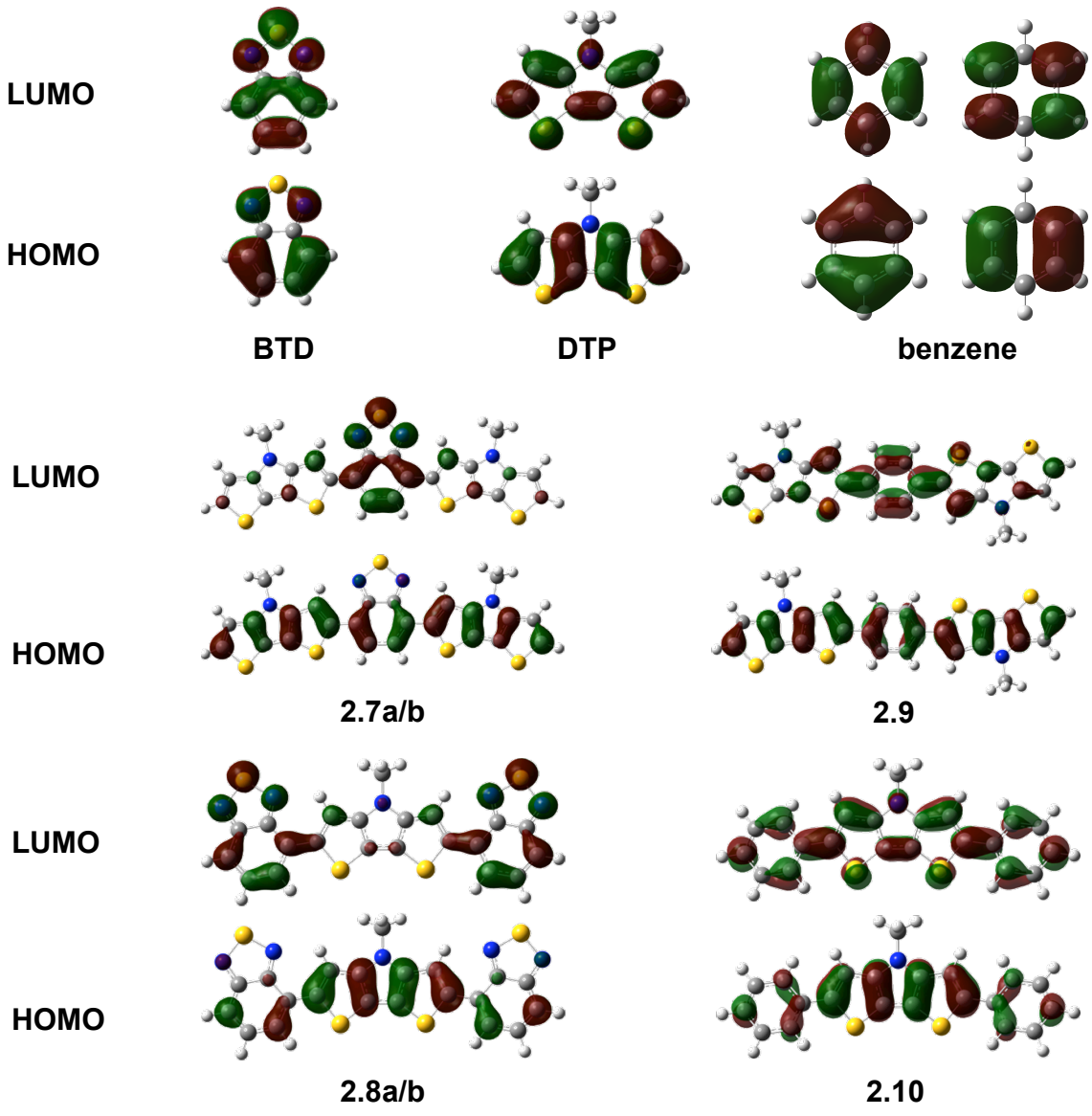

Figure 2.6. Illustrations of the HOMO and LUMO wavefunctions and energies of BTD, DTP, benzene, **2.7a/b**, **2.8a/b**, **2.9**, and **2.10**, as determined at the B3LYP/6-31G** level.

Table 2.2. B3LYP/6-31G** Frontier Orbital Energies (eV) for **2.7**-**2.10** and Their Building Blocks.[a]

cmpd	HOMO	LUMO
BTD	–6.62	–2.35
benzene	–6.72	+0.07
DTP	–5.10	–0.56
2.7a/b	–4.62	–2.52
2.7c/d	–4.48	–2.44
2.8a/b	–4.97	–2.65
2.8c/d	–4.82	–2.54
2.9	–4.68	–1.48
2.10	–4.82	–1.36

[a]Alkyl groups replaced by methyl groups.

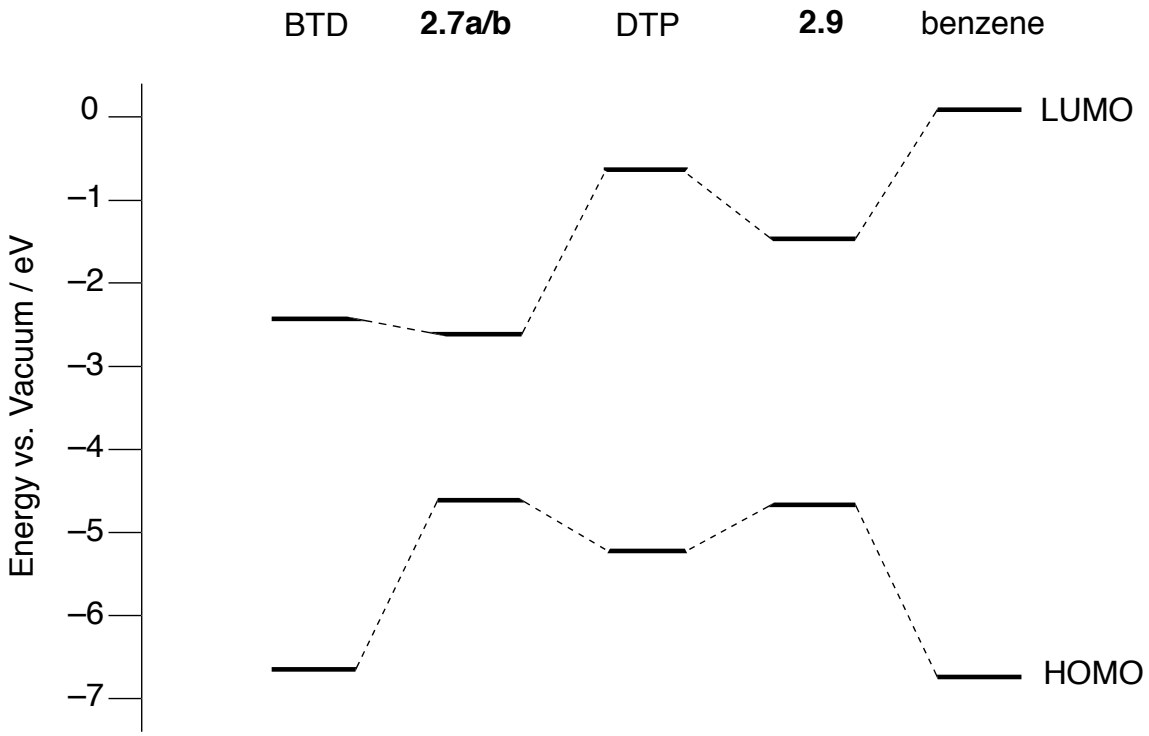

Figure 2.7. Correlation diagram showing how the DFT frontier orbital energies of the **2.7a/b** and **2.9** compare to those of their constituent building blocks. Note that the orbital energies of **2.8a/b** and **2.10** are similar to those of **2.7a/b** and **2.9**, respectively (see Table 2.2).

The relatively delocalized HOMO and localized LUMO of **2.7** are qualitatively rather similar to those previously reported for a bis(bithiophene)-BTD D-A-D triad[50] and to those calculated for extended conjugated systems incorporating thiophene-based donors and BTD acceptors, for example, model oligomers for copolymers derived from 2,6-distannyl-DTPs and 5,7-bis(5-bromo-2-thienyl)-BTD.[24]

The HOMOs of the model compounds **2.9** and **2.10** are similar to those of **2.7** and **2.8**, respectively, which is consistent with the similar appearance and energies (see Table 2.2, Figure 2.6) of the DFT HOMOs of isolated BTD and benzene molecules. The LUMOs of **2.9** and **2.10** differ significantly from those of **2.7** and **2.8**, respectively, as they are much more significantly delocalized over both benzene and DTP and significantly lower in energy than the LUMO of either building block in isolation (but much higher in energy than those of either BTD or the DTP/BTD triads); these trends are consistent with the better match in LUMO energies between DTP and benzene. Both HOMO and LUMO of **2.9** are rather similar to the respective orbitals previously reported for the closely related 1,4-(2,2'-bithiophene-5-yl)benzene.[61]

In both the radical cations and radical anions, the structures of **2.7** and **2.8** remain coplanar at the DFT level, while the DTP-benzene torsion angles in **2.9** and **2.10** are reduced to 0° and 14° upon oxidation, respectively, and to 2° and 1°, respectively, on reduction. The radical cations of series **2.7** and **2.9** and the radical anions of series **2.8** can, at least in principle, be regarded as organic mixed-valence species[62] in which the hole or electron might be either localized on one end of the molecule or delocalized between two comparable redox centers. The DFT calculations suggest all of the radical ions are symmetric systems both as isolated species or when in a dielectric continuum with a dielectric constant, ε, of 8.93 (to model solvation by dichloromethane), with symmetric geometries, distribution of LCAO coefficients in the neutral HOMO and LUMO wavefunctions, and distributions of Mulliken charges. Given the well-known tendency of

conventional DFT to give overdelocalized structures,[63] we also used Hartree-Fock (HF) calculations to investigate the radical-ion geometries. The HF radical-cation structures are fully planar (**2.7**$^{\bullet+}$ and **2.9**$^{\bullet+}$) or nearly planar (angles between DTP and BTD planes of 6º and 4º for **2.8a-b**$^{\bullet+}$ and **2.8c-d**$^{\bullet+}$, respectively), with the exception of **2.10**$^{\bullet+}$, which has an increased twist between Ph and DTP rings of 46°; these results suggest that **2.7**$^{\bullet+}$ and **2.9**$^{\bullet+}$ are symmetrical (class-III-like) species, which is consistent with the similarity of their optical spectra to those of oligothiophene radical cations (see below). The HF radical-anion structures are all planar or almost so (torsion angles of ca. 2° or less) and also point to delocalization in **2.8**$^{\bullet-}$ ions, at least in the gas phase.[64] Both DFT and HF calculations suggest that either oxidation or reduction leads to a more quinoidal pattern of bond lengths, with the DTP-BTD or DTP-benzene bonds shortening by 0.01 to 0.03 Å, a result consistent with the DTP-BTD / DTP-benzene antibonding character of the HOMOs and DTP-BTD / DTP-benzene bonding character of the LUMOs.

2.2.3 Optical Properties

Electronic spectra of **2.7**-**2.10** were recorded in dilute chloroform solution and as thin films on glass substrates. Representative spectra for the triads are shown in Figure 2.8; the corresponding absorption maxima, absorptivities, and oscillator strengths are summarized in Table 2.3. The solution absorption spectra of DTP/BTD triads **2.7** and **2.8** exhibit two prominent absorption bands with roughly comparable oscillator strengths in the near-UV / visible range. Both absorptions are observed at lower energy in the D-A-D compounds of type **2.7** than for the corresponding absorption in A-D-A compounds of type **2.8**, consistent with previously reported spectra for analogous CPBT/BTD D-A-D and A-D-A triads.[38] Terminal alkylation leads to small bathochromic shifts in the absorption maxima, these shifts being largest in **2.7**, but, as expected, the choice of DTP 4-alkyl group does not significantly affect the spectra. The spectra are generally similar

to those of previously reported triads with similar structures[38,48-51] and the two bands observed in the absorption spectra of **2.7** and **2.8** also resemble those seen for related D/A conjugated polymers, although each band is bathochromically shifted in alternating DTP/BTD conjugated polymers (low-energy bands at ca. 13000 cm^{-1} in $CHCl_3$)[25] from that in the present small molecules.

Spectra in thin films are fairly similar to those seen in solution with moderate shifts in the absorption maxima (Figure 2.9). Interestingly, the low-energy absorption maxima of both **2.7a** and **2.7b** are bathochromically shifted by ca. 700 cm^{-1}, while those of **2.7c** and **2.7d** are both bathochromically shifted by ca. 1400 cm^{-1}, suggesting that terminal alkylation can play a significant role in determining intermolecular interactions.

To gain insight into the origin of the spectroscopic properties observed in solution, vertical $S_0 \rightarrow S_n$ excitation energies for isolated molecules were calculated at the time-dependent density functional theory (TD-DFT) level of theory using the B3LYP/6-31G** functional. As shown in Figure 2.10 and Table 2.3, the TD-DFT results are in good agreement with the solution and solid-state absorption results, both in terms of excitation energies and oscillator strengths. Although the excitation energies are somewhat underestimated the differences are within the range typical for the TD-B3LYP method[65,66] and, more importantly, the experimentally observed trends between **2.7a/b**, **2.7c/d**, **2.8a/b**, and **2.8c/d** are all reproduced by the calculations.[67] According to the calculations, the strong low-energy transitions seen in the range 14200–16800 cm^{-1} for molecules of both series **2.7** and **2.8** correspond to the $S_0 \rightarrow S_1$ transitions and are predominantly HOMO→LUMO one-electron transitions in nature; therefore, they can be regarded as having considerable DTP-to-BTD quadrupolar charge-transfer (CT) character. The variations in experimental and calculated absorption maxima with molecular structure (**2.7** vs. **2.8**, **a/b** vs. **c/d**) can be rationalized by those in the energies of the DFT HOMOs and LUMOs (see above). Compounds of type **2.7** show similar low-

energy maxima to analogous BTD-based D-A-D triads with CPBT donors (17600-18100 cm^{-1}),[38,49] these being at lower energy than those for analogues with 5'-alkyl-2,2'-bithiophene-5-yl donors (19200 cm^{-1});[50,58] this is consistent with previous work showing that CPBT and DTP moieties have similar donor strength to one another and are stronger donors than bithiophenes.[43] The low-energy maxima for the A-D-A derivatives **2.8** are also similar to those of their CPTD and DTS analogues (19300 and 19900 cm^{-1}, respectively).[38,48]

Excitations to the next few excited electronic states are calculated to be very weak, with the strong higher energy (24700–27400 cm^{-1}) transitions for compounds of series **2.7** and **2.8** corresponding to $S_0 \rightarrow S_5$ and $S_0 \rightarrow S_6$, respectively. In both cases, these transitions largely correspond to excitation from the HOMO to a higher-lying unoccupied molecular orbital (LUMO+1 and LUMO+2 for **2.7** and **2.8**, respectively, see Table 2.3 and Figure 2.11) with contributions from the LUMO of the DTP fragment and from the BTD group; thus, these transitions do not exhibit the pronounced DTP-to-BTD charge-transfer character of the $S_0 \rightarrow S_1$ transitions.

Replacement of the BTD rings of **2.7** and **2.8** with benzene rings in the model compounds **2.9** and **2.10**, respectively, leads to a considerable hypsochromic shift of the lowest energy transition, in agreement with the much higher lying LUMOs calculated (see above) for the model compounds. The TD-DFT calculations indicate that the transitions observed at 24000-25400 cm^{-1} can be assigned to $S_0 \rightarrow S_1$ and are largely to HOMO→LUMO in character, both relevant orbitals being extensively delocalized along the π backbone. Indeed, the orbitals involved in these transitions are similar to those involved in the $S_0 \rightarrow S_5$ and $S_0 \rightarrow S_6$ transitions of **2.7** and **2.8**, respectively, and the transitions are observed at similar energies. The absorption maxima are also observed at similar energies to those of analogous compounds in which the DTP groups are replaced with bithiophene; absorption maxima of 25600 cm^{-1} and 26800 cm^{-1} have been

reported for 1,4-(2,2'-bithiophene-5-yl)benzene[61] and 5,5'-diphenyl-2,2'-bithiophene,[68] respectively, in CH_2Cl_2. The high-energy maxima of compounds of type **2.8** and the $S_0 \rightarrow S_1$ transition of **2.10** are seen at lower energy than the lowest energy absorption of an isolated DTP (32300 cm^{-1} in CH_2Cl_2,[42] 35200 cm^{-1} and 79% HOMO-LUMO according to TD-DFT, see SI), reflecting the additional destabilization of the HOMO and stabilization of the relevant empty orbitals by BTD or phenyl contributions. On the other hand, the $S_0 \rightarrow S_1$ transition of **2.10** is seen at very similar energy to the lowest energy transition of a 2,2'-bis(DTP), i.e., an analogous compound without the phenylene bridge (24400 cm^{-1} in CH_2Cl_2),[69] presumably due to competition between the effects of an extended π-system and disruption of that conjugation by the aromaticity and reduced coplanarity of the phenylene bridge.

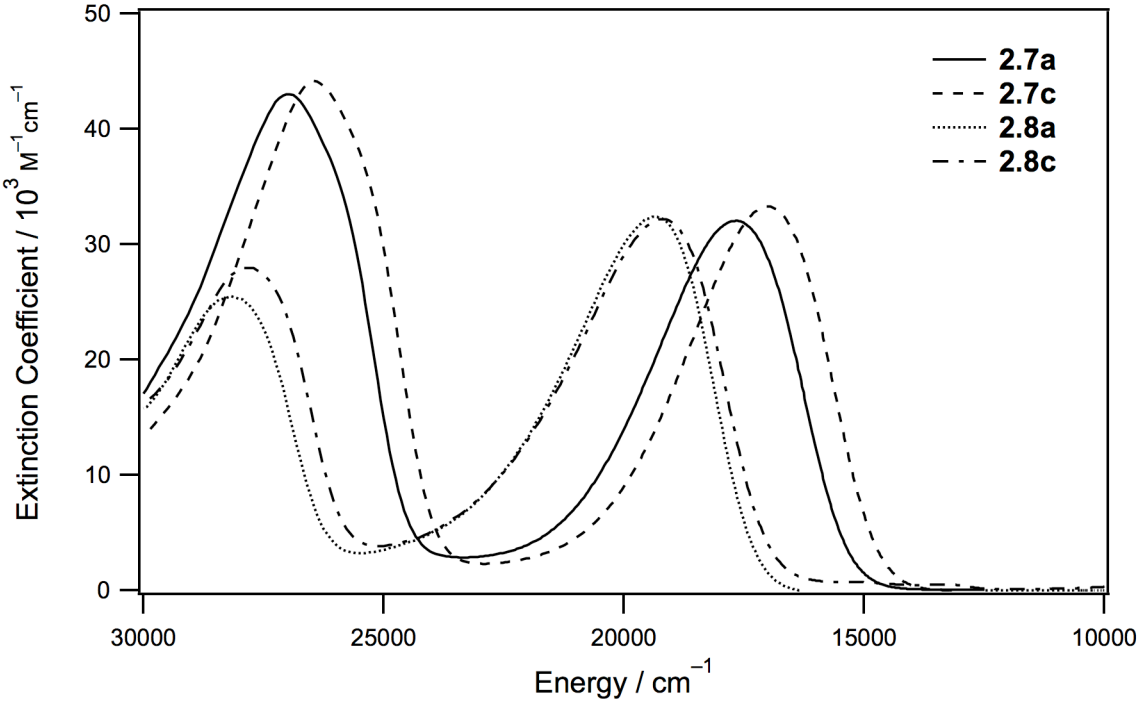

Figure 2.8. UV-vis. spectra of **2.7a**, **2.7c**, **2.8a**, and **2.8c** in chloroform.

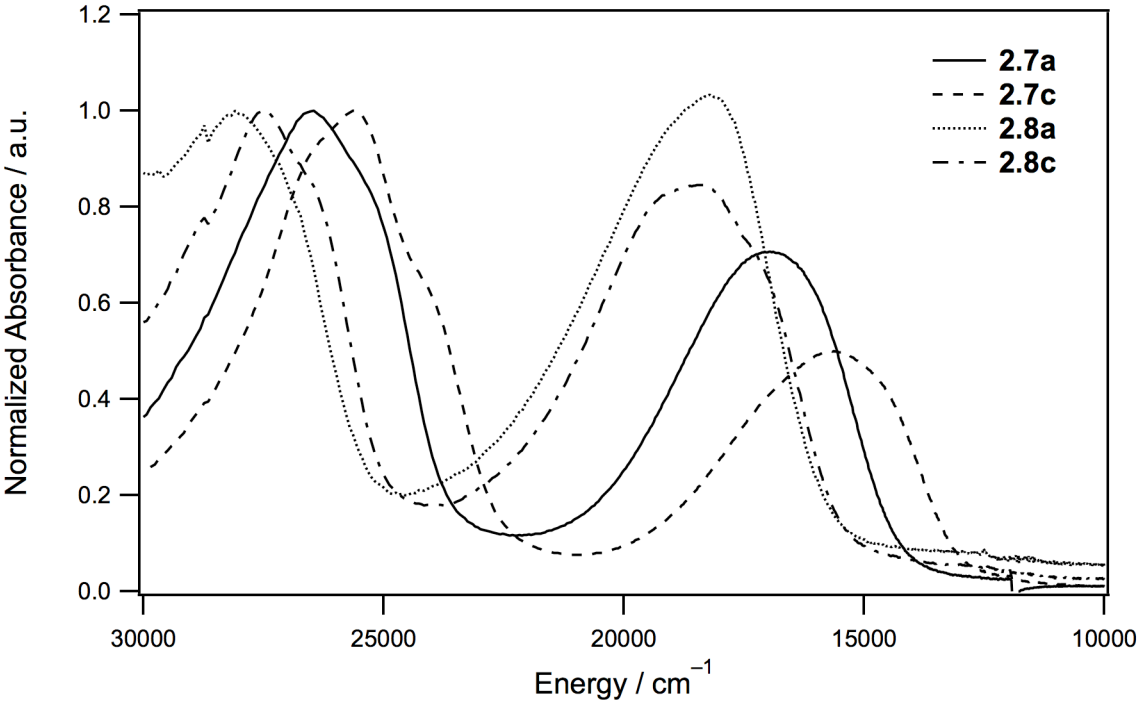

Figure 2.9. UV-vis. spectra of **2.7a**, **2.7c**, **2.8a**, and **2.8c** as films on glass.

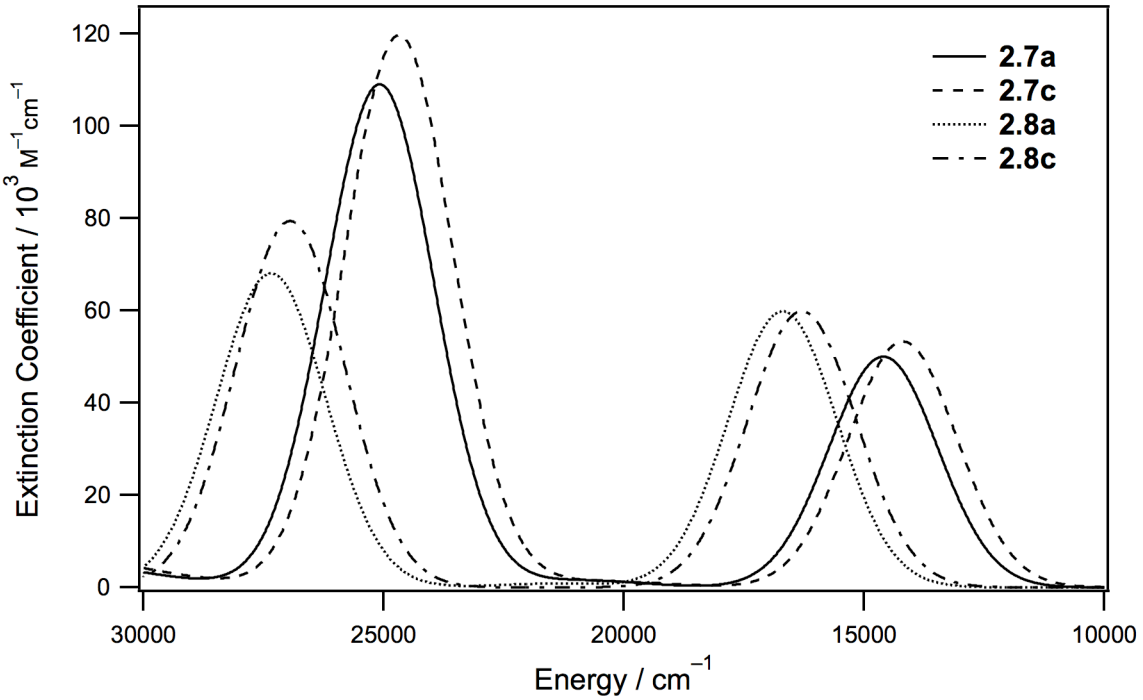

Figure 2.10. UV-vis. spectra of **2.7a**, **2.7c**, **2.8a**, and **2.8c** calculated at the TD-B3LYP/6-31G**//B3LYP/6-31G** level (obtained by applying a Gaussian broadening to the calculated oscillator strength data; full width at half maximum of 2660 cm^{-1}).

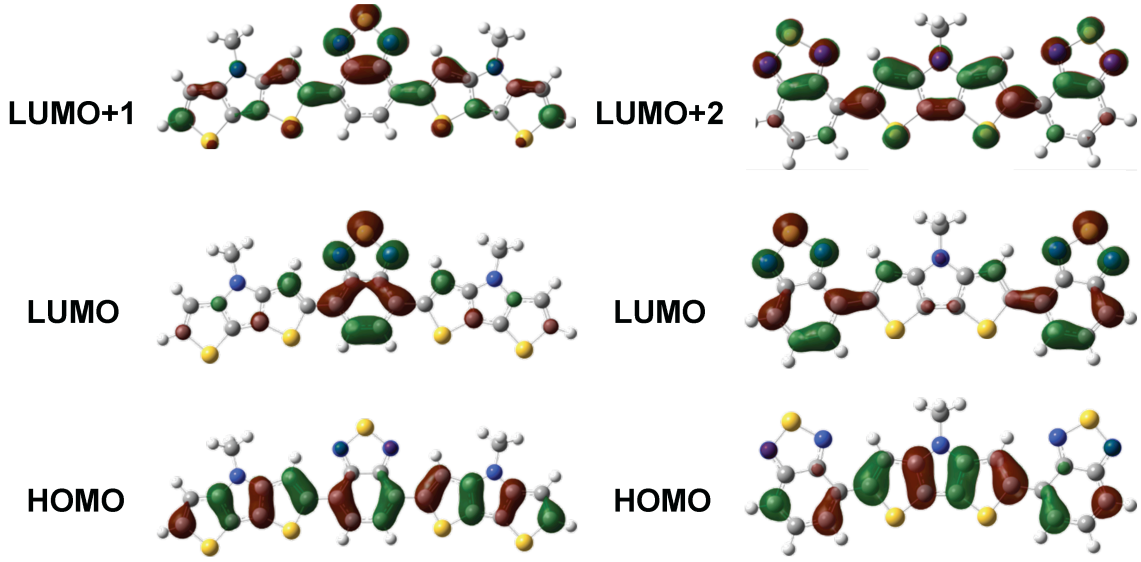

Figure 2.11. Pictorial representations of the dominant orbitals involved in the strong transitions (TD-B3LYP/6-31G**) in compounds of type **2.7** and **2.8** as determined at the B3LYP/6-31G** level.

Table 2.3. Absorption Maxima, Absorptivities, and Oscillator Strengths for the Strong UV-vis. Absorptions of **2.7**-**2.10** in Chloroform along with TD-DFT Values and Assignments (in italics) and Thin-Film Absorption Maxima.[a]

cmpd	Low-Energy Band								High-Energy Band							
	$\bar{\nu}_{max}$ / 10^3 cm^{-1}			ε_{max} / 10^4	*f*		state	CI description	$\bar{\nu}_{max}$ / 10^3 cm^{-1}			ε_{max} / 10^4	*f*		state	CI description
	soln	calc	film	$M^{-1}cm^{-1}$	soln	calc		(%)[b]	soln	calc	film	$M^{-1}cm^{-1}$	soln	calc		(%)[b]
2.7a	17.7	*14.6*	17.0	3.21	0.53	*0.61*	S_1	*H→L (98),*	27.0	*25.1*	26.5	4.31	0.82	*1.33*	S_5	*H→L (2),*
2.7b	17.7		17.0	3.13	0.53			*H→L+1 (2)*	27.0		26.5	4.20	0.82			*H→L+1 (96)*
2.7c	17.0	*14.2*	15.6	3.32	0.55	*0.65*	S_1	*H→L (98),*	26.5	*24.7*	25.7	4.39	0.83	*1.46*	S_5	*H→L (2),*
2.7d	17.0		15.6	3.39	0.56			*H→L+1 (2)*	26.5		25.7	4.49	0.87			*H→L+1 (97)*
2.8a	19.3	*16.8*	18.2	3.28	0.55	*0.73*	S_1	*H→L (82),*	28.2	*27.4*	28.1	2.57	0.34	*0.83*	S_6	*H→L+2 (84)*
2.8b	19.3		18.0	3.34	0.58			*H→L+2 (2)*	28.2		27.9	2.62	0.35			
2.8c	19.2	*16.3*	18.4	3.25	0.60	*0.73*	S_1	*H→L (98)*	27.8	*27.0*	27.5	2.82	0.40	*0.96*	S_6	*H–2→L+1 (2),*
2.8d	19.2		18.4	3.26	0.60				27.8		27.5	2.85	0.40			*H→L+2 (93)*
2.9	–	–	–	–	–	–	–	–	24.0	*23.7*	23.8	5.94	*1.24*	*1.75*	S_1	*H→L (99)*
2.10	–	–	–	–	–	–	–	–	25.4	*25.7*	27.7	4.88	1.05	*1.32*	S_1	*H→L (99)*

[a]TD-DFT Values obtained for structures in which the alkyl groups are all replaced by methyl groups at the B3LYP/6-31G** level. The two transitions reported are those seen and/or calculated at $\bar{\nu}_{max}$ < 30 000 cm^{-1} and calculated to have *f* > 0.05. [b]H and L denote HOMO and LUMO, respectively.

2.2.4 Electrochemistry, Ionization Potentials, Electron Affinities, and Reorganization Energies

The electrochemical properties of **2.7**-**2.10** were investigated using cyclic voltammetry (CV) in dichloromethane / 0.1 M tetra-*n*-butylammonium hexafluorophosphate. Representative CV traces are shown in Figure 2.12 and the redox potentials are summarized in Table 2.4. The Table also includes estimates of solid-state ionization potentials (IPs) and electron affinities (EAs) based on the electrochemical data, and values of vertical and adiabatic IPs and EAs obtained from DFT calculations for isolated molecules.

2.7 and **2.8** display reversible features corresponding to both molecular oxidation and reduction. In contrast, the CV traces of **2.9** and **2.10** only display oxidation processes (also reversible) within the accessible solvent window (down to ca. –2.5 V vs. $FeCp_2^{+/0}$) under the same conditions, consistent with the absence of the electron-accepting BTD moiety. In the case of the bis(DTP) derivatives **2.7** and **2.9** two well-separated oxidation processes are observed, whereas only one is seen for **2.8** and **2.10**. The current measured for the reduction processes of the bis(BTD) compounds **2.8** is ca. twice that for the mono-BTD species of type **2.7**, suggesting two closely overlapping reductions. This is confirmed by differential pulse voltammetry; an example is shown in Figure 5 and shows that the two reductions are separated by ca. 60 mV.

The electrochemical gaps, obtained from the difference between oxidation and reduction potentials, are rather similar to the optical gaps, obtained from the onset of absorption in solution. This suggests that the effects of exciton binding in the excited state are effectively compensated for by solvation of the ions formed in the electrochemical experiments.

The D-A-D molecules, **2.7**, are ca. 0.25 V more readily oxidized than their A-D-A, **2.8**, counterparts, in agreement with the results of the DFT calculations, which show

HOMO energies ca. 0.35 eV higher (Table 2.2) and vertical and adiabatic IPs ca. 0.45-0.50 eV lower (Table 2.4), and with the more extended conjugation in these species. The species with terminal alkylation (**2.7c/d**, **2.8c/d**) are all ca. 0.1 V more easily oxidized than their non-alkylated analogues (**2.7a/b**, **2.8a/b**), consistent with the extension of the HOMO onto the terminal alkylated rings in both D-A-D and A-D-A systems (see above) and with the DFT HOMO energies and IPs. The first oxidation potentials for triads of type **I** are similar to those previously reported for an analogous triad with CPBT donors in place of DTPs (+0.18 V vs. $FeCp_2^{+/0}$ in CH_2Cl_2)[49] and lower than those seen for one with 5'-alkyl-2,2'-bithiophene-5-yl donors (ca. +0.46 V in CH_2Cl_2);[58] these results are in line with previous comparisons of the redox properties of CPBT, bithiophene, and DTP derivatives;[43] similarly, the potentials of **2.9** and **2.10** are lower than those of analogues in which bithiophene replaces DTP (E_{ox} = +0.72 V in DMF for 1,4-di(2,2'-bithiophene-5-yl)benzene[70]; $E_{1/2}$ = +0.68 V in CH_2Cl_2 for 5,5'-diphenyl-2,2'-bithiophene[68]).

Despite the presence of two BTD acceptor moieties in the triads of type **2.8**, these species are oxidized at similar potential to DTPs (irreversibly oxidized with peak potential, E_{ox}, of ca. +0.45 V vs. $FeCp_2^{+/0}$ in MeCN),[42] or a 2,6-dialkyl-DTP (+0.23 V in CH_2Cl_2).[43] Also, the triads of type **I** are oxidized at similar potential to a 2,2'-bis(DTP) (E_{ox} = +0.08 V in CH_2Cl_2).[69] Furthermore, replacement of the BTD moieties with benzene rings has little effect on the oxidation potential or DFT IP values, consistent with the similarity of energy and extent of the HOMOs of **2.9** and **2.10** to those of **2.7** and **2.8**, respectively, and with the DFT IP values. However, in contrast to the electrochemical data, the DFT adiabatic IPs suggest that **2.7**-**2.10** are much more (0.65-1.30 eV) easily oxidized than DTP in the gas phase (6.70 eV), in agreement with the higher HOMO energies calculated for the dyads (see above). This is presumably attributable to the influence of solvation on the electrochemical values. Indeed, considerably reduced differences (0.24-0.75 eV) between the adiabatic IPs of **2.7**-**2.10** and DTP (5.17 eV) are

found when evaluated for isolated molecules embedded in a dielectric continuum (dichloromethane, ε = 8.93, see Table 2.4)

The reduction potentials of the BTD-containing triads are observed at –1.74 to –1.95 V vs. $FeCp_2^{+/0}$; potentials in the same range have previously been reported for related BTD-based triads[49,50,52,58] and for diaryl-BTD derivatives.[71] Moreover, the potentials are similar to that of benzothiadiazole itself, for which $E_{1/2}^{0/-}$ is –1.98 V vs. $FeCp_2^{+/0}$, also in dichloromethane,[72] in agreement with the highly BTD-localized nature of the LUMOs (Figure 2.6). This is broadly consistent with the similar LUMO energies calculated for the triads and BTD (Table 2.2), but is not reproduced in the DFT-calculated EA values; vertical and adiabatic values of –0.35 and –0.50 eV, respectively, are obtained for BTD, suggesting that the dyads should be ca. 0.9-1.2 eV more readily reduced than the isolated acceptor. The LUMOs and DFT EAs also suggest that the A-D-A triads, **2.8**, are more easily reduced than the D-A-D species, **2.7**, while the electrochemical data shows that the opposite is true, at least in solution. Again, solvation effects are likely to play a considerable role in accounting for this discrepancy. Indeed, adiabatic EAs computed by considering a dielectric continuum (dichloromethane, ε = 8.93) for **2.7** and **2.8** are similar (ca. –2.7 eV in both systems) and are closer to that calculated for isolated BTD in the same way (–2.37 eV). The introduction of inductively electron-donating terminal alkyl groups leads to slightly less facile reduction, both according to the electrochemical data and the DFT EA values, with the effect being larger in the **2.8** series, which confirms the BTD-localized nature of the LUMOs (see Figure 2.6).

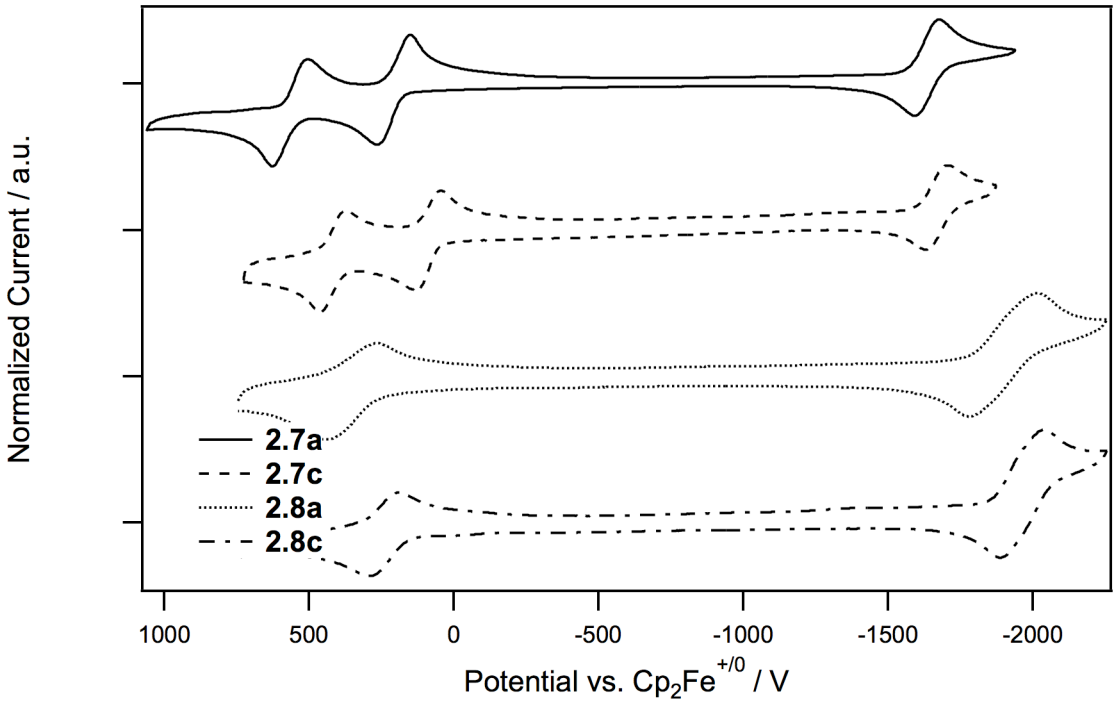

Figure 2.12. Cyclic voltammograms of **2.7a**, **2.7c**, **2.8a**, and **2.8c** in 0.1 M $^{n}Bu_4N$ PF_6 in CH_2Cl_2 recorded at a scan rate of 50 mVs^{-1}. Reported potentials are relative to ferrocenium/ferrocene ($Cp_2Fe^{+/0}$).

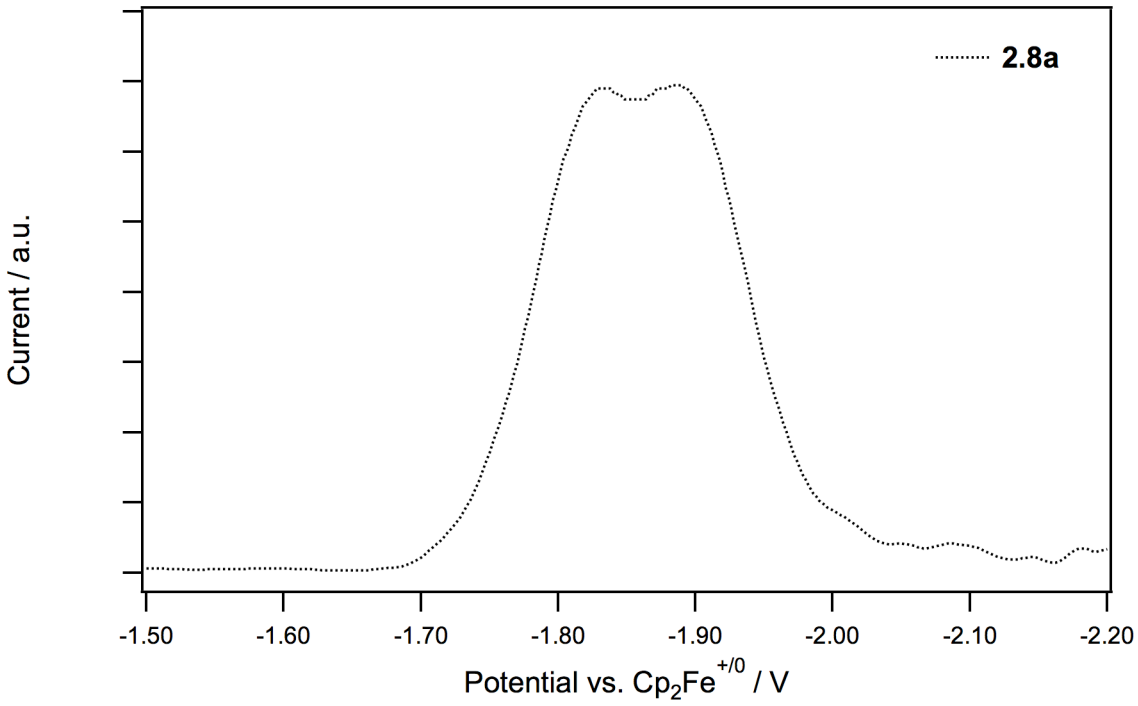

Figure 2.13. Reductive differential pulse voltammogram of **2.8a** showing two overlapping reduction processes. Reported potentials are relative to ferrocenium/ferrocene ($Cp_2Fe^{+/0}$).

Table 2.4. Electrochemical Potentials (V vs. $FeCp_2^{+/0}$),[a] Electrochemically Estimated Solid-State Ionization Potentials and Electron Affinities (eV), Estimated Electrochemical and Optical Gaps (eV), and DFT SCF Values for Ionization Potentials, Electron Affinities, and Reorganization Energies for Isolated Molecules (eV).

cmpd	Experiment							DFT					
	$E_{1/2}^{2+/+}$	$E_{1/2}^{+/0}$	$E_{1/2}^{0/-}$	IP(s)[b]	EA(s)[b]	E_{echem}[c]	E_{op}[d]	IP_{vert}[e]	IP_{adi}[e]	EA_{vert}[e]	EA_{adi}[e]	λ_h[f]	λ_e[f]
2.7a	+0.47	+0.11	–1.74	4.9	–3.1	1.9	1.9	5.70 (4.75)	5.58 (4.63)	–1.28 (–2.62)	–1.38 (–2.71)	0.259	0.194
2.7b	+0.46	+0.12	–1.74	4.9	–3.1	1.9	1.9						
2.7c	+0.34	+0.01	–1.76	4.8	–3.0	1.8	1.8	5.53 (4.64)	5.40 (4.52)	–1.22 (–2.58)	–1.32 (-2.68)	0.257	0.191
2.7d	+0.34	+0.01	–1.76	4.8	–3.0	1.8	1.8						
2.8a	g	+0.37	–1.86[h]	5.2	–2.9	2.2	2.1	6.16 (5.03)	6.06 (4.93)	–1.52 (–2.68)	–1.60 (–2.75)	0.186	0.151
2.8b	g	+0.36	–1.88[h]	5.2	–2.9	2.2	2.1						
2.8c	g	+0.28	–1.94[h]	5.1	–2.9	2.2	2.1	5.98 (4.92)	5.88 (4.82)	–1.44 (–2.60)	–1.51 (-2.67)	0.197	0.150
2.8d	g	+0.27	–1.95[h]	5.1	–2.9	2.2	2.1						
2.9	+0.49	+0.17	g	5.0	–	–	2.7	5.80 (4.82)	5.63 (4.66)	–0.34 (–1.65)	–0.52 (–1.81)	0.319	0.314
2.10	g	+0.31	g	5.1	–	–	2.9	6.13 (4.97)	5.99 (4.84)	–0.13 (–1.50)	–0.36 (–1.71)	0.268	0.407

[a]Cyclic Voltammetry in CH_2Cl_2 / 0.1 M $^nBu_4NPF_6$. [b]Estimated according to IP(s) = $eE_{1/2}^{+/0}$ + 4.8 eV and EA(s) = −($eE_{1/2}^{0/-}$ + 4.8 eV). [c]Electrochemical gap, $E_{echem} = e(E_{1/2}^{+/0} - E_{1/2}^{0/-})$. [d]Optical gap for comparison to electrochemical gap estimated from long wavelength onset of absorption in solution. [e]Gas-phase vertical and adiabatic IP / EA = SCF energy difference between the relaxed ground-state cation / anion and the ground-state neutral species (obtained for structures in which the alkyl groups are all replaced by methyl groups at the B3LYP/6-31G** level). Values in parentheses are calculated for a dielectric continuum with ε = 8.93. [f]Internal reorganization energies for $M_A^{+/-} + M_B = M_A + M_B^{+/-}$ (λ_h or λ_e for + and –, respectively) obtained as sum of the SCF energy difference between cation/anion at the neutral geometry and at cation/anion geometry and that between the neutral species at cation/anion geometry and at neutral geometry. [g]Not observed. [h]For A-D-A species, the observed feature in the cyclic voltammogram corresponds to two closely overlapping corresponding to $\mathbf{2.8}^{0/-}$ and $\mathbf{2.8}^{-/2-}$ couples.

The intramolecular reorganization energies for a self-exchange electron-transfer reaction between the neutral molecules and the corresponding radical cations and anions, λ_h and λ_e, respectively, were also calculated at the B3LYP/6-31G** level (Table 2.4). Indeed, within the framework of Marcus theory, these values are closely related to the barrier to intermolecular hole or electron transport,[73] and, therefore are critical contributors to the charge-carrier mobilities in the materials. Both λ_h and λ_e are calculated to be smallest for triads of type **2.8** and largest for the model compounds **2.9** and **2.10**. The values for **2.7** and **2.8** triads are fairly small compared with those estimated for various other charge-transport materials using similar methods; for example, λ_h values are smaller than those reported for the hole-transport materials *N,N'*-diphenyl-*N,N'*-bis(3-methylphenyl)-([1,1'-biphenyl)-4-4'-diamine, TPD, (0.29 eV)[74] and 2,2':5',2'':5'',2''':5''',2'''':5'''',2'''''-sexithiophene (0.30 eV),[75] while λ_e values are smaller than that of the electron-transport material tris(8-hydroxyquinolinato)aluminium(III), Alq3, (0.24 eV).[76] The reorganization energies are, however, larger than those calculated for certain symmetrical planar species with highly delocalized frontier orbitals such as pentacene (λ_h = 0.098 eV)[77] and 5,6,11,12,17,18-hexaazatrinaphthylene (λ_e = 0.095 eV).[78]

2.2.5 Radical-Cation Spectra

The radical cations of **2.7c**, **2.8**, **2.9**, and **2.10**, were generated in dichloromethane solution using tris(4-bromophenyl)aminium hexachloroantimonate ($E_{1/2}^{+/0}$ = 0.70 V vs. $FeCp_2^{+/0}$)[79] as an oxidant; the vis-NIR spectra of the resulting solutions are shown in Figure 2.15, 2.16 and summarized in Table 2.5. The spectra all show two conspicuous low-energy transitions consistent with what is seen for the radical

cations of other oligothiophene[80,81] and DTP[43,82] derivatives, and with the recently reported spectrum of a BTD-CPDT[38] D-A-D triad.

The vis-NIR spectra of both **2.9**$^{\bullet+}$ and **2.10**$^{\bullet+}$ show two vibronically structured bands ($\Delta\nu$ = ca. 1500 cm^{-1}). The high and low-energy bands of **2.10**$^{\bullet+}$ are bathochromically shifted by 6600 and 5100 cm^{-1} relative to those of the unsubstituted *N*-H DTP radical cation (observed in chlorobutane at 77 K);[82] this is somewhat larger than the bathochromic shifts of 2800 and 2400 cm^{-1} seen for high- and low-energy bands on terminal phenylation of terthiophene (3T) radical cations.[80,83] The vis-NIR spectrum of **2.9**$^{\bullet+}$ exhibits an additional bathochromic shift in the high and low-energy peaks of ca. 5000 and 7000 cm^{-1}, respectively, compared to **2.10**$^{\bullet+}$, which can be attributed to an increase in the conjugation length relative to **2.10**$^{\bullet+}$; for example, bathochromic shifts in the high and low-energy bands of ca. 2600 and 3500 cm^{-1} are found between 3T and 2,2':5',2'':5'',2'''-quaterthiophene (4T) radical cations.[81] Additionally, the significant hypsochromic shift in the low-energy band observed between the radical cation of 5,5'-diphenyl-2,2'-bithiophene (10700 and 26800 cm^{-1})[68] and **2.10**$^{\bullet+}$ is consistent with what is seen between the radical cations of a 2,6-dithienyl-DTP derivative and quarterthiophene analogues.[43,80,81]

The vis-NIR spectra of **2.7c**$^{\bullet+}$ and **2.8c**$^{\bullet+}$ exhibit band shapes very similar to those of **2.9**$^{\bullet+}$ and **2.10**$^{\bullet+}$, respectively, with bathochromic shifts in the high/low-energy peaks of ca. 3600/0 cm^{-1} and 3800/2600 cm^{-1}. Furthermore, the spectrum of **2.7c**$^{\bullet+}$ closely resembles that of the radical cation of a CPDT/BTD triad, for which absorption maxima of 11300 and 6500 cm^{-1} have been reported.[49]

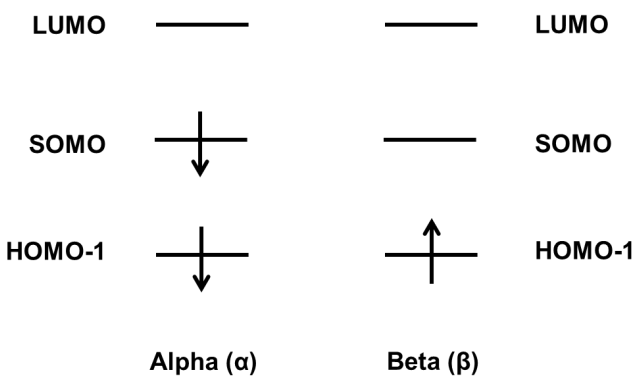

Figure 2.14. Schematic diagram representing the MO nomenclature used in the description of the vertical excited states of the radical-cations.

To gain further insight into the nature of the radical-cation excitations, TD-DFT calculations at the UB3LYP/6-31G** level were performed for **2.7c/d**$^{\bullet+}$, **2.8c/d**$^{\bullet+}$, **2.9**$^{\bullet+}$, and **2.10**$^{\bullet+}$. Note that, in discussing the configurations of the relevant states, we will refer to the SOMO (singly occupied molecular orbital) as the orbital bearing the unpaired electron so that the SOMO[α] spin orbital is the highest orbital occupied by an α spin and the SOMO[β] is vacant, with the neighboring orbitals in energy being referred to as the LUMO and HOMO–1. The cations are each calculated to exhibit two (**2.7**$^{\bullet+}$, **2.9**$^{\bullet+}$, **2.10**$^{\bullet+}$) or more (**2.8**$^{\bullet+}$) moderate to strong absorptions within the vis-NIR region (ν_{max} < 25000 cm^{-1}), with the lower energy band exhibiting smaller oscillator strengths. These features, and much of the compound-to-compound variation in transition energy, are consistent with experiment, although the transition energies are somewhat overestimated, as are the oscillator strengths for the higher energy bands. The low energy transitions of **2.7**$^{\bullet+}$ and **2.9**$^{\bullet+}$ are predominantly HOMO-1[β]→SOMO[β] in character (68 and 90%, respectively), with some SOMO[α]→LUMO[α] contribution (31 and 10%, respectively), the HOMO-1, SOMO, and LUMO closely corresponding to the HOMO–1, HOMO, and LUMO, respectively, of the neutral compounds. The transitions are qualitatively similar to HOMO-1→HOMO and HOMO→LUMO neutral ground state electronic excitations of the

neutral molecules, respectively. The strong high-energy transitions involve the same configurations, but with the SOMO[α]→LUMO[α] contribution dominating. Three one-electron excitations play and important role in both major transitions calculated for **2.8**$^{\bullet+}$ and **2.10**$^{\bullet+}$: SOMO[α]→LUMO[α], HOMO-2[β]→SOMO[β], and HOMO-1[β]→SOMO[β]. The SOMOs[α/β] essentially correspond to the HOMOs of the neutral molecules, and the HOMO–2[β] of **2.8**$^{\bullet+}$ to the HOMO–1 of **2.8**, while the HOMO-1[β] of both species and the HOMO–2[β] of **2.10**$^{\bullet+}$ do not closely resemble any of the neutral orbitals. In the case of triad **2.8**$^{\bullet+}$ an additional weak (f = 0.05) transition, again involving contributions from the same three one-electron excitations, is calculated for **2.8**$^{\bullet+}$ at 9800 cm^{-1}; this may correspond to the weak feature seen in the experimental spectrum at ca. 7000 cm^{-1}), or may overlap with the stronger low-energy transition. An additional moderately strong (f = 0.22) higher-energy transition (with a complex CI description) is also calculated for **2.8**$^{\bullet+}$ at 21200 cm^{-1} and presumably corresponds to the feature measured at ca. 22000 cm^{-1}.

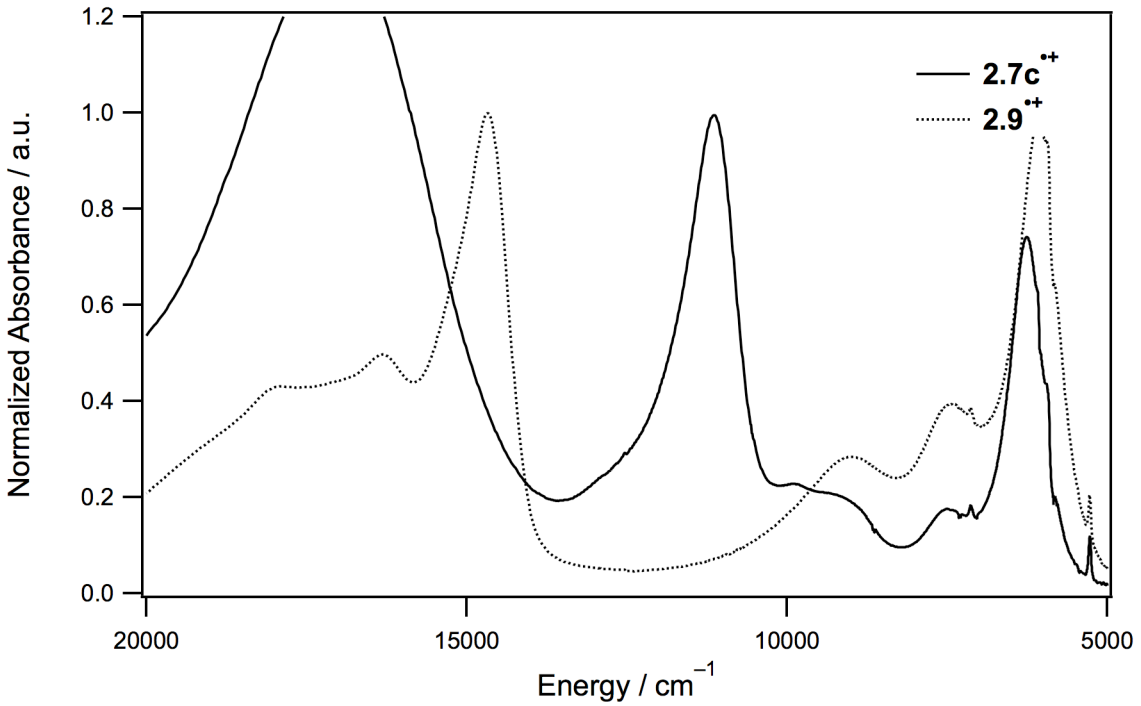

Figure 2.15. Vis-NIR absorption spectra of the radical cations of **2.7c** and **2.9** in dichloromethane. The onset of strong absorption seen at the high-energy edge of the spectrum for **2.7c**$^{\bullet+}$ is due to the presence of large excesses of the corresponding neutral species.

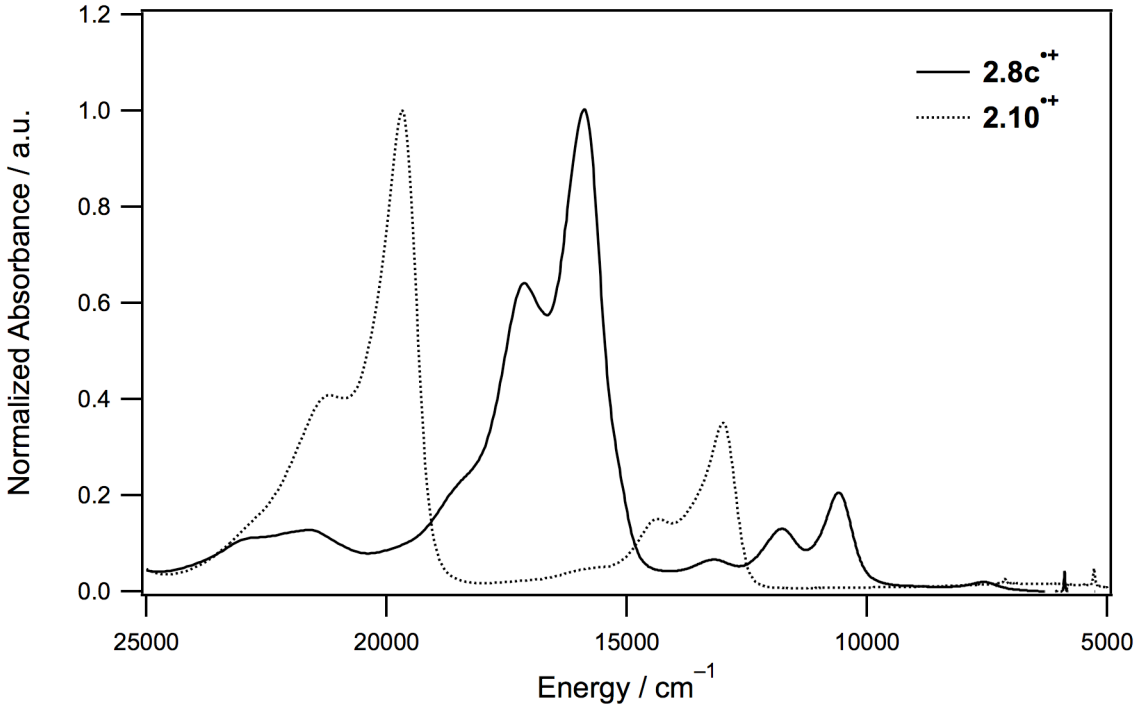

Figure 2.16. Vis-NIR absorption spectra of the radical cations of **2.8c** and **2.10** in dichloromethane.

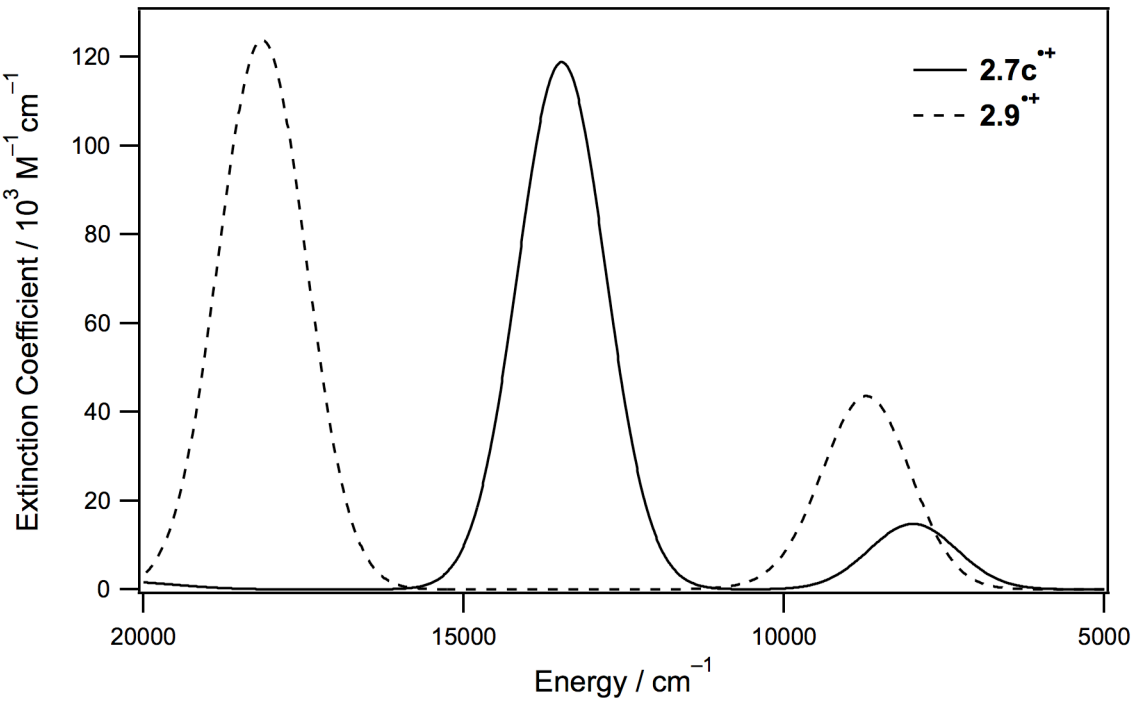

Figure 2.17. Calculated spectra of the **2.7c/d** and **2.9** radical-cation species at the TD-B3LYP/6-31G**//B3LYP/6-31G** level (obtained by applying a Gaussian broadening to the calculated oscillator strength data; full width at half maximum of 1610 cm^{-1}).

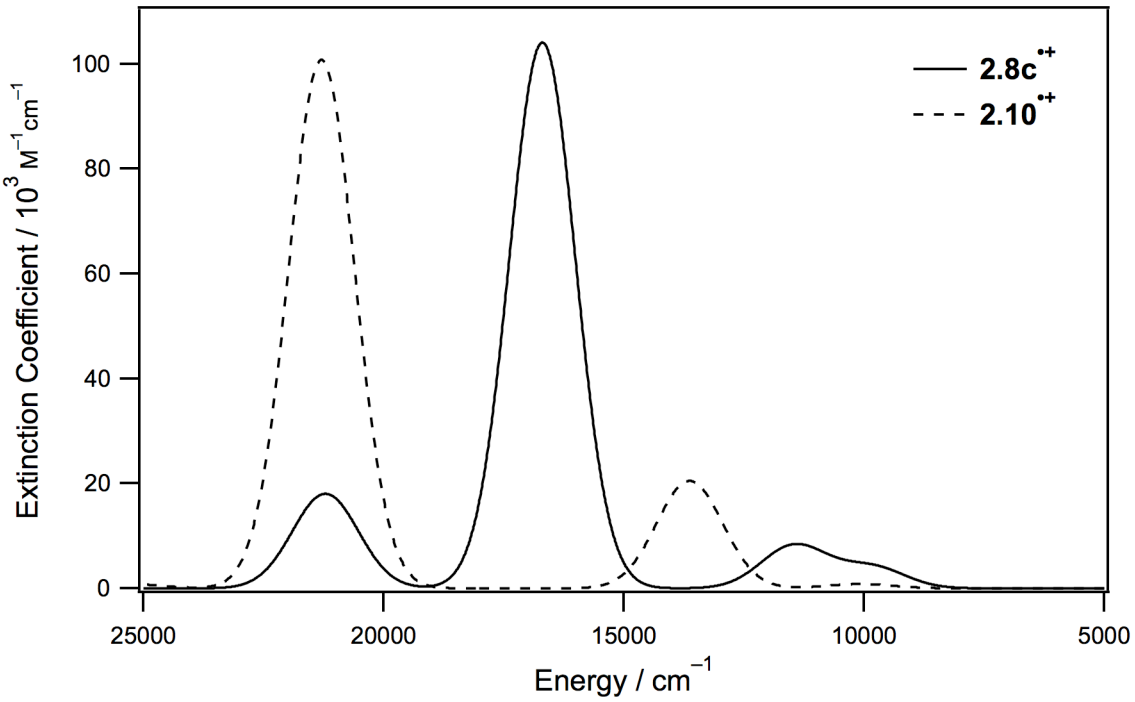

Figure 2.18. Calculated spectra of the **2.8c/d** and **2.10** radical-cation species at the TD-B3LYP/6-31G**//B3LYP/6-31G** level (obtained by applying a Gaussian broadening to the calculated oscillator strength data; full width at half maximum of 1610 cm^{-1}).

Table 2.5. Absorption Maxima, Absorptivities, and Oscillator Strengths for the Strong vis-NIR Absorptions of **2.7**-**2.10** Radical Cations in Dichloromethane along with TD-DFT Values and Assignments (in italics).[a]

cmpd	Low-Energy Band							High-Energy Band						
	$\bar{\nu}_{max}$ / 10^3 cm^{-1}		ε_{max} / 10^4	*f*		state	CI description (%)[b]	$\bar{\nu}_{max}$ / 10^3 cm^{-1}		ε_{max} / 10^4	*f*		state	CI description (%)[b]
	soln	calc	$M^{-1}cm^{-1}$	soln	calc			soln	calc	$M^{-1}cm^{-1}$	soln	calc		
2.7c$^{\bullet+}$	6.2	*8.0*	–	–	*0.18*	D_1	$S_\alpha \rightarrow L_\alpha$ (31), $H–1_\beta \rightarrow S_\beta$ (68)	11.1	*13.5*	–	–	*1.45*	D_4	$S_\alpha \rightarrow L_\alpha$ (63), $H–1_\beta \rightarrow S_\beta$ (30)
2.8c$^{\bullet+}$	10.5	*11.4*[b]	1.9	0.10	*0.10*[b]	D_2	$S_\alpha \rightarrow L_\alpha$ (21), $H–2_\beta \rightarrow H\text{-}1_\beta$ (51), $H–1_\beta \rightarrow S_\beta$ (22)	15.9	*16.7*[d]	6.0	0.58	*1.27*[d]	D_4	$S_\alpha \rightarrow L_\alpha$ (55), $H–2_\beta \rightarrow S_\beta$ (6), $H–1_\beta \rightarrow S_\beta$ (23)
2.9$^{\bullet+}$	6.1	*8.7*	6.0	0.54	*0.53*	D_1	$S_\alpha \rightarrow L_\alpha$ (10), $H–1_\beta \rightarrow S_\beta$ (90)	14.7	*18.1*	6.1	0.88	*1.51*	D_5	$S_\alpha \rightarrow L_\alpha$ (82), $H–1_\beta \rightarrow S_\beta$(11)
2.10$^{\bullet+}$	13.1	*13.6*	2.1	0.15	*0.25*	D_2	$S_\alpha \rightarrow L_\alpha$(16), $H–2_\beta \rightarrow H\text{-}1_\beta$ (58), $H–1_\beta \rightarrow S_\beta$ (23)	19.7	*21.3*	6.1	0.49	*1.23*	D_7	$S_\alpha \rightarrow L_\alpha$ (76), $H–2_\beta \rightarrow H\text{-}1_\beta$ (9), $H–1_\beta \rightarrow S_\beta$ (7)

[a]TD-DFT Values obtained for structures in which the alkyl groups are all replaced by methyl groups at the B3LYP/6-31G** level. The two transitions reported are those seen and/or calculated at $\bar{\nu}_{max} < 25\,000$ cm^{-1} and calculated to have $f \geq 0.05$. [b]H, S, and L denote HOMO, SOMO, and LUMO, respectively. [c]Excitation to D_1 is calculated at 9800 cm^{-1} (f = 0.05) with CI description: S[α]→L[α] (5), H–2[β]→H-1[β] (41), H–1[β]→S[β] (52). [d]Excitation to D_9 is calculated at 21200 cm^{-1} (f = 0.22) with CI description: S[α]→L[α] (11), S[α]→L+2[α] (12), H–3[β]→L[β] (11), H–1[β]→L+1[β] (21).

2.2.6 OFET Behavior

The electrical properties of the triads were investigated by fabricating and testing field-effect transistor devices using solution-processing techniques. Bottom-gate, top-contact geometry devices were fabricated on heavily n-doped silicon substrates, which also serve as the gate electrodes, with 200 nm thick thermally grown SiO_2 as the gate dielectric and gold source and drain electrodes (Figure 2.19). No n-channel behavior was detected, which is not very surprising given the moderate solid-state electron affinities estimated for these materials (see Table 2.4) and the use of gold electrodes. However, as shown in Table 2.6, several of the triads exhibited p-channel behavior with moderate mobility values and on / off current ratios, the variation presumably being related to differences in packing and film morphology. Interestingly, the two species showing the highest mobility values and that are most easily turned on (**2.7a** and **2.7b**) are those that DSC studies suggest form amorphous films. While falling short of the best values achieved for solution-processed small-molecule oligothiophenes (up to 0.1 $cm^2V^{-1}s^{-1}$)[75-77] and for DTP-based small molecules (up to 0.01 $cm^2V^{-1}s^{-1}$),[84] the mobility values are similar to the best achieved for related compounds such as the BTD/bithiophene triads studied by Sonar *et al.*[50,58]

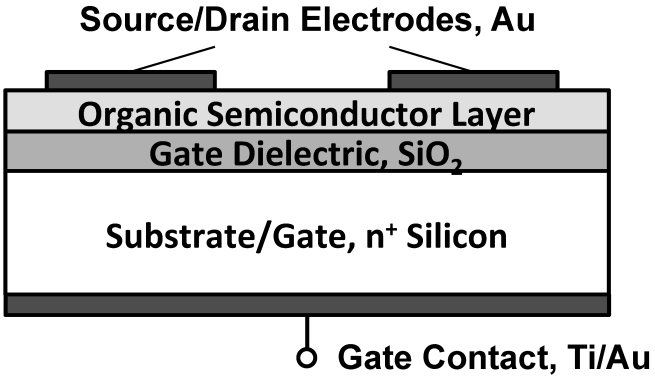

Figure 2.19. p-Channel field-effect transistor device geometry.

Table 2.6. Saturation Hole Mobility Values, Threshold Voltages, and Current On / Off Ratios for OFETs Based on DTP-BTD Triads.[a]

cmpd	μ_h[a] / $cm^2V^{-1}s^{-1}$	V_{TH} / V	I_{on} / I_{off}
2.7a	1.0 (± 0.2) × 10^{-3}	7.9 (± 2.0)	1 × 10^2
2.7b	5.9 (± 1.9) × 10^{-3}	9.5 (± 3.3)	1 × 10^3
2.7c	2.2 (± 0.1) × 10^{-4}	0.2 (± 0.8)	3 × 10^3
2.7d	2.5 (± 0.2) × 10^{-4}	–0.7 (± 1.4)	4 × 10^3
2.8a	b	b	b
2.8b	6.6 (± 1.6) × 10^{-5}	–11.0 (± 4.4)	2 × 10^2
2.8c	b	b	b
2.8d	b	b	b

[a]Average values are calculated based on 3 to 6 devices with W = 1200 and L = 100 μm from a single substrate. [b]No measurable OFET behavior.

2.2.7 Summary

D-A-D and A-D-A triads based on DTP donors and BTD acceptors have been synthesized, characterized using UV-vis. absorption and electrochemistry, and studied using (TD)DFT calculations. The HOMOs are delocalized over both DTP and BTD units, resembling those of model compounds in which benzene rings replace the BTD moieties and those of oligothiophenes, the local HOMO of the BTD building block being sufficiently high in energy for effective overlap with the DTP HOMO. On the other hand, the LUMOs are largely localized on the BTD groups. Accordingly, some properties – such as the low-energy absorptions of the neutral species, where HOMO-to-LUMO excitation is accompanied by significant DTP-to-BTD charge transfer – resemble those of other donor-acceptor systems, whereas other properties – such as the low-energy absorptions of the radical cations, where the excitation occurs predominantly from a delocalized filled orbital to the delocalized SOMO (corresponding to the HOMO of the

neutral molecule) – resemble those of other more delocalized systems, such as the benzene-containing model compounds and oligothiophenes.

Some of the triads exhibit moderate average hole mobility values (up to 5.9×10^{-3} $cm^2V^{-1}s^{-1}$) in OFETs. While higher mobility values have been observed in solution-processed p-channel OFETs based on other materials, the present values, coupled with the low-energy absorptions exhibited by the triads, do suggest possible use as donor materials for photovoltaic applications.[85]

2.3 Experimental

Experimental details describing the general synthesis and characterization methods, computational methodology, and fabrication of thin-film transistors can be found in Appendix A, C and D, respectively. Quantum chemical calculations included in this chapter were performed by Laxman Pandey under the guidance of Dr. Chad Risko in Prof. Jean-Luc Brédas' research group in the School of Chemistry and Biochemistry at Georgia Institute of Technology. Transistor fabrication and measurements included in this chapter were performed by Dr. Shree Prakash Tiwari in Prof. Bernard Kippelen's research group in the School of Electrical and Computer Engineering at Georgia Institute of Technology.

2.3.1 Synthetic Procedures

4-Bromo-7-hexylbenzo[*c*][1,2,5]thiadiazole, 2.4. A solution of hexylmagnesium bromide (9.66 g, 0.051 mol) in dry diethyl ether (25mL, 2 M) was added to a solution of zinc chloride (6.18 g, 0.061 mol) in dry THF (60 mL, 1 M) at 0 ºC and the mixture was stirred for 1 h at room temperature. The resultant hexylzinc chloride solution was added to a mixture of 4,7-dibromobenzo[*c*][1,2,5]thiadiazole (15.0 g, 0.051 mol),

tetrakis(triphenylphosphine) palladium (0.295 g, 0.255 mmol), and dry THF (25 mL) at 0 ºC. The reaction mixture was allowed to stir 2 d after which an additional aliquot of hexylzinc chloride (9.49 g, 0.025 mol) was added and the mixture was stirred at room temperature for 20 h while being monitored by GCMS. Upon completion, the reaction mixture was diluted with dichloromethane, washed with saturated aqueous ammonium chloride solution, and dried over anhydrous sodium sulfate. The combined organic washes were filtered through a plug of Celite and the filtrate was concentrated via rotary evaporation. The crude product was purified by flash chromatography (silica gel, 1:1 hexanes:toluene). The solvent was removed under reduced pressure. The product was further purified by bulb-to-bulb distillation at 135 ºC / 0.05 Torr (4.03 g, 0.013 mmol, 26%). ^{1}H NMR (400 MHz, $CDCl_3$) δ 7.72 (d, J = 7.6 Hz, 1H), 7.21 (d, *J* = 7.6 Hz, 1H), 3.05 (t, *J* = 7.6 Hz, 2H), 1.75 (quint., *J* = 7.6 Hz, 2H), 1.39-1.28 (m, 6H), 0.86 (t, *J* = 7.0 Hz, 3H). $^{13}C\{^{1}H\}$ NMR (100 MHz, $CDCl_3$) δ 154.7, 153.4, 136.0, 132.0, 127.8, 111.1, 32.0, 31.6, 29.6, 29.1, 22.6, 14.1. HRMS (EI): *m/z* calcd for $C_{12}H_{15}BrN_2S$ (M^+): 298.0139; found: 298.0163. Anal. Calcd. for $C_{12}H_{15}BrN_2S$: C, 48.17; H, 5.05; N, 9.36. Found: C, 48.30; H, 5.08; N, 9.54.

1-(3,3'-Dibromo-2,2'-bithiophen-5-yl)hexan-1-one, 2.5'. In a dry flask, a mixture of 3,3'-dibromo-2,2'-bithiophene (15.0 g, 46.3 mmol) and aluminum trichloride (7.41 g, 55.6 mmol) was purged with nitrogen. After 20 min, dry dichloromethane (460 mL) was added and the solution was cooled to 0 °C before hexanoyl chloride (7.48 g, 55.6 mmol) was added dropwise over 5 min The mixture was allowed to stir at room temperature for 3 h. Upon completion, the reaction mixture was quenched with water, extracted with dichloromethane, and dried over anhydrous sodium sulfate. The combined dichloromethane washes were concentrated via rotary evaporation and the crude product was purified by flash chromatography (silica gel, 1:1 hexanes:dichloromethane). The solvent was removed under reduced pressure. The

product was collected as a yellow oil (17.3 g, 41.0 mmol, 89%). ^{1}H NMR (400 MHz, $CDCl_3$) δ 7.62 (s, 1H), 7.44 (d, J = 5.4 Hz, 1H), 7.09 (d, J = 5.4 Hz, 1H), 2.85 (t, J = 7.4 Hz, 2H), 1.74 (p, J = 7.3 Hz, 2H), 1.35 (m, 4H), 0.90 (t, J = 7.0, 3H). ^{13}C{^{1}H} NMR (100 MHz, $CDCl_3$) δ 192.4, 143.8, 136.7, 134.4, 131.2, 128.2, 128.1, 113.0, 112.4, 39.0, 31.4, 24.2, 22.4, 13.9. HRMS (EI): *m/z* calcd for $C_{14}H_{14}Br_2OS_2$ (M^+): 419.8853; found: 418.8859. Anal. Calcd. for $C_{14}H_{14}Br_2OS_2$: C, 39.83; H, 3.34. Found: C, 39.94; H, 3.26.

3,3'-Dibromo-5-hexyl-2,2'-bithiophene, 2.5". In a dry flask, aluminum trichloride (11.9 g, 89.5 mmol) was added slowly to a solution of sodium borohydride (5.66 g, 0.149 mol) in dry THF (300 mL). A solution of 1-(3,3'-dibromo-2,2'-bithiophen-5-yl)hexan-1-one (12.6 g, 29.8 mmol) in dry THF (10 mL) was added and the mixture was allowed to stir at reflux for 20 h. Upon completion, the reaction mixture was quenched with cold water, extracted with ethyl acetate, and dried over anhydrous sodium sulfate. The combined ethyl acetate washes were concentrated via rotary evaporation and the crude product was purified by flash chromatography (silica gel, hexanes). The solvent was removed under reduced pressure. The product was collected as a yellow oil (7.31 g, 17.9 mmol, 60%). ^{1}H NMR (500 MHz, $CDCl_3$) δ 7.35 (d, J = 5.5 Hz, 1H), 7.04 (d, J = 5.5 Hz, 1H), 6.75 (d, J = 5.5 Hz, 1H), 2.77 (t, J = 7.8 Hz, 2H), 1.67 (p, J = 7.7 Hz, 2H), 1.39-1.24 (m, 6H), 0.89 (t, J = 6.8, 3H). ^{13}C{^{1}H} NMR (125 MHz, $CDCl_3$) δ 147.95, 130.70, 129.51, 127.63, 127.10, 125.84, 112.15, 111.47, 31.47, 31.03, 30.19, 28.71, 22.52, 14.05. HRMS (EI) *m/z* calcd for $C_{14}H_{16}Br_2S_2$ (M^+): 405.9060; found: 405.9065.

2,4-Dihexyl-4*H*-dithieno[3,2-*b*:2',3'-*d*]pyrrole, 2.6c. A solution of 3,3'-dibromo-5-hexyl-2,2'-bithiophene (5.00 g, 12.3 mmol), sodium *tert*-butoxide (3.53 g, 36.7 mmol), tris(dibenzylideneacetone) dipalladium ($Pd_2(dba)_3$) (0.280 g, 0.306 mmol), and BINAP (0.763 g, 1.23 mmol) in dry toluene (25 mL) was purged with nitrogen. After 20 min, 1-hexylamine (1.24 g, 12.3 mmol) was added and the mixture was stirred for 8 h at 120 °C. After cooling, the reaction mixture was filtered through silica gel eluting with 2% ethyl

acetate in hexanes. The crude product was purified by flash chromatography (silica gel, 1:5 dichloromethane in hexanes). The solvent was removed under reduced pressure. The product was collected as a yellow oil (3.64 g, 10.5 mmol, 85%). ^{1}H NMR (400 MHz, $CDCl_3$) δ 7.03 (d, J = 5.3 Hz, 1H), 6.95 (d, J = 5.3 Hz, 1H), 6.69 (s, 1H), 4.12 (t, J = 7.1 Hz, 2H), 2.86 (t, J = 7.6 Hz, 2H), 1.82 (p, J = 7.2 Hz, 2H), 1.71 (p, J = 7.5 Hz, 2H), 1.42-1.22 (m, 12H), 0.88 (t, J = 7.0, 3H), 0.85 (t, J = 7.1 Hz, 3H). ^{13}C{^{1}H} NMR (100 MHz, $CDCl_3$) δ 144.17, 144.04, 143.50, 121.56, 114.84, 112.20, 110.85, 108.26, 47.31, 31.74, 31.60, 31.49, 31.42, 30.36, 28.76, 26.66, 22.59, 22.51, 14.09, 14.00. HRMS (EI): *m/z* calcd for $C_{20}H_{29}NS_2$ (M^+): 347.1741; found: 347.1734. Anal. Calcd. for $C_{20}H_{29}NS_2$: C, 69.11; H, 8.41; N, 4.03. Found: C, 69.15; H, 8.52; N, 4.02.

4-Dodecyl-2-hexyl-4*H*-dithieno[3,2-*b*:2',3'-*d*]pyrrole, 2.6d. A solution of 3,3'-dibromo-5-hexyl-2,2'-bithiophene (4.00 g, 9.80 mmol), sodium *tert*-butoxide (2.83 g, 29.4 mmol), tris(dibenzylideneacetone) dipalladium ($Pd_2(dba)_3$) (0.224 g, 0.245 mmol), and BINAP (0.610 g, 0.980 mmol) in dry toluene (20 mL) was purged with nitrogen. After 20 min 1-dodecylamine (1.82 g, 9.80 mmol) was added and the mixture was stirred for 12 h at 120 °C. After cooling, the reaction mixture was filtered through silica gel eluting with 2% ethyl acetate in hexanes. The crude product was purified by flash chromatography (silica gel, 10% dichloromethane in hexanes). The solvent was removed under reduced pressure. The product was collected as a yellow oil (1.45 g, 3.36 mmol, 34%). ^{1}H NMR (400 MHz, $CDCl_3$) δ 7.03 (d, J = 5.3 Hz, 1H), 6.95 (d, J = 5.3 Hz, 1H), 6.69 (s, 1H), 4.11 (t, J = 7.1 Hz, 2H), 2.85 (t, J = 7.4 Hz, 2H), 1.82 (p, J = 7.0 Hz, 2H), 1.70 (p, J = 7.5 Hz, 2H), 1.40-1.22 (m, 24H), 0.88 (t, J = 7.0, 3H), 0.86 (t, J = 7.0 Hz, 3H). ^{13}C{^{1}H} NMR (100 MHz, $CDCl_3$) δ 144.17, 144.04, 143.49, 121.55, 114.84, 112.19, 110.85, 108.26, 47.30, 31.90, 31.74, 31.60, 31.49, 30.38, 29.60, 29.57, 29.47, 29.44, 29.33, 29.24, 28.77, 26.99, 22.68, 22.59, 14.11, 14.09. HRMS (EI): *m/z* calcd for $C_{26}H_{41}NS_2$ (M^+): 431.2680;

found: 431.2693. Anal. Calcd. for $C_{26}H_{41}NS_2$: C, 72.33; H, 9.57; N, 3.24. Found: C, 72.45; H, 9.72;N, 3.27.

General procedure for D-A-D Triads, 2.7, and 2.9. A 0.1 M solution of the appropriate DTP **2.6** (1 eq.) in dry THF was cooled to –78 ºC under nitrogen. After 20 min, *tert*-butyllithium (1 eq.) was added dropwise and the mixture was stirred for 2.5 h at –78 °C. Tributyltin chloride (1 eq.) was added dropwise and the mixture was allowed to warm to room temperature and stir for 1 h. This solution was transferred into a separate flask containing *trans*-dichlorobis(triphenylphosphine)palladium (5 mol%) and a 0.1 M solution of **2.3** (0.45 eq.) in dry THF; the resulting solution was heated to reflux for 19 h. After cooling, the reaction mixture was quenched with water, extracted with diethyl ether, and dried over anhydrous sodium sulfate. The combined ether washes were concentrated via rotary evaporation.

4,7-Bis(4-hexyl-4*H*-dithieno[3,2-*b*:2',3'-*d*]pyrrol-2-yl)benzo[*c*][1,2,5]thiadiazole, 2.7a. The crude product was purified by flash chromatography (silica gel, 1:1 hexanes:toluene). The product was recrystallized from isopropanol and collected as a dark purple solid (1.29 g, 3.44 mmol, 38%). ^{1}H NMR (400 MHz, $CDCl_3$) δ 8.18 (s, 2H), 7.66 (s, 2H), 7.15 (d, J = 5.3 Hz, 2H), 6.93 (d, J = 5.3 Hz, 2H), 4.12 (t, J = 7.0 Hz, 4H), 1.86 (p, J = 7.1 Hz, 4H), 1.36-1.23 (m, 12H), 0.86 (t, J = 7.0 Hz, 6H). ^{13}C{^{1}H} NMR (100 MHz, $CDCl_3$) δ 152.41, 145.70, 145.63, 136.84, 126.05, 124.25, 123.90, 115.12, 114.83, 112.04, 110.90, 47.19, 31.41, 30.34, 26.65, 22.52, 14.05. HRMS (EI): *m/z* calcd for $C_{34}H_{34}N_4S_5$ (M^+): 658.1387; found: 658.1361. Anal. Calcd. for $C_{34}H_{34}N_4S_5$: C, 61.97; H, 5.20; N, 8.50. Found: C, 61.77; H, 5.13; N, 8.44.

4,7-Bis(4-dodecyl-4*H*-dithieno[3,2-*b*:2',3'-*d*]pyrrol-2-yl)benzo[*c*][1,2,5]thiadiazole, 2.7b. The crude product was purified by flash chromatography (silica gel, 4:1 hexanes:toluene then 2:1 hexanes:toluene). The product was recrystallized from isopropanol and collected as a dark purple solid (0.580 g, 0.920

mmol, 37%). ^{1}H NMR (400 MHz, $CDCl_3$) δ 8.27 (s, 2H), 7.80 (s, 2H), 7.17 (d, J = 5.3 Hz, 2H), 6.99 (d, J = 5.3 Hz, 2H), 4.23 (t, J = 7.0 Hz, 4H), 1.91 (p, J = 6.8 Hz, 4H), 1.27 (m, 36H), 0.84 (t, J = 6.8 Hz, 6H). ^{13}C{^{1}H} NMR (100 MHz, $CDCl_3$) δ 152.9, 146.1, 146.0, 137.2, 126.6, 124.9, 124.4, 115.6, 115.2, 112.4, 111.2, 47.6, 32.2, 30.7, 30.0, 29.9, 29.9, 29.8, 29.6, 29.5, 27.3, 23.0, 14.4. HRMS (FAB): *m/z* calcd for $C_{46}H_{58}N_4S_5$ (M^+): 826.3265; found: 826.3288. Anal. Calcd. for $C_{46}H_{58}N_4S_5$: C, 66.78; H, 7.07; N, 6.77. Found: C, 66.92; H, 7.04; N, 6.70.

4,7-Bis(2,4-dihexyl-4*H*-dithieno[3,2-*b*:2',3'-*d*]pyrrol-2-yl)benzo[*c*][1,2,5]thiadiazole, 2.7c. The crude product was purified by flash chromatography (silica gel, 4:1 hexanes:toluene then 1:1 hexanes:toluene). The product was recrystallized from isopropanol and collected as a dark purple solid (0.659 g, 0.796 mmol, 26%). ^{1}H NMR (400 MHz, $CDCl_3$) δ 8.18 (s, 2H), 7.67 (s, 2H), 6.67 (s, 2H), 4.11 (t, J = 7.1 Hz, 4H), 2.87 (t, J = 7.6 Hz, 4H), 1.86 (p, J = 7.1 Hz, 4H), 1.73 (p, J = 7.5 Hz, 4H), 1.45-1.19 (m, 24H), 0.90 (t, J = 7.0 Hz, 6H), 0.87 (t, J = 7.1 Hz, 6H). ^{13}C{^{1}H} NMR (100 MHz, $CDCl_3$) δ 152.51, 145.61, 144.93, 144.42, 135.89, 125.99, 124.06, 115.52, 112.61, 111.91, 108.25, 47.15, 31.68, 31.65, 31.62, 31.43, 30.38, 28.84, 26.67, 22.61, 22.55, 14.11, 14.06. HRMS (EI): *m/z* calcd for $C_{46}H_{58}N_4S_5$ (M^+): 826.3265; found: 826.3288. Anal. Calcd. for $C_{46}H_{58}N_4S_5$: C, 66.78; H, 7.07; N, 6.77. Found: C, 66.82; H, 7.10; N, 6.69.

4,7-Bis(4-dodecyl-2-hexyl-4*H*-dithieno[3,2-*b*:2',3'-*d*]pyrrol-2-yl)benzo[*c*][1,2,5]thiadiazole, 2.7d. The crude product was purified by flash chromatography (silica gel, 4:1 hexanes:toluene then 2:1 hexanes:toluene). The product was recrystallized from isopropanol and collected as a dark purple solid (0.568 g, 0.571 mmol, 38%). ^{1}H NMR (400 MHz, $CDCl_3$) δ 8.20 (s, 2H), 7.69 (s, 2H), 6.67 (s, 2H), 4.13 (t, J = 6.9 Hz, 4H), 2.87 (t, J = 7.6 Hz, 4H), 1.87 (quint., J = 6.7 Hz, 4H), 1.73 (p, J = 7.5 Hz, 4H), 1.41-1.22 (m, 48H), 0.90 (t, J = 6.9 Hz, 6H), 0.85 (t, J = 6.8 Hz, 6H). ^{13}C{^{1}H}

NMR (100 MHz, $CDCl_3$) δ 152.56, 145.65, 144.94, 144.44, 135.90, 126.05, 124.13, 115.56, 112.63, 111.94, 108.26, 47.17, 31.90, 31.67, 31.66, 31.62, 30.40, 29.64, 29.62, 29.52, 29.33, 29.24, 28.85, 26.98, 22.68, 22.61, 14.11 (two alkyl carbon resonances not observed, presumably due to overlap). HRMS (EI): *m/z* calcd for $C_{58}H_{82}N_4S_5$ (M^+): 994.5143; found: 994.5273. Anal. Calcd. for $C_{58}H_{82}N_4S_5$: C, 69.97; H, 8.30; N, 5.63. Found: C, 69.84; H, 8.40; N, 5.57.

1,4-Bis(4-hexyl-4*H*-dithieno[3,2-*b*:2',3'-*d*]pyrrol-2-yl)benzene, **2.9**. The crude product was purified by flash chromatography (silica gel, 5:2 hexanes / CH_2Cl_2). The product was recrystallized from isopropanol and collected as small, yellow-orange needles. (0.240 g, 0.399 mmol, 47%). ^{1}H NMR (400 MHz, $CDCl_3$) δ 7.63 (s, 4H), 7.25 (s, 2H), 7.13 (d, *J* = 5.3 Hz, 2H), 6.98 (d, *J* = 5.3 Hz, 2H), 4.18 (t, *J* = 7.1 Hz, 4H), 1.88 (quint., *J* = 7.1 Hz, 4H), 1.40-1.20 (m, 12H), 0.86 (t, *J* = 7.1 Hz, 6H). ^{13}C{^{1}H} NMR (100 MHz, $CDCl_3$) δ 145.23, 144.82, 141.03, 134.27, 125.57, 123.24, 114.94, 114.22, 110.86, 106.77, 47.38, 31.41, 30.35, 26.67, 22.50, 14.00 (one aromatic carbon resonance not observed, presumably due to overlap). HRMS (EI): *m/z* calcd for $C_{34}H_{36}N_2S_4$ (M^+): 600.1761; found: 600.1754. Anal. Calcd. for $C_{34}H_{36}N_2S_4$: C, 67.96; H, 6.04; N, 4.66. Found: C, 68.00; H, 6.04; N, 4.70.

General procedure for A-D-A triads, 2.8, and 2.10. A 0.1 M solution of the appropriate DTP **2.6** (1 eq.) in dry THF was cooled to –78 ºC under nitrogen. After 20 min, *tert*-butyllithium (2 eq.) was added dropwise and the mixture was stirred for 1 h at –78 °C. The reaction was warmed to room temperature for 10 min before returning to –78 ºC. Tributyltin chloride (2.5 eq.) was added dropwise and the mixture was allowed to warm to room temperature and stir for 3 h. The solution was then transferred into a 0.1 M THF solution of the appropriate BTD derivative **2.2** or **2.4** (2.2 eq.) also containing *trans*-dichlorobis(triphenylphosphine)palladium; the mixture was heated to reflux for 19 h. After cooling, the reaction mixture was quenched with water, extracted with diethyl

ether, and dried over anhydrous sodium sulfate. The combined ether washes were concentrated via rotary evaporation.

2,6-Di(benzo[*c*][1,2,5]thiadiazol-4-yl)-4-hexyl-4*H*-dithieno[3,2-*b*:2',3'-*d*]pyrrole, 2.8a. The crude product was purified by flash chromatography (silica gel, chloroform). The product was recrystallized from 1:1 isopropanol / ethylacetate and collected as a dark red solid with a minor impurity (2.05 g, 3.86 mmol, 68%). A sample of the product (500 mg, 0.940 mmol) was purified by sublimation (85.4 mg, 0.161 mmol, 17%) and was used for electronic characterization. ^{1}H NMR (400 MHz, $CDCl_3$) δ 8.32 (s, 2H), 7.86 (d, J = 8.4 Hz, 2H), 7.83 (d, *J* = 6.8 Hz, 2H), 7.59 (dd, *J* = 8.6, 7.4 Hz, 2H), 4.34 (t, *J* = 6.8 Hz, 2H), 2.00 (quint., *J* = 7.2 Hz, 2H), 1.46-1.27 (m, 6H), 0.88 (t, *J* = 7.0 Hz, 3H). ^{13}C{^{1}H} NMR (100 MHz, $CDCl_3$) δ 155.7, 152.0, 146.4, 137.8, 129.7, 128.7, 124.2, 119.3, 115.6, 112.7, 47.4, 31.4, 30.4, 26.7, 22.5, 14.1. HRMS (EI): *m/z* calcd for $C_{26}H_{21}N_5S_4$ (M^+): 531.0680; found: 531.0658. Anal. Calcd. for $C_{26}H_{21}N_5S_4$: C, 58.79; H, 3.98; N, 13.17. Found: C, 58.67; H, 3.92; N, 13.14

2,6-Di(benzo[*c*][1,2,5]thiadiazol-4-yl)-4-dodecyl-4*H*-dithieno[3,2-*b*:2',3'-*d*]pyrrole, **2.8b.** The crude product was purified by flash chromatography (silica gel, 2:1 chloroform:hexanes). The solvent was removed under reduced pressure. The product was recrystallized from isopropanol and collected as a dark red solid with a minor impurity (1.53 g, 2.48 mmol, 49%). A sample of the product (1.20 g, 1.95 mmol) was purified by sublimation (0.374 g, 6.49 mmol, 31%) and used for electronic characterization. ^{1}H NMR (400 MHz, $CDCl_3$) δ 8.29 (s, 2H), 7.83 (d, J = 8.8 Hz, 2H), 7.80 (d, *J* = 7.2 Hz, 2H), 7.57 (dd, *J* = 8.4, 7.2 Hz, 2H), 4.34 (t, *J* = 7.2 Hz, 2H), 1.98 (quint., *J* = 7.2 Hz, 2H), 1.42-1.32 (m, 4H), 1.30-1.10 (m, 14H), 0.82 (t, *J* = 7.0 Hz, 3H). ^{13}C{^{1}H} NMR (100 MHz, $CDCl_3$) δ 155.70, 155.96, 146.35, 137.77, 129.71, 128.64, 124.21, 119.32, 115.54, 112.69, 47.34, 31.85, 30.39, 29.59, 29.47, 29.28, 29.22, 26.94, 22.63, 14.08 (two alkyl carbon resonances not observed, presumably due to overlap). HRMS

(EI): *m/z* calcd for $C_{32}H_{33}N_5S_4$ (M^+): 615.1619; found: 615.1629. Anal. Calcd. for $C_{32}H_{33}N_5S_4$: C, 62.40; H, 5.40; N, 11.37. Found: C, 62.40; H, 5.29; N, 11.51.

4-Hexyl-2,6-bis(7-hexylbenzo[*c*][1,2,5]thiadiazol-4-yl)-4*H*-dithieno[3,2-*b*:2',3'-*d*]pyrrole, 2.8c. The crude product was purified by flash chromatography (silica gel, 1:2 toluene:hexanes). The product was recrystallized from isopropanol with a small amount of chloroform and collected as a dark purple solid (0.818 g, 0.117 mmol, 56%). ^{1}H NMR (400 MHz, $CDCl_3$) δ 8.25 (s, 2H), 7.76 (d, *J* = 7.2 Hz, 2H), 7.35 (d, *J* = 7.3 Hz, 2H), 4.35 (t, *J* = 7.0 Hz, 2H), 3.11 (t, *J* = 7.6 Hz, 4H), 1.98 (quint., *J* = 7.2 Hz, 2H), 1.80 (quint., *J* = 7.6 Hz, 4H), 1.44-1.26 (m, 18H), 0.88 (t, *J* = 7.0 Hz, 6H), 0.86 (t, *J* = 7.3 Hz, 3H). ^{13}C{^{1}H} NMR (100 MHz, $CDCl_3$) δ 155.68, 152.25, 146.14, 137.98, 134.46, 127.64, 126.24, 124.72, 115.03, 11.86, 47.36, 32.27, 31.70, 31.45, 30.43, 29.73, 29.24, 26.68, 22.63, 22.55, 14.11, 14.07. HRMS (EI): *m/z* calcd for $C_{38}H_{45}N_5S_4$ (M^+): 699.2558; found: 699.2584. Anal. Calcd. for $C_{38}H_{45}N_5S_4$: C, 65.20; H, 6.48; N, 10.00. Found: C, 64.93; H, 6.53; N, 10.01.

4-Dodecyl-2,6-bis(7-hexylbenzo[*c*][1,2,5]thiadiazol-4-yl)-4*H*-dithieno[3,2-*b*:2',3'-*d*]pyrrole, 2.8d. The crude product was purified by flash chromatography (silica gel, 2:1 hexanes:chloroform). The product was recrystallized from isopropanol with a small amount of chloroform and collected as a dark purple solid (0.763 g, 0.972 mmol, 52%). ^{1}H NMR (400 MHz, $CDCl_3$) δ 8.22 (s, 2H), 7.73 (d, *J* = 7.2 Hz, 2H), 7.32 (d, *J* = 7.3 Hz, 2H), 4.31 (t, *J* = 6.9 Hz, 2H), 3.10 (t, *J* = 7.6 Hz, 4H), 1.96 (quint., *J* = 7.0 Hz, 2H), 1.79 (quint., *J* = 7.6 Hz, 4H), 1.42-1.18 (m, 32H), 0.88 (t, *J* = 7.0 Hz, 6H), 0.83 (t, *J* = 7.0 Hz, 3H). ^{13}C{^{1}H} NMR (100 MHz, $CDCl_3$) δ 155.64, 152.20, 146.13, 137.94, 134.38, 127.59, 126.22, 124.63, 114.99, 111.86, 47.29, 32.25, 31.87, 31.70, 30.40, 29.70, 29.61, 29.59, 29.49, 29.29, 29.25, 26.95, 22.64, 14.10 (four alkyl carbon resonances not observed, presumably due to overlap). HRMS (EI): *m/z* calcd for

$C_{44}H_{57}N_5S_4$ (M^+): 783.3968; found: 783.3467. Anal. Calcd. for $C_{44}H_{57}N_5S_4$: C, 67.39; H, 7.33; N, 8.93. Found: C, 67.36; H, 7.34; N, 8.90.

4-Hexyl-2,6-diphenyl-4*H*-dithieno[3,2-*b*:2',3'-*d*]pyrrole, 2.10. The crude product was purified by flash chromatography (silica gel, 5:1 hexanes:dichloromethane). The product was recrystallized from isopropanol and collected as small, yellow-orange needles. (0.246 g, 0.592 mmol, 50%). ^{1}H NMR (300 MHz, $(CD_3)_2CO$) δ 7.72 (d, J = 7.5 Hz, 4H), 7.68 (s, 2H), 7.41 (t, J = 7.4 Hz, 4H), 7.28 (t, J = 7.4 Hz, 2H), 4.38 (t, J = 6.9 Hz, 2H), 1.95 (quint., J = 6.8 Hz, 2H), 1.50-1.20 (m, 6H), 0.84 (t, J = 6.6 Hz, 3H). $^{13}C\{^1H\}$ NMR (75 MHz, $(CD_3)_2CO$) δ 146.24, 142.28, 136.45, 129.84, 127.97, 125.78, 108.83, 105.84, 47.67, 32.13, 31.06, 27.23, 23.21, 14.23 (two aromatic carbon resonances not observed, presumably due to overlap). HRMS (EI): *m/z* calcd for $C_{26}H_{25}NS_2$ (M^+): 415.1428; found: 415.1425. Anal. Calcd. for $C_{26}H_{25}NS_2$: C, 75.14; H, 6.06; N, 3.37. Found: C, 74.97; H, 5.91; N, 3.44.

2.4 References

(1) Facchetti, A. *Chem. Mater.* **2011**, *23*, 733.

(2) Bundgaard, E. *Sol. Energy Mater. Sol. Cells* **2007**, *91*, 954.

(3) Beaujuge, P. M.; Pisula, W.; Tsao, H. N.; Ellinger, S.; Müllen, K.; Reynolds, J. R. *J. Am. Chem. Soc.* **2009**, *131*, 7514.

(4) Blouin, N.; Michaud, A.; Leclerc, M. *Adv. Mater.* **2007**, *19*, 2295.

(5) Li, Y.; Zou, Y. *Adv. Mater.* **2008**, *20*, 2952.

(6) Liang, Y.; Feng, D.; Wu, Y.; Tsai, S.-T.; Li, G.; Ray, C.; Yu, L. *J. Am. Chem. Soc.* **2009**, *131*, 7792.

(7) Park, S. H.; Roy, A.; Beaupré, S.; Cho, S.; Coates, N.; Moon, J. S.; Moses, D.; Leclerc, M.; Lee, K.; Heeger, A. J. *Nature Photon.* **2009**, *3*, 297.

(8) Peet, J.; Kim, J. Y.; Coates, N. E.; Ma, W. L.; Moses, D.; Heeger, A. J.; Bazan, G. C. *Nature Mater.* **2007**, *6*, 497.

(9) Svensson, M.; Zhang, F.; Veenstra, S. C.; Verhees, W. J. H.; Hummelen, J. C.; Kroon, J. M.; Inganäs, O.; Andersson, M. R. *Adv. Mater.* **2003**, *15*, 988.

(10) Wang, E.; Wang, L.; Lan, L.; Luo, C.; Zhuang, W.; Peng, J.; Cao, Y. *Appl. Phys. Lett.* **2008**, *92*, 033307.

(11) Wang, J.-Y.; Hau, S. K.; Yip, H.-L.; Davies, J. A.; Chen, K.-S.; Zhang, Y.; Sun, Y.; Jen, A. K. Y. *Chem. Mater.* **2011**, *23*, 765.

(12) Zhang, Y.; Hau, S. K.; Yip, H.-L.; Sun, Y.; Acton, O.; Jen, A. K. Y. *Chem. Mater.* **2010**, *22*, 2696.

(13) Zou, Y.; Najari, A.; Berrouard, P.; Beaupré, S.; Réda Aïch, B.; Tao, Y.; Leclerc, M. *J. Am. Chem. Soc.* **2010**, *132*, 5330.

(14) Zhu, Y.; Champion, R. D.; Jenekhe, S. A. *Macromol.* **2006**, *39*, 8712.

(15) Mikroyannidis, J. A.; Tsagkournos, D. V.; Sharma, S. S.; Vijay, Y. K.; Sharma, G. D. *J. Mater. Chem.* **2011**, *21*, 4679.

(16) Sharma, G. D.; Balraju, P.; Mikroyannidis, J. A.; Stylianakis, M. M. *Sol. Energy Mater. Sol. Cells* **2009**, *93*, 2025.

(17) Zheng, Q.; Jung, B. J.; Sun, J.; Katz, H. E. *J. Am. Chem. Soc.* **2010**, *132*, 5394.

(18) Cheng, Y.-J.; Wu, J.-S.; Shih, P.-I.; Chang, C.-Y.; Jwo, P.-C.; Kao, W.-S.; Hsu, C.-S. *Chem. Mater.* **2011**, *23*, 2361.

(19) Li, Z.; McNeill, C. R. *J. Appl. Phys.* **2011**, *109*, 074513.

(20) Zhou, J.; Wan, X.; Liu, Y.; Wang, F.; Long, G.; Li, C.; Chen, Y. *Macromol. Chem. Phys.* **2011**, *212*, 1109.

(21) Zhang, S.; Guo, Y.; Fan, H.; Liu, Y.; Chen, H.-Y.; Yang, G.; Zhan, X.; Liu, Y.; Li, Y.; Yang, Y. *J. Polym. Sci. A Polym. Chem.* **2009**, *47*, 5498.

(22) Sonar, P.; Williams, E. L.; Singh, S. P.; Dodabalapur, A. *J. Mater. Chem.* **2011**, *21*, 10532.

(23) Hou, J.; Chen, H.; Zhang, S.; Li, G.; Yang, Y. *J. Am. Chem. Soc.* **2008**, *130*, 16144.

(24) Zhang, X.; Steckler, T. T.; Dasari, R. R.; Ohira, S.; Potscavage, W. J.; Tiwari, S. P.; Coppee, S.; Ellinger, S.; Barlow, S.; Brédas, J.-L.; Kippelen, B.; Reynolds, J. R.; Marder, S. R. *J. Mater. Chem.* **2010**, *20*, 123.

(25) Yue, W.; Zhao, Y.; Shao, S.; Tian, H.; Xie, Z.; Geng, Y.; Wang, F. *J. Mater. Chem.* **2009**, *19*, 2199.

(26) Zaumseil, J.; Sirringhaus, H. *Chem. Rev.* **2007**, *107*, 1296.

(27) Bürgi, L.; Turbiez, M.; Pfeiffer, R.; Bienewald, F.; Kirner, H.-J.; Winnewisser, C. *Adv. Mater.* **2008**, *20*, 2217.

(28) Gadisa, A.; Mammo, W.; Andersson, L. M.; Admassie, S.; Zhang, F.; Andersson, M. R.; Inganäs, O. *Adv. Funct. Mater.* **2007**, *17*, 3836.

(29) Gwinner, M. C.; Khodabakhsh, S.; Giessen, H.; Sirringhaus, H. *Chem. Mater.* **2009**, *21*, 4425.

(30) Kim, F. S.; Guo, X.; Watson, M. D.; Jenekhe, S. A. *Adv. Mater.* **2010**, *22*, 478.

(31) Zoombelt, A. P.; Mathijssen, S. G. J.; Turbiez, M. G. R.; Wienk, M. M.; Janssen, R. A. J. *J. Mater. Chem.* **2010**, *20*, 2240.

(32) Steckler, T. T.; Zhang, X.; Hwang, J.; Honeyager, R.; Ohira, S.; Zhang, X.-H.; Grant, A.; Ellinger, S.; Odom, S. A.; Sweat, D.; Tanner, D. B.; Rinzler, A. G.; Barlow, S.; Brédas, J.-L.; Kippelen, B.; Marder, S. R.; Reynolds, J. R. *J. Am. Chem. Soc.* **2009**, *131*, 2824.

(33) Usta, H.; Facchetti, A.; Marks, T. J. *J. Am. Chem. Soc.* **2008**, *130*, 8580.

(34) Yoon, M.; DiBenedetto, S.; Facchetti, A.; Marks, T. *J. Am. Chem. Soc.* **2005**, *127*, 1348.

(35) Chesterfield, R. J.; Newman, C. R.; Pappenfus, T. M.; Ewbank, P. C.; Haukaas, M. H.; Mann, K. R.; Miller, L. L.; Frisbie, C. D. *Adv. Mater.* **2003**, *15*, 1278.

(36) Beaujuge, P. M.; Pisula, W.; Tsao, H. N.; Ellinger, S.; Müllen, K.; Reynolds, J. R. *J. Am. Chem. Soc.* **2009**, *131*, 7514.

(37) Zaumseil, J.; Donley, C.; Kim, J.-S.; Friend, R.; Sirringhaus, H. *Adv. Mater.* **2006**, *18*, 2708.

(38) Welch, G. C.; Bazan, G. C. *J. Am. Chem. Soc.* **2011**, *133*, 4632.

(39) Murphy, A.; Fréchet, J. *Chem. Rev.* **2007**, *107*, 1066.

(40) Mas-Torrent, M.; Rovira, C. *Chem. Soc. Rev.* **2008**, *37*, 827.

(41) Jurchescu, O. D.; Baas, J.; Palstra, T. T. M. *Appl. Phys. Lett.* **2004**, *84*, 3061.

(42) Ogawa, K. *J. Org. Chem* **2003**, *68*, 2921.

(43) Barlow, S.; Odom, S. A.; Lancaster, K.; Getmanenko, Y. A.; Mason, R.; Coropceanu, V.; Brédas, J.-L.; Marder, S. R. *J. Phys. Chem. B* **2010**, *114*, 14397.

(44) Ohshita, J.; Nodono, M.; Kai, H.; Watanabe, T.; Kunai, A.; Komaguchi, K.; Shiotani, M.; Adachi, A.; Okita, K.; Harima, Y.; Yamashita, K.; Ishikawa, M. *Organomet.* **1999**, *18*, 1453.

(45) Chochos, C. L.; Choulis, S. A. *Prog. Polym. Sci.* **2011**, 1.

(46) Bundgaard, E.; Krebs, F. C. *Macromol.* **2006**, *39*, 2823.

(47) Horie, M.; Majewski, L. A.; Fearn, M. J.; Yu, C.-Y.; Luo, Y.; Song, A.; Saunders, B. R.; Turner, M. L. *J. Mater. Chem.* **2010**, *20*, 4347.

(48) Welch, G. C.; Coffin, R.; Peet, J.; Bazan, G. C. *J. Am. Chem. Soc.* **2009**, *131*, 10802.

(49) Karsten, B. P.; Bijleveld, J. C.; Viani, L.; Cornil, J.; Gierschner, J.; Janssen, R. A. J. *J. Mater. Chem.* **2009**, *19*, 5343.

(50) Sonar, P.; Singh, S. P.; Leclere, P.; Surin, M.; Lazzaroni, R.; Lin, T. T.; Dodabalapur, A.; Sellinger, A. *J. Mater. Chem.* **2009**, *19*, 3228.

(51) Sonar, P.; Singh, S. P.; Sudhakar, S.; Dodabalapur, A.; Sellinger, A. *Chem. Mater.* **2008**, *20*, 3184.

(52) Steinberger, S.; Mishra, A.; Reinold, E.; Levichkov, J.; Uhrich, C.; Pfeiffer, M.; Bäuerle, P. *Chem. Commun.* **2011**, *47*, 1982.

(53) Pilgram, K.; Zupan, M.; Skiles, R. *J. Heterocycl. Chem.* **1970**, *7*, 629.

(54) Gronowitz, S. *Acta Chem. Scand.* **1961**, *15*, 1393.

(55) Evenson, S. J.; Rasmussen, S. C. *Org. Lett.* **2010**, *12*, 4054.

(56) Mishra, S. P.; Palai, A. K.; Srivastava, R.; Kamalasanan, M. N.; Patri, M. *J. Polym. Sci. Pol. Chem.* **2009**, *47*, 6514.

(57) Koeckelberghs, G. *Tetrahedron* **2005**, *61*, 687.

(58) Sonar, P.; Singh, S.; Sudhakar, S.; Dodabalapur, A.; Sellinger, A. *Chem. Mater.* **2008**, *20*, 3184.

(59) Neutral ground state structures at the Hartree-Fock (HF/6-31G**) level are moderately twisted fot triads **2.7** and **2.8** (torsion angles ca. 22°) and further twisted for **2.9** and **2.10** (torsion angles ca. 39°).

(60) The compounds with terminal alkyl groups, **2.7c/d** and **2.8c/d** show very similar orbitals to their hydrogen-terminated analogues and the frontier orbitals at the HF/6-31G** level are qualitatively similar to the DFT orbitals.

(61) Sato, T.; Hori, K.; Fujitsuka, M.; Watanabe, A.; Ito, O.; Tanaka, K. *J. Chem. Soc., Faraday Trans.* **1998**, *94*, 2355.

(62) Hankache, J.; Wenger, O. S. *Chem. Rev.* **2011**, DOI: 10.1021/cr100441k.

(63) Mori-Sánchez, P.; Cohen, A. J.; Yang, W. *Phys. Rev. Lett.* **2008**, *100*, 146401.

(64) Distribution of HF Mulliken charges are broadly consistent with distribution of DFT charges.

(65) Silva-Junior, M. R.; Schreiber, M.; Sauer, S. P. A.; Thiel, W. *J. Chem. Phys.* **2008**, *129*, 104103.

(66) Peach, M. J. G.; Benfield, P.; Helgaker, T.; Tozer, D. J. *J. Chem. Phys.* **2008**, *128*, 044118.

(67) Although the transition energies obtained using the long-range corrected functionals are hypsochromically shifted from the experimental maxima, the calculated absorption profiles for the visible region are in good qualitative agreement and the CI descriptions of the transitions are qualitatively similar.

(68) Apperloo, J. J.; Groenendaal, L. B.; Verheyen, H.; Jayakannan, M.; Janssen, R. A. J.; Dkhissi, A.; Beljonne, D.; Lazzaroni, R.; Brédas, J.-L. *Chem. Eur. J.* **2002**, *8*, 2384.

(69) Yassin, A.; Leriche, P.; Roncali, J. *Macromol. Rapid Commun.* **2010**, *31*, 1467.

(70) Kojima, T.; Nishida, J.-i.; Tokito, S.; Tada, H.; Yamashita, Y. *Chem. Commun.* **2007**, 1430.

(71) Omer, K. M.; Ku, S.-Y.; Wong, K.-T.; Bard, A. J. *J. Am. Chem. Soc.* **2009**, *131*, 10733.

(72) Watanabe, M.; Goto, K.; Shibahara, M.; Shinmyozu, T. *J. Org. Chem* **2010**, *75*, 6104.

(73) Marcus, R. A. *Rev. Mod. Phys.* **1993**, *65*, 599.

(74) Malagoli, M.; Brédas, J.-L. *Chem. Phys. Lett.* **2000**, *327*, 13.

(75) da Silva Filho, D. A.; Coropceanu, V.; Fichou, D.; Gruhn, N. E.; Bill, T. G.; Gierschner, J.; Cornil, J.; Brédas, J.-L. *Philos. Trans. R. Soc. A: Math. Phys. Eng. Sci.* **2007**, *365*, 1435.

(76) Lin, B. C.; Cheng, C. P.; You, Z.-Q.; Hsu, C.-P. *J. Am. Chem. Soc.* **2004**, *127*, 66.

(77) Coropceanu, V.; Malagoli, M.; da Silva Filho, D. A.; Gruhn, N. E.; Bill, T. G.; Br; eacute; das, J. L. *Phys. Rev. Lett.* **2002**, *89*, 275503.

(78) Barlow, S.; Zhang, Q.; Kaafarani, B. R.; Risko, C.; Amy, F.; Chan, C. K.; Domercq, B.; Starikova, Z. A.; Antipin, M. Y.; Timofeeva, T. V.; Kippelen, B.; Brédas, J.-L.; Kahn, A.; Marder, S. R. *Chem. Eur. J.* **2007**, *13*, 3537.

(79) Connelly, N.; Geiger, W. *Chem. Rev.* **1996**, *96*, 877.

(80) Guay, J.; Kasai, P.; Diaz, A.; Wu, R.; Tour, J.; Dao, L. *Chem. Mater.* **1992**, *4*, 1097.

(81) Fichou, D.; Horowitz, G.; Xu, B.; Garnier, F. *Synth. Met.* **1990**, *39*, 243.

(82) Fujitsuka, M.; Sato, T.; Sezaki, F.; Tanaka, K.; Watanabe, A.; Ito, O. *J. Chem. Soc., Faraday Trans.* **1998**, *94*, 3331.

(83) Graf, D.; Duan, R.; Campbell, J.; Miller, L.; Mann, K. *J. Am. Chem. Soc.* **1997**, *119*, 5888.

(84) Polander, L. E.; Tiwari, S. P.; Pandey, L.; Seifried, B. M.; Zhang, Q.; Barlow, S.; Risko, C.; Brédas, J.-L.; Kippelen, B.; Marder, S. R. *Chem. Mater.* **2011**, *23*, 3408.

(85) From the estimated solid-state IPs and excited-state energies, E_{op}, of Table 2.4, and using a value of –3.8 eV for the solid-state EA of PCBM (Guan, Z.-L.; Kim, J. B.; Wang, H.; Jaye, C.; Fischer, D. A.; Loo, Y.-L.; Kahn, A. *Org. Electron.* **2010**, *11*, 1779), a commonly used acceptor in photovoltaic studies, one can estimate ΔG for electron transfer from the photoexcited dyads to PCBM to be in the range –0.7 to –0.8 eV.

CHAPTER 3

DONOR-ACCEPTOR TRIADS BASED ON NAPHTHALENE DIIMIDE WITH HIGH ELECTRON MOBILITY

3.1 Introduction

Organic semiconductors have attracted interest for electronic applications due to their potential for use in low-cost, large-area, flexible electronic devices.[1-3] While many examples of organic semiconductors for p-channel and n-channel organic field-effect transistors (OFETs) have been reported in the recent literature,[4-6] there is a paucity of high-performance, solution-processable small molecule materials for n-channel OFETs. In order to take advantage of the technological potential of organic semiconducting materials, solution-processable, ideally air-stable, electron-transport (ET) materials with low barriers for charge injection, high charge-carrier mobility values (> 1 $cm^2V^{-1}s^{-1}$), large current on/off ratios (I_{on}/I_{off} > 10^6), and low threshold voltage (< ±2.5 V) are still desirable.

Rylene diimides are interesting candidates and many high-mobility examples have been reported.[7] In particular, materials based on naphthalene-1,8:4,5-bis(dicarboximide)s (NDIs) are among the best organic ET materials to date; some examples show air-stable n-channel mobility values of up to 1.2 $cm^2V^{-1}s^{-1}$ when incorporated in OFETs by vacuum deposition.[8,9] However, solution-processed ET materials based on NDI derivatives typically exhibit lower mobility values[10] and only recently have values exceeding ~ 0.1 $cm^2V^{-1}s^{-1}$ been reported. An ET copolymer of NDI and bithiophene reported by Facchetti *et. al.*[11] represents the highest mobility example of a solution-processable polymer, with an OFET mobility value of 0.85 $cm^2V^{-1}s^{-1}$. The

highest OFET electron mobility values reported to date for solution-cast small molecules have been measured on core-expanded NDIs reported by Zhu *et al.*;[12,13] very recently one of these derivatives was shown to exhibit values as high as 0.55-1.2 $cm^2V^{-1}s^{-1}$ when appropriately processed,[13] further demonstrating the potential of rylene-based materials for high-performance solution-processed n-channel OFETs.

This chapter shows that bis(NDI) derivatives with conjugated bridging groups based on fused heterocycle ring systems can be processed from solution into films that exhibit OFET electron mobility values of up to 1.5 $cm^2V^{-1}s^{-1}$, which is among the highest yet reported for an n-channel OFET based on a solution-processed small molecule.

3.2 Molecular Bis(Naphthalene Diimide) Derivatives

3.2.1 Synthesis

As shown in Scheme 3.1, commercially available NDA, **3.1**, was converted to its 4-bromo derivative, **3.2**, according to literature procedures.[14,15] Palladium-catalyzed Stille coupling of **3.2** and bis(tributylstannyl) fused-ring heterocycle derivatives, **3.3**,[16,17] yields the bis(NDI) derivatives, **3.4**, in 30-60% yield; these compounds were characterized by ^1H and $^{13}C\{^1H\}$ NMR spectroscopy, high-resolution mass spectrometry, and elemental analysis.

The thermal properties of the compounds were investigated by thermogravimetric analysis (TGA, Figure 3.1, Table 3.1) and three repeated heating-cooling cycles using differential scanning calorimetry (DSC). TGA showed decomposition temperatures (defined as that at which 5 wt% loss is observed) above 400 ºC for all three bis(NDI)s. In the DSC trace, **3.4** exhibited one endothermic transition, presumably attributable to melting, at 279 ºC, 300 ºC and 361 ºC on heating **3.4a**, **3.4b** and **3.4c**, respectively (and one corresponding exothermic transitions on cooling).

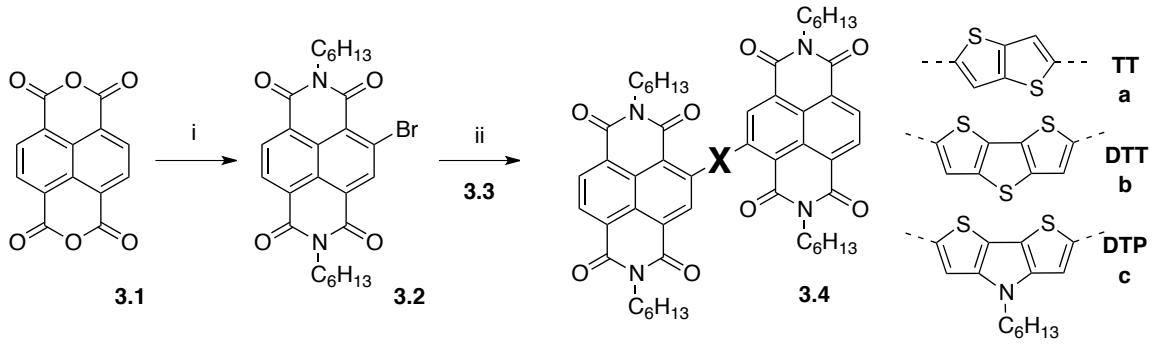

Scheme 3.1. Preparation of **3.4**. (i) 1) DBI, H_2SO_4, 2) hexanoyl chloride, AcOH; (ii) Pd_2dba_3, P(*o*-tol)$_3$, toluene.

Table 3.1. Decomposition (T_d), glass transition (T_g) and melting point (T_m) temperatures.

cmpd	T_d / ºC	T_g / ºC	T_m / ºC
3.4a	400	95	279
3.4b	402	94	300
3.4c	409	96	361

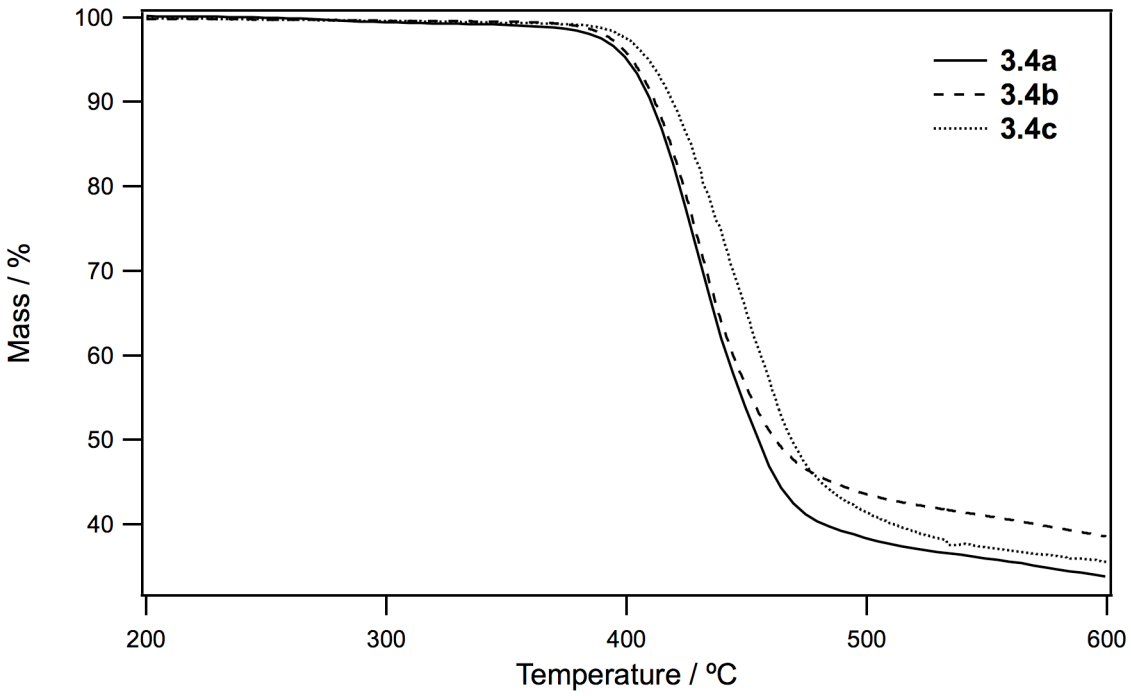

Figure 3.1. Thermogravimetric analysis of **3.4**.

3.2.2 Molecular Geometry and Frontier Orbitals

The neutral ground-state structures obtained at the DFT (B3LYP/6-31G**) level for **3.4** (with all alkyl groups replaced by methyl groups) are characterized by conformation type A for **3.4b** and **3.4c**, whereas **3.4a** is characterized by conformation type B (Figure 3.2). These respective confirmations are ~ 0.2 kcal/mol, 0.1 kcal/mol, and 0.6 kcal/mol more stable than the alternate confirmations, respectively, for **3.4a**, **3.4b**, and **3.4c**. The NDI units are (on average) twisted 47°, 46°, and 42° out-of-plane with respect to the central TT, DTT, and DTP units, respectively. This is consistent with the effects of steric interactions between hydrogen atoms in the 3 / 3' positions of the oligothiophene bridges with hydrogen atoms on the NDI rings. Due to the tendency of DFT methods to overestimate the extent of delocalization and conjugation, geometries were also obtained at Hartree-Fock (HF/6-31G**); the neutral ground state structures obtained for **3.4** retain the symmetrical torsion angles seen in the DFT results, but with values of 78º, 78º and 75º for **3.4a**, **3.4b**, and **3.4c**, respectively.

The HOMO and LUMO single-electron wavefunctions (B3LYP/6-31G**) are illustrated for **3.4** and their building blocks in Figure 3.3 and Figure 3.4. The HOMO wavefunctions are localized on the central electron-rich units for all three derivatives with similar energies to that of an isolated TT, DTT, and DTP molecule, respectively (see Table 3.2 and Figure 3.5). The LUMOs are strongly localized on the two NDI segments and their energies are within 0.13 eV of that of an isolated NDI. This can be attributed to the large mismatch in the energies of the NDI and oligothiophene LUMOs.

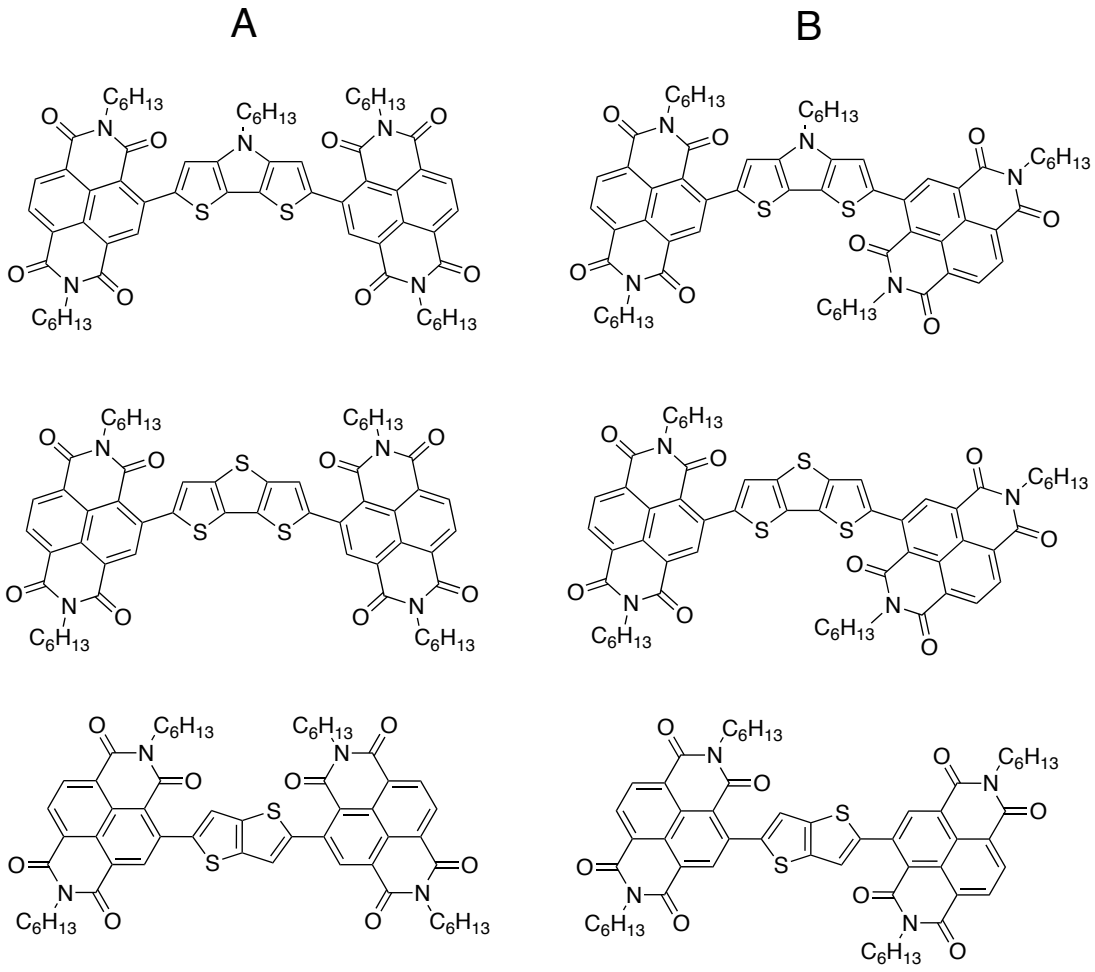

Figure 3.2. Structural representation of conformation type A and B.

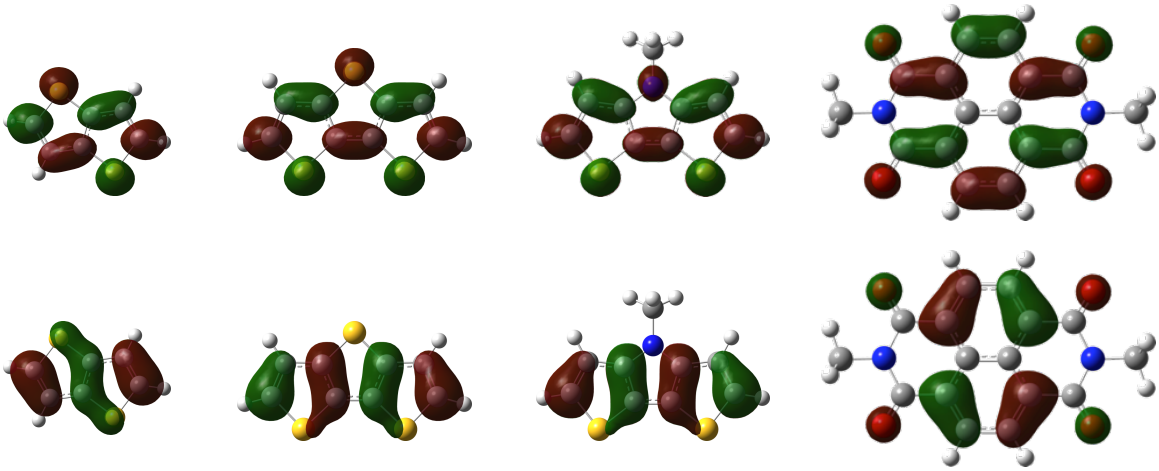

Figure 3.3. Pictorial representation of the HOMO (bottom) and LUMO (top) wave functions and energies for TT (left), DTT (left, middle), DTP (right, middle) and NDI (right) as determined at the B3LYP/6-31G** level of theory.

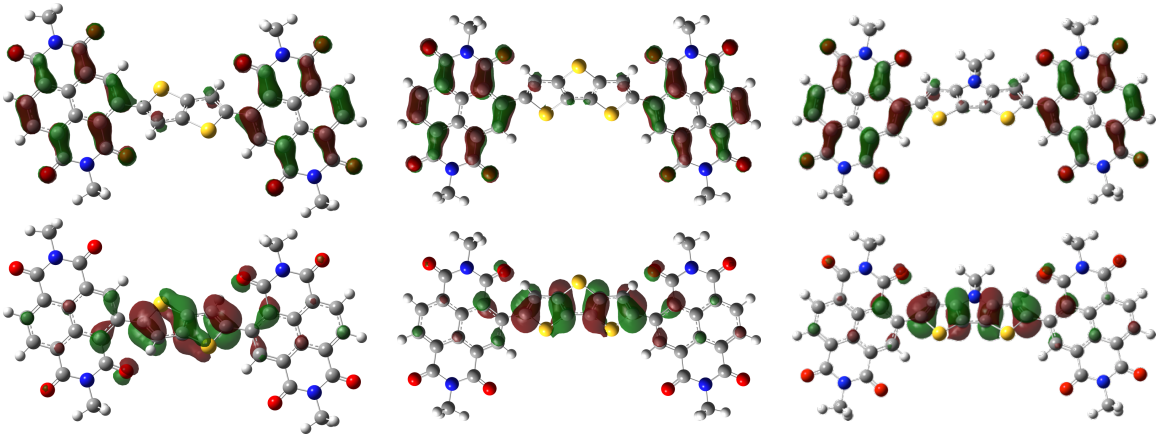

Figure 3.4. Pictorial representations of the HOMO (bottom) and LUMO (top) wavefunctions and energies for **3.4a** (left), **3.4b** (middle), and **3.4c** (right) as determined at the B3LYP/6-31G(d,p) level of theory.

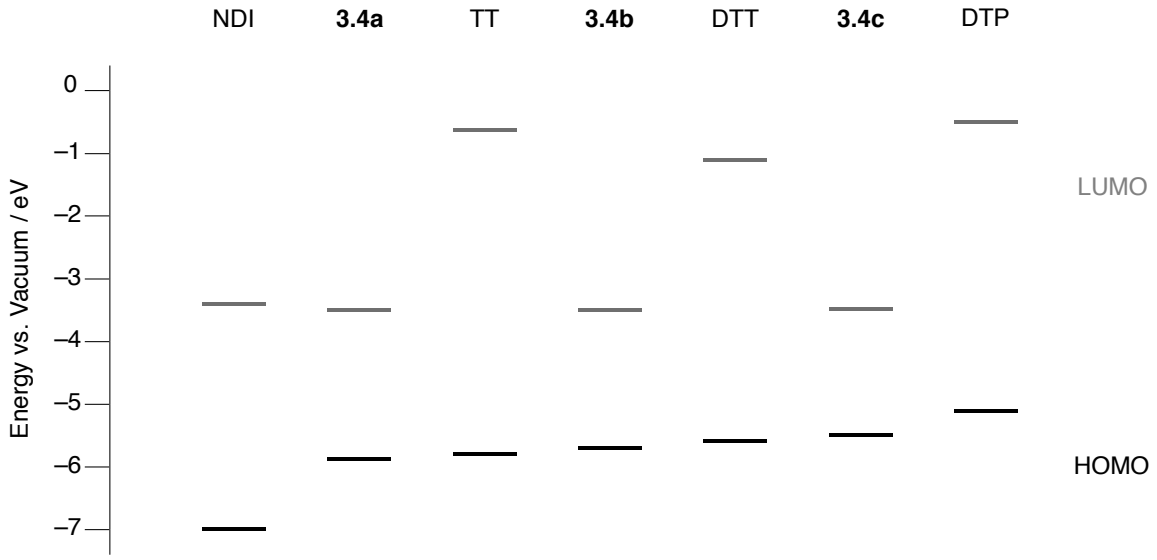

Figure 3.5. Schematic showing how the DFT frontier orbital energies of **3.4** compared to those of their constituent building blocks.

Table 3.2. B3LYP/6-31G** Frontier Orbital Energies (eV) for **3.4** and Their Building Blocks.[a]

Compound	HOMO	LUMO
NDI	–7.04	–3.41
TT	–5.86	–0.74
DTT	–5.61	–1.10
DTP	–5.10	–0.56
3.4a	–5.88	–3.54
3.4b	–5.73	–3.54
3.4c	–5.46	–3.47

[a]Alkyl groups replaced by methyl groups throughout.

In the radical cations of **3.4**, the average twist angles of the NDI units increase (symmetrically) to 54°, 60° and 70°, while for reduction the twist angles decrease (symmetrically) to 36°, 38° and 34°, respectively, for **3.4a**, **3.4b**, and **3.4c** at the DFT level. The radical anions of **3.4** can, at least in principle, be regarded as organic mixed-valence species[18] in which the electron might be either localized on one end of the molecule or delocalized between two comparable redox centers. In particular, the NDI-localized LUMOs suggest the possibility of localized (class II)[19] behavior. The DFT calculations suggest all these species are delocalized (class III) systems, but, given the well-known tendency of DFT to give overdelocalized structures, we also used HF calculations to investigate the radical-anion geometries. The HF radical-anion structures of **3.4b** and **3.4c** are calculated to have twist angles (unsymmetrical) of 84º/29º and 85º/31º, while the twist angles for **3.4a** are largely symmetrical at 33º/30º. The HF calculations suggest all three species are mainly localized systems with electronic charges of 0.86*e*, 0.87*e* and 0.88*e* for **3.4a**, **3.4b**, and **3.4c**, respectively.

3.2.3 Optical Properties

The UV-vis. absorption spectra (Table 3.3, Figure 3.6) of the **3.4** derivatives in chloroform have maxima at 382-385 nm, similar to that of the corresponding monomeric NDI derivative (383 nm). Additionally, **3.4a**, **3.4b**, and **3.4c** exhibit long-wavelength absorption maxima at 543, 566, and 681 nm, respectively. The bathochromic shift of this long-wavelength absorption with increasing electron-richness of the bridging group is suggestive of a charge-transfer (CT) type origin. Moreover, the low-energy band is similar to that seen in other thiophene-substituted NDIs.[11] Spectra in thin films are fairly similar to those seen in solution with moderate shifts in the absorption maxima (Table 3.3, Figure 3.7).

Table 3.3. Absorption Maxima, Absorptivities, and Oscillator Strengths for the Strong UV-vis. Absorptions of **3.4** in Chloroform along with TD-DFT Values and Assignments (in italics) and Thin-Film Absorption Maxima.[a]

cmpd	$\bar{\nu}_{max}$ / 10^3 cm^{-1} (nm)			ε_{max} / 10^4	*f*		state	CI description
	soln	calc	film	$M^{-1}cm^{-1}$	soln	calc		(%)[b]
3.4a	18.9 (543)	*15.7*	17.4 (572)	1.28	0.47	*0.48*	S_1	*H→L (98)*
	26.2 (383)	*26.7*	29.9 (335)	4.17	0.25	*0.22*	S_{10}	*H–9→L (2), H–8→L (13), H–7→L+1 (10), H–3→L (52), H–2→L+1 (11), H→L+2 (2)*
3.4b	17.6 (566)	*14.8*	17.6 (570)	1.48	0.56	*0.62*	S_1	*H→L (88)*
	27.6 (382)	*26.0*	27.6 (362)	4.05	0.30	*0.49*	S_8	*H–7→L (8), H–6→L+1 (8), H–5→L (7), H–2→L+1 (13), H→L+2 (49)*
3.4c	14.9 (681)	*13.7*	13.4 (744)	1.99	0.79	*0.75*	S_1	*H→L (85)*
	26.1 (385)	*25.3*	24.9 (400)	5.29	*0.37*	*0.74*	S_7	*H–7→L (4), H–6→L+1 (5), H–5→L (13), H→L+2 (66)*

[a]TD-DFT Values obtained for structures in which the alkyl groups are all replaced by methyl groups at the B3LYP/6-31G** level. [b]H and L denote HOMO and LUMO, respectively.

To gain insight into the origin of the spectroscopic properties observed in solution, the vertical $S_0 \rightarrow S_n$ excitation energies for isolated molecules were calculated at the time-dependent density functional theory (TD-DFT) level of theory using the B3LYP/6-31G** or long-range-corrected CAM-B3LYP and ωB97X functionals. As shown in Table 3.3 and Figure 3.8, the TD-DFT results are in reasonable agreement with the solution and solid-state absorption results, both in terms of excitation energies and oscillator strengths.[20] Although the excitation energies are somewhat underestimated, the experimentally observed trends between **3.4a**, **3.4b** and **3.4c** are all reproduced by the TD-DFT calculations. According to the calculations, the strong low-energy transitions correspond to the $S_0 \rightarrow S_1$ transitions and are predominantly HOMO→LUMO excitations and, therefore, can be regarded as having considerable DTP-to-NDI quadrupolar charge-transfer (CT) character.

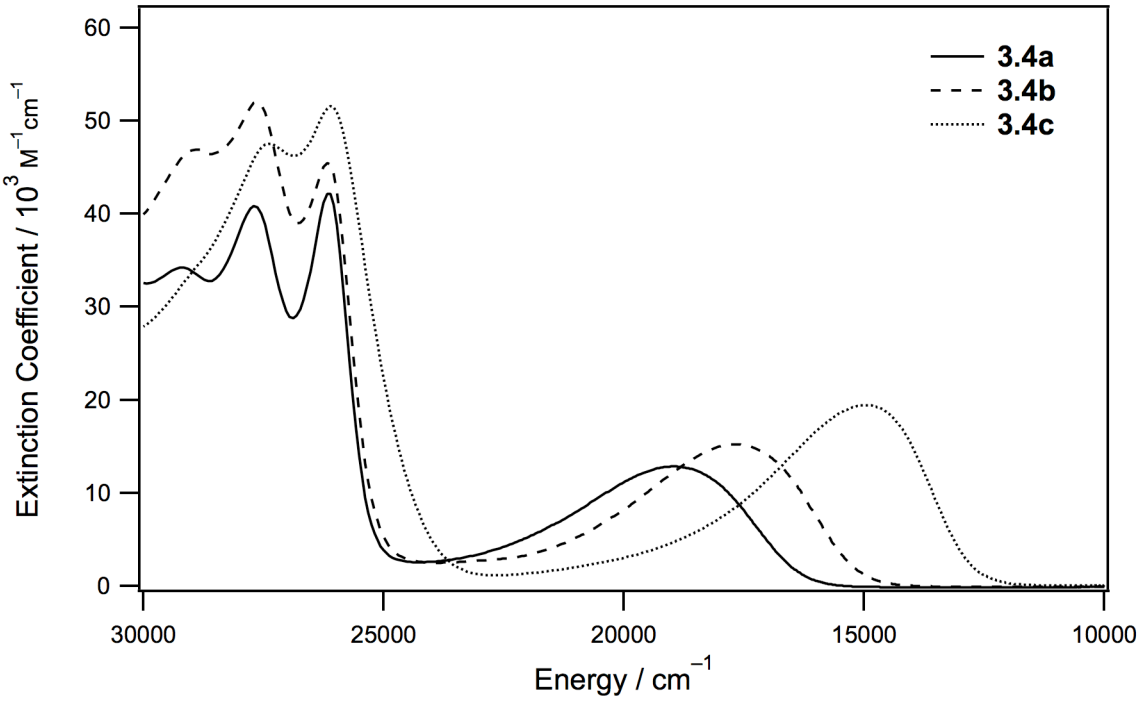

Figure 3.6. UV-vis. spectra of **3.4** in dilute chloroform solution.

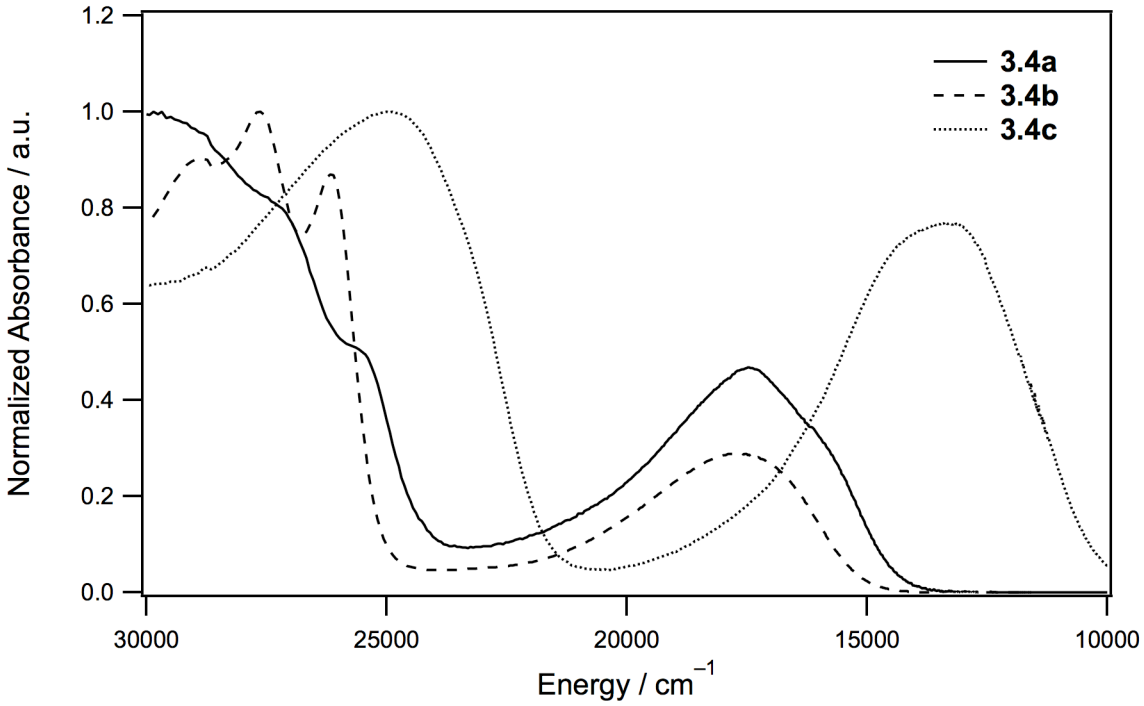

Figure 3.7. UV-vis. spectra of **3.4** as films on glass substrates.

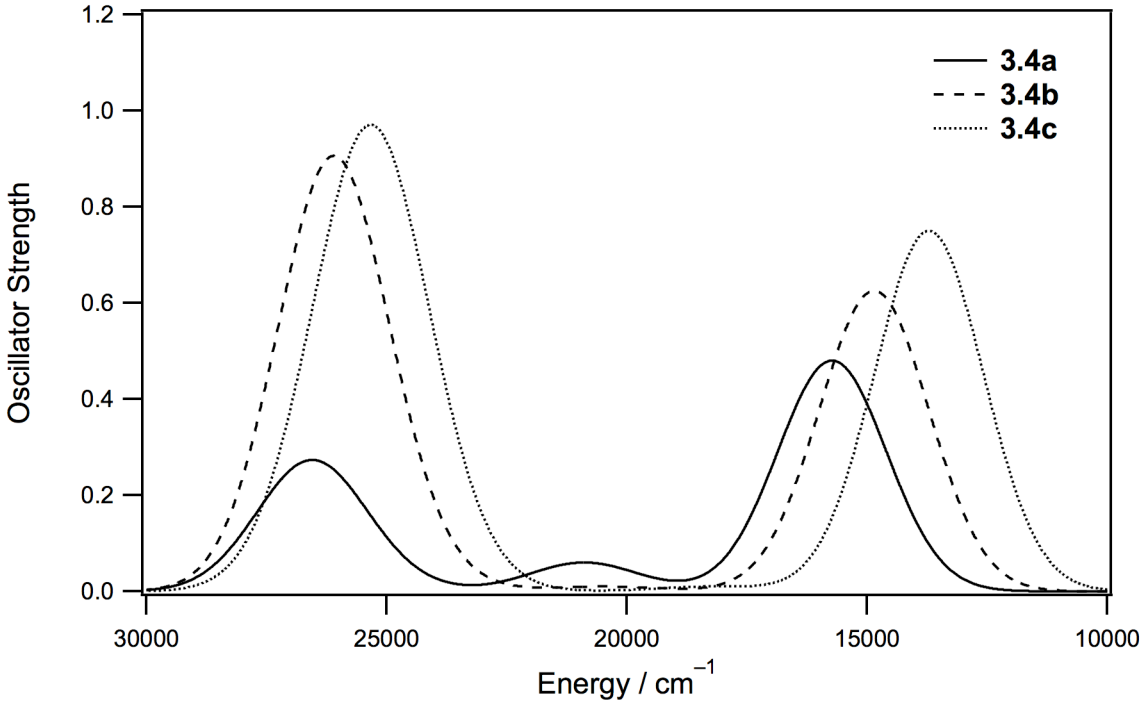

Figure 3.8. UV-vis. spectra of **3.4** predicted by DFT (bottom).

3.2.4 Electrochemistry, Ionization Potentials and Electron Affinities

Cyclic voltammetry (CV) was used to measure the electrochemical properties of the **3.4** derivatives in CH_2Cl_2 / 0.1 M $^nBu_4NPF_6$ (Table 3.4, Figure 3.9). In each case, a one-electron reversible oxidation process was observed along with two reversible reduction processes, each with approximately twice the current of that found for the oxidation; these are assigned to essentially independent reduction of both NDIs to their radical anions to give a molecular dianion and then a second reduction of both NDIs to give a tetraanion. The first half-wave reduction ($E_{1/2}^{0/-}$) potentials are very similar to that of an isolated NDI core ($E_{1/2}^{0/-}$ = – 1.13 V), consistent with the similarity in the DFT LUMO energies of the **3.4** compounds and isolated NDIs noted above. The half-wave oxidation ($E_{1/2}^{+/0}$) potentials show a difference between the potentials for DTT and DTP, which reflects that between 2,6-dibutyl-4H-dithieno[3,2-*b*:2',3'-*d*]thiophene and 4-(tert-butyl)-2,6-dibutyl-4H-dithieno[3,2-*b*:2',3'-*d*]pyrrole ($E_{1/2}^{+/0}$ = 0.69 and 0.23 V, respectively),[21] consistent with DFT data showing the HOMOs to be largely localized on the bridging groups; DFT adiabatic ionization potentials also show similar trends (6.83, 6.65, and 6.35 eV in **3.4a**, **3.4b** and **3.4c**, respectively, Table 3.5).

Table 3.4. Electrochemical Potentials (V vs. $FeCp_2^{+/0}$)[a] and Electrochemically Estimated Solid-State Ionization Potentials and Electron Affinities (eV).

cmpd	$E_{1/2}^{+/0}$	$E_{1/2}^{0/2-}$	$E_{1/2}^{2-/4-}$	IP(s)[b]	EA(s)[b]	E_{echem}[c]	E_{op}[d]
3.4a	1.10	-1.05	-1.48	5.9	–3.8	2.2	2.0
3.4b	0.93	-1.03	-1.45	5.7	–3.8	2.0	1.9
3.4c	0.56	-1.09	-1.50	5.4	–3.7	1.7	1.6

[a]Cyclic Voltammetry in CH_2Cl_2 / 0.1 M $^nBu_4NPF_6$. [b]Estimated according to IP(s) = $eE_{1/2}^{+/0}$ + 4.8 eV and EA(s) = $-(eE_{1/2}^{0/-} + 4.8$ eV). [c]Electrochemical gap, $E_{echem} = e(E_{1/2}^{+/0} - E_{1/2}^{0/-})$. [d]Optical gap estimated from long wavelength onset of absorption in solution.

Table 3.5. DFT SCF Values for Ionization Potentials, Electron Affinities, and Reorganization Energies for Isolated Molecules (eV).

cmpd	IP_{vert}[a]	IP_{adi}[a]	EA_{vert}[a]	EA_{adi}[a]	λ_h[b]	λ_e[b]
3.4a	7.01	6.83	–2.57	–2.67	0.391	0.210
3.4b	6.81	6.65	–2.61	–2.70	0.384	0.186
3.4c	6.51	6.35	–2.54	–2.64	0.452	0.189

[a]Vertical IP / EA = SCF energy difference between cation / anion at the ground-state neutral geometry and the ground-state neutral species; adiabatic IP / EA = SCF energy difference between the relaxed ground-state cation / anion and the ground-state neutral species (obtained for structures in which the alkyl groups are all replaced by methyl groups at the B3LYP/6-31G** level). [b]Internal reorganization energies for $M_A^{+/-} + M_B = M_A + M_B^{+/-}$ (λ_h or λ_e for + and –, respectively) obtained as sum of the SCF energy difference between cation/anion at the neutral geometry and at cation/anion geometry and that between the neutral species at cation/anion geometry and at neutral geometry.

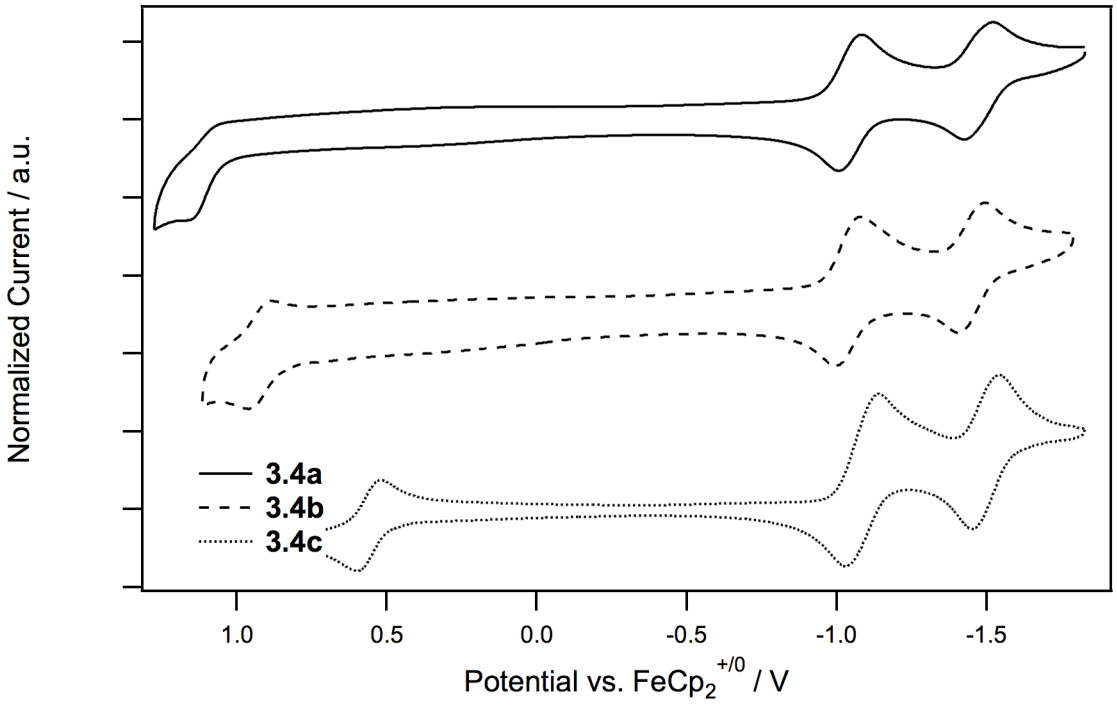

Figure 3.9. Cyclic voltammograms of **3.4** in 0.1 M $^nBu_4N$ PF_6 in CH_2Cl_2 recorded at a scan rate of 50 mVs^{-1}.

3.2.5 Radical-Anion Spectra

In order to study the potential mixed valence characteristics of **3.4**, the vis-NIR spectra of the radical anion and dianion of **3.4c** was investigated by optical spectroscopy. Robin and Day presented a classification of MV species based on the electronic coupling between the redox centers that divided MV species into three classes. In Class I, there is no electronic coupling between redox centers. In Class II, the redox centers are localized with measurable electronic coupling, which gives rise to an intervalence charge transfer (IVCT) band observed in the vis-NIR spectrum. In Class III, the redox centers are indistinguishable, and the charge is delocalized equally over both redox sites.[18,19] As mentioned earlier, the NDI-localized LUMOs suggest the possibility of localized (Class II) behavior.

The radical anion of **3.4c** was generated in dichloromethane solution using bis(cyclopentadienyl)cobalt(II) (cobaltocene, $E_{1/2}^{+/0}$ = –1.3 V vs. $FeCp_2^{+/0}$)[22] as an reductant; the vis-NIR spectra of the resulting solutions are shown in Figure 3.10 and Figure 3.11. The progression of **3.4c** to **3.4c**$^{\bullet-}$ and **3.4c**$^{2\bullet-}$ was observed through the portionwise addition of a sub-stoichiometric amount of the cobaltacene reductant (up to 2 eq. total added) and was performed on both a high (A_{max} > 4 a.u.) and low (A_{max} < 2 a. u.) concentration samples of **3.4**. The radical anion spectrum is characterized by a set of intense and characteristic visible and NIR absorption bands above 450 nm, consistent with what is seen for the radical anion of an isolated NDI unit.[23,24]

At high concentration, the evolution of an absorption band at considerably lower energy than the lowest energy absorption of the corresponding dianion was observed with a maximum absorption occurring at 1 eq. of cobaltocene reductant added; this band is attributed to an IVCT band associated with the radical anion species, which is consistent with a Class II mixed valence system (Figure 3.11).

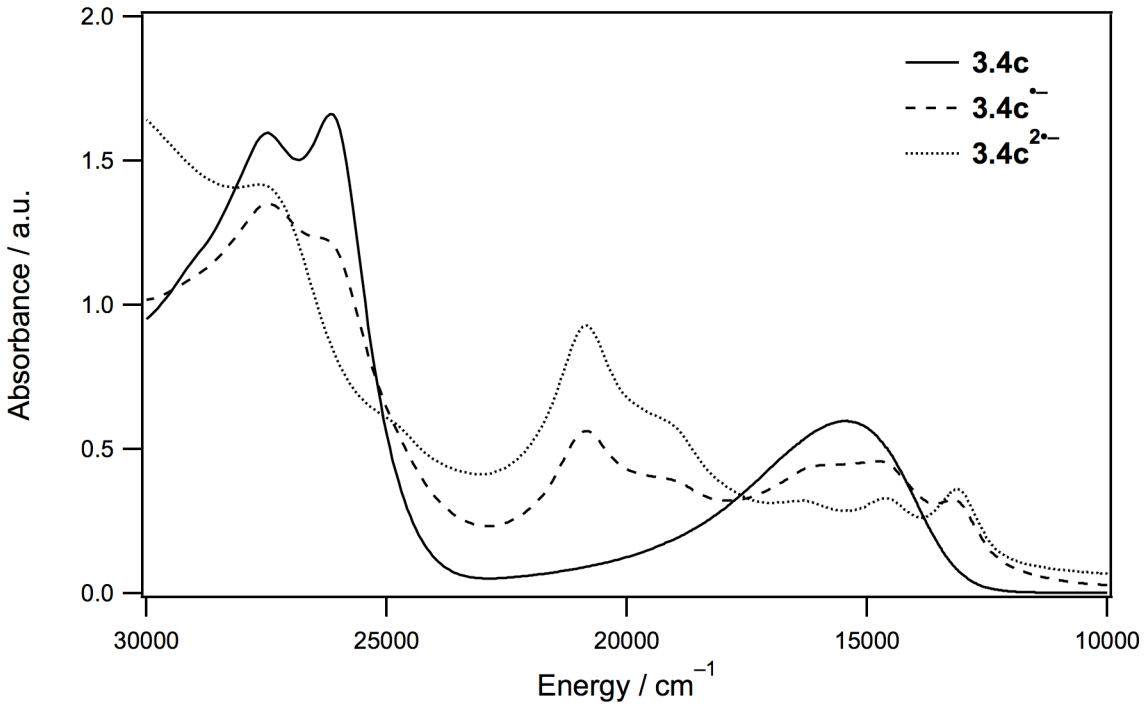

Figure 3.10. Vis-NIR absorption spectra of the neutrail, radical anion, and radical dianion of **3.4c** in dichloromethane (dilute, A_{max} < 2 a.u.).

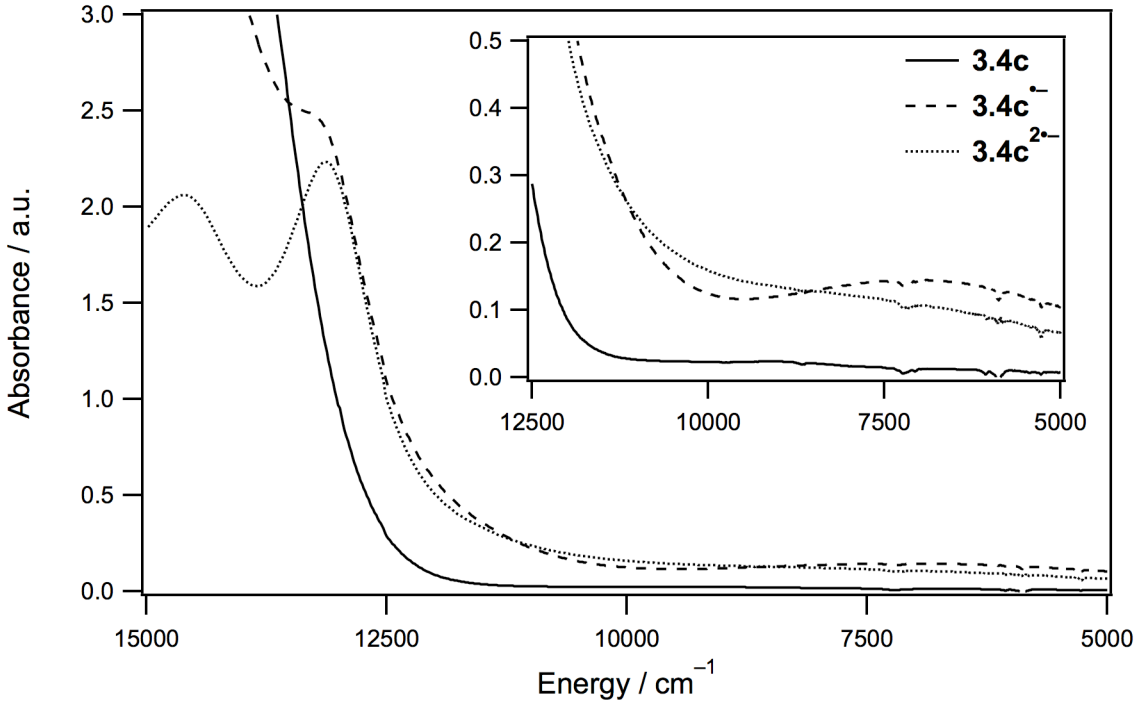

Figure 3.11. Vis-NIR absorption spectra of the neutral, radical anion, and radical dianion of **3.4c** in dichloromethane (concentrated, A_{max} > 4 a.u.).

3.2.6 OFET Behavior

Electrical characterization studies (Table 3.7) were performed on top-gate OFETs with a CYTOP / Al_2O_3 bilayer gate dielectric[25] and Au source / drain electrodes. **3.4** was spin-coated from 1,2-dichlorobenzene solutions; however, uniform films were not obtained from spin-casting of **3.4a** and **3.4b** due to reduced solubility of these materials in dichlorobenzene, and so films of these materials were prepared by drop casting.

OFETs fabricated using **3.4c** showed ambipolar electrical characteristics with dominant n-channel transistor behavior. Devices exhibited electron mobility values of up to 1.5 $cm^2V^{-1}s^{-1}$ with a rather high threshold voltage of 13.0 V. In p-channel transistor operation, a hole mobility of up to 9.8×10^{-3} $cm^2V^{-1}s^{-1}$ with a threshold voltage of 14.4 V was observed. The ambipolarity of **3.4c** means that the transistors are not fully turned off at zero gate bias and that no current on / off ratio can be measured, which is problematic for applications. On the other hand, decreasing the donor character of the bridge led to purely n-channel device performance and moderate on / off ratios; devices based on **3.4a** and **3.4b** function solely as n-channel transistors, albeit with lower mobility values than that seen for **3.4c** and with comparably high threshold voltages.

Table 3.7. Saturation Electron Mobilities, Threshold Voltages, and Current On / Off Ratios for OFETs Based on **3.4**.

cmpd	μ_e[a] / $cm^2V^{-1}s^{-1}$	V_{TH} / V	I_{on} / I_{off}
3.4a	0.12 (± 0.02)	12.3 (± 0.7)	1×10^4
3.4b	0.14 (± 0.07)	9.0 (± 0.3)	2×10^3
3.4c	1.2 (± 0.3)	13.0 (± 0.9)	b

[a] Average values are calculated based on 3 to 6 devices from a single substrate. [b] Not determined due to ambipolarity of sample.

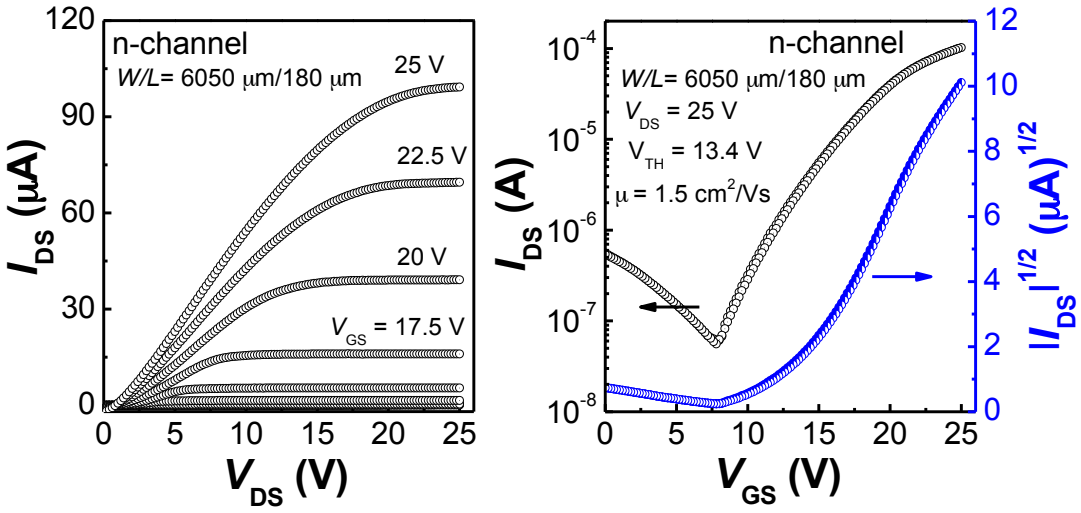

Figure 3.12. Output (left) and transfer (right) characteristics of a particular n-channel top-gate OFET with **3.4c** as semiconductor and CYTOP/Al_2O_3 gate dielectric layer with Au source/drain electrodes (*W/L*= 6050 μm/180 μm).

3.3 A Naphthalene Diimide / Dithienopyrrole D-A-D Triad

In order to understand the factors contributing to the exceptionally high electron mobility values associated with **3.4c**, it was hoped to study of the single-crystal structure and associated electronic coupling values of this bis(NDI) deriavtive. However, despite many attempts, single crystals suitable for X-ray structure were not obtained. On the other hand, suitable single crystals were grown for **3.6**, a D-A-D analogue of **3.4c**, and, although direct comparisons cannot be made, the packing structure of **3.6** is helpful in understanding a little bit more about the interactions between NDI and DTP in the solid state. A brief summary of the synthetic procedure, packing in the crystal structure, optical and electrochemical properties, and charge-transport characteristics are included for **3.6** below.

3.3.1 Synthesis

As shown in Scheme 3.2, 4-hexyl-4*H*-dithieno[3,2-*b*:2',3'-*d*]pyrrole, **2.6a**, was converted to 4-hexyl-2-(tributylstannyl)-4*H*-dithieno[3,2-*b*:2',3'-*d*]pyrrole, **3.5**, via lithiation using one equivalent of *tert*-butyllithium in THF at –78 ºC. The lithiated intermediate was converted to **3.5** by the addition of tributylchlorostannane at –78 ºC. After warming to room temperature, the freshly prepared stannyl derivative was purified by triethylamine-washed silica gel chromatography eluting with hexanes to separate unsubstituted, mono- and di-stannyl DTP products. Palladium-catalyzed Stille coupling of 2,6-dibromo-NDI (**4.2**, described in Chapter 4) and tributylstannyl-functionalized, fused-ring heterocycle derivative, **3.5**, yields the DTP-NDI-DTP triad, **3.6**, in 60% yield. The final product was characterized by ^{1}H and $^{13}C\{^{1}H\}$ NMR spectroscopy, high-resolution mass spectrometry, elemental analysis, and X-ray crystal structure.

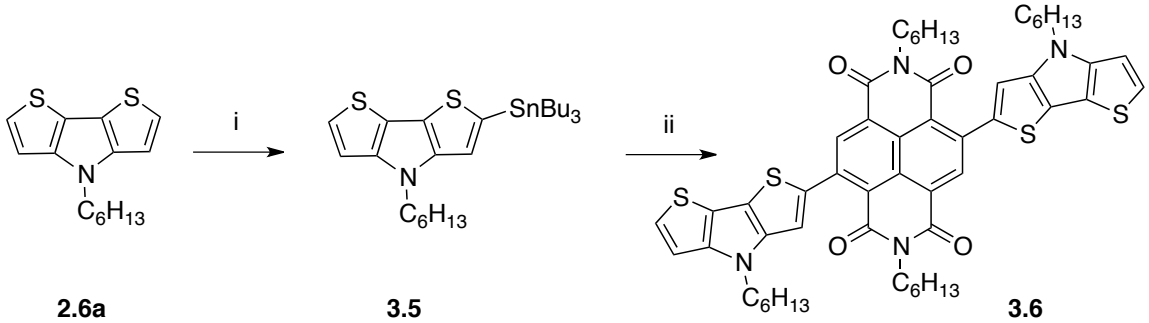

2.6a **3.5** **3.6**

Scheme 3.2. Preparation of compound **3.6**. i) 1) ^{t}BuLi (1 eq.), THF, 2) Bu_3SnCl; ii) *N,N'*-di(*n*-hexyl)-2,6-dibromonaphthalene-1,8:4,5-bis(dicarboximide), Pd_2dba_3, P(*o*-tol)$_3$, toluene.

3.3.2 Crystal Structure

Compound **3.6** produced crystals suitable for single-crystal X-ray structural analysis by liquid-liquid diffusion of a chloroform solution with methanol. The compound crystallized with two halves of the molecules (A and B) in the asymmetric unit; the

independent A and B molecules have similar geometries that vary with the rotation of the DTP substituents (Figure 3.16). The NDI-based central aromatic core deviates significantly from planarity, with the root mean square deviation of plane formed by $N_2O_4C_{14}$ of 0.17 and 0.19 Å, for A and B, respectively. The corresponding DTP units are twisted from the plane of the NDI core by ca. 25-30º. The molecules are packed in A-B-A-B sequence stacks, related by translations along *a*-axis, with a shortest distance between marked atoms of 3.2 Å (Figure 3.17).

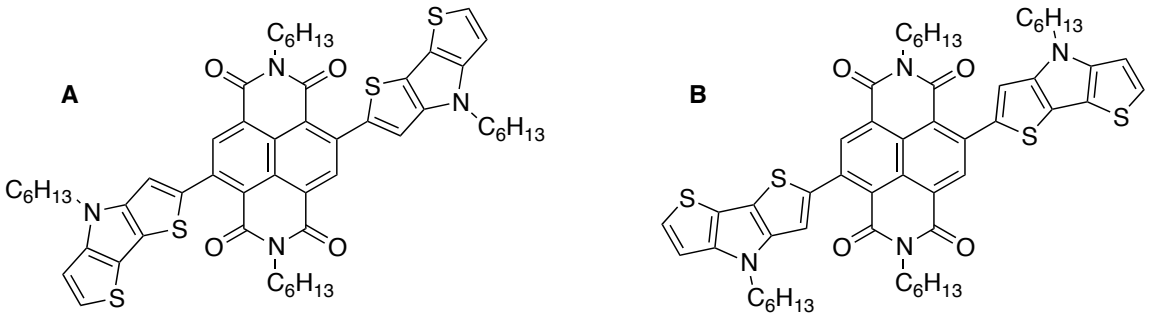

Figure **3.13.** Specific configurations of A and B geometries of **3.6**.

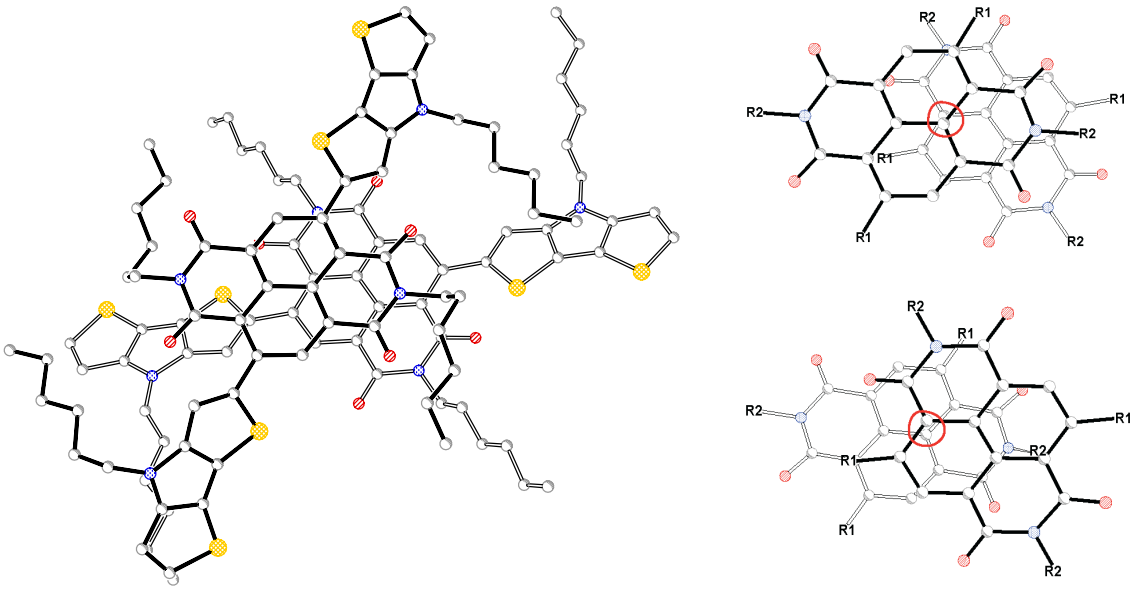

Figure 3.14. (left) Overlap of B over A molecule. Overlap of the cores, with the shortest distance between marked atoms being 3.2 Å. (top) B over A. (bottom) A over B'.

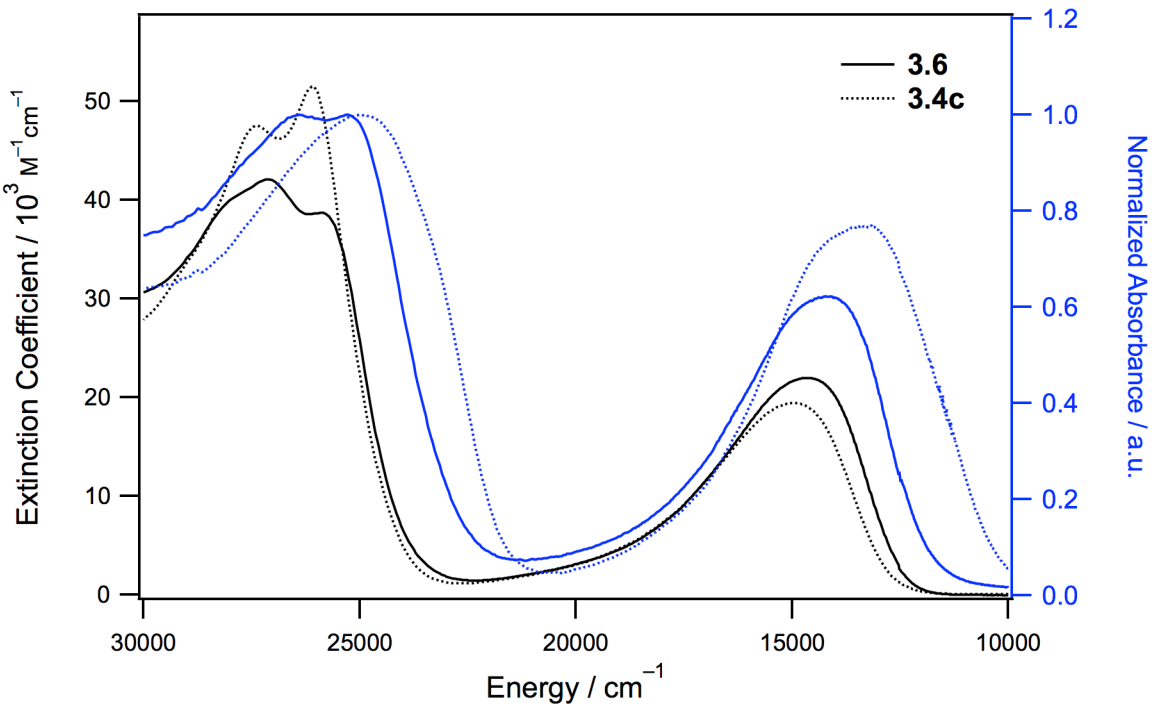

Figure 3.15. UV-vis. spectra of **3.6** compared to **3.4c** in dilute chloroform solution (black) and as a film on glass (blue).

3.3.3 Optical and Electrochemical Properties

The optical and electrochemical properties of compound **3.6** were investigated and compared to those of **3.4c**. The UV-vis. absorption spectrum of **3.6** is similar in shape to that of **3.4c** with λ_{max} (ε_{max} in 10^4 $M^{-1}cm^{-1}$) of 27100 (4.0) / 14600 (2.1) cm^{-1} and 26100 (5.3) / 14900 (2.0) cm^{-1}, respectively (Figure 3.16). The two high energy transitions exhibit different relative extinction coefficients with the band at 26100 cm^{-1} having larger extinction coefficient in **3.4c** due to the increased NDI character (two NDI untis) and the band at 27100 cm^{-1} exhibiting slightly broader band shape and having larger extinction coefficient in **3.6** due to increased DTP character (two DTP units). The electrochemical potentials for **3.6** are quite similar to those observed for **3.4c**, which is attributed mainly to the individual one-electron oxidation and two-electron reduction of the DTP and NDI units, respectively; **3.6** exhibited an oxidation potential of +0.52 V

($E_{1/2}^{2+/0}$) corresponding to the overlapping independent oxidations of each DTP unit, first reduction potential of –1.06 V, and a second reduction potential of –1.44 V vs. $FeCp_2^{+/0}$. The first half-wave reduction ($E_{1/2}^{0/-}$) potential is very similar to that of an isolated NDI core ($E_{1/2}^{0/-}$ = – 1.13 V) and the half-wave oxidation ($E_{1/2}^{2+/0}$) is slightly larger than that of an isolated DTP ($E_{1/2}^{+/0}$ = 0.23 V for 4-(tert-butyl)-2,6-dibutyl-4H-dithieno[3,2-*b*:2',3'-*d*]pyrrole),[21] in agreement with what is described above for **3.4c**.

3.3.4 OFET Behavior

Bottom-gate, top-contact geometry devices were fabricated on heavily n-doped silicon substrates, which also serve as the gate electrodes, BCB (see experimental details) coated SiO_2 as the gate dielectric and gold source and drain electrodes. Solutions (20 mg / mL) of **3.6** and a 1:1 by weight mixture of **3.6** and **3.4c** were spin-coated from 1,2-dichlorobenzene solutions as the active layer. This device design is used to screen materials for potential charge-transport properties and usually gives lower electron mobility values for NDI-based materials when compared to the top-gate structure used above for compounds **3.4** (as observed by Dr. Do Kyung Hwang in Prof. Bernard Kippelen's research group at Georgia Institute of Technology). For comparison, devices with this bottom-gate, top-contact design based on **3.4c** exhibited mobility values of 0.92 (± 0.1) × 10^{-3} $cm^2V^{-1}s^{-1}$, threshold voltages of 12.9 (± 0.9) V, and current on / off ratios of 10^4, which are much lower than the values determined for top-gate geometry devices as described above. Devices based on **3.6** exhibited electron mobility values two orders of magnitude lower than those observed for **3.4c** in the same device geometry (μ = 1.1 (± 0.1) × 10^{-5} $cm^2V^{-1}s^{-1}$, V_{TH} = 1.6 (± 2.4) V, $I_{ON/OFF}$ = 10^2). Devices based on the mixture of **3.4c** and **3.6** exhibited slightly improved electron mobility values of up to 5.4 (± 0.5) × 10^{-5} $cm^2V^{-1}s^{-1}$; however, the mobility values are still quite low. This could be attributed to a variety of reasons, but film quality and its effect on solid-state

packing is presumably a major influence in this case. Devices to test p-channel transistor operation were not fabricated.

3.4 Summary

In summary, this chapter describes the synthesis and characterization of a new class of small-molecule ET materials based on naphthalene diimide. DTP derivative **3.4c** exhibits ambipolar OFET properties with electron mobility up to 1.5 $cm^2V^{-1}s^{-1}$, this being the highest electron mobility measured for solution-processed small-molecule OFETs to date. Studies are underway to further optimize the properties and device characteristics of this class of materials.

Additionally, a D-A-D analogue of **3.4c** was synthesized and characterized by single crystal x-ray diffraction. Correlations cannot be made directly to **3.4c**; however, the very close π-π stacking distances observed between the NDI cores for **3.6** could lead to large electronic coupling values, which can correlate to high mobility values.

3.5 Experimental

Experimental details describing the general synthesis and characterization methods, X-ray crystal structure measurements, computational methodology, and fabrication of thin-film transistors can be found in Appendix A, B, C and D, respectively. X-ray crystal structure measurements included in this chapter were performed by Alexandr Fonari in Prof. Tatiana Timofeeva's research group in the Department of Chemistry at New Mexico Highlands University. Quantum chemical calculations included in this chapter were performed by Laxman Pandey under the guidance of Dr. Chad Risko in Prof. Jean-Luc Brédas' research group in the School of Chemistry and

Biochemistry at Georgia Institute of Technology. Transistor fabrication and measurements included in this chapter were performed by Dr. Shree Prakash Tiwari in Prof. Bernard Kippelen's research group in the School of Electrical and Computer Engineering at Georgia Institute of Technology.

3.5.1 Synthetic Procedures

2,5-Bis(tributylstannyl)thieno[3,2-*b*]thiophene. *n*-Butyllithium (14.7 mL, 36.7 mmol) was added slowly to 2,5-dibromothieno[3,2-*b*]thiophene (5.34 g, 17.9 mmol) in tetrahydrofuran (50 mL) at -78 ^{o}C. After addition, the mixture was stirred at -78 ^{o}C for 30 min. Tributyltin chloride (11.7 g, 35.9 mmol) was added slowly and the mixture was stirred for 30 min at -78 ^{o}C then warm to room temperature. The reaction was quenched by addition of brine. The mixture was extracted with ether and the combined organic layer was dried with anhydrous magnesium sulfate. Solvent was removed under reduced pressure to obtain an oil (12.5 g, 97%). ^{1}H NMR ^{1}H NMR (400 MHz, $CDCl_3$) δ 7.23 (s, 2H), 1.56 (quint., *J* = 7.2 Hz, 12H), 1.34 (sext, *J* = 7.1 Hz, 12H), 1.12 (t, *J* = 7.8 Hz, 12H), 0.90 (t, *J* = 7.8 Hz, 18H). ^{13}C{^{1}H} NMR (100 MHz, $CDCl_3$) δ 147.83, 140.39, 126.48, 29.21, 27.53, 13.92, 11.12. Anal. Calcd for $C_{30}H_{56}S_2Sn_2$: C, 50.16; H, 7.86; Found: C, 49.88; H, 7.71.

4-Hexyl-2,6-bis(tributylstannyl)-4*H*-dithieno[3,2-*b*:2',3'-*d*]pyrrole.[17] A solution of 4-hexyl-4*H*-dithieno[3,2-*b*:2',3'-*d*]pyrrole (10.0 g, 38.0 mmol) in dry THF (350 mL) was cooled in an acetone/dry ice bath. After 20 min, *tert*-butyllithium (4.86 g, 75.9 mmol) was added dropwise and the mixture was stirred for 1 h at -78 °C. The reaction was warmed to room temperature for 10 min before cooling to -78 ºC. Tributyltin chloride (30.9 g, 94.9 mmol) was added dropwise and the mixture was allowed to warm to room temperature and stir for 3 h. The reaction mixture was quenched with water, extracted with dichloromethane, washed with saturated brine solution, and dried over anhydrous

sodium sulfate. The combined organic washes were concentrated via rotary evaporation. The crude product was purified by flash chromatography (silica gel prewashed with triethylamine, hexanes). The solvent was removed under reduced pressure and the product was used without further purification (27.3 g, 32.4 mmol, 85% assuming it to be pure). ^{1}H NMR (300 MHz, $CDCl_3$) δ 6.93 (s, 2H), 4.17 (t, *J* = 6.8 Hz, 2H), 1.86 (quint., *J* = 7.2 Hz, 2H), 1.73-1.50 (m, 12H), 1.50-0.98 (m, 30H), 0.98-0.74 (m, 21H).

***N,N'*-Bis(*n*-hexyl)-2-bromonaphthalene-1,4:5,8-bis(dicarboximide).**[14,15] A solution of naphthalene-1,4:5,8-tetracarboxydianhydride (10.0 g, 37.3 mmol) in concentrated sulfuric acid (370 mL) was heated to 85 ºC. Potassium 1,5-dibromo-4,6-dioxo-1,4,5,6-tetrahydro-1,3,5-triazin-2-olate (6.06 g, 18.64 mmol) was dissolved in concentrated sulfuric acid and added via cannula. The mixture was allowed to stir at 85 ºC for 48 h. After cooling, the reaction mixture was poured into ice. The resulting yellow precipitate was collected by filtration, washed with methanol, and dried under vacuum. The yellow solid was transferred to a flask with glacial acetic acid (370 mL) and *n*-hexylamine (15.1 g, 0.149 mol). The reaction mixture was refluxed for 20 min, allowed to cool overnight, and poured into methanol (1500 mL). The resulting precipitate was collected by filtration, washed with methanol, and dried under vacuum. The crude product was purified by column chromatography (silica, dichloromethane) to yield a white solid (2.38 g, 4.64 mmol, 12%). ^{1}H NMR (400 MHz, $CDCl_3$) δ 8.88 (s, 1H), 8.77 (d, *J* = 7.6 Hz, 1H), 8.72 (d, *J* = 7.6 Hz, 1H), 4.16 (t, *J* = 6.9 Hz, 2H), 4.14 (t, *J* = 6.6 Hz, 2H), 1.71 (quint., *J* = 7.1 Hz, 2H), 1.69 (quint., *J* = 7.6 Hz, 2H), 1.45-1.24 (m, 12H), 0.87 (t, *J* = 7.0 Hz, 6H). ^{13}C{^{1}H} NMR (100 MHz, $CDCl_3$) δ 162.40, 161.79, 161.67, 160.99, 138.3, 131.62, 130.67, 128.62, 128.54, 126.79, 125.99, 125.92, 125.64, 123.85, 41.47, 41.09, 31.46, 31.44, 27.93, 27.88, 26.76, 26.67, 22.54, 22.50, 14.02. HRMS (EI) calcd for $C_{26}H_{29}BrN_2O_4$ (M^+), 512.13107; found, 512.1280. Anal. Calcd. for $C_{26}H_{29}BrN_2O_4$: C, 60.82; H, 5.69; N, 5.46. Found: C, 59.91; H, 5.60; N, 5.36.

2,2'-(Thieno[3,2-*b*]thiophene-2,5-diyl)bis(*N,N'*-bis(*n*-hexyl)naphthalene-1,4:5,8-bis(dicarboximide), 3.4a. A solution of *N,N'*-bis(*n*-hexyl)-2-bromonaphthalene-1,4:5,8-bis(dicarboximide) (1.00 g, 1.96 mmol), crude 2,5-bis(tributylstannyl)thieno[3,2-b]thiophene (0.683 g, 0.951 mmol), and copper iodide (0.022 g, 0.117 mmol) in dry toluene (20 mL) was deoxygenated with nitrogen for 5 min. Tetrakis(triphenylphosphine)palladium (0.584 g, 0.506 mmol) was added and the reaction was heated to 90 ºC for 18 h. After cooling, the reaction mixture was diluted with dichloromethane and filtered through a plug of Celite and the filtrate was concentrated via rotary evaporation. The crude product was purified by flash chromatography (silica gel, 2.0% ethyl acetate in chloroform). The product was precipitated from isopropanol and collected as a purple solid (0.257 g, 0.256 mmol, 27%). ^{1}H NMR (300 MHz, $CDCl_3$) δ 8.84 (d, *J* = 7.6 Hz, 2H), 8.79 (s, 2H), 8.77 (d, *J* = 7.4 Hz, 2H), 7.51 (s, 2H), 4.27-4.05 (m, 8H), 1.81-1.63 (m, 8H), 1.50-1.25 (m, 24H), 0.96-0.83 (m, 12H). ^{13}C NMR (100 MHz, $CDCl_3$) δ 162.69, 162.38, 162.36, 161.87, 143.22, 140.91, 140.10, 136.08, 131.51, 130.82, 127.83, 126.87, 126.57, 126.35, 125.30, 123.63, 120.60, 41.22, 41.02, 31.48, 31.46, 28.00, 26.75, 26.70, 22.55, 22.51, 14.00 (two aliphatic resonances not observed due to overlap). HRMS (MALDI) calcd for $C_{58}H_{60}N_4O_8S_2$ (MH^+), 1005.3925; found, 1005.3912. Anal. Calcd. for $C_{58}H_{60}N_4O_8S_2$: C, 69.30; H, 6.02; N, 5.57. Found: C, 69.18; H, 6.06; N 5.48.

2,2'-(Dithieno[3,2-*b*:2',3'-*d*]thiophene-2,6-diyl)bis(*N,N'*-bis(*n*-hexyl)naphthalene-1,4:5,8-bis(dicarboximide), 3.4b. A solution of *N,N'*-bis(*n*-hexyl)-2-bromonaphthalene-1,4:5,8-bis(dicarboximide) (1.50 g, 2.92 mmol), crude 2,6-bis(tributylstannyl)dithieno[3,2-*b*:2',3'-*d*]thiophene[16] (1.08 g, 1.39 mmol), and tri*o*-tolylphosphine (0.085 g, 0.278 mmol) in dry toluene (30 mL) was deoxygenated with nitrogen for 5 min. Tris(dibenzylideneacetone)dipalladium (0.064 g, 0.070 mmol) was added and the reaction was heated to 90 ºC for 1 h. After cooling, the reaction mixture

was precipitated in methanol. The solid was dissolved in chloroform, eluted through a plug of silica gel (dichloromethane:methanol), and concentrated via rotary evaporation. The crude product was purified by column chromatography (silica, 1.0% ethyl acetate in chloroform) followed by precipitation in methanol to yield a purple (0.744 g, 0.701 mmol, 50%). ^{1}H NMR (400 MHz, $CDCl_3$) δ 8.80 (d, *J* = 7.6 Hz, 2H), 8.77 (s, 2H), 8.73 (d, *J* = 7.7 Hz, 2H), 7.52 (s, 2H), 4.17 (t, *J* = 7.4 Hz, 4H), 4.11 (t, *J* = 7.5 Hz, 4H), 1.77-1.60 (m, 8H), 1.46-1.23 (m, 24H), 0.93-0.77 (m, 12H). $^{13}C\{^{1}H\}$ NMR (100 MHz, $CDCl_3$) δ 162.62, 162.34, 162.32, 161.84, 141.91, 141.84, 139.76, 135.98, 132.80, 131.48, 130.74, 127.82, 126.79, 126.48, 126.27, 125.24, 123.45, 121.87, 41,16, 20.95, 31.41, 27.94, 26.70, 26.64, 22.51, 22.46, 13.96 (three aliphatic resonances not observed due to overlap). HRMS (MALDI) calcd for $C_{60}H_{60}N_4O_8S_3$ (MH^+), 1060.3573; found, 1060.3504. Anal. Calcd. for $C_{60}H_{60}N_4O_8S_3$: C, 67.90; H, 5.70; N, 5.28. Found: C, 67.69; H, 5.60; N, 5.26.

2,2'-(4-Hexyl-4*H*-dithieno[3,2-*b*:2',3'-*d*]pyrrole-2,6-diyl)bis(*N,N'*-bis(*n*-hexyl)naphthalene-1,4:5,8-bis(dicarboximide), 3.4c. A solution of *N,N'*-bis(*n*-hexyl)-2-bromonaphthalene-1,4:5,8-bis(dicarboximide) (0.577 g, 1.12 mmol), crude 4-hexyl-2,6-bis(tributylstannyl)-4*H*-dithieno[3,2-*b*:2',3'-*d*]pyrrole (0.450 g, 0.535 mmol), and tri-*o*-tolylphosphine (0.033 g, 0.107 mmol) in dry THF (10 mL) was deoxygenated with nitrogen for 5 min. Tris(dibenzylideneacetone)dipalladium (0.024 g, 0.027 mmol) was added and the reaction was heated to reflux for 18 h. After cooling, the reaction mixture was quenched with water, extracted with chloroform, and dried over anhydrous magnesium sulfate. The combined organic washes were filtered through a plug of silica gel eluting with chloroform and concentrated via rotary evaporation. The crude product was purified by column chromatography (silica, 1% ethylacetate in chloroform) followed by precipitation in *iso*-propanol to yield a dark blue solid (0.355 g, 0.315 mmol, 59%). ^{1}H NMR (400 MHz, $CDCl_3$) δ 8.76 (s, 2H), 8.74 (d, *J* = 7.7 Hz, 2H), 8.65 (d, *J* = 7.7 Hz, 2H),

7.34 (s, 2H), 4.24 (t, *J* = 7.0 Hz, 2H), 4.19-4.06 (m, 8H), 1.96 (quint., *J* = 7.6, 2H), 1.77-1.62 (m, 8H), 1.48-1.20 (m, 30 H), 0.94-0.80 (m, 15H). $^{13}C\{^{1}H\}$ NMR (100 MHz, $CDCl_3$) δ 162.70, 162.54, 162.45, 162.05, 145.52, 141.17, 139.30, 136.28, 131.25, 130.19, 128.12, 126.61, 126.34, 125.78, 124.73, 122.42, 118.34, 112.99, 41.20, 40.94, 31.52, 31.48, 31.47, 30.46, 28.01, 27.99, 26.86, 26.78, 26.70, 22.57, 22.53, 22.51, 14.02 (three aliphatic carbon signals are not observed due to overlapping resonances). HRMS (MALDI) calcd for $C_{66}H_{73}N_5O_8S_2$ (MH^+), 1128.4978; found, 1128.4761. Anal. Calcd. for $C_{66}H_{73}N_5O_8S_2$: C, 70.25; H, 6.52; N, 6.21. Found: C, 69.99; H, 6.45; N, 6.22.

4-Hexyl-2-(tributylstannyl)-4*H*-dithieno[3,2-*b*:2',3'-*d*]pyrrole, 3.5. A solution of 4-hexyl-4*H*-dithieno[3,2-*b*:2',3'-*d*]pyrrole (1.00 g, 3.80 mmol) in dry THF (38 mL) was cooled in an acetone / dry ice bath. After 20 minutes, *tert*-butyllithium (0.243 g, 3.80 mmol) was added dropwise and the mixture was stirred for 2.5 hours at –78 °C. Tributyltinchloride (1.24 g, 3.80 mmol) was added dropwise and the mixture was allowed to warm to room temperature and stir overnight. The reaction mixture was quenched with water, extracted with dichloromethane, and dried over anhydrous sodium sulfate. The combined organic washes were concentrated via rotary evaporation. The crude product was purified by flash chromatography (silica gel prewashed with triethylamine, hexanes). The solvent was removed under reduced pressure and the product was used without further purification (1.34 g, 2.43 mmol, 64 %). ^{1}H NMR (400 MHz, $CDCl_3$) δ 7.24 (s, 1H), 7.07 (d, *J* = 5.3 Hz, 1H), 6.96 (d, *J* = 5.7 Hz, 2H), 4.17 (t, *J* = 7.0 Hz, 2H), 1.85 (quint., *J* = 7.2 Hz, 2H), 1.70-1.46 (m, 6H), 1.40-1.22 (m, 12H), 1.12 (t, *J* = 8.1 Hz, J_{Sn} = 52.2 Hz, 6H), 0.87 (t, *J* = 6.2 Hz, 9H), 0.84 (t, *J* = 7.1 Hz, 3H). $^{13}C\{^{1}H\}$ NMR (100 MHz, $CDCl_3$) δ 147.77, 145.06, 135.27, 122.28, 120.19, 117.96, 114.53, 110.97, 47.38, 31.42, 30.36, 28.98, 27.27, 26.68, 22.51, 14.00, 13.67, 10.90. HRMS (EI) *m/z* $[M]^+$ calcd for $C_{26}H_{43}NS_2Sn$, 553.18589; found, 553.18626. Anal. Calcd for $C_{26}H_{43}NS_2Sn$: C, 56.52; H, 7.85; N, 2.54. Found: C, 56.11; H, 7.66; N, 2.72.

***N,N'*-bis(*n*-hexyl)-2,6-bis(4-hexyl-4*H*-dithieno[3,2-*b*:2',3'-*d*]pyrrol-2-yl) naphthalene-1,8:4,5-bis(dicarboximide), 3.6.** A solution of *N,N'*-bis(*n*-hexyl)-2,6-dibromonaphthalene-1,8:4,5-bis(dicarboximide) (1.00 g, 1.69 mmol), 4-hexyl-2-(tributylstannyl)-4*H*-dithieno[3,2-*b*:2',3'-*d*]pyrrole (1.91 g, 3.46 mmol), and tri*o*-tolylphosphine (0.103 g, 0.338 mmol) in dry THF (33 mL) was degassed with nitrogen for 5 minutes. Tris(dibenzylideneacetone)dipalladium (0.077 g, 0.084 mmol) was added and the reaction was heated to reflux for 18 hours. After cooling, the reaction mixture was diluted with hexanes and filtered through celite. The combined organic washes were concentrated via rotary evaporation. The crude product was purified by column chromatography (silica, 5:1 chloroform:hexanes) followed by recrystallization from isopropanol to yield a dark blue solid (0.913 g, 0.954 mmol, 57%). ^{1}H NMR (400 MHz, $CDCl_3$) δ 8.84 (s, 2H), 7.34 (s, 2H), 7.20 (d, *J* = 5.6 Hz, 2H), 7.00 (d, *J* = 5.6 Hz, 2H), 4.21 (t, *J* = 7.0 Hz, 4H), 4.12 (t, *J* = 7.6 Hz 4H), 1.90 (quint., *J* = 7.3, 4H), 1.69 (quint., *J* = 7.5 Hz, 4H), 1.45-1.20 (m, 24 H), 0.94-0.80 (m, 12H). $^{13}C\{^{1}H\}$ NMR (100 MHz, $CDCl_3$) δ 162.44, 162.30, 145.86, 144.71, 140.58, 137.61, 136.78, 127.47, 124.92, 124.85, 122.07, 118.23, 115.11, 112.94, 110.85, 47.57, 41.19, 31.54, 31.45, 30.39, 28.03, 26.77, 22.53, 14.03 (three aliphatic resonances not observed, presumably due to overlap). HRMS (MALDI) *m/z* $[M]^+$ calcd for $C_{54}H_{60}N_4O_4S_4$, 956.3497; found, 956.3491. Anal. Calcd. for $C_{54}H_{60}N_4O_4S_4$: C, 67.75; H, 6.32; N, 5.85. Found: C, 67.75; H, 6.14; N, 5.86.

3.6 References

(1) Dimitrakopoulos, C.; Malenfant, P. *Adv. Mater.* **2002**, *14*, 99.

(2) Sirringhaus, H.; Ando, M. *MRS Bull.* **2008**, *33*, 676.

(3) Garnier, F.; Hajlaoui, R.; Yassar, A.; Srivastava, P. *Science* **1994**, *265*, 1684.

(4) Murphy, A. R.; Fréchet, J. M. J. *Chem. Rev.* **2007**, *107*, 1066.

(5) Anthony, J. E.; Facchetti, A.; Heeney, M.; Marder, S. R.; Zhan, X. *Adv. Mater.* **2010**, *22*, 3876.

(6) Dong, H.; Wang, C.; Hu, W. *Chem. Commun.* **2010**, *46*, 5211.

(7) Zhan, X.; Facchetti, A.; Barlow, S.; Marks, T. J.; Ratner, M. A.; Wasielewski, M. R.; Marder, S. R. *Adv. Mater.* **2010**, *23*, 268.

(8) Shukla, D.; Nelson, S. F.; Freeman, D. C.; Rajeswaran, M.; Ahearn, W. G.; Meyer, D. M.; Carey, J. T. *Chem. Mater.* **2008**, *20*, 7486.

(9) See, K. C.; Landis, C.; Sarjeant, A.; Katz, H. E. *Chem. Mater.* **2008**, *20*, 3609.

(10) Katz, H.; Lovinger, A.; Johnson, J.; Kloc, C.; Siegrist, T.; Li, W.; Lin, Y.; Dodabalapur, A. *Nature* **2000**, *404*, 478.

(11) Yan, H.; Chen, Z.; Zheng, Y.; Newman, C.; Quinn, J. R.; Dötz, F.; Kastler, M.; Facchetti, A. *Nature* **2009**, *457*, 679.

(12) Gao, X.; Di, C.-A.; Hu, Y.; Yang, X.; Fan, H.; Zhang, F.; Liu, Y.; Li, H.; Zhu, D. *J. Am. Chem. Soc.* **2010**, *132*, 3697.

(13) Zhao, Y.; Di, C.-A.; Gao, X.; Hu, Y.; Guo, Y.; Zhang, L.; Liu, Y.; Wang, J.; Hu, W.; Zhu, D. *Adv. Mater.* **2011**, *23*, 2448.

(14) Chaignon, F.; Falkenstrom, M.; Karlsson, S.; Blart, E.; Odobel, F.; Hammarstrom, L. *Chem. Commun.* **2007**, 64.

(15) Jones, B. A.; Facchetti, A.; Marks, T. J.; Wasielewski, M. R. *Chem. Mater.* **2007**, *19*, 2703.

(16) Zhan, X.; Tan, Z. a.; Domercq, B.; An, Z.; Zhang, X.; Barlow, S.; Li, Y.; Zhu, D.; Kippelen, B.; Marder, S. R. *J. Am. Chem. Soc.* **2007**, *129*, 7246.

(17) Zhang, X.; Steckler, T. T.; Dasari, R. R.; Ohira, S.; Potscavage, W. J.; Tiwari, S. P.; Coppee, S.; Ellinger, S.; Barlow, S.; Brédas, J.-L.; Kippelen, B.; Reynolds, J. R.; Marder, S. R. *J. Mater. Chem.* **2010**, *20*, 123.

(18) Hankache, J.; Wenger, O. S. *Chem. Rev.* **2011**, *111*, 5138.

(19) Robin, M. B.; Day, P. *Adv. Inorg. Chem.* **1968**, *10*, 247.

(20) While the TDDFT vertical transition energies to the first excited states determined with the B3LYP functional are red-shifted with respect to the experiment, those determined with both the CAM-B3LYP and ωB97X functionals are blue-shifted.

(21) Barlow, S.; Odom, S. A.; Lancaster, K.; Getmanenko, Y. A.; Mason, R.; Coropceanu, V.; Brédas, J.-L.; Marder, S. R. *J. Phys. Chem. B* **2010**, *114*, 14397.

(22) Connelly, N.; Geiger, W. *Chem. Rev.* **1996**, *96*, 877.

(23) Bhosale, S. V.; Jani, C. H.; Langford, S. J. *Chem. Soc. Rev.* **2008**, *37*, 331.

(24) Andric, G.; Boas, J. F.; Bond, A. M.; Fallon, G. D.; Ghiggino, K. P.; Hogan, C. F.; Hutchison, J. A.; Lee, M. A. P.; Langford, S. J.; Pilbrow, J. R.; Troup, G. J.; Woodward, C. P. *Aust. J. Chem.* **2004**, *57*, 1011.

(25) Hwang, D. K.; Fuentes-Hernandez, C.; Kim, J.; Potscavage, W. J.; Kim, S.-J.; Kippelen, B. *Adv. Mater.* **2011**, *23*, 1293.

CHAPTER 4

STANNYL DERIVATIVES OF NAPHTHALENE DIIMIDES AND THEIR APPLICATION TO OLIGOMER AND TRIAD SYNTHESIS

4.1 Introduction

Tetracarboxylic diimide derivatives of rylenes, particularly of napthalene and perylene (NDIs and PDIs, respectively), represent one of the most extensively studied classes of functional materials in the field of organic electronics.[1,2] The thermal, chemical, and photochemical stability as well as their high electron affinities and charge-carrier mobilities render these materials attractive for applications in organic field-effect transistors (OFETs)[3-15] and organic photovoltaic cells (OPVs).[12,16-20] They have also been widely used as acceptors in transient absorption studies of photoinduced electron-transfer, again due to their redox potentials, and to the stability and distinctive absorption spectra of the corresponding radical anions.[21-24]

The *N,N′*-substituents of PDIs and NDIs generally only have minimal influence on the optical and electronic properties of isolated molecules, although they can be used to control solubility, aggregation, and intermolecular packing in the solid-state. Core substitution of these species typically has a much more significant effect on the redox potentials (enabling, in some cases, the electron affinities to be brought within a range in which air-stable OFET operation can be achieved[5,13,25]) and optical spectra of these species. Moreover, core substitution can be used as a means of constructing more elaborate architectures such as conjugated polymers[7,11,20,26,27] and donor or acceptor functionalized products.[13,14,28-32]

Functionalized NDIs are most effectively obtained through the selective bromination of naphthalene-1,4:5,8-tetracarboxylic dianhydride (NDA) with dibromoisocyanuric acid (DBI) in concentrated sulfuric acid or oleum, followed by imidization with the primary amine of choice in refluxing acetic acid.[5,27,32] NDA can also be brominated using Br_2 in concentrated sulfuric acid or oleum.[5,33] The brominated NDI can then serve as an intermediate for further functionalization through either nucleophilic substitution to afford amino, thiol or alkoxy substituted derivatives,[31,32] or through palladium-catalyzed coupling reactions to yield cyano,[5,29] phenyl,[28,29] alkynyl[29] and thienyl[11,14,28] functionalized products. However, the range of conjugated species that can be obtained by palladium-catalyzed methods is determined by the availability of appropriate candidate coupling partners. In particular, metallated reagents such as stannanes and boronates can be difficult to obtain for electron-poor (acceptor) building blocks. Accordingly, metallated NDI species would be valuable building blocks for new types of conjugated NDI derivatives in which acceptor groups are directly conjugated to the NDI core.

This chapter describes the synthesis, using palladium-catalyzed coupling[34,35] of brominated NDIs and hexabutylditin, and characterization of the first stannyl derivatives of NDIs and their use as reagents in Stille coupling reactions to obtain bi- and ter-NDIs along with two bis(NDI) derivatives containing electron-poor conjugated bridging groups based on 2,2'-bithiophene.

4.2 Stannyl and Oligomeric Derivatives of Naphthalene Diimides

4.2.1 Synthesis

N,N'-di(*n*-hexyl)-2-tri(*n*-butyl)stannylnaphthalene-1,8:4,5-bis(dicarboximide), **4.3**, and *N,N'*-di(*n*-hexyl)-2,6-bis(tri(*n*-butyl)stannyl)naphthalene-1,8:4,5-bis(dicarboximide), **4.4**, were obtained in good to moderate yields, respectively, according to Scheme 4.1: a mixture of the appropriate mono- or dibromo derivative, **4.1** or **4.2**, and hexabutylditin (1 eq. per bromo substituent) was heated in toluene in the presence of Pd_2dba_3 (0.05 eq. per bromo) and P(*o*-tol)$_3$ (0.2 eq. per bromo substitution). Purification of the reaction products by silica gel chromatography and recrystallization from methanol afforded the mono- and distannyl derivatives as long yellow needles; these compounds were characterized by NMR spectroscopy, mass spectrometry, elemental analysis, and, in the case of **4.4**, X-ray crystal structure (Figure 4.1).[36] The ability to isolate and thoroughly purify the distannyl derivative is important for potential applications in conjugated-polymer syntheses, where the ability to obtain high-molecular-weight material is critically dependent on precise control of monomer stoichiometry.

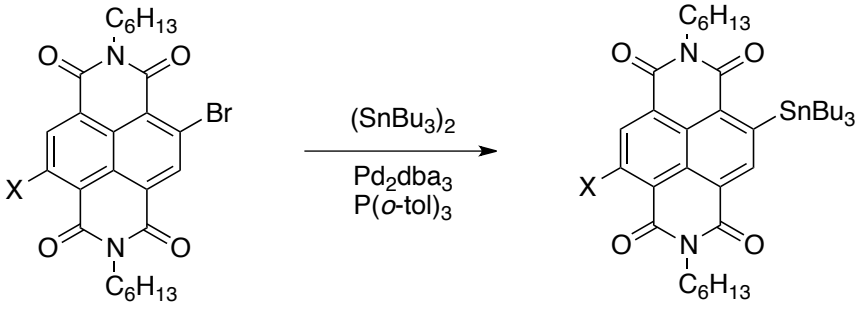

4.1: X = H
4.2: X = Br

4.3: X = H (Yield 90 %)
4.4: X = $SnBu_3$ (Yield 48%)

Scheme 4.1. Preparation of stannyl NDI derivatives.

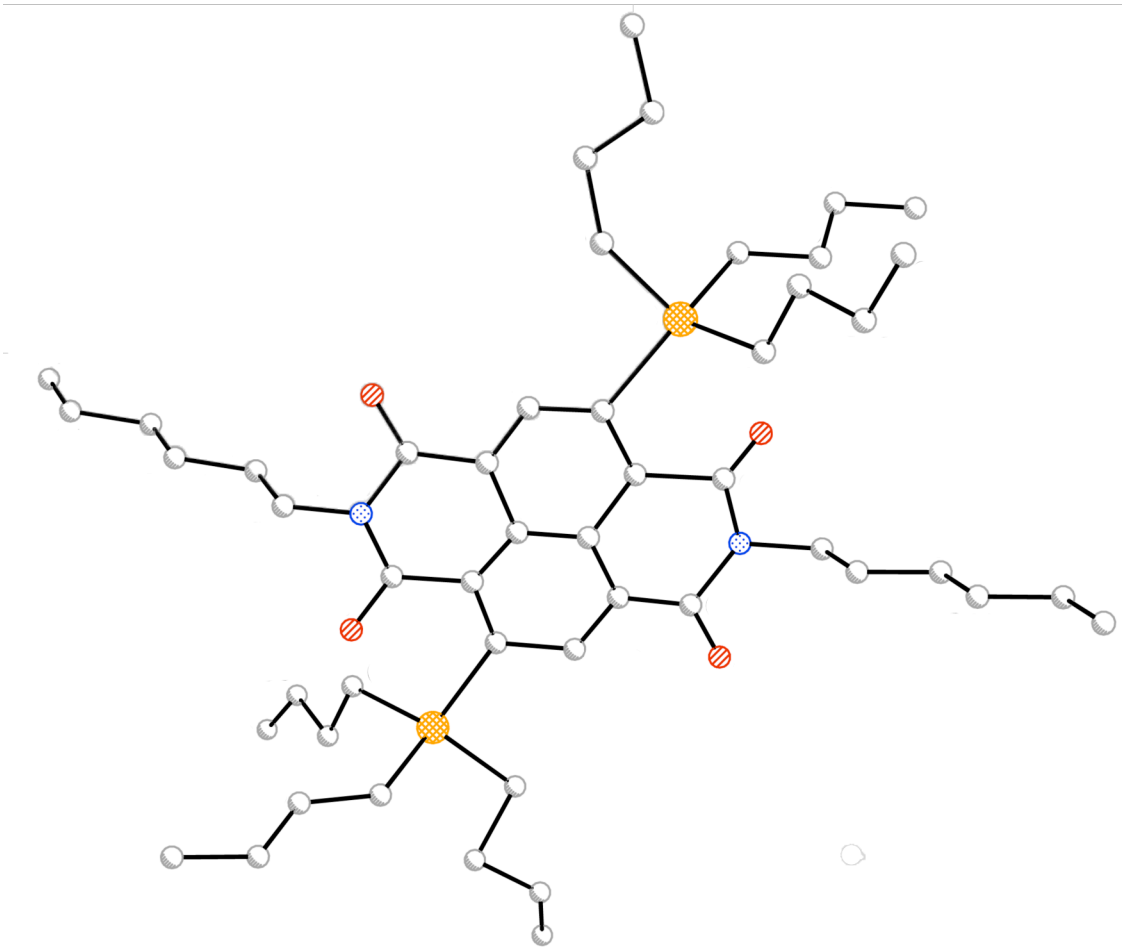

Figure 4.1. Crystal structure of **4.4** for independent molecule B. Hydrogen atoms are omitted for clarity. Atoms are shown as spheres of arbitrary size. More details can be found in Appendix B.

Moreover, the different chromatographic behavior of **4.3** and **4.4** (**4.3**: R_f = 0.3 on silica, eluting with 1:1 dichloromethane / hexanes; **4.4**: R_f = 0.3 on silica, eluting with 1:10 dichloromethane / hexanes) suggested to us the possibility of carrying out this reaction using a mixture of mono- and dibromo species obtained from bromination and imidization of NDA, only purifying at the final stage. This transformation can indeed be carried out without separation of the mono- and difunctionalized intermediates to give isolated yields of mono- and distannyl derivatives of ca. 20% and 5%, respectively. As shown in Scheme 4.2, in addition to **4.3** and **4.4**, their *N,N'*-bis(*n*-dodecyl) analogues **4.5**

and **4.6** have also been obtained in similar isolated yield. The facile separation of the highly soluble mono- and distannyl NDI products via column chromatography is an attractive alternative to the more difficult purification of that of the mono- and dibromo-NDI intermediates, such as **4.1** and **4.2**, which are both less soluble in common organic solvents and less well-differentiated in R_f (0.4 and 0.3 for **4.1** and **4.2** on silica, eluting with dichloromethane). As such, a two-step isolation and purification of the brominated species followed by stannylation results in overall yields with respect to NDA of ca. 9% and 2% for the mono- and distannyl NDI, respectively.

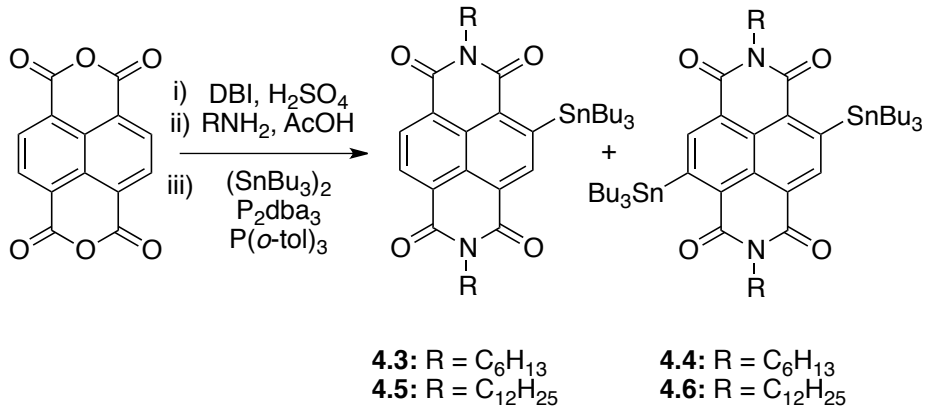

Scheme 4.2. Preparation of stannyl NDI derivatives from commercially available NDA.

As an example of the utility of stannyl NDI derivatives as reagent for cross-coupling with electron-poor moieties, we carried out stannyl-NDI / bromo-NDI cross-couplings to obtain *N,N′,N″,N‴*-tetra(*n*-hexyl)-[2,2'-binaphthalene]-1,8:4,5:1',8':4',5'-tetra(dicarboximide), **4.7**, and *N,N′,N″,N‴,N⁗,N⁗′*-hexa(*n*-hexyl)-[2,2':6',2''-ternaphthalene]-1,8:4,5:1',8':4',5':1'',8'':4'',5''-hexa(dicarboximide) **4.8** (Scheme 4.3). In addition to using the cross-coupling of **4.1** and **4.3** (Scheme 4.3, B), **4.7** was also obtained by the one-pot homo-coupling of **4.1** (Scheme 4.3, A) using 5.0 mol% of $Pd(PPh_3)_4$, 10 mol% of CuI, and 0.5 eq. hexabutylditin in hot toluene over 6 d, a reaction

that presumably involves the in situ generation and reaction of **4.3**. Purification of the reaction mixture by silica-gel chromatography and recrystallization from isopropanol afforded **4.7** in 25% yield. The cross-coupling of **4.1** and **4.3** was performed in the presence of 5.0 mol% of $Pd(PPh_3)_4$ and 10 mol% of CuI in hot toluene over only 3 h and afforded **4.7** in 59% yield after identical purification procedures.

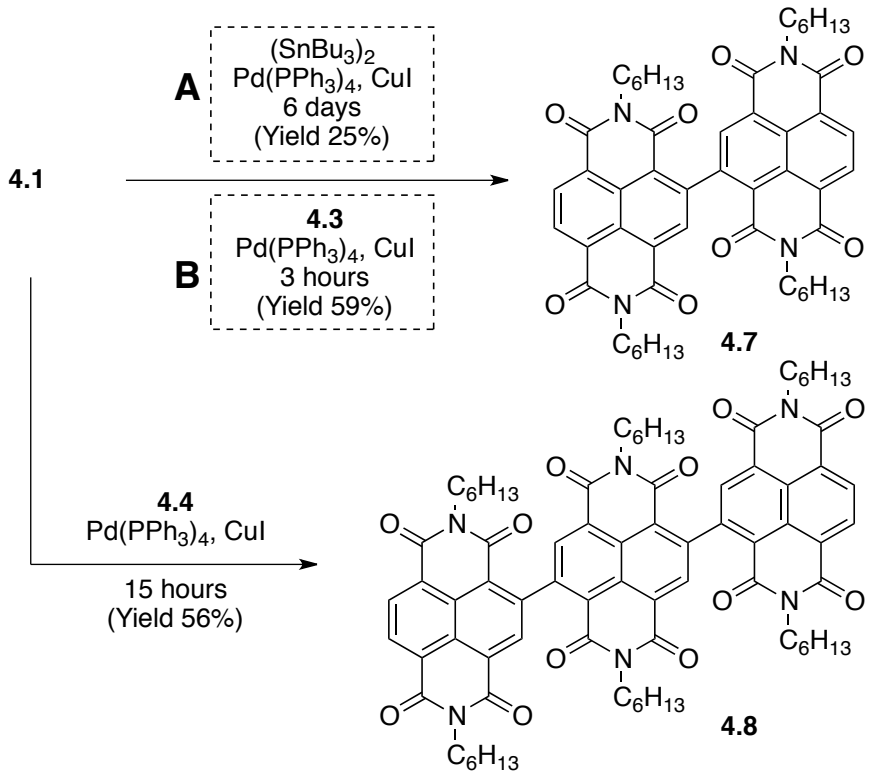

Scheme 4.3. Preparation of bi- and ter-NDI derivatives.

The preparation of **4.8** was performed by cross-coupling of **4.1** and **4.4** in the presence of 5.0 mol% of $Pd(PPh_3)_4$ and 10 mol% of CuI in hot toluene over 15 h. Purification of the reaction mixture by silica-gel chromatography and recrystallization from isopropanol afforded **4.8** in 56% yield.

4.2.2 Optical Properties and Electrochemistry

The optical and electrochemical properties of compounds **4.7** and **4.8** were compared to those of the corresponding monomeric parent NDI, *N,N'*-bis(*n*-hexyl)naphthalene-1,4:5,8-bis(dicarboximide), **4.9**. The UV-vis. absorption spectra of **4.7** and **4.8** are similar in shape to that of **4.9** and the molar absorptivity, ε_{max}, increases with the number of NDI units, suggesting that each NDI sub-unit behaves largely independently of the other(s), consistent with inter-NDI steric interactions leading to significant deviation of the NDI sub-units from coplanarity (Figure 4.2). However, the nonlinear increase of ε_{max} with the degree of oligomerization, some broadening seen in the spectra of **4.7** and **4.8**, and the appearance of a distinct shoulder on the low-energy side of the main absorption of **8** indicates that there are some interactions, possibly excitonic coupling, between the NDI sub-units (differences in band shape are more clearly seen in normalized spectra of **4.7**, **4.8** and **4.9**, Figure 4.3).

Cyclic voltammetry showed four reversible reduction waves for **4.7** and six reversible reduction waves for **4.8** corresponding to the sequential reduction of each NDI to the radical anions and then to dianions (Figure 4.5). No oxidation could be observed in the potential window investigated. The first halfwave reduction potentials are reported in Table 1. **4.7** and **4.8** are reduced at very similar potential to one another and at only marginally more anodic potential than the monomeric NDI, **4.9**, suggesting no significant delocalization of the charge between the NDI units, consistent with the picture of weakly interacting NDIs indicated by the optical data. The slight anodic shift in the oligomeric species is perhaps attributable to the inductive electron-withdrawing effect of one NDI upon another, while the separation between the multiple reductions is likely to be due to electrostatic effects, given the close proximity of the multiple redox centers.

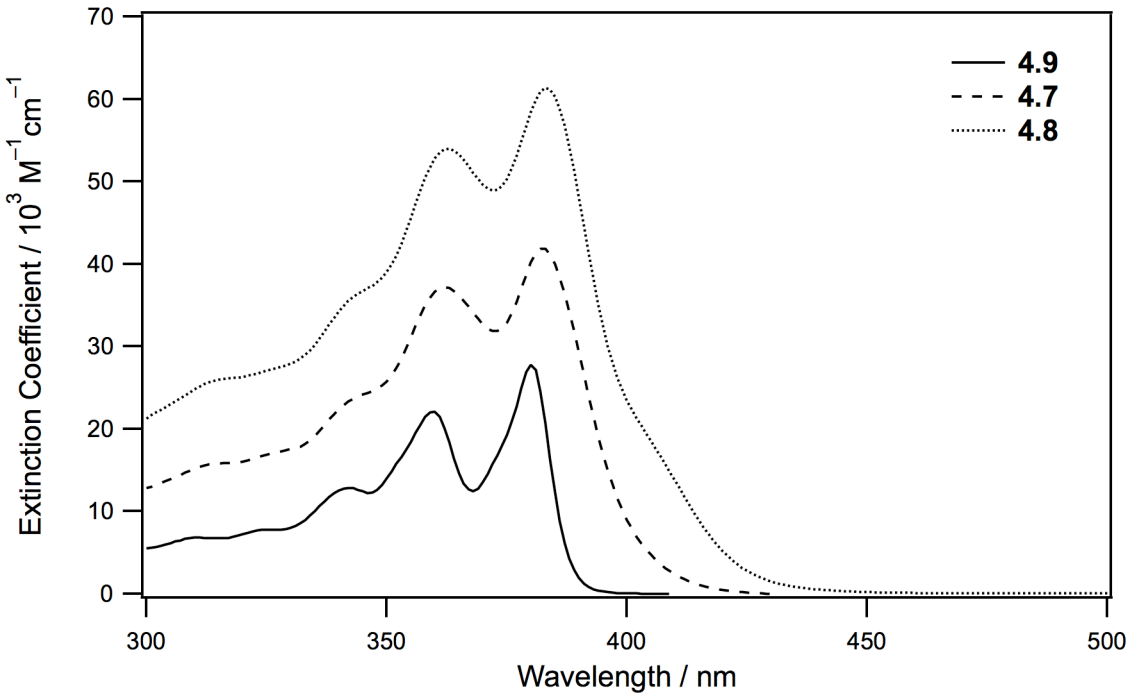

Figure 4.2. UV-vis. spectra in dichloromethane of **4.7**-**4.9**.

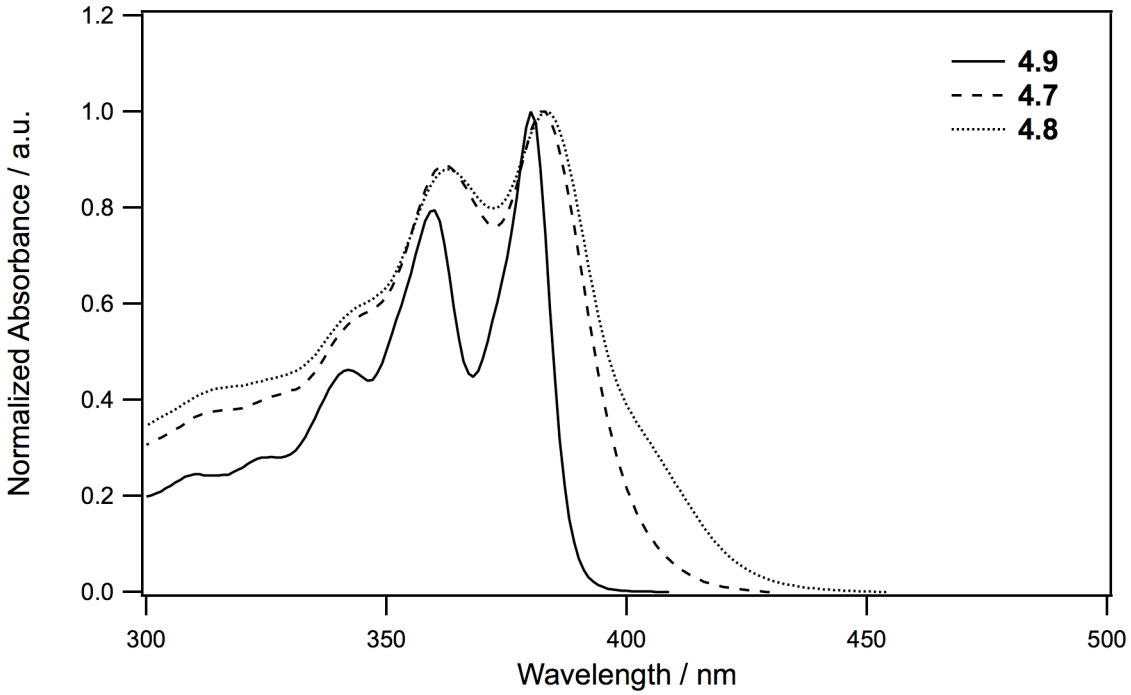

Figure 4.3. Normalized UV-vis. spectra in dichloromethane of **4.7**-**4.9**.

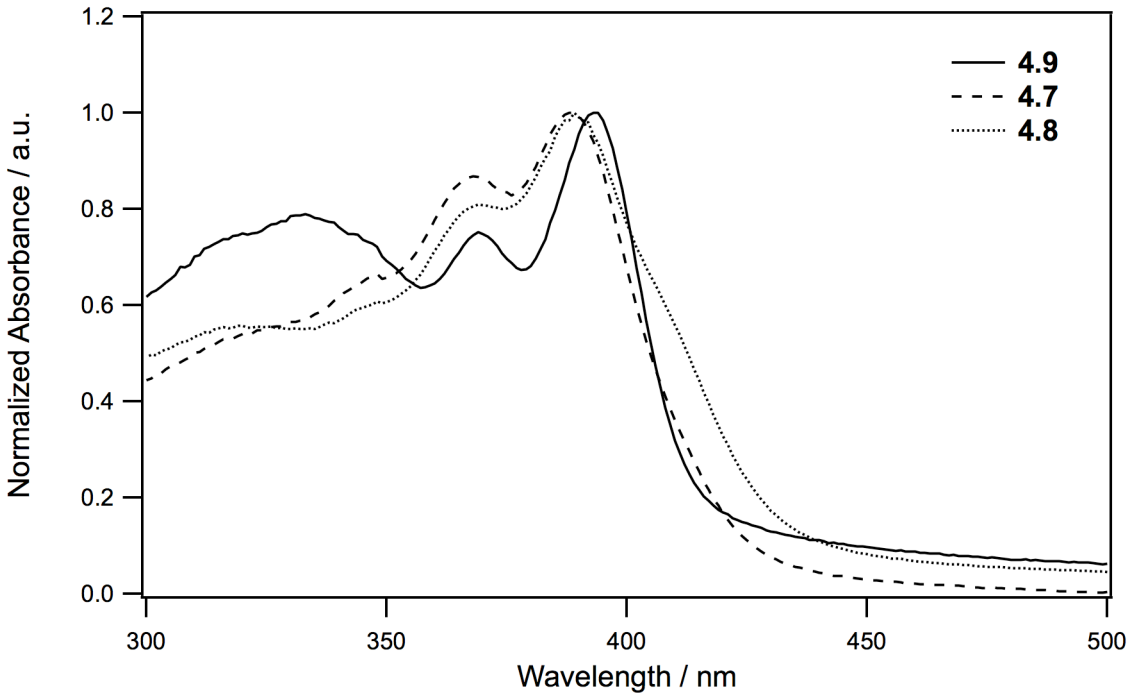

Figure 4.4. Normalized UV-vis. spectra as films on glass of **4.7**-**4.9**.

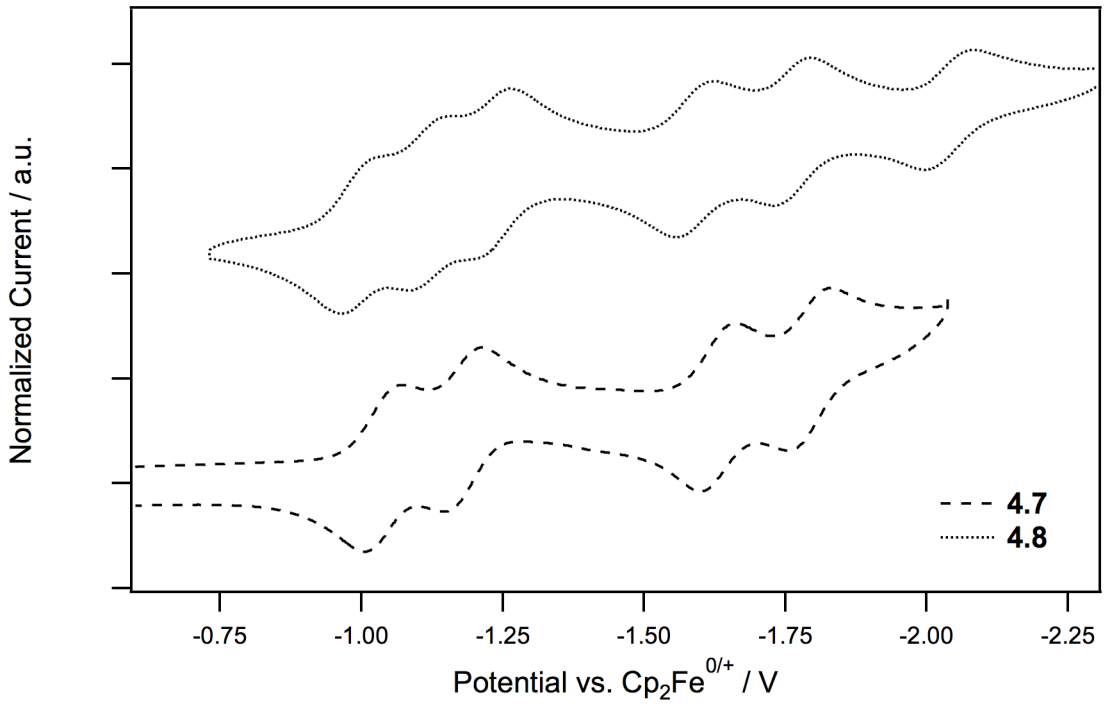

Figure 4.5. Cyclic voltammograms of **4.7** and **4.8** in dichloromethane / $^{n}Bu_4NPF_6$.

Table 4.1. Absorption Maxima (nm) and Absorptivities (10^4 $M^{-1}cm^{-1}$) for the Strong UV-vis. Absorptions of **4.7**-**4.9** in Dichloromethane along with Thin-Film Absorption Maxima and Electrochemical Potentials (V vs. $FeCp_2^{+/0}$).[a] Saturation Electron Mobility Values ($cm^2V^{-1}s^{-1}$), Threshold Voltages (V), and Current On / Off Ratios for OFETs Based on **4.7** and **4.8**.[b]

cmpd	λ_{max}		ε_{max}	$E_{1/2}^{0/-}$	μ_e[a]	V_{TH}	I_{on} / I_{off}
	soln	film					
4.9	380	393	2.76	–1.13	c	c	c
4.7	381	388	4.10	–1.03	0.27 (± 0.04)	7.5 (± 0.5)	10^4
4.8	383	390	6.09	–1.00	0.010 (± 0.004)	12.5 (± 1.2)	10^3

[a]Cyclic Voltammetry in CH_2Cl_2 / 0.1 M $^nBu_4NPF_6$. [b]Average values are calculated based on 6 to 9 devices with W = 2550 and L = 180 μm from a single substrate. [c]Not reported for solution-processed devices.

4.2.3 OFET Behavior

Top-gate, bottom-contact geometry devices were fabricated with a CYTOP / Al_2O_3 bilayer gate dielectric, **4.7** and **4.8** as the active layer and Au source / drain electrodes (Table 4.1). The materials were spin-coated from 1,1',2,2'-tetrachloroethane solutions. OFETs fabricated with **4.7** showed n-channel electrical characteristics with moderate electron mobility values of up to 0.34 $cm^2V^{-1}s^{-1}$, a moderate threshold voltage of 7.9 V and current on / off ratio of 10^4. Devices based on **4.8** also showed n-channel transistor behavior, however with much lower electron mobility values of up to 0.014 $cm^2V^{-1}s^{-1}$, a rather high threshold voltage of 13.1 V and a current on / off ratio of 10^3. No p-channel transistor behavior was observed for either material. Although the mobility value measured for **4.7** is not state of the art for solution-processed n-channel devices (μ_e = 1.5 $cm^2V^{-1}s^{-1}$, Chapter 3), it is an order of magnitude higher than the electron mobility reported for solution-processed devices based on an unsubstituted NDI core (μ_e = 0.01 $cm^2V^{-1}s^{-1}$).[3]

4.3 Bis(Naphthalene Diimide) Derivatives with Electron-Poor Bridging Groups

4.3.1 Synthesis

In addition to the bi- and ter-NDI derivatives described above, two bis(NDI) derivatives containing electron-poor conjugated bridging groups, cyclopenta[2,1-*b*;3,4-b']dithiophen-4-one and benzo[2,1-*b*:3,4-*b'*]dithiophene-4,5-dione, were synthesized. As shown in Scheme 4.4, 2,6-dibromo-cyclopenta[2,1-*b*;3,4-b']dithiophen-4-one **4.11** and 2,7-dibromo-benzo[2,1-*b*:3,4-*b'*]dithiophene-4,5-dione **4.13** were synthesized from their silyl precursors, 2,6-bis(trimethylsilyl)-4H-cyclopenta[2,1-b;3,4-b']dithiophen-4-one **4.10** and 2,7-bis(trimethylsilyl)benzo[1,2-*b*:6,5-*b'*]dithiophene-4,5-dione **4.12**, via simultaneous deprotection / bromination using bromine in dichloromethane. One of the ketone groups in compound **4.13** was protected, using ethylene glycol and 10-camphorsulfonic acid in methanol, to prevent adverse reactions during Stille coupling. Preparation and full characterization of intermediates **4.11** and **4.14** was performed by Yulia Getmanenko in Prof. Seth Marder's research group at Georgia Institute of Technology.[40,41]

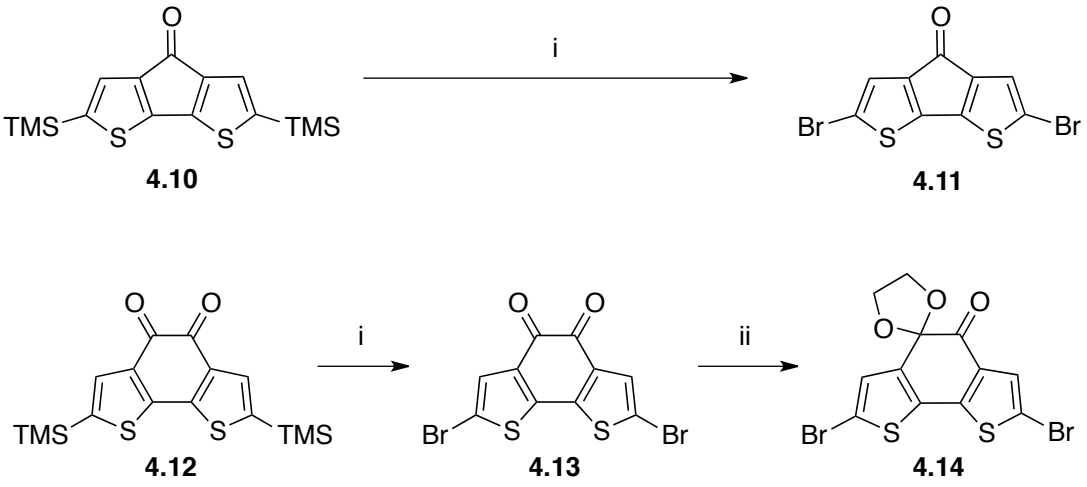

Scheme 4.4. Preparation of ketone-functionalized bithiophene bridges. i) Br_2, dichloromethane; iii) 1,2-ethanediol, 10-camphorsulfonic acid, methanol.

2,2'-(4-Oxo-4*H*-cyclopenta[1,2-*b*:5,4-*b'*]dithiophene-2,6-diyl)bis(2,7-dihexylnaphthalene-1,8:4,5-bis(dicarboximide)**,** **4.15**, and 2,2'-(4,5-dioxo-4,5-dihydrobenzo[1,2-*b*:6,5-*b'*]dithiophene-2,7-diyl)bis(2,7-dihexylnaphthalene-1,8:4,5-bis(dicarboximide), **4.17**, were obtained via copper-mediated Stille coupling of **4.3** with dibromides **4.11** and **4.14**, respectively, to yield **4.15** and the ethylene glycol-protected derivative of **4.17**, 2,2'-(5-oxo-5*H*-spiro[benzo[1,2-*b*:6,5-*b'*]dithiophene-4,2'-[1,3]dioxolane]-2,7-diyl)bis(2,7-dihexylnaphthalene-1,8:4,5-bis(dicarboximide), **4.16**. Compound **4.17** was obtained after deprotection of **4.16** using hydrochloric acid in acetic acid. The final products and intermediates were characterized by ^{1}H and $^{13}C\{^{1}H\}$ NMR spectroscopy, high-resolution mass spectrometry, and elemental analysis.

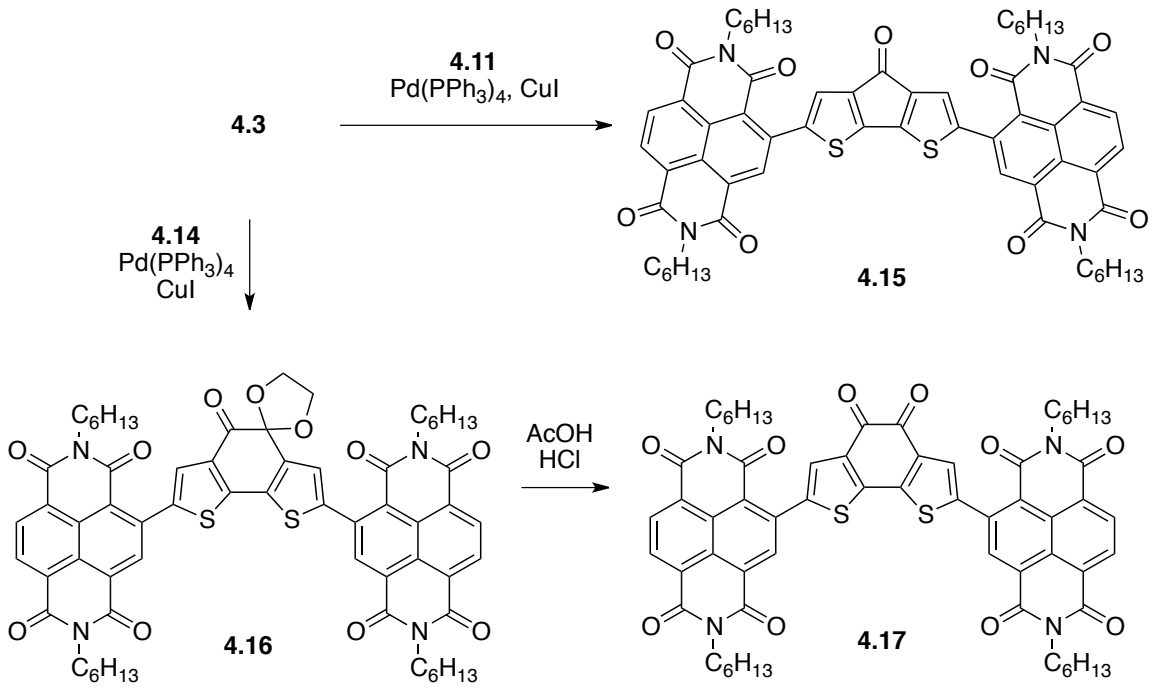

Scheme 4.5. Preparation of electron-poor bridged bis(NDI) derivatives.

4.3.2 Optical Properties and Electrochemistry

Electronic spectra of **4.15** and **4.17** were recorded in dilute chloroform solution and as films on glass substrates. Representative spectra are shown in Figure 4.6 and the corresponding absorption maxima are summarized in Table 4.2. The absorption spectra of **4.15** and **4.17** in solution exhibit two prominent absorption bands: a band at ca. 382 nm and a lower energy band at 568 nm and 497 nm, respectively. The low energy band in **4.15** presumably corresponds to a charge transfer band between the predominantly bithiophene-based HOMO and NDI based LUMO similar to that observed for bis(NDI) derivatives in Chapter 3. The low energy band in **4.17**, on the other hand, is consistent with that observed for the bithiophene-based bridge and is assigned to a HOMO to LUMO electronic excitation of the bridge unit.[40]

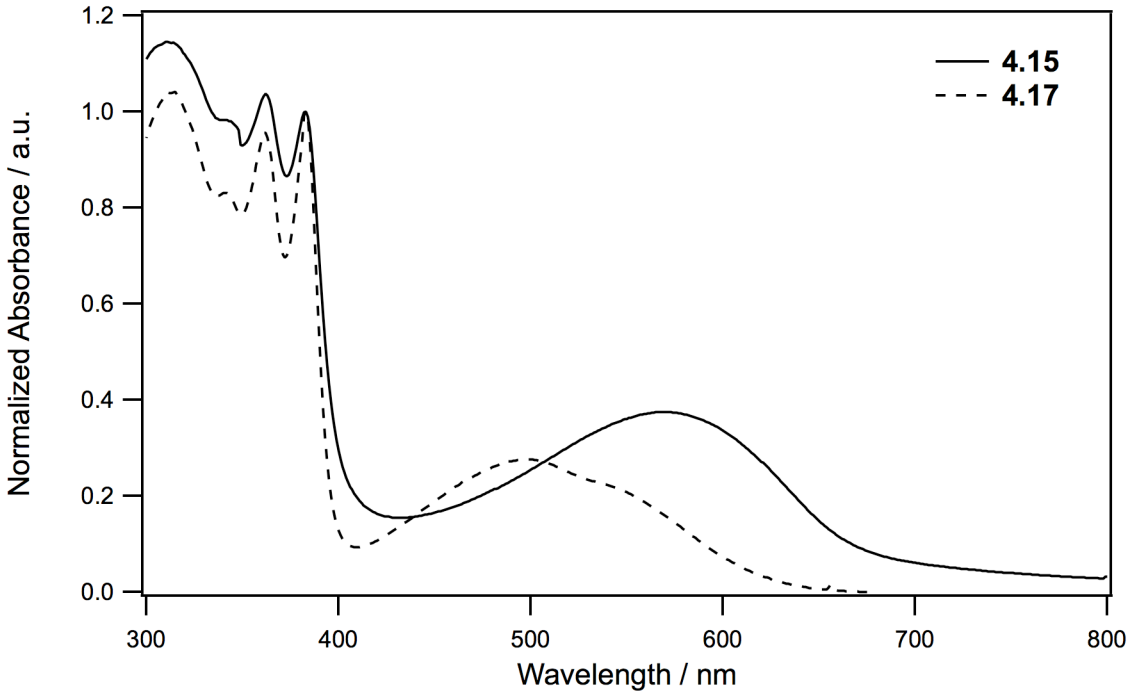

Figure 4.6. Normalized UV-vis. spectra in dichloromethane of **4.15** and **4.17**.

Cyclic voltammetry (CV) was used to measure the electrochemical properties of **4.15** and **4.17** in CH_2Cl_2 / 0.1 M $^nBu_4NPF_6$ (Table 4.2, Figure 4.7). In the case of compound **4.15**, a one-electron reversible oxidation process was observed along with two reversible reduction processes, each with approximately twice the current of that found for the oxidation; these are assigned to essentially independent reduction of both NDIs to their radical anions to give a molecular dianion and then a second reduction of both NDIs to give a tetraanion. The first half-wave oxidation ($E_{1/2}^{+/0}$) potential of **4.15** is similar to that observed for the silyl-functionalized bridge analogue **4.10** ($E_{1/2}^{+/0}$ = +0.96 V)[40] The first half-wave reduction ($E_{1/2}^{0/-}$) potential of **4.15** is very similar to that of an isolated NDI core ($E_{1/2}^{0/-}$ = –1.13 V), consistent with the a predominantly NDI-based LUMO. The negligible shift in the first reduction potential of **4.15** relative to **4.9** is also consistent with that observed in similarly structured bis(NDI) derivatives discussed in Chapter 3.

Compound **4.17**, on the other hand, exhibited four reversible reduction processes. The first three processes are assigned to essentially independent one-electron reduction of the bithophene bridge, one NDI unit and the other NDI unit, respectively. The last process is assigned to an overlap of the second reduction of the bridge and each NDI unit, respectively. These assumptions are supported by differential pulse voltammetry (Figure 4.8). No oxidation could be observed for **4.17** in the potential window investigated. The first half-wave reduction ($E_{1/2}^{0/-}$) potential **4.17** is slightly more positive than the first reduction potential of **4.12**. This shift is perhaps attributable to the inductively withdrawing effect of the NDI substituents on the bithophene-based bridge and is consistent with a similar shift observed for **4.13**, which contains strong inductively withdrawing bromine substitution.[41]

Table 4.2. Absorption Maxima and Absorptivities for the Strong UV-vis. Absorptions of **4.10**, **4.12**, **4.13**, **4.15** and **4.17** in Chloroform along with Thin-Film Absorption Maxima and Electrochemical Potentials (V vs. $FeCp_2^{+/0}$)[a].

cmpd	λ_{max} / nm		ε_{max}	$E_{1/2}^{+/0}$	$E_{1/2}^{0/-}$
	soln	film	/10^4 $M^{-1}cm^{-1}$	/ V	/ V
4.10[40]	282 494	–	5.2 0.17	+0.96	–1.67
4.12[40]	285 501	–	2.6 0.28	c	–1.10
4.13[41]	–	–	–	c	–0.81
4.15	381 568	b	b	+0.94	–1.10[d]
4.17	383 497	385 517	3.49 1.09	c	–0.91

[a]Cyclic Voltammetry in CH_2Cl_2 / 0.1 M $^nBu_4NPF_6$. [b]Not measured due to limited sample quantitiy. [C]Not observed within the electrochemical solvent window. [d]Represents two overlapping transitions ($E_{1/2}^{0/2-}$).

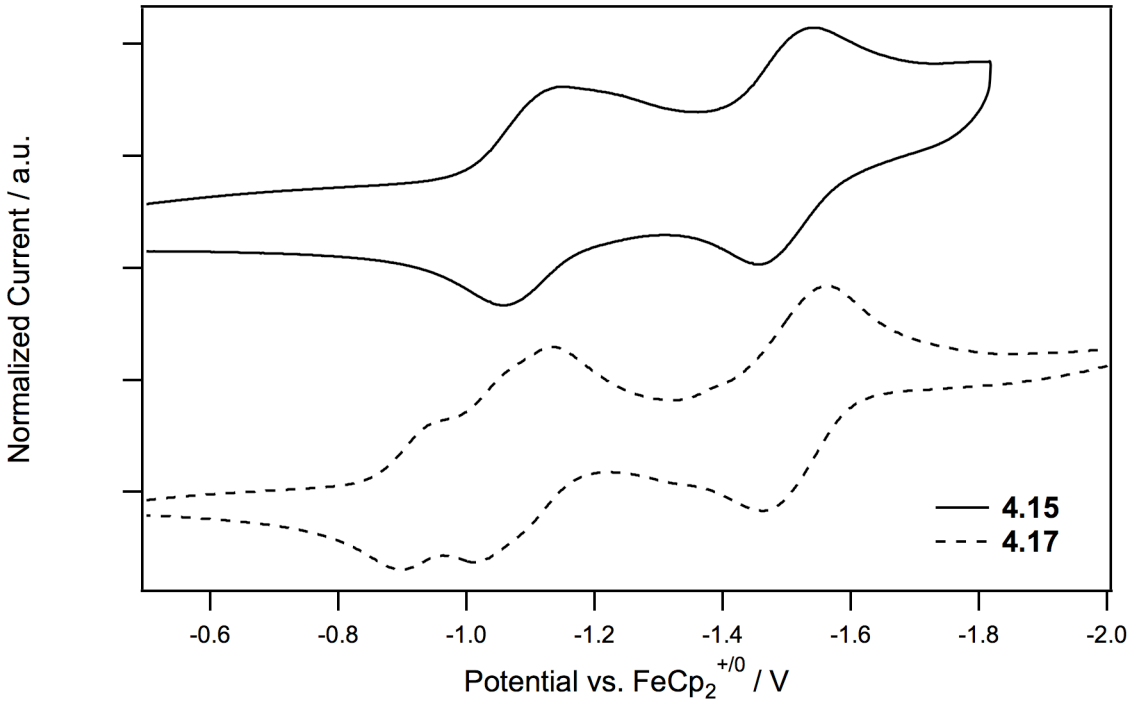

Figure 4.7. Cyclic voltammograms of **4.15** and **4.17** in dichloromethane / $^nBu_4NPF_6$.

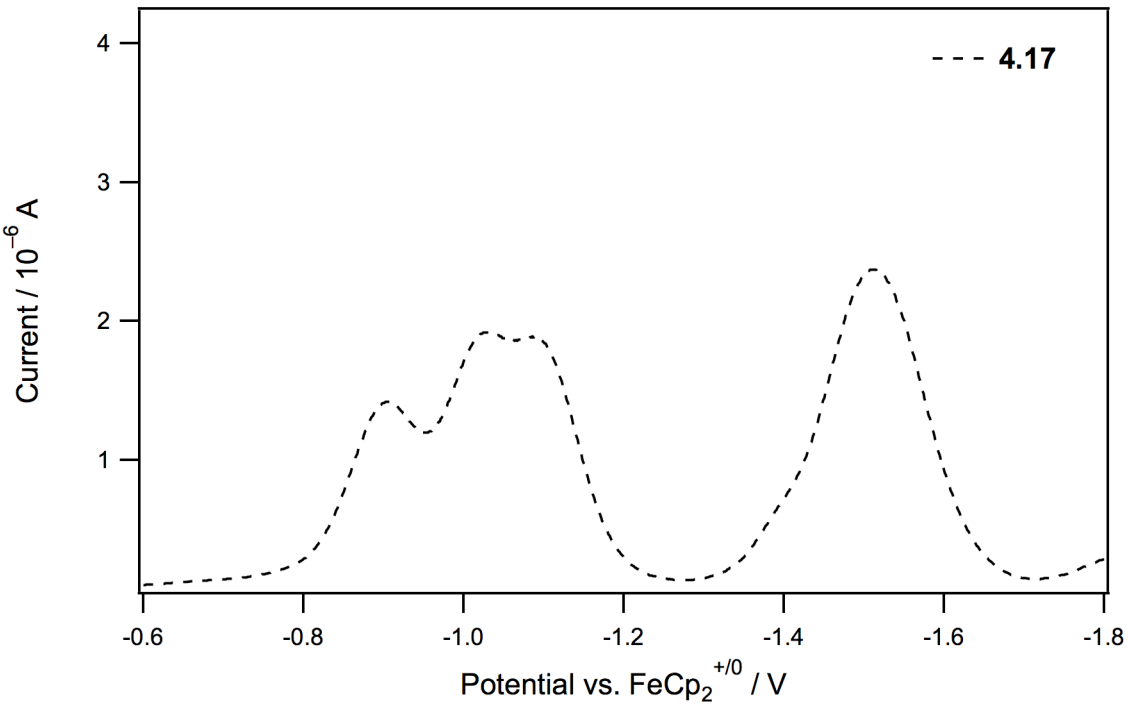

Figure 4.8. Differential Pulse Voltammogram of **4.17** in dichloromethane / $^{n}Bu_4NPF_6$.

4.3.3 OFET Behavior

The electrical properties of the **4.15** and **4.17** were investigated by fabricating top-gate, bottom-contact geometry devices with a CYTOP / Al_2O_3 bilayer gate dielectric and Au source / drain electrodes (Table 4.3). A 1,1',2,2'-tetrachloroethane solution of **4.15** and a 1,2-dichlorobenzene solution of **4.17** was used for spin-coating the active layer. Thin-film transistors fabricated with **4.15** and **4.17** exhibited n-channel mobility values of up to 0.19 and 0.009 $cm^2V^{-1}s^{-1}$, respectively, with moderate threshold voltages of 11.8 V and 8.5 V, respectively, and fairly low current on / off ratios of ca. 10^3. The increased mobility observed for **4.15** is potentially due to the predominantly NDI-based nature of the LUMO; the large, planar NDI cores tend to stack in the solid state potentially leading to improved orbital overlap relative to **4.17**, where the LUMO is largely bridge-based.

Table 4.3. Saturation Electron Mobility Values, Threshold Voltages, and Current On / Off Ratios for OFETs Based on **4.15** and **4.17**.[a]

cmpd	μ_e[a] / $cm^2V^{-1}s^{-1}$	V_{TH} / V	I_{on} / I_{off}
4.15	0.17 (± 0.01)	11.5 (± 0.3)	5×10^3
4.17	0.007 (± 0.002)	8.1 (± 0.4)	2×10^3

[a]Average values are calculated based on 6 to 9 devices with W = 2550 and L = 180 μm from a single substrate.

4.4 Summary

To conclude, this chapter describes an efficient and straightforward method for the synthesis of 2-stannyl and 2,6-distannyl NDIs. The ability of these derivatives to act as reagents in palladium-catalyzed coupling reactions was successfully demonstrated in the synthesis of bi- and ter-NDI (**4.7** and **4.8**) along with two electron-poor bithiophene-bridged bis(NDI) derivatives. Compounds **4.7** and **4.15** were found to exhibit moderate electron mobility values of up to 0.34 and 0.19 $cm^2V^{-1}s^{-1}$, respectively, demonstrating the use of stannyl NDI derivatives in the synthesis of new electronic materials. We expect that these stannyl NDI derivatives will be important building blocks for new small-molecule and polymeric NDIs and may facilitate the synthesis of structures that are otherwise difficult to obtain.

4.5 Experimental

Experimental details describing the general synthesis and characterization methods, X-ray crystal structure measurements, and fabrication of thin-film transistors can be found in Appendix A, B and D, respectively. X-ray crystal structure measurements included in this chapter were performed by Alexander Romanov in Prof.

Tatiana Timofeeva's research group in the Department of Chemistry at New Mexico Highlands University. Transistor fabrication and measurements included in this chapter were performed by either Dr. Do Kyung Hwang (**4.7**, **4.8** and **4.15**) or Dr. Shree Tiwari (**4.17**) in Prof. Bernard Kippelen's research group in the School of Electrical and Computer Engineering at Georgia Institute of Technology.

4.5.1 Synthetic procedures

***N,N'*-Di(*n*-hexyl)-2-bromonaphthalene-1,8:4,5-bis(dicarboximide), 4.1, and *N,N'*-di(*n*-hexyl)-2,6-dibromonaphthalene-1,8:4,5-bis(dicarboximide), 4.2.** A solution of naphthalene-1,8:4,5-tetracarboxydianhydride (NDA) (10.0 g, 37.3 mmol) in concentrated sulfuric acid (370 mL) was heated to 55 ºC. In a separate flask, potassium dibromoisocyanurate (6.06 g, 18.6 mmol) was dissolved in concentrated sulfuric acid (90 mL) while stirring at room temperature for 1 h. Once dissolved, the solution was added to the reaction flask and the mixture was allowed to stir at 85 ºC for 24 h. The mixture was poured into ice water (1 L) and allowed to stir for 2 h, while warming to room temperature. The resulting yellow precipitate was collected by filtration, washed with methanol, and dried under vacuum. The yellow solid was transferred to a flask with glacial acetic acid (380 mL) and *n*-hexylamine (15.1 g, 0.149 mol). The reaction mixture was refluxed for 2 h, allowed to cool overnight, and poured into methanol (1 L). The resulting precipitate was collected by filtration, washed with methanol, and dried under vacuum (11.6 g). The crude product was purified by column chromatography (silica, 3:2 dichloromethane / hexanes). The first band from the column afforded **4.2** as a yellow solid (1.13 g, 1.90 mmol, 5%). The second band gave **4.1** as a white solid (2.38 g, 4.64 mmol, 12%).

Data for **4.1**: ^{1}H NMR (400 MHz, $CDCl_3$) δ 8.88 (s, 1H), 8.77 (d, J = 7.6 Hz, 1H), 8.72 (d, J = 7.6 Hz, 1H), 4.16 (t, J = 6.9 Hz, 2H), 4.14 (t, J = 6.6 Hz, 2H), 1.71 (quint., J = 7.1 Hz,

2H), 1.69 (quint., J = 7.6 Hz, 2H), 1.45-1.24 (m, 12H), 0.87 (t, J = 7.0 Hz, 6H). $^{13}C\{^1H\}$ NMR (100 MHz, $CDCl_3$) δ 162.40, 161.79, 161.67, 160.99, 138.3, 131.62, 130.67, 128.62, 128.54, 126.79, 125.99, 125.92, 125.64, 123.85, 41.47, 41.09, 31.46, 31.44, 27.93, 27.88, 26.76, 26.67, 22.54, 22.50, 14.02 (one aliphatic resonance not observed, presumably due to overlap). HRMS (EI) *m/z* calcd for $C_{26}H_{29}BrN_2O_4$ (M^+), 512.1311; found, 512.1280. Anal. Calcd. for $C_{26}H_{29}BrN_2O_4$: C, 60.82; H, 5.69; N, 5.46. Found: C, 59.91; H, 5.60; N, 5.36.

Data for **4.2**: ^1H NMR (400 MHz, $CDCl_3$): δ 8.98 (s, 2H), 4.17 (t, J = 7.8 Hz, 4H), 1.72 (quint., J = 7.8 Hz, 4H), 1.49-1.20 (m, 12H), 0.88 (t, J = 7.1 Hz, 6H). $^{13}C\{^1H\}$ NMR (100 MHz, $CDCl_3$) δ 160.73, 139.06, 128.96, 128.32, 127.72, 125.34, 124.08, 41.61, 31.45, 27.84, 26.73, 22.54, 14.02. HRMS (EI) *m/z* calcd for $C_{26}H_{28}Br_2N_2O_4$ (M^+), 590.0416; found, 590.0394. Anal. Calcd. for $C_{26}H_{28}Br_2N_2O_4$: C, 52.72; H, 4.76; N, 4.73. Found: C, 52.71; H, 4.69; N, 4.70.

***N,N'*-Di(*n*-hexyl)-2-tri(*n*-butyl)stannylnaphthalene-1,8:4,5-bis(dicarboximide), 4.3, from 4.1.** A solution of **4.1** (1.45 g, 2.82 mmol), 1,1,1,2,2,2-hexabutyldistannane (1.64 g, 2.82 mmol), and tri-*o*-tolylphosphine (0.172 g, 0.565 mmol) in dry toluene (30 mL) was deoxygenated with nitrogen for 5 min. Tris(dibenzylideneacetone)dipalladium (0.129 g, 0.141 mmol) was added and the reaction was heated to 90 ºC for 24 h. After cooling, the reaction mixture was precipitated in methanol (100 mL), the solid was removed via filtration, and the solvent was removed under reduced pressure. The crude product was purified by column chromatography (silica, dichloromethane) to yield a yellow solid (1.53 g, 2.11 mmol, 75%). ^1H NMR (400 MHz, $CDCl_3$) δ 8.94 (s, 1H), 8.70 (d, J = 7.6 Hz, 1H), 8.67 (d, J = 7.6 Hz, 1H), 4.18 (t, J = 7.6 Hz, 2H), 4.16 (t, J = 8.0 Hz, 2H), 1.75-1.64 (m, 4H), 1.55-1.45 (m, 6H), 1.40-1.23 (m, 18H), 1.19 (t, J = 8.2 Hz, 6H), 0.90-0.80 (m, 15H). $^{13}C\{^1H\}$ NMR (100 MHz, $CDCl_3$) δ 164.91, 163.62, 163.12, 163.04, 156.00, 138.65, 131.67,

130.24, 130.13, 126.84, 126.72, 126.70, 125.98, 123.64, 53.40, 41.00, 40.91, 31.50, 29.20, 28.25, 28.07, 28.02, 27.39, 26.76, 26.65, 22.54, 22.48, 17.27, 14.02, 13.69, 13.58, 11.58. HRMS (MALDI) *m/z* calcd for $C_{38}H_{56}N_2O_4Sn$ (M^+), 725.3340; found, 725.3325. Anal. Calcd. for $C_{38}H_{56}N_2O_4Sn$: C, 63.08; H, 7.80; N, 3.87. Found: C, 62.81; H, 7.99; N, 3.93.

***N,N'*-Di(*n*-hexyl)-2,6-bis(tri(n-butyl)stannyl)naphthalene-1,8:4,5-bis(dicarboximide), 4.4, from 4.2.** A solution of **4.2** (0.500 g, 0.844 mmol), 1,1,1,2,2,2-hexabutyldistannane (1.00 g, 1.73 mmol), and tri*o*-tolylphosphine (0.051 g, 0.169 mmol) in dry toluene (10 mL) was deoxygenated with nitrogen for 5 min. Tris(dibenzylideneacetone)dipalladium (0.039 g, 0.042 mmol) was added and the reaction was heated to 90 ºC for 24 h. Additional portions of tri-*o*-tolylphosphine (0.051 g, 0.169 mmol) and tris(dibenzylideneacetone)dipalladium (0.039 g, 0.042 mmol) were added and the reaction was stirred at 90 ºC for an additional 2 d. After cooling, the reaction mixture was filtered through a plug of silica gel eluting with chloroform / hexanes (1:1) and the solvent was removed under reduced pressure. The crude product was recrystallized from methanol to yield a yellow solid (0.407 g, 0.402 mmol, 48%). ^{1}H NMR (400 MHz, $CDCl_3$) δ 8.92 (s, 2H), 4.18 (t, J = 7.4 Hz, 4H), 1.68 (quint., J = 7.5 Hz, 4H), 1.53-1.46 (m, 12H), 1.45-1.36 (m, 4H), 1.35-1.25 (m, 20H), 1.23-1.09 (m, 12H), 0.90-0.80 (m, 24H). ^{13}C{^{1}H} NMR (100 MHz, $CDCl_3$) δ 165.12, 163.82, 154.61, 138.04, 131.84, 126.90, 123.11, 40.92, 31.53, 29.22, 28.08, 27.39, 26.69, 22.49, 14.02, 13.69, 11.54. MS (MALDI) *m/z* 898.3 (M-$(C_4H_9)_2^+$). Anal. Calcd. for $C_{50}H_{82}N_5O_4Sn_2$: C, 59.31; H, 8.16; N, 2.77. Found: C, 59.30; H, 7.98; N, 2.83.

4.3 and 4.4 from naphthalene-1,8:4,5-tetracarboxydianhydride. A solution of naphthalene-1,8:4,5-tetracarboxydianhydride (NDA) (5.00 g, 18.6 mmol) in concentrated sulfuric acid (180 mL) was heated to 55 ºC. In a separate flask, potassium dibromoisocyanurate (6.06 g, 18.6 mmol) was dissolved in concentrated sulfuric acid (90

mL) while stirring at room temperature for 1 h. Once dissolved, the solution was added to the reaction flask and the mixture was allowed to stir at 85 ºC for 48 h. The mixture was poured into ice water (1 L) and allowed to stir for 2 h, while warming to room temperature. The resulting yellow precipitate was collected by filtration, washed with methanol, and dried under vacuum (4.51 g). The yellow solid was transferred to a flask with glacial acetic acid (100 mL) and *n*-hexylamine (7.2 g, 71.1 mmol). The reaction mixture was refluxed for 2 h, allowed to cool overnight, and poured into methanol (1 L). The resulting precipitate was collected by filtration, washed with methanol, and dried under vacuum (5.51 g). The orange solid was transferred to a dry Schlenk flask with 1,1,1,2,2,2-hexabutyldistannane (11.3 g, 19.5 mmol), tri-*o*-tolylphosphine (1.13 g, 3.71 mmol) and tris(dibenzylideneacetone)dipalladium (0.850 g, 0.930 mmol). The flask was pump-filled three times with nitrogen. Anhydrous toluene (80 mL) was added and the reaction was heated to 100 ºC for 18 h. After cooling, the reaction mixture was diluted with hexanes (100 mL) and filtered through a plug of silica gel eluting with hexanes. Dichloromethane / hexanes (1:1) was used to elute the first yellow band (impure **4.4**). The second yellow band was collected using dichloromethane as an eluent and was evaporated to give **4.3** as a yellow solid (2.60 g, 3.59 mmol, 19% overall yield from NDA). The first fraction was further purified by column chromatography (silica gel, 10:1 hexanes / dichloromethane) to yield **4.4** a yellow solid (0.780 g, 0.770 mmol, 4% from NDA). ^{1}H NMR data were consistent with those obtained for **4.3** and **4.4** synthesized from **4.1** and **4.2**, respectively.

***N,N'*-Di(*n*-dodecyl)-2-tri(*n*-butyl)stannylnaphthalene-1,8:4,5-bis(dicarboximide), 4.5, and *N,N'*-di(*n*-dodecyl)-2,6-bis(tri(*n*-butyl)stannyl)naphthalene-1,8:4,5-bis(dicarboximide), 4.6, from naphthalene-1,8:4,5-tetracarboxydianhydride.** A solution of NDA (5.00 g, 18.6 mmol) in concentrated sulfuric acid (180 mL) was heated to 55 ºC. In a separate flask, potassium

dibromoisocyanurate (6.06 g, 18.6 mmol) was dissolved in concentrated sulfuric acid (90 mL) while stirring at room temperature for 1 h. Once dissolved, the solution was added to the reaction flask and the mixture was allowed to stir at 85 ºC for 48 h. The mixture was poured into ice water (1 L) and stirred for 2 h, while allowing to warm to room temperature. The resulting yellow precipitate was collected by filtration, washed with methanol, and dried under vacuum (8.33 g). The yellow solid was transferred to a flask with glacial acetic acid (190 mL) and *n*-dodecylamine (14.2 g, 76.4 mmol). The reaction mixture was refluxed for 2 h, allowed to cool overnight, and poured into methanol (1 L). The resulting precipitate was collected by filtration, washed with methanol, and dried under vacuum. The resultant orange solid (10.0 g) was transferred to a dry schlenk flask with 1,1,1,2,2,2-hexabutyldistannane (16.0 g, 27.6 mmol), tri-*o*-tolylphosphine (1.60 g, 5.26 mmol) and tris(dibenzylideneacetone)dipalladium (1.20 g, 1.31 mmol). The flask was pump-filled three times with nitrogen. Anhydrous toluene (60 mL) was added and the reaction was heated to 90 ºC for 24 h. After cooling, the reaction mixture was diluted with hexanes, filtered through a plug of Celite, and the solvent was removed under reduced pressure. The crude product was purified by column chromatography (silica gel): the first band was eluted using hexanes / dichloromethane (10:1) and, on evaporation, gave a yellow oil (impure **4.6**). The second band was eluted using hexanes / dichloromethane (1:1) and was evaporated to give **4.5** as a yellow solid (3.87 g, 4.34 mmol, 23% overall yield from NDA). The first yellow fraction was further purified by column chromatography (silica gel, 10:1 hexanes / toluene) to yield pure **4.6** as a yellow oil (1.25 g, 1.06 mmol, 6% overall yield from NDA).

Data for **4.5**: ^{1}H NMR (400 MHz, $CDCl_3$) δ 8.95 (s, 1H), 8.70 (d, J = 7.6 Hz, 1H), 8.67 (d, J = 7.7 Hz, 1H), 4.18 (m, 4H), 1.78-1.64 (m, 4H), 1.58-1.45 (m, 6H), 1.40-1.15 (m, 48 H), 0.90-0.82 (m, 15H). $^{13}C\{^{1}H\}$ NMR (100 MHz, $CDCl_3$) δ 164.90, 163.60, 163.09, 163.02, 155.98, 138.63, 131.65, 130.22, 130.12, 126.82, 126.71, 126.69, 125.96, 123.62, 40.98,

40.91, 31.89, 31.57, 28.61, 28.52, 29.48, 29.33, 29.20, 29.10,28.12, 28.06, 27.39, 27.11, 26.99, 22.67, 14.09, 13.70, 11.57 (five aliphatic resonances not observed, presumably due to overlap). MS (MALDI) *m/z* 893.5 (7 %, M^+), 835.4 (100 %, M-$(C_4H_9)^+$). Anal. Calcd. for $C_{50}H_{80}N_2O_4Sn$: C, 67.33; H, 9.04; N, 3.14. Found: C, 67.40; H, 9.03; N, 3.13.

Data for **4.6**: ^{1}H NMR (300 MHz, $CDCl_3$) δ 8.93 (s, 2H), 4.19 (t, *J* = 7.2 Hz, 4H), 1.71 (quint., *J* = 7.3 Hz, 4H), 1.53-1.46 (m, 12H), 1.57-1.42 (m, 12H), 1.42-1.02 (m, 60H), 0.94-0.76 (m, 24H). $^{13}C\{^1H\}$ NMR (75 MHz, $CDCl_3$) δ 165.11, 163.82, 154.60, 138.04, 131.84, 126.89, 123.10, 40.93, 31.90, 29.64, 29.62, 29.50, 29.38, 29.34, 29.23, 28.12, 27.41, 27.04, 22.67, 14.10, 13.72, 11.52 (one aliphatic resonance not observed, presumably due to overlap). MS (MALDI) *m/z* 1066.4 (M-$(C_4H_9)_2^+$). Anal. Calcd. for $C_{62}H_{106}N_2O_4Sn_2$: C, 63.06; H, 9.05; N, 2.37. Found: C, 62.87; H, 9.09; N, 2.32.

***N,N',N'',N'''*-Tetra(*n*-hexyl)-[2,2'-binaphthalene]-1,8:4,5:1',8':4',5'-tetra(dicarboximide), 4.7, from homocoupling of 4.1.** A solution of **4.1** (1.00 g, 1.95 mmol), 1,1,1,2,2,2-hexabutyldistannane (0.551 g, 0.950 mmol), and copper(I) iodide (0.018 g, 0.095 mmol) in dry toluene (20 mL) was heated to 50 ºC to dissolve the reagents and deoxygenated with nitrogen for 5 min. Tetrakis(triphenylphosphine)palladium (0.055 g, 0.048 mmol) was added and the reaction was heated to 90 ºC for 6 d while monitoring by TLC. After cooling, the reaction mixture was diluted with dichloromethane, filtered through a plug of Celite, and the solvent was removed under reduced pressure. The crude product was purified by column chromatography (silica, dichloromethane) followed by precipitation in methanol to yield a yellow solid (0.202 g, 0.233 mmol, 25%). ^{1}H NMR (400 MHz, $CDCl_3$) δ 8.83 (d, *J* = 7.6 Hz, 2H), 8.79 (d, *J* = 7.6 Hz, 2H), 8,43 (s, 2H), 4.17 (t, *J* = 7.6 Hz, 4H), 3.95-3.90 (m, 4H), 1.72 (quint., *J* = 7.6, 4H), 1.59-1.48 (m, 4H), 1.48-1.35 (m, 4H), 1.35-1.27 (m, 8H), 1.27-1.13 (m, 12H), 0.87 (t, *J* = 6.9 Hz, 6H), 0.78 (t, *J* = 6.6 Hz, 6H). $^{13}C\{^1H\}$ NMR (100 MHz, $CDCl_3$) δ 162.76, 162.74, 162.51, 146.38, 132.28, 131.61, 130.86, 127.44,

126.80, 126.36, 126.15, 122.41, 41.03, 41.96, 31.46, 31.37, 27.99, 27.86, 26.70, 26.62, 22.50, 22.48, 14.01, 13.92 (one C=O and one aromatic resonance not observed, presumably due to overlap). HRMS (MALDI) *m/z* calcd for $C_{52}H_{59}N_4O_8$ (MH^+), 867.4333; found, 867.4349. Anal. Calcd. for $C_{52}H_{58}N_4O_8$: C, 72.03; H, 6.74; N, 6.46. Found: C, 71.77; H, 6.71; N, 6.43.

4.7 from cross-coupling of 4.1 and 4.3. A solution of **4.1** (0.071 g, 0.138 mmol), **4.3** (0.095 g, 0.131 mmol), and copper(II) iodide (0.002 g, 0.013 mmol) in dry toluene (5 mL) was heated to 50 ºC to dissolve the reagents and deoxygnated with nitrogen for 5 min. Tetrakis(triphenylphosphine)palladium (0.008 g, 0.007 mmol) was added and the reaction was heated to 90 ºC for 3 h while monitoring by TLC. After cooling, the reaction mixture was diluted with dichloromethane, filtered through a plug of Celite, and the solvent was removed under reduced pressure. The crude product was purified by column chromatography (silica, dichloromethane) followed by recrystallization from isopropanol to yield **7** as a yellow solid (0.067 g, 0.077 mmol, 59%). The ^{1}H NMR spectrum was consistent with that obtained for **4.7** synthesized by the homocoupling of **4.3**.

***N,N',N'',N''',N'''',N'''''*-Hexa(*n*-hexyl)-[2,2':6',2''-ternaphthalene]-1,8:4,5:1',8':4',5':1'',8'':4'',5''-hexa(dicarboximide), 4.8.** A solution of **4.1** (0.958 g, 1.87 mmol), **4.4** (0.900 g, 0.889 mmol), and copper(I) iodide (0.034 g, 0.178 mmol) in dry toluene (10 mL) was deoxygenated with nitrogen for 5 min. Tetrakis(triphenylphosphine)palladium (0.102 g, 0.088 mmol) was added and the reaction was heated to 90 ºC for 26 h while monitoring by TLC. After cooling, the reaction mixture was diluted with dichloromethane, filtered through a plug of Celite, and the solvent was removed under reduced pressure. The crude product was purified by column chromatography (silica, dichloromethane to 3% methanol in dichloromethane) followed by recrystallization from isopropanol to yield **4.8** as a yellow solid (0.644 g,

0.496 mmol, 56%). ^{1}H NMR (400 MHz, $CDCl_3$) δ 8.86 (d, J = 7.6 Hz, 2H), 8.81 (d, J = 7.6 Hz, 2H), 8.53 (d, J = 2.0 Hz, 2H), 8.46 (d, J = 3.7 Hz, 2H), 4.20 (t, J = 7.4 Hz, 4H), 4.45-3.88 (m, 8H), 1.85-1.69 (m, 4H), 1.67-1.55 (m, 8H), 1.48-1.40 (m, 4H), 1.38-1.30 (m, 8H), 1.30-1.15 (m, 24H), 0.87 (t, J = 7.1 Hz, 6H), 0.87-0.70 (m, 12H). ^{13}C{^{1}H} NMR (100 MHz, $CDCl_3$) δ 162.81, 162.79, 162.77, 162.56, 162.49, 162.25, 146.34, 146.30, 132.92, 132.21, 131.68, 130.93, 127.48, 127.16, 126.86, 126.82, 126.43, 126.37, 126.28, 122.70, 122.46, 41.11, 41.02, 31.51, 31.42, 31.29, 28.05, 27.90, 28.87, 26.77, 26.73, 26.67, 26.63, 22.56, 22.52, 22.50, 14.05, 13.98, 13.95. HRMS (MALDI) *m/z* calcd for $C_{78}H_{87}N_6O_{12}$ (MH^+), 1299.6391; found, 1299.6382. Anal. Calcd. for $C_{78}H_{86}N_6O_{12}$: C, 72.09; H, 6.67; N, 6.47. Found: C, 71.84; H, 6.56; N, 6.37.

2,6-Dibromo-cyclopenta[2,1-*b*;3,4-b']dithiophen-4-one, 4.11 (performed by Yulia Getmanenko).[41] 2,6-Bis-trimethylsilyl-cyclopenta[2,1-*b*;3,4-*b*']dithiophen-4-one[40] (3.0 mmol, 1.01 g) was dissolved in 20 mL of dichloromethane, cooled in ice-water bath and a solution of bromine (2.1 eq., 6.3 mmol, 1.01 g) in 10 mL of dichloromethane was added to a dark red solution. The reaction mixture became purple in color and after stirring for about 0.5 h it was allowed to warm to room temperature. Aqueous solution of $Na_2S_2O_3$ was added and organic solvent was removed by rotary evaporation. The dark purple solid was filtered off, washed with ethanol and dried. Crude product was obtained in 92% yield (0.96 g). This material was purified by column chromatography (150 mL of silica gel, CH_2Cl_2 as eluant; material was dissolved in boiling chloroform to apply to the column). Fractions with pure material were combined, the solvent was removed and product 2,6-dibromo-cyclopenta[2,1-*b*;3,4-*b*']dithiophen-4-one was obtained as dark purple solid. ^{1}H NMR ($CDCl_3$, 400 MHz): δ 7.00 (s, 2H). ^{13}C{^{1}H} NMR ($CDCl_3$, 100 MHz) δ 180.52, 148.72, 139.54, 124.43, 113.97. Anal. Calc. for $C_9H_2Br_2OS_2$: C, 30.88; H, 0.58. Found: C, 30.87; H, 0.47.

2,7-Dibromo-benzo[2,1-*b*:3,4-*b'*]dithiophene-4,5-dione, 4.13 (performed by Yulia Getmanenko).[41] 2,7-Bis-trimethylsilyl-benzo[2,1-*b*:3,4-*b'*]dithiophene-4,5-dione[40] (4.0 mmol, 1.46 g) was dissolved in dichloromethane (40 mL) and bromine (2.2 eq., 8.8 mmol, 1.41 g) was added dropwise to a red-black solution. The reaction mixture became purple-black. The reaction mixture was analyzed by TLC (CH_2Cl_2 as eluant), and a new product and a minor impurity was detected. Additional amount of bromine (0.33 g) was added, the mixture was stirred for 0.5 h and treated with 10 ml of aqueous $Na_2S_2O_3$. The organic solvent was removed by rotary evaporation and the crude product was separated by vacuum filtration (1.95 g). This crude material was purified by column chromatography (300 ml of silica gel, CH_2Cl_2 as eluant). The solvent was removed from the combined fractions, and very dark shiny microcrystalline material was obtained (0.90 g, 60% yield). The heavily stained column was eluted with chloroform, the solvent was removed from the combined fractions and additional amount of product was obtained as very dark microcrystalline solid (0.52 g, 34% yield). ^{1}H NMR (400 MHz, $CDCl_3$) δ 7.47 (s, 2H). $^{13}C\{^1H\}$ NMR (100 MHz, $CDCl_3$) δ 172.51, 143.59, 135.38, 130.07, 114.67. HRMS (EI) calculated for $C_{10}H_2Br_2O_2S_2$ 375.7863; found 375.7869. Anal. Calc. for $C_{10}H_2Br_2O_2S_2$: C, 31.77; H, 0.53. Found: C, 32.06; H, 0.40.

2,7-Bibromo-5*H*-spiro[benzo[1,2-*b*:6,5-*b'*]dithiophene-4,2'-[1,3]dioxolan]-5-one, 4.14 (performed by Yulia Getmanenko).[41] 2,7-Dibromo-benzo[2,1-*b*:3,4-*b'*]dithiophene-4,5-dione[41] (0.50 mmol, 0.19 g) was mixed with ethylene glycol (20 ml), MeOH (5 ml) and 10-camphorsulfonic acid (0.07 mol%, 0.035 mmol, 8.0 mg). The reaction mixture was heated to a vigorous reflux (145-155 ºC bath temperature) for 7.5 h, cooled to room temperature and treated with MeOH. Hexanes was added and the mixture was vigorously stirred for ~20 min. The organic phase contained some insoluble dark solid and was diluted with dichloromethane. The organic phase was separated, the aqueous phase was extracted with hexanes, and combined organic phases were dried

over $MgSO_4$. The solvents were removed by rotary evaporation and the residue (reddish-brownish solid) was purified by column chromatography (100 ml of silica gel, hexanes:CH_2Cl_2 (3:2). The solvents were removed from combined fractions and yellow solid was recrystallized from 2-PrOH to give bright yellow fluffy needles (0.090 g, 43% yield). ^{1}H NMR (400 MHz, $CDCl_3$) δ 7.35 (s, 1H), 7.13 (s, 1H), 4.47 (m, 2H), 4.31 (m, 2H); $^{13}C\{^1H\}$ NMR (100 MHz, $CDCl_3$) δ 189.03, 144.91, 139.47, 132.44, 131.71, 130.31, 128.21, 114.28, 111.61, 98.68, 66.17. HRMS (EI) m/z $[M]^+$ calcd. for $C_{12}H_6Br_2O_3S_2$ 419.8125; found 419.8134. Anal. Calcd. for $C_{12}H_6Br_2O_3S_2$: C, 34.14; H, 1.43. Found: C, 38.38; H, 1.32.

2,2'-(4-Oxo-4*H*-cyclopenta[1,2-*b*:5,4-*b*']dithiophene-2,6-diyl)bis(2,7-dihexylnaphthalene-1,4:5,8-bis(dicarboximide), 4.15. A solution of **4.3** (1.00 g, 1.38 mmol), **4.11** (0.236 g, 0.670 mmol), and copper(I) iodide (0.013 g, 0.067 mmol) in dry toluene (14 mL) was degassed with nitrogen for 5 minutes. Tetrakis(triphenylphosphine)palladium (0.039 g, 0.034 mmol) was added and the reaction was heated to 100 ºC for 17 hours while monitoring by TLC. Added a second portion of copper iodide (0.013 g, 0.067 mmol), tetrakis(triphenylphosphine)palladium (0.039 g, 0.034 mmol), and **4.3** (0.050 g, 0.069 mmol) and let stir at 100 ºC for 20 hours while monitoring by TLC. After cooling, the reaction mixture was diluted with chloroform and filtered through a short plug of silica gel (chloroform:ethyl acetate). The crude product was purified by column chromatography (silica gel, 3-5% ethyl acetate in chloroform). Preparatory TLC (silica gel, 1.5% ethyl acetate in chloroform) was performed on the desired fraction and a purple solid was obtained (0.080 g, 0.076 mmol, 11%). ^{1}H NMR (400 MHz, $CDCl_3$) δ 8.82 (d, *J* = 7.5 Hz, 2H), 8.75 (d, *J* = 7.5 Hz, 2H), 8.70 (s, 2H), 7.33 (s, 2H), 4.16 (m, 4H), 1.85-1.67 (m, 8H), 1.54-1.20 (m, 24H), 1.00-0.80 (m, 12H). $^{13}C\{^1H\}$ NMR (100 MHz, $CDCl_3$) δ 181.79, 162.47, 136.16, 132.11, 161.92, 151.00, 143.96, 141.83, 138.29, 135.36, 131.60, 130.78, 127.77, 126.57, 126.31,

126.21, 125.48, 126.13, 122.91, 41.16, 40.98, 31.40, 31.35, 27.86, 26.70, 26.60, 22.54, 22.47, 14.06 (two aliphatic resonances not observed due to overlap). HRMS (MALDI) m/z $[M]^+$ calcd for $C_{61}H_{60}N_4O_9S_2$ 1056.3802; found, 1056.3728. Anal. Calcd. for $C_{61}H_{60}N_4O_9S_2$: C, 69.30; H, 5.72; N, 5.30. Found: C, 69.18; H, 5.88; N 5.13.

2,2'-(5-Oxo-5*H*-spiro[benzo[1,2-*b*:6,5-*b'*]dithiophene-4,2'-[1,3]dioxolane]-2,7-diyl)bis(2,7-dihexylnaphthalene-1,8:4,5-bis(dicarboximide)), 4.16. A solution of **4.3** (0.500 g, 0.691 mmol), **4.14** (0.142 g, 0.337 mmol), and copper(I) iodide (0.013 g, 0.069 mmol) in dry toluene (7 mL) was deoxygenated with nitrogen for 5 min. Tetrakis(triphenylphosphine)palladium (0.019 g, 0.017 mmol) was added and the reaction was heated to 90 ºC for 3 hours. After cooling, the reaction mixture was precipitated in methanol. The solid was dissolved in dichloromethane, eluted through a plug of silica gel (dichloromethane:methanol), and concentrated via rotary evaporation. The crude product was purified by column chromatography (silica, 3% ethyl acetate in dichloromethane) to yield a purple solid (0.197 g, 0.174 mmol, 52%). ^{1}H NMR (400 MHz, $CDCl_3$) δ 8.80 (dd, *J* = 7.8, 2.2 Hz, 2H), 8.75 (dd, *J* = 7.6, 2.0 Hz, 2H), 8.73 (s, 1H), 8.68 (s, 1H), 7.56 (s, 1H), 7.37 (s, 1H), 4.53 (m, 2H), 4.36 (m, 2H), 4.17 (t, *J* = 7.4 Hz, 4H), 4.11 (m, 4H), 1.78-1.62 (m, 8H), 1.46-1.20 (m, 24H), 0.92-0.80 (m, 12H). ^{13}C{^{1}H} NMR (100 MHz, $CDCl_3$) δ 190.25, 162.61, 162.58, 162.34, 162.26, 162.23, 162.20, 161.88, 161.83, 146.22, 141.85, 139.72, 139.62, 138.80, 138.30, 135.70, 135.61, 134.04, 132.01, 131.69, 131.63, 131.04, 130.95, 128.89, 128.86, 128.85, 127.75, 127.71, 126.80, 126.58, 126.56, 126.45, 125.72, 125.55, 123.70, 123.51, 99.49, 66.17, 41.24, 41.21, 41.03, 41.01, 31.44, 27.96, 26.71, 26.66, 22.52, 22.49, 14.00 (one aliphatic resonance not observed due to overlap). HRMS (MALDI) *m/z* $[M+H]^+$ calcd for $C_{64}H_{64}N_4O_{11}S_2$, 1129.4091; found, 1129.4045. Anal. Calcd. for $C_{64}H_{64}N_4O_{11}S_2$: C, 68.06; H, 5.71; N, 4.96. Found: C, 68.02; H, 5.71; N, 4.86.

4,4'-(4,5-Dioxo-4,5-dihydrobenzo[1,2-*b*:6,5-*b'*]dithiophene-2,7-diyl)bis(2,7-dihexylnaphthalene-1,8:4,5-bis(dicarboximide)), 4.17. A solution of 4,4'-(5-oxo-5*H*-spiro[benzo[1,2-*b*:6,5-*b'*]dithiophene-4,2'-[1,3]dioxolane]-2,7-diyl)bis(2,7-dihexylnaphthalene-1,4:5,8-bis(dicarboximide)) (0.150 g, 0.133 mmol), acetic acid (25 mL), and concentrated hydrochloric acid (5 mL) was deoxygenated with nitrogen for 10 min. The reaction was heated to reflux for 2 h. After cooling, the reaction mixture was diluted with water to precipitate a purple solid. The solid was filtered, washed with water and methanol, and dried under vacuum. The crude product was purified by column chromatography (silica, 3% ethyl acetate in dichloromethane) followed by precipitation in methanol to yield a purple solid (0.094 g, 0.087 mmol, 65%). ^{1}H NMR (400 MHz, $CDCl_3$) δ 8.82 (d, *J* = 7.6 Hz, 2H), 8.77 (d, *J* = 7.6 Hz, 2H), 8.67 (s, 2H), 7.62 (s, 2H), 4.15 (t, *J* = 7.6 Hz, 4H), 4.10 (t, *J* = 7.6 Hz, 4H), 1.76-1.63 (m, 8H), 1.45-1.23 (m, 24H), 0.90-0.78 (m, 12H). $^{13}C\{^{1}H\}$ NMR (100 MHz, $CDCl_3$) δ 173.93, 162.37, 162.05, 162.04, 161.85, 144.52, 141.86, 137.26, 135.54, 135.07, 131.88, 131.36, 128.04, 127.56, 126.75, 126.70, 126.58, 125.82, 124.07, 41.25, 41.02, 31.38, 27.90, 26.67, 26.61, 22.49, 22.45, 13.95 (three aliphatic resonances not observed due to overlap). HRMS (MALDI) *m/z* $[M+H]^+$ calcd for $C_{62}H_{60}N_4O_{10}S_2$, 1085.3829; found, 1085.3790. Anal. Calcd. for $C_{62}H_{60}N_4O_{10}S_2$: C, 68.61; H, 5.57; N, 5.16. Found: C, 68.64; H, 5.56; N, 5.18.

4.6 References

(1) Zhan, X.; Facchetti, A.; Barlow, S.; Marks, T. J.; Ratner, M. A.; Wasielewski, M. R.; Marder, S. R. *Adv. Mater.* **2010**, *23*, 268.

(2) Huang, C.; Barlow, S.; Marder, S. R. *J. Org. Chem.* **2011**, *76*, 2386.

(3) Katz, H.; Lovinger, A.; Johnson, J.; Kloc, C.; Siegrist, T.; Li, W.; Lin, Y.; Dodabalapur, A. *Nature* **2000**, *404*, 478.

(4) Singh, T. B.; Erten, S.; Guenes, S.; Zafer, C.; Turkmen, G.; Kuban, B.; Teoman, Y.; Sariciftci, N. S.; Icli, S. *Org. Elect.* **2006**, *7*, 480.

(5) Jones, B. A.; Facchetti, A.; Marks, T. J.; Wasielewski, M. R. *Chem. Mater.* **2007**, *19*, 2703.

(6) Lee, Y.-L.; Hsu, H.-L.; Chen, S.-Y.; Yew, T.-R. *J. Phys. Chem. C* **2008**, *112*, 1694.

(7) Chen, Z.; Zheng, Y.; Yan, H.; Facchetti, A. *J. Am. Chem. Soc.* **2009**, *131*, 8.

(8) Gawrys, P.; Boudinet, D.; Zagorska, M.; Djurado, D.; Verilhac, J.-M.; Horowitz, G.; Pecaud, J.; Pouget, S.; Pron, A. *Synth. Met.* **2009**, *159*, 1478.

(9) Molinari, A.; Alves, H.; Chen, Z.; Facchetti, A.; Morpurgo, A. *J. Am. Chem. Soc.* **2009**, *131*, 2462.

(10) Piliego, C.; Jarzab, D.; Gigli, G.; Chen, Z.; Facchetti, A.; Loi, M. A. *Adv. Mater.* **2009**, *21*, 1573.

(11) Yan, H.; Chen, Z.; Zheng, Y.; Newman, C.; Quinn, J. R.; Dötz, F.; Kastler, M.; Facchetti, A. *Nature* **2009**, *457*, 679.

(12) Zhan, X.; Tan, Z. a. a.; Zhou, E.; Li, Y.; Misra, R.; Grant, A.; Domercq, B.; Zhang, X.-H.; An, Z.; Zhang, X.; Barlow, S.; Kippelen, B.; Marder, S. R. *J. Mater. Chem.* **2009**, *19*, 5794.

(13) Hu, Y.; Gao, X.; Di, C.-A.; Yang, X.; Zhang, F.; Liu, Y.; Li, H.; Zhu, D. *Chem. Mater.* **2011**, *23*, 1204.

(14) Polander, L. E.; Tiwari, S. P.; Pandey, L.; Seifried, B. M.; Zhang, Q.; Barlow, S.; Risko, C.; Brédas, J.-L.; Kippelen, B.; Marder, S. R. *Chem. Mater.* **2011**, *23*, 3408.

(15) Würthner, F.; Stolte, M. *Chem. Commun.* **2011**, *47*, 5109.

(16) Halls, J.; Friend, R. *Synth. Met.* **1997**, *85*, 1307.

(17) Hou, J.; Zhang, S.; Chen, T. L.; Yang, Y. *Chem. Commun.* **2008**, 6034.

(18) Sharma, G. D.; Balraju, P.; Mikroyannidis, J. A.; Stylianakis, M. M. *Sol. Energy Mater. Sol. Cells* **2009**, *93*, 2025.

(19) Shibano, Y.; Imahori, H.; Adachi, C. *J. Phys. Chem. C* **2009**, *113*, 15454.

(20) Wei, Y.; Zhang, Q.; Jiang, Y.; Yu, J. *Macromol. Chem. Phys.* **2009**, *210*, 769.

(21) Schenning, A. P. H. J.; von Herrikhuyzen, J.; Jonkheijm, P.; Chen, Z.; Würthner, F.; Meijer, E. W. *J. Am. Chem. Soc.* **2002**, *124*, 10252.

(22) O'Neil, M. P.; Niemczyk, M. P.; Svec, W. A.; Gosztola, D.; Gaines, G. L.; Wasielewski, M. R. *Science* **1992**, *257*, 63.

(23) An, Z.; Odom, S. A.; Kelley, R. F.; Huang, C.; Zhang, X.; Barlow, S.; Padilha, L. A.; Fu, J.; Webster, S.; Hagan, D. J.; Van Stryland, E. W.; Wasielewski, M. R.; Marder, S. R. *J. Phys. Chem. A* **2009**, *113*, 5585.

(24) Fukuzumi, S.; Ohkubo, K.; Ortiz, J.; Gutierrez, A. M.; Fernandez-Lazaro, F.; Sastre-Santos, A. *Chem. Commun.* **2005**, 3814.

(25) Oh, J. H.; Suraru, S.-L.; Lee, W.-Y.; Koenemann, M.; Hoeffken, H. W.; Roeger, C.; Schmidt, R.; Chung, Y.; Chen, W.-C.; Wuerthner, F.; Bao, Z. *Adv. Funct. Mater.* **2010**, *20*, 2148.

(26) Durban, M. M.; Kazarinoff, P. D.; Luscombe, C. K. *Macromol.* **2010**, *43*, 6348.

(27) Guo, X.; Watson, M. *Org. Lett.* **2008**, *10*, 5333.

(28) Bhosale, S. V.; Kalyankar, M. B.; Bhosale, S. V.; Langford, S. J.; Reid, E. F.; Hogan, C. F. *New J. Chem.* **2009**, *33*, 2409.

(29) Chopin, S.; Chaignon, F.; Blart, E.; Odobel, F. *J. Mater. Chem.* **2007**, *17*, 4139.

(30) Suraru, S.-L.; Würthner, F. *Synthesis* **2009**, *11*, 1841.

(31) Thalacker, C.; Roeger, C.; Wuerthner, F. *J. Org. Chem.* **2006**, *71*, 8098.

(32) Roeger, C.; Wuerthner, F. *J. Org. Chem.* **2007**, *72*, 8070.

(33) Gao, X.; Qiu, W.; Yang, X.; Liu, Y.; Wang, Y.; Zhang, H.; Qi, T.; Liu, Y.; Lu, K.; Du, C.; Shuai, Z.; Yu, G.; Zhu, D. *Org. Lett.* **2007**, *9*, 3917.

(34) Stille, J. *Angew. Chem. Int. Ed.* **1986**, *25*, 508.

(35) Azizian, H.; Eaborn, C. *J. Organomet. Chem.* **1981**, *214*, 49.

(36) Under identical conditions, the monobrominated PDI derivative undergoes homocoupling to yeild the bi-PDI product and the stannyl PDI intermediate cannot be isolated.

(37) Rademacher, A.; Märkle, S.; Langhals, H. *Chem. Ber.* **1982**, *115*, 2927.

(38) G. Hamilton, D.; Prodi, L.; Feeder, N.; K. M. Sanders, J. *J. Chem. Soc., Perkin Trans. 1* **1999**, 1057.

(39) Reczek, J. J.; Villazor, K. R.; Lynch, V.; Swager, T. M.; Iverson, B. L. *J. Am. Chem. Soc.* **2006**, *128*, 7995.

(40) Getmanenko, Y. A.; Risko, C.; Tongwa, P.; Kim, E.-G.; Li, H.; Sandhu, B.; Timofeeva, T.; Brédas, J.-L.; Marder, S. R. *J. Org. Chem.* **2011**, *76*, 2660.

(41) Getmanenko, Y. A.; Marder, S. R. Method of Making Coupled Heteroaryl Compounds via Rearrangement of Halogenated Heteroaromatics Followed by Oxidative Coupling. WO 2011098495. August 18, 2011.

CHAPTER 5

DIACYL-FUNCTIONALIZED AND EXTENDED-CORE NAPHTHALENE DIIMIDES: AIR-STABLE ELECTRON AFFINITIES AND IMPROVED SOLID-STATE PACKING

5.1 Introduction

As discussed in previous chapters, research focused on the development of materials for n-channel organic transistors that can be operated in air has afforded several series of new electron transport materials in which electron-withdrawing substituents, such as perfluoralkyl, perfluorophenyl, halo, cyano, and acyl groups, are attached to thiophene-, phenylene- and arylene-based cores.[1-14] In particular, naphthalene diimide (NDI) has been functionalized with a variety of halo[5,15] and cyano[6-8,16] substituents resulting in moderate to high air-stable electron mobility values measured in OFETs.

Air-stable device operation in NDIs is generally achieved through two methods: 1) incorporation of kinetic barriers and / or 2) increasing the magnitude of the electron affinity (EA). In NDI chemistry, kinetic barriers have been achieved using fluoroalkyl substitution, which, through dense packing of the chains in the thin film, is believed to act as a barrier against ambient species penetration.[17-19] However, performance in devices fabricated with materials of this type has been shown to degrade over time.[20-22] On the other hand, an increase in the electron affinity, which is generally achieved through functionalization with electron-withdrawing substituents, can lead to materials with a thermodynamic stability towards oxidation in air that does not rely on the packing of the material in the film.[8,20,23] Materials exhibiting intrinsically air-stable electron transport, i.e.; in which electron transport is not affected by environmental conditions and / or molecular

arrangement in the film, are desirable. Cyano-functionalized PDIs and NDIs represent the first-generation examples of thermodynamically air-stable, n-channel semiconductors and have exhibited electron mobility values up to 0.64 $cm^2V^{-1}s^{-1}$ and current on / off ratios of 10^4-10^7 when processed by vacuum deposition.[4,8,12]

Additionally, contrary to their inorganic counterparts where the atoms are held together by strong covalent bonds, the interactions between molecules in organic semiconductors are much weaker. Such intermolecular interactions are responsible for the formation of a conduction path; therefore, the mobility in organic materials is highly dependent on the molecular ordering.[24] In other words, a stronger electronic coupling, such as that resulting from strong intermolecular π-overlap, leads to higher mobility values (as discussed in Chapter 1).[2]

This chapter describes previously unexplored 2,6-diacyl-NDI derivatives, which offer the benefit of versatile functionalization through the use of different acyl-halide precursors and lead to electrochemical potentials below the air stability threshold. The diacyl-NDIs were also condensed with hydrazine to yield planar, fused-ring NDI cores with extended π-systems; these new cores exhibit improved solid-state packing characteristics over their acyl-NDI analogues.

5.2 2,6-Diacyl-Naphthalene Diimide Derivatives

5.2.1 Synthesis

2,6-Diacyl-derivatives of NDI have not been reported in the literature due to a lack of synthetic methodology; however, the 2,6-distannyl-NDIs reported in Chapter 4 offer a synthetic route using well known palladium-catalyzed Stille coupling of aryl-stannanes with acyl-halides.[25]

N,N'-Di(*n*-hexyl)-2,6-bis(tri(*n*-butyl)stannyl)naphthalene-1,8:4,5-bis(dicarboximide) (**4.4**, described in Chapter 4) was converted via palladium-catalyzed Stille coupling with $Pd(PPh_3)_2Cl_2$, CuI and the appropriate acylhalide, **XCOR**, to *N,N'*-bis(*n*-hexyl)-2,6-di(acyl)naphthalene-1,8:4,5-bis(dicarboximide) derivatives, **5.1**-**5.5**, in 20-40% yield. These compounds were characterized by ^{1}H and $^{13}C\{^{1}H\}$ NMR spectroscopy, high-resolution mass spectrometry, and elemental analysis.

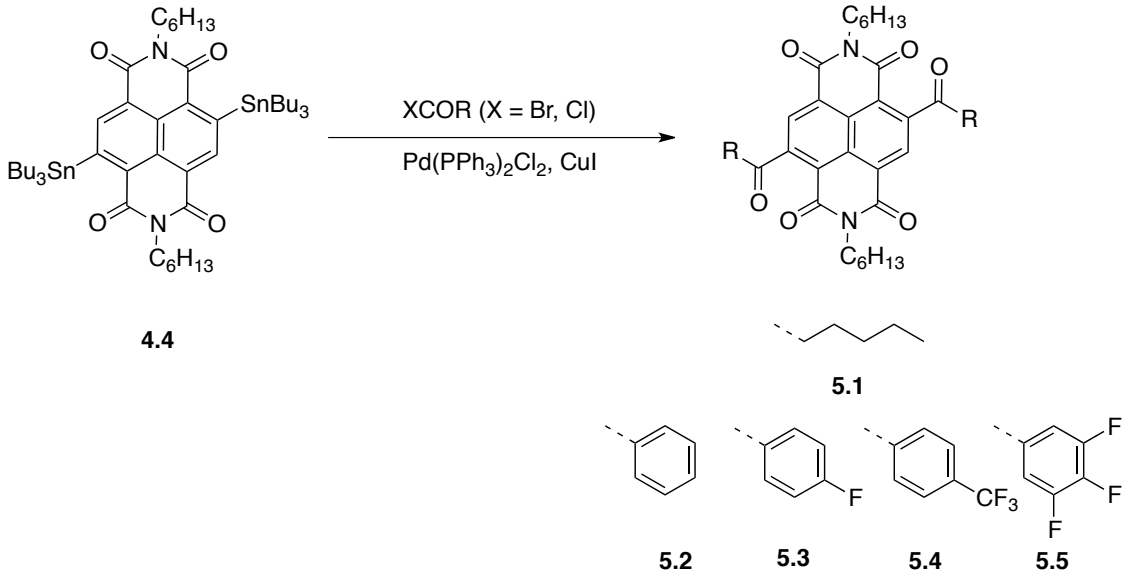

4.4 **5.1** **5.2** **5.3** **5.4** **5.5**

Scheme 5.1. Preparation of alkyl- and aryl- substituted diacyl-NDI derivatives.

The solubility of **5.1**-**5.5** was poor in common solvents (dichloromethane, chloroform, THF, toluene) and purification was difficult for these materials. Several groups have studied the effect of alkyl groups incorporated into π-conjugated materials for improved solubility and the influence of these groups on the self-assembly, solid-state morphology, and resulting device performance.[26-28] Varying lengths of *N,N'*-alkyl substitution on NDI cores have been reported, with longer *n*-alkyl and branched alkyl chains typically leading to improved solubility without significantly disrupting the solid-

state packing or inhibiting charge transport.[7] Therefore, a *N,N′*-dodecyl substitution was selected to improve the solubility of the diacyl-NDI derivatives. *N*,*N′*-Bis(*n*-dodecyl)-2,6-di(thiophene-2-carbonyl)naphthalene-1,8:4,5-bis(dicarboximide), **5.6**, was synthesized via Stille coupling from *N,N′*-di(*n*-dodecyl)-2,6-bis(tri(*n*-butyl)stannyl)naphthalene-1,8:4,5-bis(dicarboximide) (**4.6**, described in Chapter 4) and characterized by ^{1}H and $^{13}C\{^{1}H\}$ NMR spectroscopy, high-resolution mass spectrometry, and elemental analysis (Scheme 5.2).

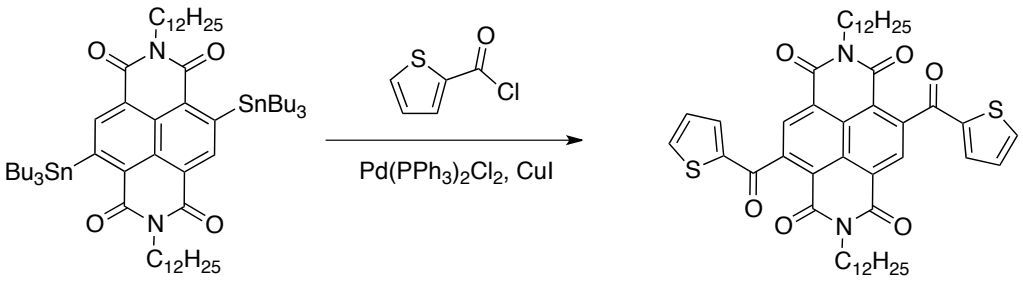

Scheme 5.2. Preparation of thienyl-substituted diacyl-NDI derivative.

5.2.2 Molecular Geometry and Frontier Orbitals

The neutral ground-state structures obtained at the DFT (B3LYP/6-31G**) level for **5.1**-**5.6** (with all *N,N′*-alkyl groups replaced by methyl groups and R = C_5H_{11} replaced by ethyl groups) are characterized by a large torsion angle between the plane of the NDI core and a plane containing the C(O)C moiety of the ketone functional groups. The alkyl and aryl ketone units are (on average) estimated to be twisted 71° and 76° out-of-plane with respect to the central NDI units, respectively. This is consistent with the effects of steric interactions between the C=O group of the ketone functionality with the C=O of the NDI imide and the hydrogen atoms in the 3 and 7 positions on the NDI rings.

Table 5.1. B3LYP/6-31G** Frontier Orbital Energies (eV) for **5.1**-**5.6**.[a]

Compound	HOMO	LUMO
NDI	–7.04	–3.41
5.1	–7.02	–3.66
5.2	–6.98	–3.53
5.3	–7.05	–3.63
5.4	–7.35	–3.86
5.5	–7.31	–3.80
5.6	–6.79	–3.53

[a]Alkyl groups replaced by methyl groups throughout.

The HOMO and LUMO wavefunctions (B3LYP/6-31G**) are illustrated for **5.1**-**5.6** in Figure 5.1 and Figure 5.2. The HOMO wavefunctions of **5.3, 5.4**, and **5.6** are strongly localized on the C(O)R segments while ones for **5.1**, **5.2**, and **5.5** are characterized by partial delocalization onto the core of the NDI. The HOMO wavefunctions for this diacyl-NDI series are structurally complex and further studies are required to elucidate their origin. The LUMO wavefunctions, on the other hand, are strongly localized on the NDI core for all derivatives. The LUMO energy of **5.1** is stabilized relative to that of an isolated NDI; this is attributed to the inductive withdrawing effect of the C=O functionality on the NDI-based LUMO – the Hammett parameter, σ, reported for a C(O)Me group is 0.33.[29] The LUMO energies of **5.2** and **5.6** are also stabilized with respect to that of NDI; however, the effect is slightly less pronounced than that observed for **5.1** – based on the Hammett parameters of a C(O)Me and C(O)Ph group (0.33 and 0.31, respectively), the inductive withdrawing effect should be similar. This observation is potentially due to the π-donating effect of the aryl groups on the C=O moiety, rendering it less inductively withdrawing towards the NDI core. With the increasingly inductive withdrawing fluoroaryl substituents present in **5.3** to **5.5**, a corresponding sequential increase in stabilization of

the LUMO energies is observed; LUMO energies of up to 0.4 eV lower than those of NDI are obtained.

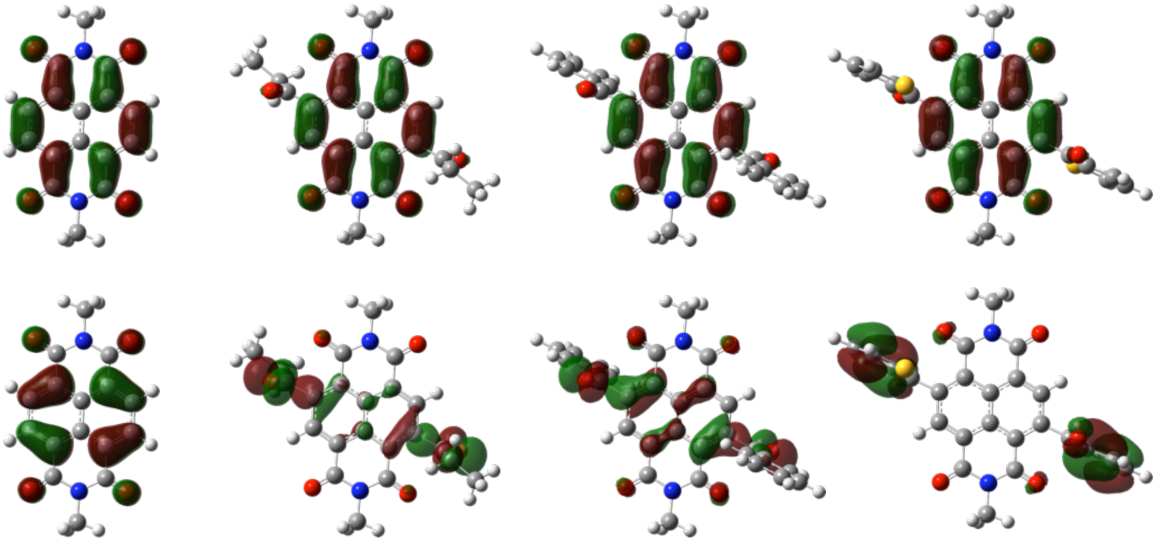

Figure 5.1. Pictorial representations of the HOMO and LUMO wavefunctions for (left to right) NDI, **5.1**, **5.2**, and **5.6** as determined at the B3LYP/6-31G** level of theory.

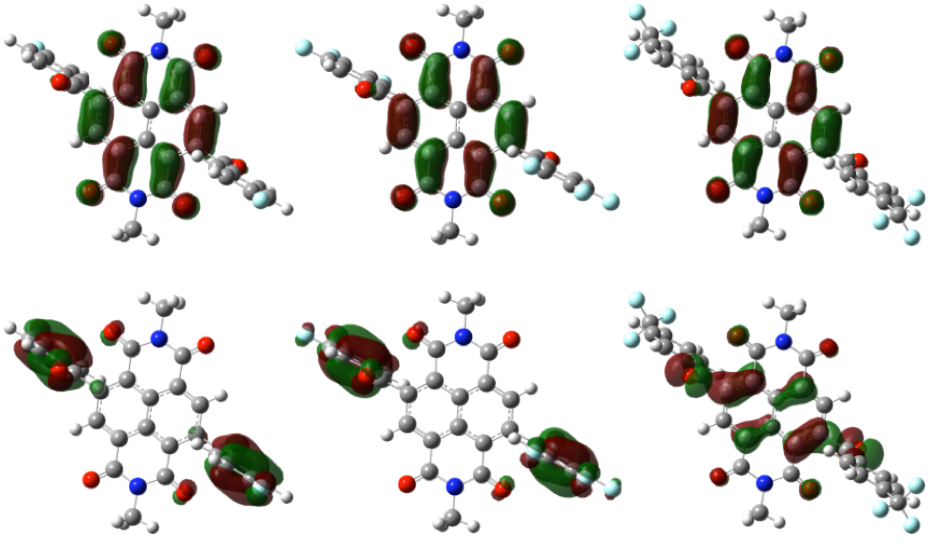

Figure 5.2. Pictorial representations of the HOMO and LUMO wavefunctions for (left to right) **5.3**, **5.4**, and **5.5** as determined at the B3LYP/6-31G** level of theory.

5.2.3 Crystal Structure and Electronic Coupling

Crystals of **5.2** and **5.6** suitable for single-crystal X-ray structural analysis were obtained by slow evaporation of a 1:1 dichloromethane:ethyl acetate solution and liquid / liquid diffusion of a 1,1',2,2'-tetrachloroethane / pentanol mixture, respectively. The structures are described using pitch and roll angles / distances as described by Curtis *et al.* (Figure 5.3)[30] where *P* and *R* are the pitch and roll angles corresponding to the molecular slipping along the long (z_L) and short (z_S) axis of the molecule, respectively; d is the π-π distance between two stacked molecular planes; d_P and d_R are the slip distances along the long and short axis, respectively; and d_{tot} is defined as the total slip distance ($d_{tot} = (d_P^2 + d_R^2)^{1/2}$). These values are summarized for each crystal in Table 5.2.

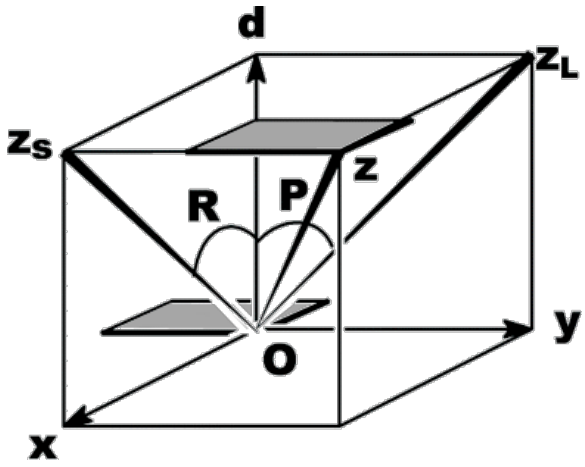

Figure 5.3. Illustration of the terminology used in this section. Adapted from Ref. 30.

The X-ray single crystal structure of *N,N'*-bis(n-hexyl) naphthalene diimide (**4.9**) reported by Shukla *et al.* was used for comparison purposes.[31] The crystal is characterized as a slipped π-stack with close π-π distances (*d* = 3.3 Å) and a total slip distance, d_{tot}, of 3.6 Å resulting in substantial overlap of the NDI cores (Figure 5.3). The stacks are arranged in parallel with respect to neighboring stacks leading to long-range structural order in the crystal.

Table 5.2. Pitch and Roll Angles (deg) and Distances (Å) along with Electronic Coupling[a] (B3LYP/6-31G**) between Nearest Pairs (meV) for **4.9**, **5.2**, and **5.6**.

cmpd	*P*	*R*	*d*	d_P	d_R	d_{tot}	t_a	t_b	t_c
4.9	19.4	45.6	3.3	1.2	3.4	3.6	85	31	0
5.2	13.0	47.6	3.8	0.88	4.2	4.3	0	20	0
5.6	11.2	51.1	3.6	0.71	4.5	4.6	13	2	–

[a]Electronic coupling calculated along the *a*- (t_a), *b*- (t_b), and *c*- (t_c) axes, respectively, between LUMO levels of adjacent pairs with intermolecular distances less than 7 Å along the specified axis.

Compound **5.2** and **5.6** also adopt a slipped π-stack structure with much larger π-π and total slip distances when compared to **4.9** (Table 5.2). The large distances observed in **5.2** and **5.6** are attributed to the aryl-ketone units, which are approximately perpendicular to the plane of the NDI core in **5.2** and only slightly less than perpendicular in **5.6** (the angles between planes formed by the carbon atoms of the NDI and C(O)C of the ketone moiety are 86.5º and 80.9º, respectively), consistent with large torsion angles predicted by DFT. The major difference observed in the structure of **5.2** relative to **4.9** and **5.6**, is in the arrangement of neighboring molecular stacks (Figure 5.4). As mentioned, the molecular stacks in **4.9** are arranged in parallel (planes of neighboring stacked molecules are parallel), which is also the case in **5.6**; however, planes of neighboring molecular stacks in **5.2** are arranged almost perpendicular to each other (tilted ca. 83.4º from parallel).

On the basis of the crystal structures of **4.9**, **5.2**, and **5.6**, DFT evaluations of the intermolecular effective electronic couplings (B3LYP/6-31G**, using the fragment orbital approach[32]) were explored. The electronic couplings (*t*) for **4.9** were performed for comparison purposes and were determined to be moderate for electrons along the *a*-axis (π-π stacking direction, 85 meV, LUMO-LUMO) and relatively low along the *b*-axis (31 meV, LUMO-LUMO). In general, these values are comparable to the effective

electronic coupling calculated based on single crystal structures of *N,N'*-cyclohexyl NDI by similar methods (91 and 19 meV for *a*- and *b*-axis, respectively; LUMO-LUMO).[33]

For **5.2**, electronic coupling along the π-π stacking direction (*b*-axis) is determined to be low for electrons (20 meV) compared to **4.9**, while along the *a*- and *c*-axis it is negligible. Similarly, the electronic coupling along the π-π stacking direction in **5.6** is also low (13 meV, *a*-axis, LUMO-LUMO) with negligible values calculated along the *b*-axis. These results suggest that the packing of the cores in **5.2** and **5.6** is not conducive to electron transport in devices; if mobility values are observed, they have the potential to be lower than those reported for NDI based on the differences in electronic coupling relative to **4.9**.

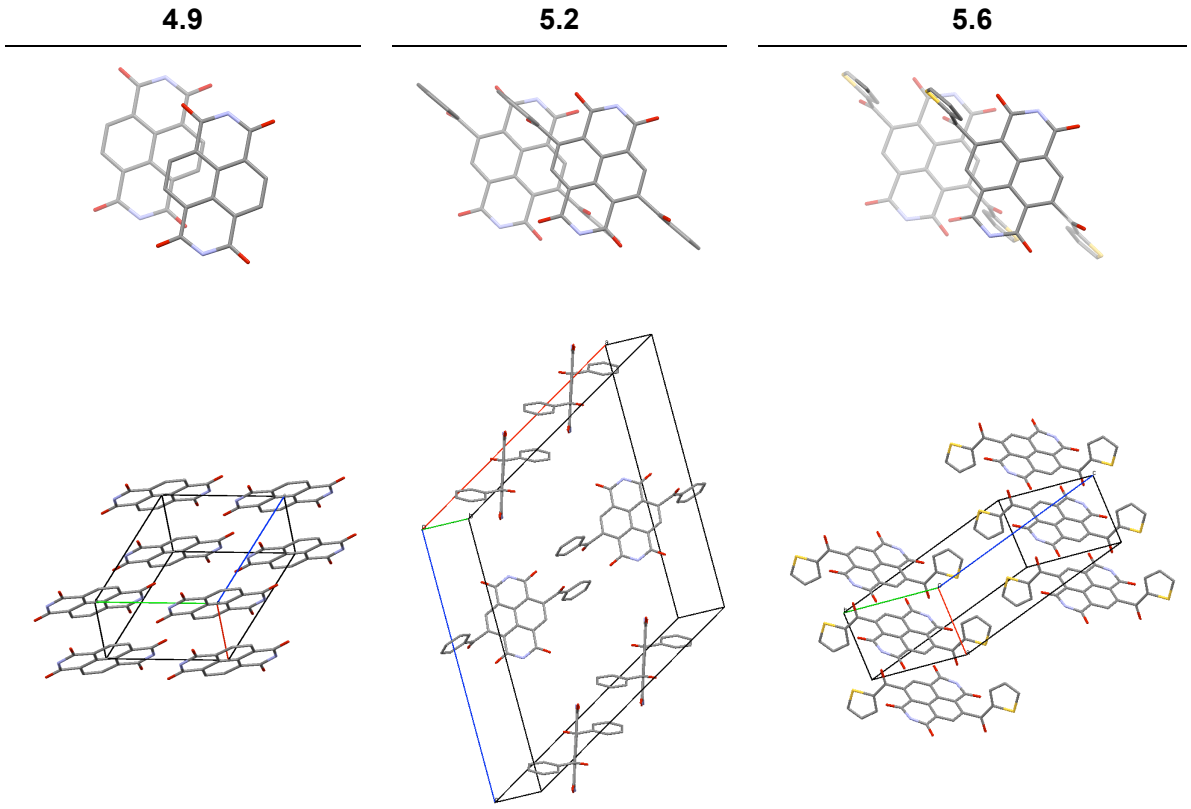

Figure 5.4. Crystal structure of **4.9**, **5.2** and **5.6** showing the overlap of the cores (top) and the packing motif (bottom). The axes are depicted according to: *a*-axis (red), *b*-axis (green), *c*-axis (blue). *N,N'*-alkyl groups have been removed for clarity.

5.2.4 Optical Properties and Electrochemistry

Electronic spectra of **5.1**-**5.6** were recorded in dilute dichloromethane solution and as thin films on glass substrates. Representative spectra are shown in Figure 5.5 and Figure 5.6; the corresponding absorption maxima and molar absorptivities are summarized in Table 5.3. The solution absorption spectra of **5.1**-**5.6** exhibit one prominent absorption band with maxima at 380-381 nm, similar to that of the corresponding monomeric NDI derivative (**4.9**, Chapter 4, 380 nm), and roughly comparable oscillator strengths with the exception of **5.6**, which has a slightly larger extinction coefficient and similar band shape. Fluorination of the phenyl moiety does not significantly affect the spectra, which is consistent with the fluoro-phenyl groups participating as inductively-withdrawing substituents. Thin film absorption spectra are fairly similar to those seen in solution with moderate shifts in the absorption maxima and a slight broadening. The film of **5.6** appeared, by both eye and UV-vis. spectroscopy, to be higher quality relative to **5.1** and **5.2**, which is attributed to an increased solubility of the material in the processing solvent.

Cyclic voltammetry (CV) was used to measure the electrochemical properties of **5.1**-**5.6** in CH_2Cl_2 / 0.1 M $^nBu_4NPF_6$ (Table 5.3 and Figure 5.7). Two reversible reduction processes were observed for each system **5.1**-**5.6** corresponding to the first and second reduction of the NDI unit. The first half-wave reduction ($E_{1/2}^{0/-}$) potentials of **5.2**-**5.5** are cathodically shifted with increasing fluorine substitution, as expected based on the Hammett parameters[29] of the appropriate fluoro-phenyl substituents (see Figure 5.8) and consistent with the trend observed in the DFT calculated adiabatic EA values (Table 5.3). Additionally, the first reduction potential values approach and surpass the estimated air-stability threshold (–0.4 V vs. SCE) making these materials potential candidates for air-stable electron transport.

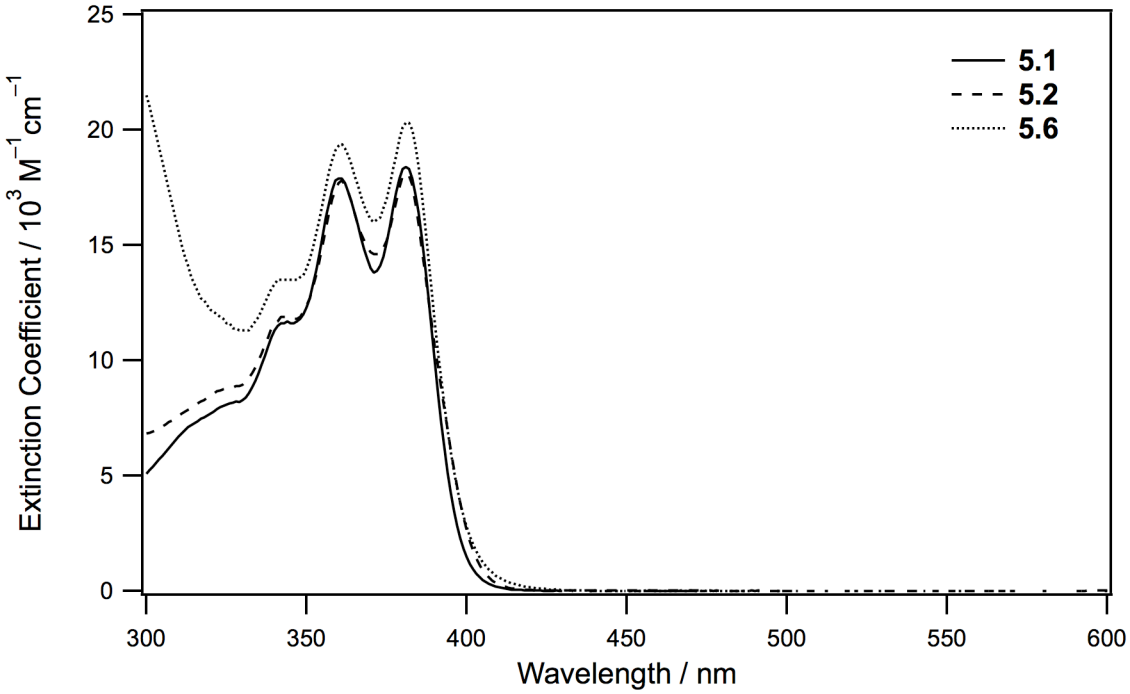

Figure 5.5. Representative UV-vis. spectra of **5.1**, **5.2** and **5.6** in dilute dichloromethane solutions.

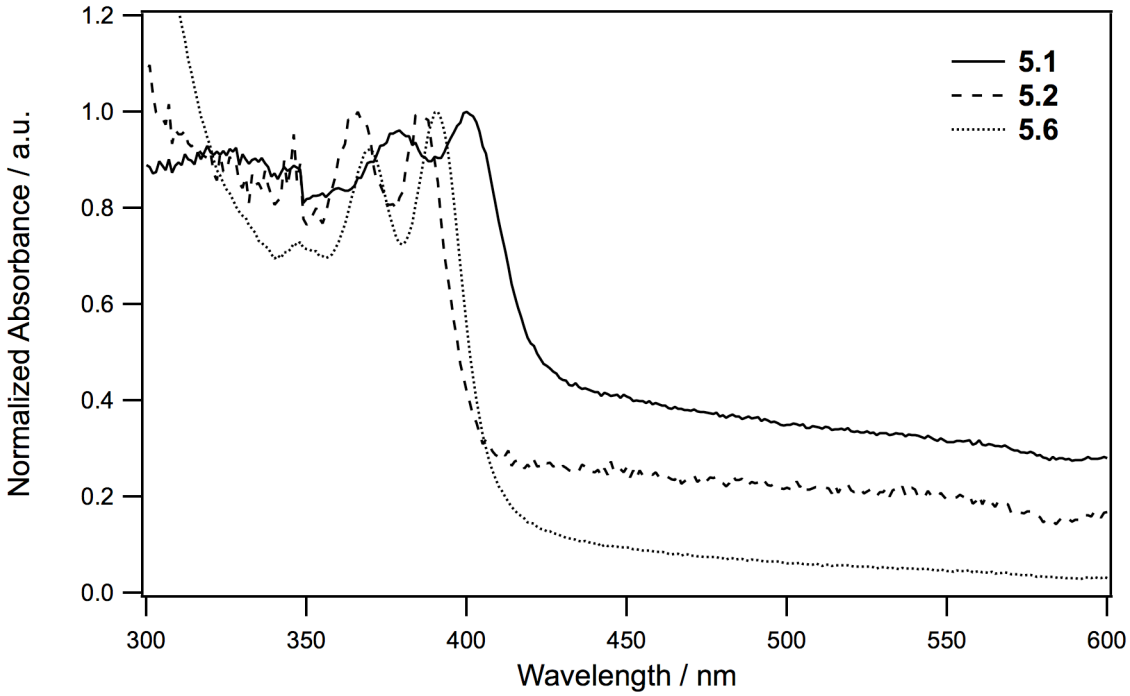

Figure 5.6. Representative UV-vis. spectra of **5.1**, **5.2** and **5.6** as films on glass.

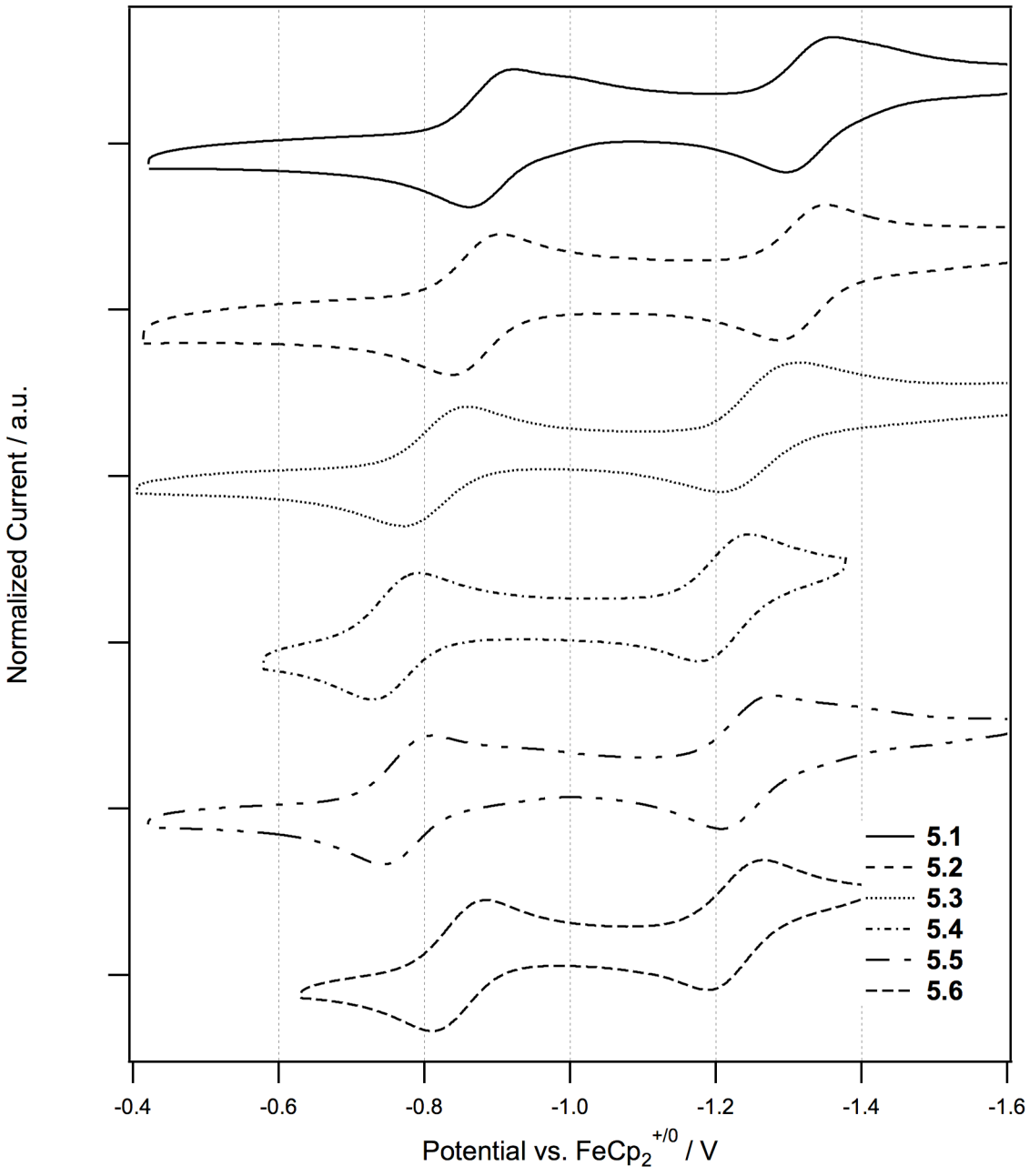

Figure 5.7. Cyclic voltammograms of **5.1**-**5.6** in 0.1 M $^{n}Bu_4N$ PF_6 in CH_2Cl_2 recorded at a scan rate of 50 mVs^{-1}.

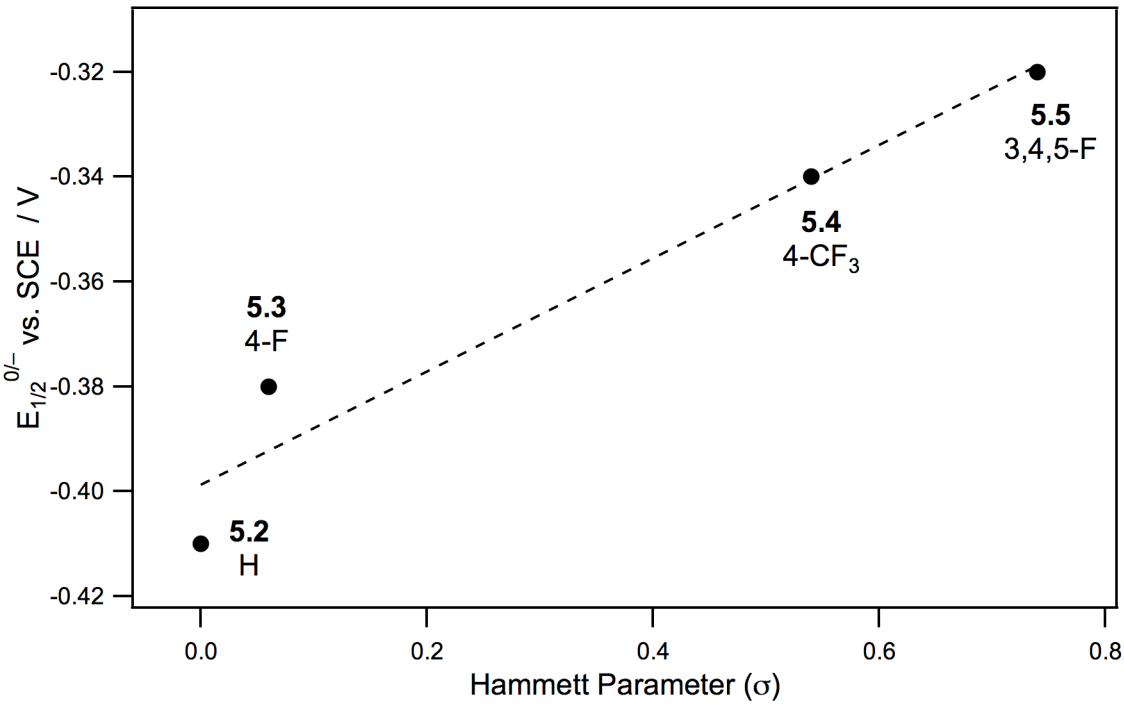

Figure 5.8. Correlation between the first reduction potential vs. SCE of **5.2**-**5.5** and the corresponding Hammett parameter for the fluoro-phenyl substituents. Dashed line depicts a linear fit. Hammet parameters taken from Ref. 29 ($\sigma_{3,4,5\text{-F}} = 2\sigma_{m\text{-F}} + \sigma_{p\text{-F}}$).

The intramolecular reorganization energies for a self-exchange electron-transfer reaction between the neutral molecules and the corresponding radical anions, λ_e, were also calculated at the B3LYP/6-31G** level (Table 5.3). Within the framework of Marcus theory, these values are closely related to the electron transfer rate,[34] and, therefore are critical contributors to the charge-carrier mobility values in the materials. The calculated λ_e values for all six diacyl-NDI derivatives are similar (within a 40 meV range) and they are significantly larger (by 100-140 meV) than those estimated for **4.9**. Large reorganization energies, along with small electronic coupling values estimated based on the crystal structures of **5.2** and **5.6**, suggest that if electron mobility is observed in these materials, it will be low relative to that observed for **4.9**.[34]

Table 5.3. Absorption Maxima (nm) and Absorptivities (10^4 $M^{-1}cm^{-1}$) for the Strong UV-vis. Absorptions of **5.1**-**5.6** in Dichloromethane along with Thin-Film Absorption Maxima (nm), Electrochemical Potentials (V vs. $FeCp_2^{+/0}$)[a] and Electrochemically Estimated Solid-State Electron Affinities (eV). DFT SCF Values for Electron Affinities and Reorganization Energies for Isolated Molecules (eV).

cmpd	λ_{max}		ε_{max}	$E_{1/2}^{0/-}$	$E_{1/2}^{-/2-}$	$E_{1/2}^{0/-}$ SCE[b]	EA(s)[c]	EA_{adi}[d]	λ_e[e]
	soln	film							
4.9	380	393	2.76	–1.13	–1.70	–0.67	–3.7	–2.03	0.336
5.1	380	401	1.79	–0.90	–1.34	–0.44	–3.9	–2.45	0.432
5.2	380	386	1.88	–0.87	–1.32	–0.41	–3.9	–2.40	0.452
5.3	381	d	d	–0.84	–1.28	–0.38	–4.0	–2.50	0.464
5.4	381	d	d	–0.80	–1.26	–0.34	–4.0	–2.74	0.470
5.5	381	d	d	–0.78	–1.24	–0.32	–4.0	–2.69	0.477
5.6	380	391	2.03	–0.86	–1.27	–0.40	–3.9	–2.39	0.439

[a]Cyclic Voltammetry in CH_2Cl_2 / 0.1 M $^nBu_4NPF_6$. [b]Estimated according to $E_{1/2}^{0/-}$(vs SCE) = $E_{1/2}^{0/-}$(vs. $FeCp_2^{+/0}$) + 0.46 V (for CH_2Cl_2). [c]Estimated according to EA(s) = −($eE_{1/2}^{0/-}$ vs. $FeCp_2^{+/0}$ + 4.8 eV). [d]Not measured due to solubility limitations. [d]Adiabatic EA = SCF energy difference between the relaxed ground-state anion and the ground-state neutral species (obtained for structures in which the alkyl groups are all replaced by methyl groups at the B3LYP/6-31G** level). [e]Internal reorganization energies for $M_A^- + M_B = M_A + M_B^-$ obtained as sum of the SCF energy difference between anion at the neutral geometry and at anion geometry and that between the neutral species at anion geometry and at neutral geometry.

5.2.5 OFET Behavior

Top-gate OFETs were fabricated with **5.1**, **5.2** and **5.6** as the active layer, CYTOP / Al_2O_3 as a bilayer gate dielectric[35] and Au source / drain electrodes (Table 5.4). The devices fabricated with **5.1** and **5.2** did not exhibit field-effect transistor function; therefore, no mobility values were measurable. This result could be either due to low solubility of the materials in the processing solvent (1,2-dichlorobenzene, 30 mg / mL) resulting in poor film quality and / or the poor orbital overlap of the NDI cores as suggested by the large π-π and slip distances observed in the crystal structure of **5.1**. Compound **5.6** was processed from 15 mg / mL solutions in 1,1',2,2'-tetrachloroethane resulting in improved film quality. Although electron mobility values were obtained for this

material, the values were quite low (≤ 3.8 × 10^{-4} $cm^2V^{-1}s^{-1}$) relative to the electron mobility values reported for solution-processed devices based on NDIs without core substitution (0.01 $cm^2V^{-1}s^{-1}$).[36] Considering the larger π-π and slip distances and smaller electronic coupling values associated with the molecules in the single crystal structure of **5.6** relative to that of **4.9**, this result is not surprising and similar effects have been observed between the packing distances / mobility values of other NDI structures.[31]

Table 5.4. Saturation Electron Mobilities, Threshold Voltages, and Current On / Off Ratios for OFETs Based on **5.1**-**5.6**.

cmpd	μ_e[a] / $cm^2V^{-1}s^{-1}$	V_{TH} / V	I_{on} / I_{off}
5.1	b	b	b
5.2	b	b	b
5.6	3.3 (± 0.5) × 10^{-4}	3.4 (± 0.5)	50

[a] Average values are calculated based on 3 to 7 devices from a single substrate. [b]No OFET behavior observed in the devices.

5.3 Extended-Core Naphthalene Diimide Derivatives

5.3.1 Synthesis

1,7-Di(alkyl/aryl)-4,10-di(*n*-alkyl)phthalazino[6,7,8,1-*lmna*]pyridazino[5,4,3-*gh*][3,8]phenanthroline-5,11(4*H*,10*H*)-dione derivatives **5.7**-**5.9** were synthesized from *N,N'*-bis(*n*-alkyl)-2,6-di(acyl)naphthalene-1,8:4,5-bis(dicarboximide) derivatives **5.1**, **5.2** and **5.6** via condensation with hydrazine hydrate in either ethanol or *n*-butanol at reflux (Scheme 5.3).[37,38] These compounds were characterized by ^1H and $^{13}C\{^1H\}$ NMR spectroscopy, high-resolution mass spectrometry, and elemental analysis.

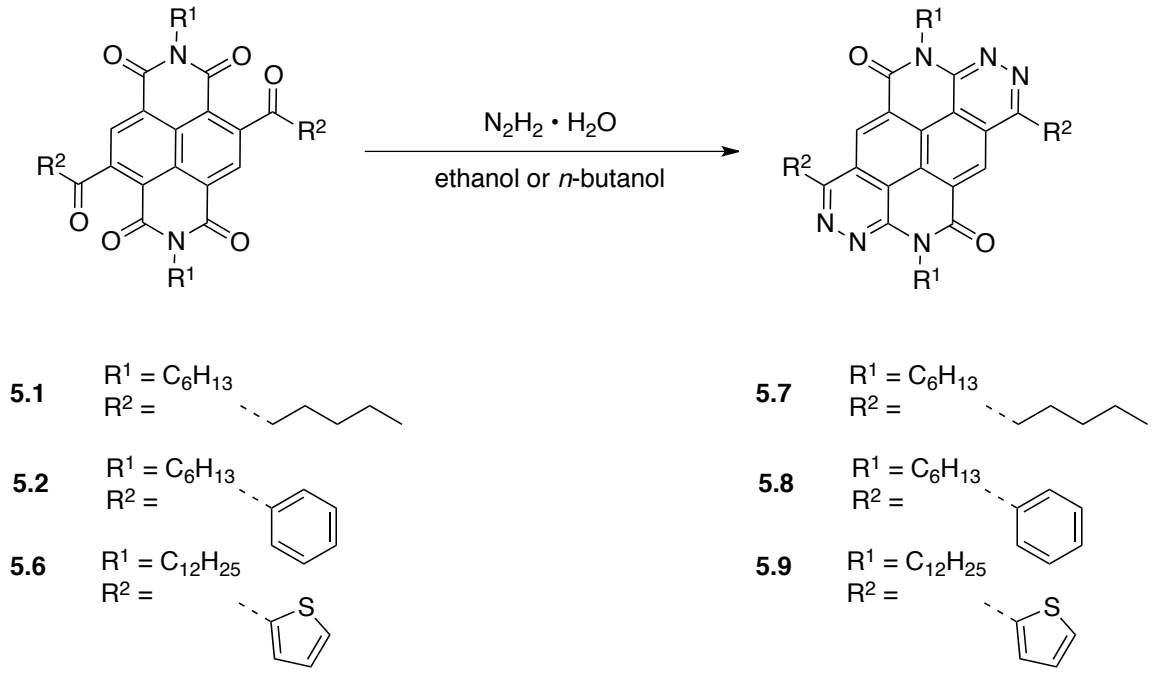

Scheme 5.3. Preparation of alkyl- and aryl- substituted fused ring NDI derivatives.

5.3.2 Molecular Geometry and Frontier Orbitals

The neutral ground-state structures obtained at the DFT (B3LYP/6-31G**) level for **5.7**-**5.9** (with all *N,N'*-alkyl groups replaced by methyl groups and R = C_5H_{11} replaced by ethyl groups) are characterized by a planar fused core. The benzene and thiophene units are (on average) estimated to be twisted 41° and 26° out-of-plane with respect to the central cores, respectively. This is consistent with the effects of steric interactions between hydrogen atoms in the *ortho*-position on the benzene ring and in the 3-position on the thiophene ring with the hydrogen atoms on the core structure.

The HOMO and LUMO single-electron wavefunctions (B3LYP/6-31G**) are illustrated for **5.7**-**5.9** in Figure 5.9. The HOMO of **5.7** is largely delocalized over the core while the HOMOs of **5.8** and **5.9** show increasing pyridizine-aryl (C=N-N=C-R) character, presumably associated with an increase in the π-donor strength of the aryl group, with little to no delocalization through the core. The LUMO wavefunctions are similar for **5.7**-

5.9 and are delocalized over the core of the fused-ring structure The HOMO and LUMO energies are destabilized relative to those of an isolated NDI by 0.51-1.03 and 0.26-0.36 eV, respectively (Table 5.5).

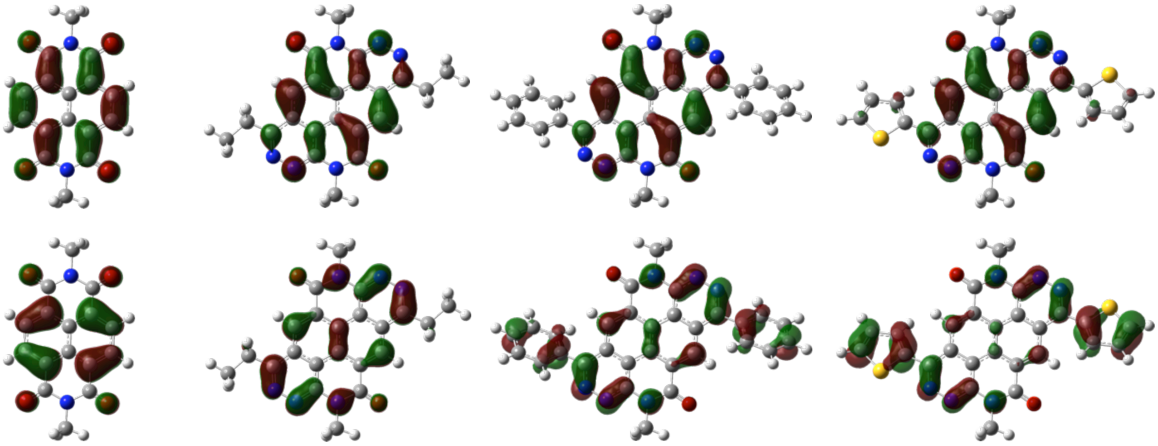

Figure 5.9. Pictorial representations of the HOMO (bottom) and LUMO (top) wavefunctions and energies for (left to right) NDI, **5.7**, **5.8**, and **5.9** as determined at the B3LYP/6-31G** level of theory.

Table 5.5. B3LYP/6-31G** Frontier Orbital Energies (eV) for **5.7**-**5.9**.[a]

Compound	HOMO	LUMO
NDI	–7.04	–3.41
5.7	–6.53	–3.08
5.8	–6.24	–3.05
5.9	–6.01	–3.15

[a]Alkyl groups replaced by methyl groups throughout.

5.3.3 Crystal Structure and Electronic Coupling

Compound **5.7** and **5.8** adopt a slipped π-stack structure with parallel neighboring molecular stacks similar to that observed for **4.9** (Figure 5.10 and 5.11). Although the relative pitch and roll angles / distances are different, the π-π and total slip

distances for **5.7** and **5.8** are very similar or the same as those measured in the crystal structure of **4.9** (Table 5.6) and allow for a significant amount of overlap between the cores (Figure 5.10). Furthermore, the aryl moiety in **5.8** does not impede π-π interactions and the torsion angle between this group and the plane of the core is 60.7º, consistent with a decrease in torsion angle calculated for **5.8** relative to **5.2** using DFT.

On the basis of the crystal structures of **5.7** and **5.8**, DFT evaluations of the intermolecular effective electronic couplings (B3LYP/6-31G**, using the fragment orbital approach[32]) were explored (Table 5.6). The electronic coupling for **5.7** along the π-π stacking direction (*a*-axis) is determined to be very low for electrons (7 meV, LUMO-LUMO) compared to **4.9**; however, the electronic coupling along the π-π stacking direction in **5.8** is similar to that seen in **4.9**, with a value of 63 meV (*a*-axis, LUMO-LUMO). These results suggest that, while the packing of **5.7** may not be conducive to electron transport in devices, **5.8** has an electronic coupling value much larger than its corresponding diacyl-NDI analogue, **5.2**, as predicted based on the extended core structure, and may be a good candidate for electron transport. However, additional properties must also be considered including reorganization energy and electron injection barriers from gold electrodes.

Table 5.6. Pitch and Roll Angles (deg) and Distances (Å) along with Electronic Coupling[a] (B3LYP/6-31G**) between Nearest Pairs (meV) for **4.9**, **5.7**, and **5.8**.

cmpd	*P*	*R*	*d*	d_P	d_R	d_{tot}	t_a	t_b	t_c
4.9	19.4	45.6	3.3	1.2	3.4	3.6	85	31	–
5.7	45.4	11.3	3.3	3.3	0.67	3.4	7	–	–
5.8	45.7	18.1	3.3	3.4	1.1	3.6	63	–	0

[a]Electronic coupling calculated along the *a*- (t_a), *b*- (t_b), and *c*- (t_c) axes, respectively, between LUMO levels of adjacent pairs with intermolecular distances less than 7 Å along the specified axis.

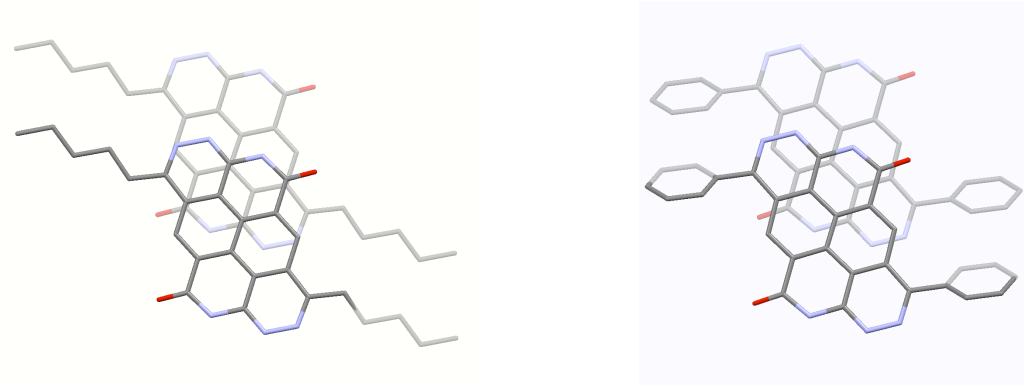

Figure 5.10. Crystal structure of **5.7** and **5.8** showing the overlap of the cores. *N,N'*-alkyl groups have been removed for clarity.

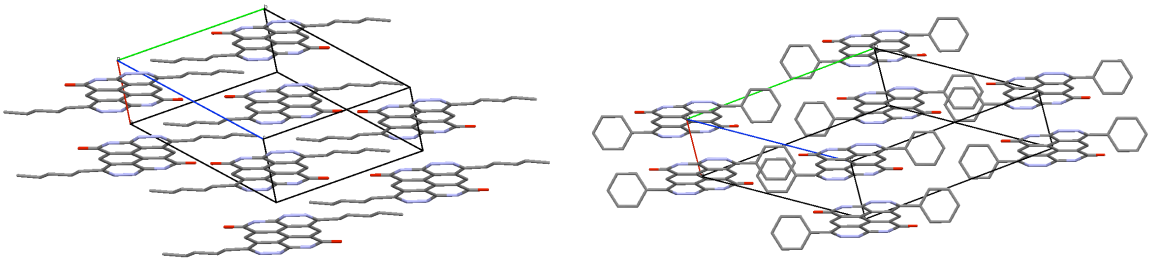

Figure 5.11. Crystal structure of **5.7** and **5.8** showing the packing motif. The axes are depicted according to: *a*-axis (red), *b*-axis (green), *c*-axis (blue). *N,N'*-alkyl groups have been removed for clarity.

5.3.4 Optical Properties and Electrochemistry

Electronic spectra of **5.7**-**5.9** were recorded in dilute dichloromethane solution and as thin films on glass substrates. Representative spectra are shown in Figure 5.12 and Figure 5.13; the corresponding absorption maxima and molar absorptivities are summarized in Table 5.7. The solution absorption spectra of **5.7**, **5.8** and **5.9** exhibit one prominent absorption band with maxima at 423, 433 and 450 nm, respectively. The oscillator strengths of **5.7** and **5.8** are fairly similar while that of **5.9** is much larger; **5.9** exhibits a larger extinction coefficient and broader absorption band than **5.7** and **5.8**. The absorption maxima are bathochromically shifted by ca. 50-80 nm relative to that of NDI

4.9 and the diacyl-NDI analogues **5.1**-**5.6**. This shift is attributed to the extended conjugation of the planar NDI core. Thin film absorption spectra exhibit bathochromic shifts in the absorption maxima, relative to solution, of 20, 10 and 70 nm in **5.7**, **5.8** and **5.9**, respectively; a change in the relative absorbtivity of the two prominent bands is also observed in each case compared to solution spectra.

Cyclic voltammetry (CV) was used to measure the electrochemical properties of **5.7**-**5.9** in CH_2Cl_2 / 0.1 M $^nBu_4NPF_6$ (Table 5.7 and Figure 5.14). Two reversible reduction processes were observed for **5.7**-**5.9** corresponding to the first and second reduction of the core. The first half-wave reduction ($E_{1/2}^{0/-}$) potentials of the aryl-substituted derivatives **5.8** and **5.9** are similar in magnitude, while the alkyl-substituted derivative **5.7** is ca. 0.10 V harder to reduce. All of the hydrazine-fused products, however, are significantly more difficult to reduce than **4.9**; this is consistent with the trend in the EA values observed using quantum-chemical calculations (Table 5.7).

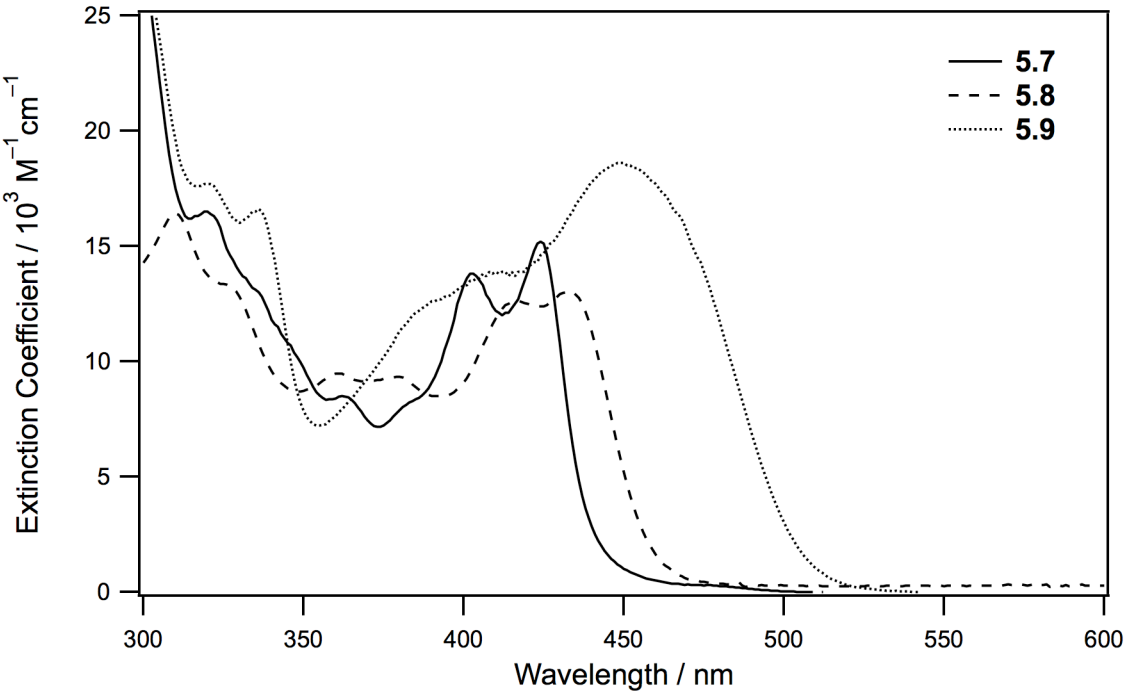

Figure 5.12. UV-vis. spectra of **5.7**-**5.9** in dilute dichloromethane solution.

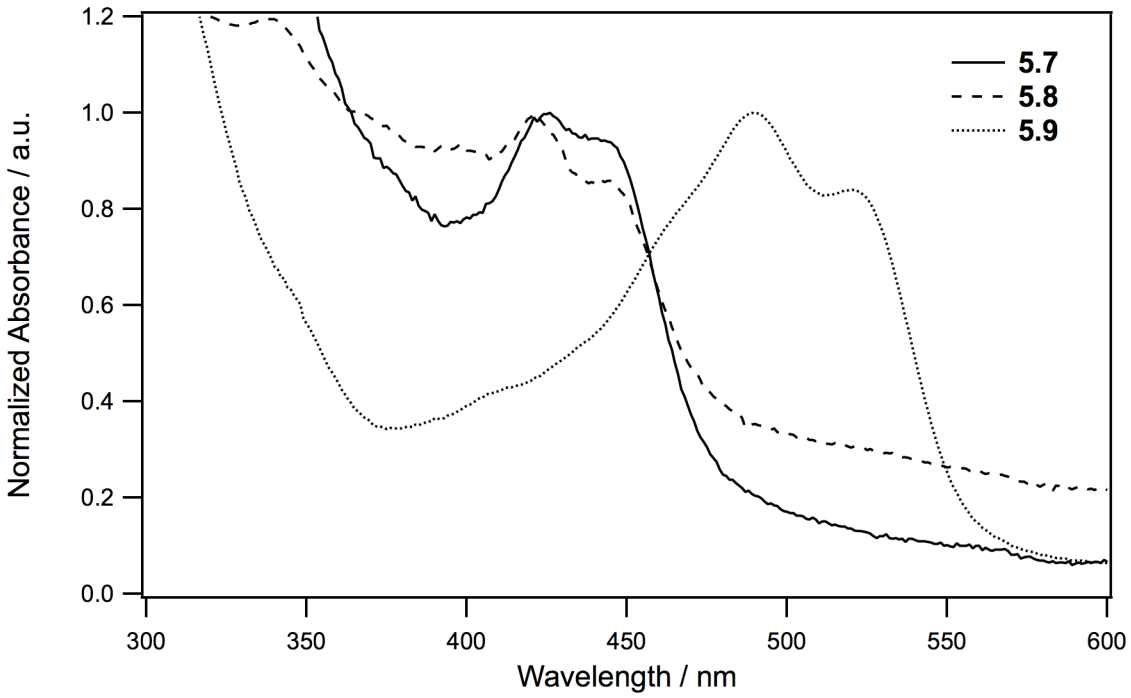

Figure 5.13. UV-vis. spectra of **5.7**-**5.9** as films on glass.

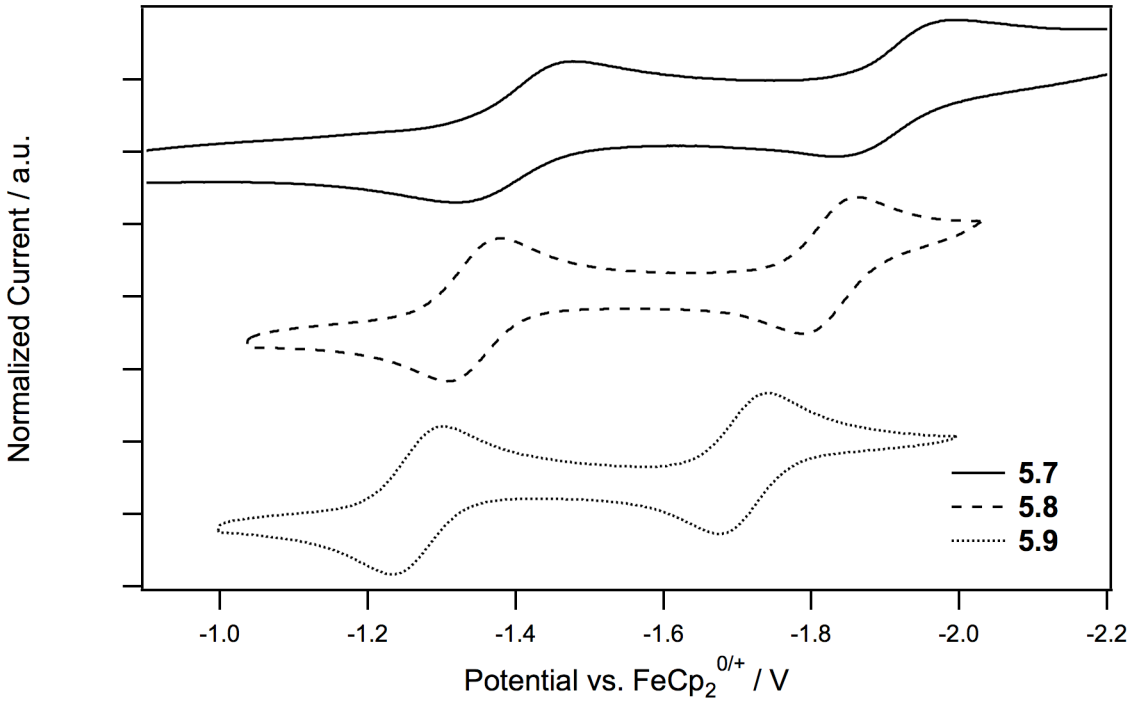

Figure 5.14. Cyclic voltammograms of **5.7**-**5.9** in 0.1 M $^{n}Bu_4N$ PF_6 in CH_2Cl_2 recorded at a scan rate of 50 mVs^{-1}.

The intramolecular reorganization energies for a self-exchange electron-transfer reaction between the neutral molecules and the corresponding radical anions were also calculated at the B3LYP/6-31G** level (Table 5.7). The calculated λ_e values are similar for all three fused-ring NDI derivatives. The values for **5.7**-**5.9** are smaller by ca. 60 meV compared with those estimated for **4.9** and are much smaller than the values calculated for the diacyl-NDI derivatives (by ca. 200 meV). The moderate electronic coupling and small reorganization energy observed in **5.9**, relative to **4.9**, suggest large electron transfer rates for **5.9** compared to the other molecules discussed in this chapter.

Table 5.7. Absorption Maxima (nm) and Absorptivities (10^4 $M^{-1}cm^{-1}$) for the Strong UV-vis. Absorptions of **5.7**-**5.9** in Dichloromethane along with Thin-Film Absorption Maxima (nm), Electrochemical Potentials (V vs. $FeCp_2^{+/0}$)[a] and Electrochemically Estimated Solid-State Electron Affinities (eV). DFT SCF Values for Electron Affinities and Reorganization Energies for Isolated Molecules (eV).

cmpd	λ_{max}		ε_{max}	$E_{1/2}^{0/-}$	$E_{1/2}^{-/2-}$	EA(s)[c]	EA_{adi}[d]	λ_e[e]
	soln	film						
4.9	380	393	2.76	–1.13	–1.70	–3.7	–2.03	0.336
5.7	402	425	1.38	–1.40	–1.91	–3.4	–1.83	0.271
	423	444	1.52					
5.8	416	433	1.26	–1.30	–1.73	–3.5	–1.91	0.276
	433	443	1.30					
5.9	450	489 520	1.87	–1.27	–1.71	–3.5	–2.03	0.269

[a]Cyclic Voltammetry in CH_2Cl_2 / 0.1 M $^nBu_4NPF_6$. [b]Estimated according to $E_{1/2}^{0/-}$(vs SCE) = $E_{1/2}^{0/-}$(vs. $FeCp_2^{+/0}$) + 0.46 V (for CH_2Cl_2). [c]Estimated according to EA(s) = −($eE_{1/2}^{0/-}$ vs. $FeCp_2^{+/0}$ + 4.8 eV). [d]Not measured due to solubility limitations. [d]Adiabatic EA = SCF energy difference between the relaxed ground-state anion and the ground-state neutral species (obtained for structures in which the alkyl groups are all replaced by methyl groups at the B3LYP/6-31G** level). [e]Internal reorganization energies for $M_A^- + M_B = M_A + M_B^-$ obtained as sum of the SCF energy difference between anion at the neutral geometry and at anion geometry and that between the neutral species at anion geometry and at neutral geometry.

5.3.5 OFET Behavior

Top-gate OFETs were fabricated with **5.7** and **5.8** as the active layer, CYTOP / Al_2O_3 as a bilayer gate dielectric[35] and Au source / drain electrodes (Table 5.8). The devices fabricated with **5.7** did not exhibit field-effect transistor function and no mobility values were measured. This result could be either due to the large barrier for electron injection due to the small EA associated with **5.7** and / or potentially poor electronic coupling between adjacent cores (as observed in **5.8**). Compound **5.9** was processed from 15 mg / mL solutions in 1,1',2,2'-tetrachloroethane resulting in improved film quality. Although electron mobility values were obtained for this material, the threshold is quite high, presumably due to large injection barriers associated with the small EA values, and the current on / off ratio is low. The mobility values were measured of up to 3.8×10^{-4} $cm^2V^{-1}s^{-1}$, which are two orders of magnitude smaller relative to the electron mobility values reported for solution-processed devices based on an unsubstituted NDI core ($0.01\ cm^2V^{-1}s^{-1}$).[36]

Table 5.8. Saturation Electron Mobilities, Threshold Voltages, and Current On / Off Ratios for OFETs Based on **5.7**-**5.9**.

cmpd	μ_e[a] / $cm^2V^{-1}s^{-1}$	V_{TH} / V	I_{on} / I_{off}
5.7	b	b	b
5.9	6.1 (± 2.3) × 10^{-4}	13.7 (± 2.1)	50

[a] Average values are calculated based on 3 to 7 devices from a single substrate. [b]No OFET behavior observed in the devices.

5.4 Summary

In this chapter, diacyl-NDIs and fused-ring NDIs were synthesized and characterized by quantum chemical calculations, X-ray crystallography, UV-vis.

spectroscopy, cyclic voltammetry, and OFET device performance. The diacyl-NDI derivatives are characterized by poor solubility, small electronic coupling values, and large reorganization energies resulting in a failure to fabricate functioning OFETs from **5.1** and **5.2**, and very low mobility values measured for a more soluble derivative, **5.6**. Aryl ketone derivatives of NDI with increasing fluorine substitution were also synthesized to investigate the inductive withdrawing effect of fluorine on the EA of the NDI structure. The measured first reduction potentials of **5.3**-**5.5** are below the estimated air-stability threshold of –0.4 V vs. SCE making them suitable candidates for air-stable electron transport; however, the solubility of these particular materials was not conducive to solution processing techniques and devices based on **5.3**-**5.5** were not fabricated. Fused-ring NDI derivatives **5.7**-**5.9** were synthesized in order to improve the intermolecular packing of the NDI cores. X-ray crystal structures of **5.7** and **5.8** indicated vary close π-π stacking distances of ca. 3.3 Å and moderate electronic coupling was estimated for **5.9**. Relatively small reorganization energies were also observed compared to NDI; however, electrochemically estimated EA values were smaller in magnitude than NDI by ca. 0.1 eV and very low mobility values were obtained, presumably at least partially due to large injection barriers.

Acylation of NDI and fused-ring NDI derivatives of this type are unexplored in the literature and the versatility of this method is attractive for the synthesis of new NDI cores. In particular, the solubility and EA values of these materials are easily tuned through varying the *N,N'*-alkyl substitution and the use of electron-poor acyl-halide coupling partners. A large variety of commercially available coupling candidates can be applied in this general synthetic method to develop new diacyl-NDI and fused-ring NDI derivatives.

5.5 Experimental

Experimental details describing the general synthesis and characterization methods, X-ray crystal structure measurements, computational methodologies, and fabrication of thin-film transistors can be found in Appendix A, B, C and D, respectively. X-ray crystal structure measurements included in this chapter were performed by either Alexandr Fonari (**5.2** and **5.7**) or Alexander Romanov (**5.6** and **5.8**) in Prof. Tatiana Timofeeva's research group in the Department of Chemistry at New Mexico Highlands University. Quantum chemical calculations included in this chapter were performed by Laxman Pandey and Dr. Chad Risko in Prof. Jean-Luc Brédas' research group in the School of Chemistry at Georiga Institute of Technology. Transistor fabrication and measurements included in this chapter were performed by either Dr. Shree Tiwari (**5.1** and **5.2**) or Dr. Do Kyung Hwang (**5.6**, **5.7** and **5.9**) in Prof. Bernard Kippelen's research group in the School of Electrical and Computer Engineering at Georgia Institute of Technology.

5.5.1 Synthetic procedures

***N*,*N'*-Bis(*n*-hexyl)-2,6-dihexanoylnaphthalene-1,8:4,5-bis(dicarboximide),** **5.1**. A solution of *N*,*N'*-bis(*n*-hexyl)-2,6-bis(tributylstannyl)naphthalene-1,8:4,5-bis(dicarboximide) (2.00 g, 1.98 mmol), hexanoyl chloride (0.798 g, 5.93 mmol), and copper(I) iodide (0.038 g, 0.198 mmol) in dry toluene (40 mL) was degassed with nitrogen for 5 min. Dichloro-bis(triphenylphosphine)palladium (0.069 g, 0.099 mmol) was added and the reaction was heated to 100 ºC for 2 h. After cooling, the reaction mixture was filtered through a plug of Celite eluting with toluene and the filtrate was concentrated via rotary evaporation. The crude product was purified by flash chromatography (silica gel, 0-2% methanol in dichloromethane). The product was recrystallized twice from ethyl

acetate and collected as a white solid (0.333 g, 0.518 mmol, 26%). ^{1}H NMR (400 MHz, $CDCl_3$) δ 8.46 (s, 2H), 4.11 (t, *J* = 7.6 Hz, 4H), 2.86 (t, *J* = 7.4 Hz, 4H), 1.85 (quint., *J* = 7.4 Hz, 4H), 1.66 (quint., *J* = 7.5 Hz, 4H), 1.50-1.20 (m, 20H), 0.92 (t, *J* = 7.0 Hz, 6H), 0.87 (t, *J* = 6.9 Hz, 6H). ^{13}C NMR (100 MHz, $CDCl_3$) δ 204.96, 162.18, 161.75, 146.88, 129.39, 126.91, 126.38, 122.24, 43.23, 41.17, 31.39, 31.25, 27.88, 26.64, 23.42, 22.50, 22.44, 13.98, 13.91. HRMS (MALDI) m/z $[M+H]^+$ calcd for $C_{38}H_{50}N_2O_6$ 631.3747; found,631.3580. Anal. Calcd. for $C_{38}H_{50}N_2O_6$: C, 72.35; H, 7.99; N, 4.44. Found: C,72.65; H, 7.94; N 4.47.

***N,N'*-Bis(*n*-hexyl)-2,6-dibenzoylnaphthalene-1,8:4,5-bis(dicarboximide), 5.2**. A solution of *N*,*N'*-bis(*n*-hexyl)-2,6-bis(tributylstannyl)naphthalene-1,8:4,5-bis(dicarboximide) (2.00 g, 1.98 mmol), benzoyl bromide (1.10 g, 5.93 mmol), and copper(I) iodide (0.038 g, 0.198 mmol) in dry toluene (40 mL) was degassed with nitrogen for 5 min. Dichloro-bis(triphenylphosphine)palladium (0.069 g, 0.099 mmol) was added and the reaction was heated to 100 ºC for 2 h. After cooling, the reaction mixture was filtered through a plug of Celite eluting with toluene and the filtrate was concentrated via rotary evaporation. The crude product was purified by flash chromatography (silica gel, 0-2% methanol in dichloromethane). The product was recrystallized twice from ethyl acetate and collected as a white solid (0.376 g, 0.596 mmol, 30%). ^{1}H NMR (400 MHz, $CDCl_3$) δ 8.63 (s, 2H), 7.79 (d, *J* = 7.3 Hz, 4H), 7.62 (dd, *J* = 7.4, 7.4 Hz, 2H), 7.47 (dd, *J* = 7.8, 7.8 Hz, 4H), 4.02 (t, *J* = 7.1 Hz, 4H), 1.59 (m, 4H), 1.33-1.15 (m, 12H), 0.81 (t, *J* = 6.9 Hz, 6H). ^{13}C NMR (100 MHz, $CDCl_3$) δ 194.79, 161.75, 161.71, 145.02, 135.49, 134.08, 130.55, 129.23, 128.91, 126.77, 126.64, 123.88, 41.15, 31.34, 27.79, 26.53, 22.44, 13.94. HRMS (MALDI) m/z $[M+H]^+$ calcd for $C_{40}H_{38}N_2O_6$ 643.2808; found, 643.2679. Anal. Calcd. for $C_{40}H_{38}N_2O_6$: C, 74.75; H, 5.96; N, 4.36. Found: C,74.49; H, 5.85; N 4.29.

***N,N'*-Bis(*n*-hexyl)-2,6-bis(4-fluorobenzoyl)naphthalene-1,8:4,5-bis(dicarboximide), 5.3**. A solution of *N,N'*-bis(*n*-hexyl)-2,6-bis(tributylstannyl)naphthalene-1,8:4,5-bis(dicarboximide) (0.500 g, 0.490 mmol), 4-fluorobenzoyl chloride (0.141 g, 0.890 mmol), and copper(I) iodide (0.004 g, 0.020 mmol) in dry toluene (5 mL) was degassed with nitrogen for 5 min. Dichloro-bis(triphenylphosphine)palladium (0.007 g, 0.010 mmol) was added and the reaction was heated to 100 ºC for 2 h. After cooling, the reaction mixture was filtered through a plug of Celite eluting with toluene and the filtrate was concentrated via rotary evaporation. The crude product was purified by flash chromatography (silica gel, 0-1% ethyl acetate in chloroform). The product was recrystallized twice from ethyl acetate and collected as a white solid (60.1 mg, 0.089 mmol, 18%). ^{1}H NMR (400 MHz, $CDCl_3$) δ 8.61 (s, 2H), 7.81 (dd, *J* = 8.8, 8.8 Hz, 4H), 7.14 (t, *J* = 8.6 Hz, 4H), 4.02 (t, *J* = 7.3 Hz, 4H), 1.67-1.53 (m, 4H), 1.35-1.13 (m, 12H), 0.82 (t, *J* = 6.9 Hz, 6H). ^{13}C NMR (100 MHz, $CDCl_3$) δ 193.16, 166.28 (d, *J* = 255 Hz), 161.71, 161.59, 144.68, 132.10, 131.89, 131.79, 130.48, 126.80 (d, *J* = 20 Hz), 123.5, 116.22 (d, *J* = 22 Hz), 41.20, 31.31, 27.80, 26.53, 22.44, 13.89. ^{19}F NMR (375 MHz, $CDCl_3$, referenced to trifluorotoluene in $CDCl_3$) δ –104.15. HRMS (EI) m/z $[M]^+$ calcd for $C_{40}H_{36}F_2N_2O_6$ 678.2541; found, 678.2557. Anal. Calcd. for $C_{40}H_{36}F_2N_2O_6$: C, 70.78; H, 5.35; N, 4.13. Found: C,70.55; H, 5.42; N 4.09.

***N,N'*-Bis(*n*-hexyl)-2,6-bis(4-(trifluoromethyl)benzoyl)naphthalene-1,8:4,5-bis(dicarboximide), 5.4**. A solution of *N,N'*-bis(*n*-hexyl)-2,6-bis(tributylstannyl)naphthalene-1,8:4,5-bis(dicarboximide) (0.500 g, 0.490 mmol), 4-(trifluoromethyl)benzoyl chloride (0.215 g, 1.03 mmol), and copper(I) iodide (0.004 g, 0.020 mmol) in dry toluene (5 mL) was degassed with nitrogen for 5 min. Dichloro-bis(triphenylphosphine)palladium (0.007 g, 0.010 mmol) was added and the reaction was heated to 100 ºC for 1.5 h. After cooling, the reaction mixture was diluted with 1,1',2,2'-tetrachloroethane and filtered through a plug of silica gel eluting with 1,1',2,2'-

tetrachloroethane:ethyl acetate. The filtrate was diluted with hexanes (1:1 hexanes:$C_2H_2Cl_4$) and placed at –20 ºC for 1 h to precipitate a white solid. The crude product was recrystallized from dichloromethane and collected as a white solid (0.112 mg, 0.144 mmol, 29%). ^{1}H NMR (400 MHz, $C_2D_2Cl_4$) δ 8.64 (s, 2H), 7.92 (d, *J* = 8.0 Hz, 4H), 7.76 (d, *J* = 8.3 Hz, 4H), 4.03 (t, *J* = 7.3 Hz, 4H), 1.70-1.50 (m, 4H + H_2O overlap), 1.35-1.15 (m, 12H), 0.83 (t, *J* = 6.6 Hz, 6H). ^{19}F NMR (375 MHz, $C_2D_2Cl_4$, referenced to trifluorotoluene in $CDCl_3$) δ -62.94. HRMS (EI) m/z $[M]^+$ calcd for $C_{42}H_{36}F_6N_2O_6$ 778.2478; found, 778.2477. Anal. Calcd. for $C_{42}H_{36}F_6N_2O_6$: C, 64.78; H, 4.66; N, 3.60. Found: C, 64.58; H, 4.54; N 3.59.

***N,N'*-Bis(*n*-hexyl)-2,6-bis(3,4,5-trifluorobenzoyl)naphthalene-1,8:4,5-bis(dicarboximide), 5.5**. A solution of *N*,*N'*-bis(*n*-hexyl)-2,6-bis(tributylstannyl)naphthalene-1,8:4,5-bis(dicarboximide) (0.500 g, 0.490 mmol), 3,4,5-trifluorobenzoyl chloride (0.202 g, 1.04 mmol), and copper(I) iodide (0.004 g, 0.020 mmol) in dry toluene (5 mL) was degassed with nitrogen for 5 min. Dichloro-bis(triphenylphosphine)palladium (0.007 g, 0.010 mmol) was added and the reaction was heated to 100 ºC for 4 h. After cooling, the reaction mixture was diluted with 1,1',2,2'-tetrachloroethane and filtered through a plug of Celite. The solvent was removed under reduced pressure. The crude product was recrystallized from chlorobenzene and collected as a white solid (0.034 mg, 0.045 mmol, 9.2%). recrystallized from dichloromethane and collected as a white solid (0.112 mg, 0.144 mmol, 29%). ^{1}H NMR (400 MHz, $C_2D_2Cl_4$) δ 8.62 (s, 2H), 7.45 (m, 4H), 4.04 (m, 4H), 1.70-1.50 (m, 4H + H_2O overlap), 1.40-1.20 (m, 12H), 0.85 (m, 6H). HRMS (EI) m/z $[M]^+$ calcd for $C_{40}H_{32}F_6N_2O_6$ 750.2165; found, 750.2150. Anal. Calcd. for $C_{40}H_{32}F_6N_2O_6$: C, 64.00; H, 4.30; N, 3.73. Found: C, 63.72; H, 4.34; N 3.79.

***N,N'*-Bis(*n*-dodecyl)-2,6-di (thiophene-2-carbonyl)naphthalene-1,8:4,5-bis(dicarboximide), 5.6**. A solution of *N*,*N'*-bis(*n*-dodecyl)-2,6-

bis(tributylstannyl)naphthalene-1,8:4,5-bis(dicarboximide) (2.70 g, 2.33 mmol), thiophenoyl chloride (0.719 g, 4.90 mmol), and copper(I) iodide (0.044 g, 0.233 mmol) in dry toluene (25 mL) was degassed with nitrogen for 5 min. Dichloro-bis(triphenylphosphine)palladium (0.082 g, 0.117 mmol) was added and the reaction was heated to 100 ºC for 1 h. After cooling, the reaction mixture was filtered through a plug of Celite eluting with dichloromethane and the filtrate was concentrated via rotary evaporation. The crude product was purified by flash chromatography (silica gel, dichloromethane). The product was recrystallized from ethyl acetate and from isopropanol and collected as a yellow solid (0.426 g, 0.518 mmol, 22%). ^{1}H NMR (400 MHz, $C_2D_2Cl_4$) δ 8.69 (s, 2H), 7.79 (dd, *J* = 4.9, 1.1 Hz, 2H), 7.30 (m, 2H), 7.10 (dd, *J* = 4.8, 3.9 Hz, 2H), 4.05 (m, 4H), 1.62 (m, 4H), 1.35-1.15 (m, 36H), 0.85 (t, *J* = 6.9 Hz, 6H). ^{13}C NMR (100 MHz, $C_2D_2Cl_4$) δ 186.83, 161.58, 161.46, 144.21, 142.71, 135.54, 134.45, 130.65, 128.40, 128.37, 126.80, 123.65, 41.23, 31.86, 29.56, 29.51, 29.45, 29.60, 29.20, 27.85, 26.93, 22.64, 14.08 (one alkyl resonance not observed, presumably due to overlap). HRMS (MALDI) m/z $[M+H]^+$ calcd for $C_{48}H_{58}N_2O_6S_2$ 822.3736; found, 822.3719. Anal. Calcd. for $C_{48}H_{58}N_2O_6S_2$: C, 70.04; H, 7.10; N, 3.40. Found: C, 70.04; H, 7.02; N, 3.57.

1,7-Di(*n*-pentyl)-4,10-di(*n*-hexyl)phthalazino[6,7,8,1-*lmna*]pyridazino[5,4,3-*gh*][3,8]phenanthroline-5,11(4*H*,10*H*)-dione, 5.7. To solution of **5.1** (0.200 g, 0.317 mmol) in ethanol (6 mL) at 80 ºC was added hydrazine monohydrate (0.5 mL). The reaction was heated at 100 ºC in a pressure tube for 2 d while being monitored by TLC. After cooling, the reaction mixture was diluted with dichloromethane and filtered. Removed solvent under reduced pressure. The crude product was purified by flash chromatography (silica gel, 0-3% methanol in dichloromethane). The product was recrystallized from dichloromethane and twice from methanol to yield yellow crystals (0.073 g, 0.117 mmol, 37%). ^{1}H NMR (400 MHz, $CDCl_3$) δ 9.47 (s, 2H), 4.86 (t, *J* = 7.6

Hz, 4H), 3.65 (t, *J* = 7.8 Hz, 4H), 2.08 (quint., *J* = 7.6 Hz, 4H), 1.97 (quint., *J* = 7.6 Hz, 4H), 1.60-1.50 (m, 8H), 1.50-1.25 (m, 12H), 0.93 (t, *J* = 7.2 Hz, 6H), 0.88 (t, *J* = 7.1 Hz, 6H). ^{13}C NMR (100 MHz, $CDCl_3$) δ 160.58, 157.37, 149.72, 128.34, 125.74, 124.39, 123.28, 110.87, 42.36, 33.27, 31.78, 31.58, 29.36, 27.81, 26.78, 22.58, 22.49, 14.03, 13.96. HRMS (MALDI) m/z $[M+H]^+$ calcd for $C_{38}H_{51}N_6O_2$ 623.4034; found,623.4074. Anal. Calcd. for $C_{38}H_{50}N_6O_2$: C, 73.28; H, 8.09; N, 13.49. Found: C, 72.57; H, 7.93; N 13.24.

4,10-Di(*n*-hexyl)-1,7-diphenylphthalazino[6,7,8,1-*lmna*]pyridazino[5,4,3-*gh*][3,8]phenanthroline-5,11(4*H*,10*H*)-dione, 5.8. To solution of **5.2** (0.200 g, 0.311 mmol) in ethanol (6 mL) at 80 ºC was added hydrazine monohydrate (0.2 mL). The reaction was heated at 100 ºC in a pressure tube for 2 d while being monitored by TLC. Additional hydrazine monohydrate (0.5 mL) was added and the reaction was heated at 100 ºC for 2 more d while being monitored by TLC. After cooling, the reaction mixture was diluted with chloroform and filtered. Removed solvent under reduced pressure. The product was purified by flash chromatography (silica gel, 5% ethyl acetate in chloroform). Upon fraction collection, yellow solid began to precipitate from chloroform solution. Placed product fraction in the freezer and collected the product as a yellow solid (0.019 g, 0.030 mmol, 10%). ^{1}H NMR (400 MHz, $C_2D_2Cl_4$) δ 9.57 (s, 2H), 7.97 (m, 4H), 7.76 (m, 6H), 4.92 (t, *J* = 7.7 Hz, 4H), 2.01 (quint., *J* = 7.7 Hz, 4H), 1.60-1.50 (m, 4H), 1.50-1.30 (m, 8H), 0.91 (t, *J* = 7.2 Hz, 6H). ^{13}C NMR (100 MHz, $C_2D_2Cl_4$) δ 160.45, 156.22, 149.59, 134.91, 130.27, 130.07, 129.18, 128.33, 127.84, 124.09, 123.23, 111.07, 42.54, 31.54, 27.81, 26.77, 22.56, 14.10. HRMS (MALDI) m/z $[M+H]^+$ calcd for $C_{40}H_{39}N_6O_2$ 635.3134; found,635.3140. Anal. Calcd. for $C_{40}H_{38}N_6O_2$: C, 75.69; H, 6.03; N, 13.24. Found: C, 75.40; H, 6.04; N 13.08.

4,10-Di(*n*-dodecyl)-1,7-di(thiophen-2-yl)phthalazino[6,7,8,1-*lmna*]pyridazino[5,4,3-*gh*][3,8]phenanthroline-5,11(4*H*,10*H*)-dione, 5.9. A solution of

5.6 (0.200 g, 0.243 mmol) in *n*-butanol (5 mL) was heated at 120 ºC for 15 min. Hydrazine monohydrate (0.5 mL) was added and the reaction mixture turned black. After 10 min, a large amount of orange solid began to precipitate in the reaction flask. Atfter 30 min, the TLC indicated the reaction was complete and the mixture was cooled to room temperature. After cooling, the reaction mixture was diluted with ethanol, filtered and the orange solid was dried on the filter. The crude product was dissolved in dichloromethane, filtered through a plug of Celite, and purified by flash chromatography (silica gel, dichloromethane). The product was recrystallized from ethyl acetate to yield an orange solid (0.045 g, 0.055 mmol, 23%). ^{1}H NMR (400 MHz, $C_2D_2Cl_4$) δ 9.89 (s, 2H), 7.97 (d, *J* = 3.1 Hz, 2H), 7.78 (d, *J* = 5.0 Hz, 2H), 7.42 (dd, *J* = 4.3, 4.3 Hz, 2H), 4.89 (t, *J* = 7.4 Hz, 4H), 2.01 (quint., *J* = 7.6 Hz, 4H), 1.59 (quint., *J* = 7.6 Hz, 4H), 1.42 (quint., *J* = 7.2 Hz, 4H), 1.35-115 (m, 32H), 086 (t, *J* = 6.7 Hz, 6H). ^{13}C NMR (100 MHz, $C_2D_2Cl_4$) δ 160.23, 150.15, 149.12, 137.68, 130.47, 130.21, 128.68, 128.56, 127.29, 123.26, 111.0, 42.62, 31.78, 29.52, 29.43, 29.23, 27.91, 27.14, 22.60, 14.14 (one aromatic and three alkyl resonances not observed, presumably due to overlap). HRMS (MALDI) m/z $[M+H]^+$ calcd for $C_{48}H_{59}N_6O_2S_2$: 815.4141; found, 815.4126. Anal. Calcd. for $C_{48}H_{58}N_6O_2S$: C, 70.73; H, 7.17; N, 10.31. Found: C, 70.43; H, 7.17; N 10.22.

5.6 References

(1) Murphy, A.; Fréchet, J. *Chem. Rev.* **2007**, *107*, 1066.

(2) Anthony, J. E.; Facchetti, A.; Heeney, M.; Marder, S. R.; Zhan, X. *Adv. Mater.* **2010**, *22*, 3876.

(3) Dimitrakopoulos, C.; Malenfant, P. *Adv. Mater.* **2002**, *14*, 99.

(4) Jones, B. A.; Facchetti, A.; Wasielewski, M. R.; Marks, T. J. *J. Am. Chem. Soc.* **2007**, *129*, 15259.

(5) Oh, J. H.; Suraru, S.-L.; Lee, W.-Y.; Koenemann, M.; Hoeffken, H. W.; Roeger, C.; Schmidt, R.; Chung, Y.; Chen, W.-C.; Wuerthner, F.; Bao, Z. *Adv. Funct. Mater.* **2010**, *20*, 2148.

(6) Gao, X.; Di, C.-A.; Hu, Y.; Yang, X.; Fan, H.; Zhang, F.; Liu, Y.; Li, H.; Zhu, D. *J. Am. Chem. Soc.* **2010**, *132*, 3697.

(7) Hu, Y.; Gao, X.; Di, C.-A.; Yang, X.; Zhang, F.; Liu, Y.; Li, H.; Zhu, D. *Chem. Mater.* **2011**, *23*, 1204.

(8) Jones, B. A.; Facchetti, A.; Marks, T. J.; Wasielewski, M. R. *Chem. Mater.* **2007**, *19*, 2703.

(9) Letizia, J. A.; Cronin, S.; Ortiz, R. P.; Facchetti, A.; Ratner, M. A.; Marks, T. J. *Chem. Eur. J.* **2010**, *16*, 1911.

(10) Usta, H.; Risko, C.; Wang, Z.; Huang, H.; Deliomeroglu, M. K.; Zhukhovitskiy, A.; Facchetti, A.; Marks, T. J. *J. Am. Chem. Soc.* **2009**, *131*, 5586.

(11) Usta, H.; Facchetti, A.; Marks, T. J. *J. Am. Chem. Soc.* **2008**, *130*, 8580.

(12) Jones, B.; Ahrens, M.; Yoon, M.; Facchetti, A.; Marks, T.; Wasielewski, M. *Angew. Chem. Int. Ed.* **2004**, *43*, 6363.

(13) Piliego, C.; Jarzab, D.; Gigli, G.; Chen, Z.; Facchetti, A.; Loi, M. A. *Adv. Mater.* **2009**, *21*, 1573.

(14) Suzuki, Y.; Miyazaki, E.; Takimiya, K. *J. Am. Chem. Soc.* **2010**, *132*, 10453.

(15) Yuan, Z.; Li, J.; Xiao, Y.; Li, Z.; Qian, X. *J. Org. Chem.* **2010**, *75*, 3007.

(16) Chopin, S.; Chaignon, F.; Blart, E.; Odobel, F. *J. Mater. Chem.* **2007**, *17*, 4139.

(17) Jung, B. J.; Sun, J.; Lee, T.; Sarjeant, A.; Katz, H. E. *Chem. Mater.* **2009**, *21*, 94.

(18) See, K. C.; Landis, C.; Sarjeant, A.; Katz, H. E. *Chem. Mater.* **2008**, *20*, 3609.

(19) Katz, H.; Lovinger, A.; Johnson, J.; Kloc, C.; Siegrist, T.; Li, W.; Lin, Y.; Dodabalapur, A. *Nature* **2000**, *404*, 478.

(20) Jones, B.; Ahrens, M.; Yoon, M.; Facchetti, A.; Marks, T.; Wasielewski, M. *Angew. Chem. Int. Ed.* **2004**, *43*, 6363.

(21) Oh, J.; Liu, S.; Bao, Z.; Schmidt, R.; Wurthner, F. *Appl. Phys. Lett.* **2007**, *91*.

(22) Chen, H.; Ling, M.; Mo, X.; Shi, M.; Wang, M.; Bao, Z. *Chem. Mater.* **2007**, *19*, 816.

(23) Ahrens, M.; Fuller, M.; Wasielewski, M. *Chem. Mater.* **2003**, *15*, 2684.

(24) Mas-Torrent, M.; Rovira, C. *Chem. Rev.* **2011**, *111*, 4833.

(25) Stille, J. *Angew. Chem. Int. Ed.* **1986**, *25*, 508.

(26) Sauvé, G.; Javier, A. E.; Zhang, R.; Liu, J.; Sydlik, S. A.; Kowalewski, T.; McCullough, R. D. *J. Mater. Chem.* **2010**, *20*, 3195.

(27) Ellinger, S.; Kreyes, A.; Ziener, U.; Hoffmann-Richter, C.; Landfester, K.; Moller, M. *European J. Org. Chem.* **2007**, 5686.

(28) Kastler, M.; Pisula, W.; Wasserfallen, D.; Pakula, T.; Müllen, K. *J. Am. Chem. Soc.* **2005**, *127*, 4286.

(29) Hansch, C.; Leo, A.; Taft, R. W. *Chem. Rev.* **1991**, *91*, 165.

(30) Curtis, M. D.; Cao, J.; Kampf, J. W. *J. Am. Chem. Soc.* **2004**, *126*, 4318.

(31) Shukla, D.; Nelson, S. F.; Freeman, D. C.; Rajeswaran, M.; Ahearn, W. G.; Meyer, D. M.; Carey, J. T. *Chem. Mater.* **2008**, *20*, 7486.

(32) Valeev, E. F.; Coropceanu, V.; da Silva Filho, D. A.; Salman, S.; Brédas, J.-L. *J. Am. Chem. Soc.* **2006**, *128*, 9882.

(33) Adiga, S. P.; Shukla, D. *J. Phys. Chem. C* **2010**, *114*, 2751.

(34) Marcus, R. *Rev. Mod. Phys.* **1993**.

(35) Hwang, D. K.; Fuentes-Hernandez, C.; Kim, J.; Potscavage, W. J.; Kim, S.-J.; Kippelen, B. *Adv. Mater.* **2011**, *23*, 1293.

(36) Katz, H.; Johnson, J.; Lovinger, A.; Li, W. *J. Am. Chem. Soc.* **2000**, *122*, 7787.

(37) Wharton, C. J.; Wrigglesworth, R. *J. Chem. Soc., Perkin Trans. 1* **1985**, 809.

(38) Warner, C. R.; Walsh, E. J.; Smith, R. F. *J. Chem. Soc.* **1962**, 1232.

CHAPTER 6

CONCLUSIONS

Overview. The research in this thesis focused on understanding the physical and electronic properties of donor (D) and acceptor (A) based D-A-D, A-D-A, and A-A-A structured small-molecules and specifically addressed the ability to tune these properties through synthetic design. The objectives of the research were 1) to design and synthesize a range of conjugated D/A small molecules, 2) to understand the structure-property relationships for these materials, and 3) to assess their utility as solution-processed active layers in organic field-effect transistors (OFETs). The main focus of this thesis is on the synthesis and physical properties associated with oligothiophene and naphthalene diimide (NDI) based small-molecules with different D-A combinations explored in Chapter 2, NDI-D-NDI structures described in Chapters 3, and NDI-A combinations investigated in Chapters 4 and 5. A summary of the more specific results of each chapter can be found below.

In order to obtain materials, which exhibit appropriate molecular order in the solid state, energy levels for charge injection, and solubility in solvents conducive to solution-processing techniques, efforts were paid to synthesize planar, fused-ring systems incorporating electron-deficient cores with appropriate alkyl substitution. In order to do this, the synthesis of a variety of precursors were developed and / or optimized including that of 2-(tributylstannyl)dithienopyrrole (DTP), 2-hexyl-2'-(tributylstannyl)-DTP, 4-bromo-7-hexylbenzothiadiazole (BTD), 2-bromo-NDI, and both 2-(tributylstannyl) and 2,6-di(tributylstannyl)-NDI derivatives, which had not previously been described. These precursors can be applied towards the synthesis of a diverse set of products leading to new materials for various organic electronic applications including, but not limited to,

OFETs, organic photovoltaics (OPVs), and dye-sensitized solar cells (DSSC). The final products were then built from these novel intermediates using well-known palladium-catalyzed coupling techniques.

Upon successful synthesis of the molecular D/A materials, their structure-property relationships were studied using optical and electrochemical techniques along with the single-crystal structure, in some cases, and comparison to quantum-chemical calculations. These studies indicated that the physical properties of the materials could be tuned by varying the degree of D and / or A character of the individual components. In the case of the D-A-D and A-D-A small molecules incorporating BTD and NDI, the low energy UV-vis. absorptions were found to have considerable D-to-A charge transfer character, which could be tuned depending on the strength of the D and A components. Additionally, as expected based on the literature, the ionization potential (IP) and electron affinity (EA) of the materials were found to be highly dependent on the D and A, respectively. The solid-state structures of a number of D-A-D and A-A-A structured materials were also studied, based on the X-ray single-crystal structure, with comparisons to electronic coupling values determined by DFT. In general, it was found that planar, fused-ring structures led to larger electronic coupling values. The estimated reorganization energies were also described by DFT and, along with the electronic coupling, predictions were made regarding the electron transfer rates of the materials. The results correlated small reorganization energies and large electronic coupling to improved electron mobility values as described by Marcus Theory.

The potential utility of the products as charge-transport materials was tested in OFET devices. Devices based on D-A small molecules, with BTD as the A, exhibited only p-channel characteristics, while increasing the electron affinity through the incorporation of NDI as the A unit led to the observation of n-channel and ambipolar mobility. The charge-transport materials reported in this thesis are interesting for a

variety of organic electronic applications in addition to OFETs. In particular, the D-A materials containing DTP and BTD or NDI are of interest for use in bulk-heterojunction organic photovoltaics where solution processability and charge-transport properties are required.

Chapter Summary. In Chapter 2, the main goal was to understand the basic properties of D-A-D and A-D-A triads based on DTP donors and BTD acceptors and the structural effects of these systems on the physical properties of the materials. The triads were synthesized, characterized using UV-vis absorption and electrochemistry, and studied using (TD)DFT calculations. Previously, a few examples of small-molecule D-A-D and A-D-A structures with BTD acceptors and various oligothiophene and planarized oligothiophene donors had been synthesized and incorporated into organic photovoltaic (OPV) and field-effect transistor (OFET) applications; however, the majority of work done had focused on D-A conjugated copolymers. The study presented here provided a thorough investigation of the fundamental nature of the specific D/A interactions, which are not readily studied in the polymer analogues. Comparisons were also made to benzene derivatives, highlighting the nature of BTD in D/A functional materials.

The research in Chapter 3 focused on the effects of incorporating NDI into A-D-A structures and studying the extent to which these cores were influenced by the varied length and donor character of the bridging groups. Molecular NDI derivatives had been reported with varied *N,N'*-alkyl / *N,N'*-aryl substitution, with only a few examples of core functionalization, exhibiting good to excellent electrical characteristics in OFETs. The synthesis of D-A small-molecules or polymers incorporating NDI as the acceptor and the synthesis of solution-processable NDI derivatives, however, was relatively unexplored. These A-D-A derivatives exhibited moderate to high electron mobility values of up to 1.5 $cm^2V^{-1}s^{-1}$ being classified as the highest electron mobility observed to date for solution-processed small-molecule or polymeric materials.

Chapter 4 described the synthesis and characterization of the first stannyl derivatives of NDIs and their use as reagents in Stille coupling reactions to obtain bi- and ter-NDIs. The *N,N′*-substituents of NDIs generally only exibited minimal influence on the optical and electronic properties of isolated molecules and core substitution of these species had led to significant effects on the redox potentials and optical spectra of the products. Core functionalization of NDIs had been explored using nucleophilic substitution and palladium-catalyzed coupling reactions of NDI bromides; however, the availability of appropriate metallated coupling partners, such as stannanes and boronates, limited the use of electron-poor moieties. Core stannylated derivatives of NDI were introduced in Chapter for representing important building blocks that allow for the synthesis of new small-molecule and polymeric NDIs. The rest of Chapter 4 demonstrated the potential of this stannyl-NDI derivative through the synthesis and characterization of new NDI-A-NDI structures, which could not be synthesized through alternative methods. Moderate solution-processed electron mobility values were also obtained for this series (up to 0.3 $cm^2V^{-1}s^{-1}$) further validating the utility of this new stannyl-NDI derivative.

The NDI precursor synthesized in Chapter 4 was applied again in Chapter 5 to develop previously unexplored A-NDI-A structured diacyl-NDI derivatives. The effect of alky, aryl, and fluoroaryl substituents on the solid-state packing relative to NDI and the electron affinity relative to the air stability threshold was explored. NDI cores functionalized with electron withdrawing groups such as halo and cyano derivatives had been synthesized leading to electrochemical potentials above the air stability threshold and air-stable electron transport. This type of functionalization, however, was very limited and did not leave room for further synthetic modification. The acyl-NDIs reported in Chapter 5 offered a versatile way for functionalizing the NDI core with electron-poor side groups while still allowing for side group variety, which allowed for changes in

solubility, solid state packing, and electron mobility. The second study in Chapter 5 investigated the condensation of the diacyl-NDIs to form planar, extended-core structures. The solid-state packing of these structures were explored relative the their acyl-NDI analogues and to the NDI core structure. Although a few other types of extended-core functionalization had been employed for NDI derivatives, this field was relatively unexplored compared to unsubstituted NDI core analogues; the extended core structure led to an improvement in the electronic coupling relative to the acyl-NDI derivatives and a decrease in the reorganization energy relative to NDI making them attractive candidates for electron transport.

Conclusion. Naphthalene diimide-based structures have grown popular in OFET literature due to the advantageous solid-state packing, large electron affinity, and large vacuum-processed mobility values that have often been associated with this core. The research presented in this thesis, however, has shown that through simple synthetic modifications, NDI cores can be applied successfully as solution-processed active layers with very high mobility values. Based on this work, the synthesis of new solution-processable electron-transport materials should be focused on the NDI-A framework, as presented in Chapters 4 and 5, incorporating solubilizing *N,N′*-substituents and electron-poor A groups. The synthetic design strategies presented in this work enable the synthesis of new NDI-A structures and the research reported here will serve as a framework for the development of new solution-processable, n-channel and ambipolar charge-transport materials for OFETs, and potentially, for other organic electronic applications.

APPENDIX A

GENERAL METHODS FOR SYNTHESIS AND CHARACTERIZATION

A.1 Materials

Starting materials were reagent grade and were used without further purification unless otherwise indicated. Solvents were dried by passing through columns of activated alumina (toluene, CH_2Cl_2), by distillation from Na/benzophenone (THF), or were obtained as anhydrous grade from Acros Organics.

A.2 Characterization

Chromatography. Chromatographic separations were performed using standard flash column chromatography methods using silica gel purchased from Sorbent Technologies (60 Å, 32-63 μm).

Nuclear Magnetic Resonance. ^{1}H and $^{13}C\{^{1}H\}$ NMR spectra were obtained on either a Varian Mercury 300 MHz or a Bruker AMX 400 MHz spectrometer with chemical shifts referenced to $CDCl_3$ or $C_2D_2Cl_4$, as specified, using the ^{1}H resonance of the residual protio solvent signal or the ^{13}C resonance of the deuterated solvent, respectively.

Mass Spectrometry. EI and FAB mass spectra were recorded on a VG Instruments 70SE or a Micromass AutoSpec and MALDI spectra were recorded on an Applied Biosystems 4700 Proteomics Analyzer by the Georgia Tech Mass Spectrometry Facility. GCMS data were acquired on an Agilent 5790 GC / 6850 MS.

Thermal Properties. Differential scanning calorimetry (DSC) was carried out under nitrogen on a TA Instruments Q200 (scanning rate of 5 ºC min^{-1}). Thermogravimetric analysis (TGA) was carried out using a Netzsch STA 449 C Jupiter (heating rate of 5 ºC min^{-1}).

Electrochemical Measurements. Electrochemical measurements were carried out under nitrogen in dry deoxygenated 0.1 M tetra-*n*-butylammonium hexafluorophosphate in dichloromethane using a conventional three-electrode cell with a glassy carbon working electrode, platinum wire counter electrode, and a Ag wire coated with AgCl as pseudo-reference electrode. Potentials were referenced to ferrocenium / ferrocene by using decamethylferrocene (–0.55 V vs. ferrocenium / ferrocene) for ferrocene as an internal reference, as specified. Cyclic voltammagrams were recorded at a scan rate of 50 mVs^{-1}.

Optical Spectroscopy. UV-vis-NIR spectra were recorded in 1 cm cells using a Varian Cary 5E spectrometer in either chloroform or dichloromethane solvents, as specified in the text.

Elemental Analysis. Elemental analyses were performed by Atlantic Microlabs.

APPENDIX B

X-RAY DIFFRACTION DETAILS AND CRYSTAL IDENTIFICATION FILES

The measurement of the X-ray crystal structures presented in this thesis was performed by Alexandr Fonari (**3.6**, **5.2** and **5.7**) and Alexander Romanov (**4.4**, **5.6** and **5.8**) while working in Prof. Tatiana Timofeeva's research group in the Department of Chemistry at New Mexico Highlands University.

B.1 Experimental Details

The X-ray diffraction data were collected with a Bruker Apex II CCD area detector at 100 K using graphite monochromated Mo Kα radiation (λ = 0.71073 Å). Absorption correction was applied semi-empirically using APEX2 program.[1] The structures were solved by direct methods and refined by full matrix least-squares on F^2 in the anisotropic approximation for non-hydrogen atoms. The phenyl-ring of molecule **5.8** were disordered into two positions with the occupancies 0.51/0.49. For the final refinement, the contribution of the severely disordered 1,1',2,2'-tetrachloroethane molecule of crystallization were removed from the diffraction data with *PLATON*[2] / *SQUEEZE*[3]. All hydrogen atom positions were refined in isotropic approximation in "riding" model with the $U_{iso}(H)$ parameters equal to 1.2 $U_{eq}(C_i)$, for methyl groups equal to 1.5 $U_{eq}(C_{ii})$, where $U(C_i)$ and $U(C_{ii})$ are respectively the equivalent thermal parameters of the carbon atoms to which the corresponding H atoms are bonded. Data reduction and further calculations were performed by using the SHELXS-97[4] and SHELXL-97[5] (**3.6**, **5.2** and **5.7**) or SHELXTL[6] (**4.4**, **5.6** and **5.8**) program packages. Selected refinement data and structure parameters are shown in Table C.1.

Table B.1. Summary of the details for the structure determinations performed.

	3.6	**5.2**	**5.6**	**5.7**	**5.8**
Empirical formula	$C_{54}H_{60}N_4O_4S_4$	$C_{40}H_{38}N_2O_6$	$C_{48}H_{58}N_2O_6S_2$	$C_{38}H_{50}N_6O_2$	$C_{41}H_{38}N_6O_2$
Formula weight	957.30	642.72	823.08	622.84	634.76
Crystal appearance	Purple plate	Colorless needle	Colorless needle	Yellow needle	Yellow needle
Crystal system	Triclinic	Monoclinic	Triclinic	Triclinic	Triclinic
Space group	$P\bar{1}$	C2/c	$P\bar{1}$	$P\bar{1}$	$P\bar{1}$
a / Å	8.578(4)	27.241(10)	5.714(3)	4.8953(10)	4.806(6)
b / Å	17.526(9)	5.734(2)	9.811(4)	12.709(3)	14.85(2)
c / Å	17.614(9)	23.284(8)	19.638(9)	14.175(3)	14.93(2)
α / Å	68.617(7)	90	100.270(8)	88.727(4)	60.43(2)
β / Å	81.197(11)	112.558(7)	97.424(9)	83.038(4)	85.26(2)
γ / Å	89.749(9)	90	94.807(9)	79.127(4)	89.20(2)
Volume / $Å^3$	2433(2)	3358(2)	1067.8(8)	859.7(3)	923(2)
Z	2	4	1	1	1
ρ_{calc} / gcm^{-3}	1.307	1.271	1.280	1.203	1.142
μ / mm^{-1}	0.246	0.086	0.177	0.076	0.072
F(000)	1016	1360	400	336	336
Crystal size / mm^3	–	–	0.59×0.05×0.05	–	0.23×0.07×0.05
θ range for data / °	1.41-25.00	1.89-25.00	2.12-26.00	2.18-25.00	1.58-26.00
Reflns collected	15213	18860	13255	10272	3546
Unique reflections	7746	2958	4164	3022	3546
R_{int}	0.0309	0.0495	0.0756	0.0264	0.000
Reflns with $I>2\sigma(I)$	5728	1882	2821	2123	1257
No. of parameters	599	230	262	215	194
R [$I>2\sigma(I)$]	0.0589	0.0516	0.0760	0.0485	0.1000
wR	0.2022	0.1549	0.1894	0.1562	0.2218
S	1.005	1.013	1.057	0.929	0.997

B.2 Chapter 3

B.2.1 Compound 3.6

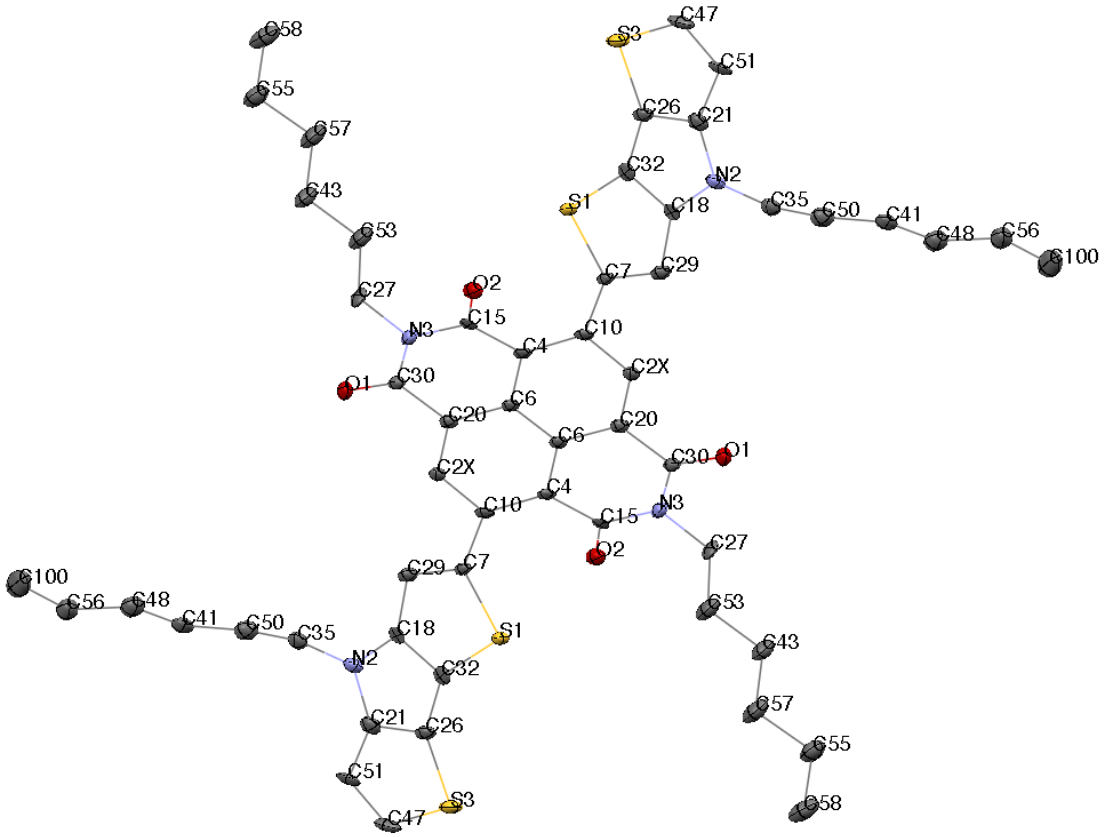

Figure B.1. The structure of compound **3.6**, structure A. Ellipsoids are shown at the 50% level. Hydrogen atoms are omitted for clarity.

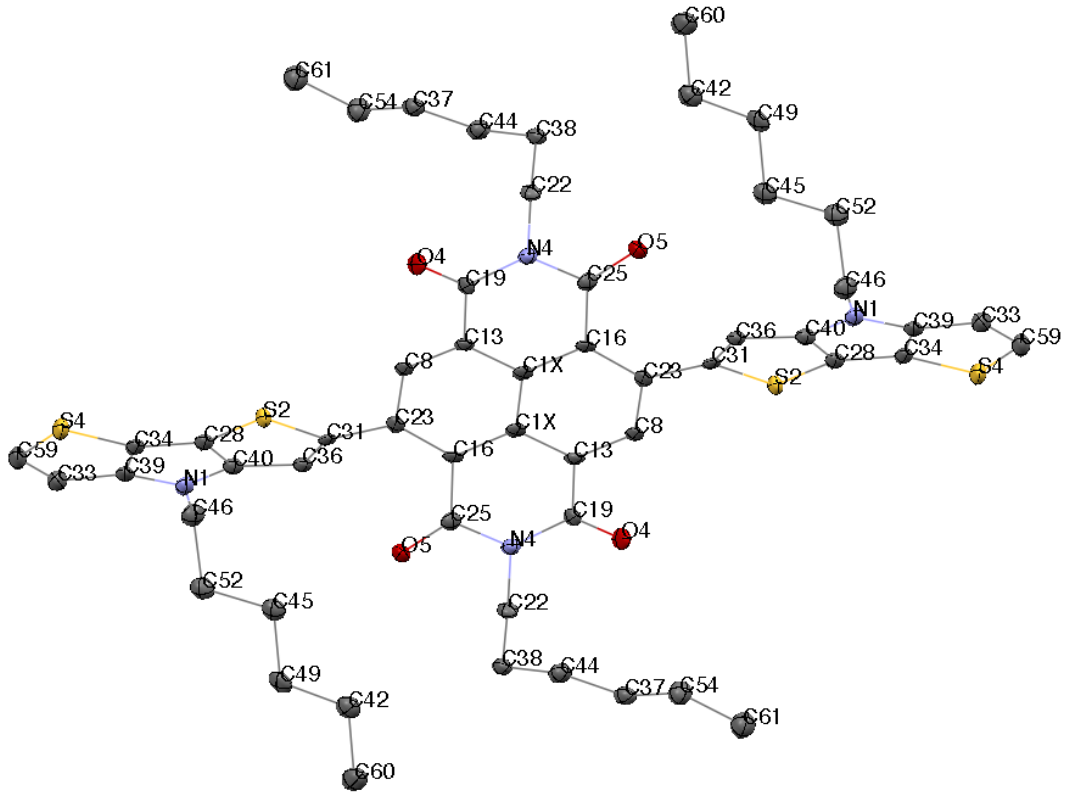

Figure B.2. The structure of compound **3.6**, structure type B. Ellipsoids are shown at the 50% level. Hydrogen atoms are omitted for clarity.

*Crystal Identification File for Compound **3.6***

```
data_2

_audit_creation_method            SHELXL-97
_chemical_name_systematic
;
 ?
;
_chemical_name_common             ?
_chemical_melting_point           ?
_chemical_formula_moiety          ?
_chemical_formula_sum
 'C54 H60 N4 O4 S4'
_chemical_formula_weight          957.30

loop_
 _atom_type_symbol
 _atom_type_description
 _atom_type_scat_dispersion_real
 _atom_type_scat_dispersion_imag
 _atom_type_scat_source
 'C'  'C'   0.0033   0.0016
 'International Tables Vol C Tables 4.2.6.8 and 6.1.1.4'
 'H'  'H'   0.0000   0.0000
 'International Tables Vol C Tables 4.2.6.8 and 6.1.1.4'
 'N'  'N'   0.0061   0.0033
 'International Tables Vol C Tables 4.2.6.8 and 6.1.1.4'
 'O'  'O'   0.0106   0.0060
 'International Tables Vol C Tables 4.2.6.8 and 6.1.1.4'
 'S'  'S'   0.1246   0.1234
 'International Tables Vol C Tables 4.2.6.8 and 6.1.1.4'

_symmetry_cell_setting            ?
_symmetry_space_group_name_H-M    ?

loop_
 _symmetry_equiv_pos_as_xyz
 'x, y, z'
 '-x, -y, -z'

_cell_length_a                    8.578(4)
_cell_length_b                    17.526(9)
_cell_length_c                    17.614(9)
_cell_angle_alpha                 68.617(7)
_cell_angle_beta                  81.197(11)
_cell_angle_gamma                 89.749(9)
_cell_volume                      2433(2)
_cell_formula_units_Z             2
_cell_measurement_temperature     100(2)
_cell_measurement_reflns_used     ?
_cell_measurement_theta_min       ?
_cell_measurement_theta_max       ?

_exptl_crystal_description        ?
_exptl_crystal_colour             ?
_exptl_crystal_size_max           ?
_exptl_crystal_size_mid           ?
_exptl_crystal_size_min           ?
_exptl_crystal_density_meas       ?
_exptl_crystal_density_diffrn     1.307
_exptl_crystal_density_method     'not measured'
_exptl_crystal_F_000              1016
_exptl_absorpt_coefficient_mu     0.246
```

```
_exptl_absorpt_correction_type    ?
_exptl_absorpt_correction_T_min   ?
_exptl_absorpt_correction_T_max   ?
_exptl_absorpt_process_details    ?

_exptl_special_details
;
 ?
;

_diffrn_ambient_temperature       100(2)
_diffrn_radiation_wavelength      0.71073
_diffrn_radiation_type            MoK\a
_diffrn_radiation_source          'fine-focus sealed tube'
_diffrn_radiation_monochromator   graphite
_diffrn_measurement_device_type   ?
_diffrn_measurement_method        ?
_diffrn_detector_area_resol_mean  ?
_diffrn_standards_number          ?
_diffrn_standards_interval_count  ?
_diffrn_standards_interval_time   ?
_diffrn_standards_decay_%         ?
_diffrn_reflns_number             15213
_diffrn_reflns_av_R_equivalents   0.0309
_diffrn_reflns_av_sigmaI/netI     0.0532
_diffrn_reflns_limit_h_min        -9
_diffrn_reflns_limit_h_max        10
_diffrn_reflns_limit_k_min        -20
_diffrn_reflns_limit_k_max        20
_diffrn_reflns_limit_l_min        -20
_diffrn_reflns_limit_l_max        20
_diffrn_reflns_theta_min          1.41
_diffrn_reflns_theta_max          25.00
_reflns_number_total              7746
_reflns_number_gt                 5728
_reflns_threshold_expression      >2sigma(I)

_computing_data_collection        ?
_computing_cell_refinement        ?
_computing_data_reduction         ?
_computing_structure_solution     'SHELXS-97 (Sheldrick, 1990)'
_computing_structure_refinement   'SHELXL-97 (Sheldrick, 1997)'
_computing_molecular_graphics     ?
_computing_publication_material   ?

_refine_special_details
;
 Refinement of F^2^ against ALL reflections.  The weighted R-factor wR and
 goodness of fit S are based on F^2^, conventional R-factors R are based
 on F, with F set to zero for negative F^2^. The threshold expression of
 F^2^ > 2sigma(F^2^) is used only for calculating R-factors(gt) etc. and is
 not relevant to the choice of reflections for refinement.  R-factors based
 on F^2^ are statistically about twice as large as those based on F, and R-
 factors based on ALL data will be even larger.
;

_refine_ls_structure_factor_coef  Fsqd
_refine_ls_matrix_type            full
_refine_ls_weighting_scheme       calc
_refine_ls_weighting_details
 'calc w=1/[\s^2^(Fo^2^)+(0.1456P)^2^+0.0000P] where P=(Fo^2^+2Fc^2^)/3'
_atom_sites_solution_primary      direct
_atom_sites_solution_secondary    difmap
_atom_sites_solution_hydrogens    geom
_refine_ls_hydrogen_treatment     mixed
```

```
_refine_ls_extinction_method      none
_refine_ls_extinction_coef        ?
_refine_ls_number_reflns          7746
_refine_ls_number_parameters      599
_refine_ls_number_restraints      0
_refine_ls_R_factor_all           0.0796
_refine_ls_R_factor_gt            0.0589
_refine_ls_wR_factor_ref          0.2022
_refine_ls_wR_factor_gt           0.1759
_refine_ls_goodness_of_fit_ref    1.005
_refine_ls_restrained_S_all       1.005
_refine_ls_shift/su_max           0.000
_refine_ls_shift/su_mean          0.000

loop_
 _atom_site_label
 _atom_site_type_symbol
 _atom_site_fract_x
 _atom_site_fract_y
 _atom_site_fract_z
 _atom_site_U_iso_or_equiv
 _atom_site_adp_type
 _atom_site_occupancy
 _atom_site_symmetry_multiplicity
 _atom_site_calc_flag
 _atom_site_refinement_flags
 _atom_site_disorder_assembly
 _atom_site_disorder_group
S1 S 0.25211(10) 0.35176(5) 0.28918(5) 0.0150(2) Uani 1 1 d . . .
S2 S 0.54870(10) 0.19335(5) 0.02059(5) 0.0166(2) Uani 1 1 d . . .
S3 S 0.47366(11) 0.20713(6) 0.51633(5) 0.0234(3) Uani 1 1 d . . .
S4 S 0.69054(11) -0.04875(6) 0.03491(6) 0.0233(3) Uani 1 1 d . . .
N3 N 0.1001(3) 0.61310(18) 0.11650(18) 0.0165(6) Uani 1 1 d . . .
O2 O 0.3057(3) 0.51068(15) 0.17940(15) 0.0183(5) Uani 1 1 d . . .
O5 O 0.2548(3) 0.70849(14) -0.19204(15) 0.0196(6) Uani 1 1 d . . .
C4 C 0.1282(4) 0.4801(2) 0.09519(19) 0.0131(7) Uani 1 1 d . . .
O1 O -0.0960(3) 0.71939(15) 0.04451(15) 0.0198(6) Uani 1 1 d . . .
C6 C 0.0214(4) 0.5208(2) 0.0248(2) 0.0130(7) Uani 1 1 d . . .
C7 C 0.2788(4) 0.3397(2) 0.1956(2) 0.0137(7) Uani 1 1 d . . .
C8 C 0.4785(4) 0.3805(2) -0.0412(2) 0.0161(7) Uani 1 1 d . . .
H8A H 0.4534 0.3439 -0.0668 0.019 Uiso 1 1 calc R . .
N4 N 0.2601(3) 0.57697(18) -0.18374(17) 0.0168(6) Uani 1 1 d . . .
C10 C 0.1840(4) 0.3941(2) 0.11986(19) 0.0135(7) Uani 1 1 d . . .
O4 O 0.2580(3) 0.44412(15) -0.17374(16) 0.0229(6) Uani 1 1 d . . .
N2 N 0.5522(3) 0.15506(18) 0.32599(17) 0.0178(6) Uani 1 1 d . . .
C13 C 0.4116(4) 0.4619(2) -0.0719(2) 0.0146(7) Uani 1 1 d . . .
N1 N 0.9607(3) 0.06961(18) 0.10693(18) 0.0185(7) Uani 1 1 d . . .
C15 C 0.1870(4) 0.5332(2) 0.1342(2) 0.0140(7) Uani 1 1 d . . .
C16 C 0.6175(4) 0.3969(2) 0.0699(2) 0.0149(7) Uani 1 1 d . . .
C2X C 0.1438(4) 0.3545(2) 0.0678(2) 0.0151(7) Uani 1 1 d . . .
H2XA H 0.1776 0.3007 0.0766 0.018 Uiso 1 1 calc R . .
C18 C 0.4409(4) 0.2246(2) 0.2852(2) 0.0138(7) Uani 1 1 d . . .
C19 C 0.3041(4) 0.4915(2) -0.1464(2) 0.0164(7) Uani 1 1 d . . .
C20 C -0.0471(4) 0.6052(2) 0.0029(2) 0.0139(7) Uani 1 1 d . . .
C21 C 0.5594(4) 0.1475(2) 0.4066(2) 0.0197(8) Uani 1 1 d . . .
C22 C 0.1696(4) 0.6102(2) -0.2642(2) 0.0158(7) Uani 1 1 d . . .
H22A H 0.1060 0.5641 -0.2662 0.019 Uiso 1 1 calc R . .
H22B H 0.0966 0.6525 -0.2587 0.019 Uiso 1 1 calc R . .
C23 C 0.5874(4) 0.3446(2) 0.0291(2) 0.0162(7) Uani 1 1 d . . .
C1X C 0.4478(4) 0.5174(2) -0.0362(2) 0.0149(7) Uani 1 1 d . . .
C25 C 0.2953(4) 0.6352(2) -0.1515(2) 0.0165(7) Uani 1 1 d . . .
C26 C 0.4555(4) 0.2120(2) 0.4166(2) 0.0177(8) Uani 1 1 d . . .
C27 C 0.1373(4) 0.6567(2) 0.1700(2) 0.0191(8) Uani 1 1 d . . .
H27A H 0.2526 0.6566 0.1702 0.023 Uiso 1 1 calc R . .
H27B H 0.1101 0.7146 0.1453 0.023 Uiso 1 1 calc R . .
```

```
C28 C 0.7056(4) 0.1126(2) 0.0517(2) 0.0185(8) Uani 1 1 d . . .
C29 C 0.3809(4) 0.2680(2) 0.2037(2) 0.0162(7) Uani 1 1 d . . .
H29A H 0.4075 0.2500 0.1588 0.019 Uiso 1 1 calc R . .
C30 C -0.0208(4) 0.6511(2) 0.0552(2) 0.0149(7) Uani 1 1 d . . .
C31 C 0.6594(4) 0.2577(2) 0.0483(2) 0.0157(7) Uani 1 1 d . . .
C32 C 0.3800(4) 0.2610(2) 0.3394(2) 0.0158(7) Uani 1 1 d . . .
C33 C 0.9771(5) -0.0767(2) 0.1003(2) 0.0237(9) Uani 1 1 d . . .
H33A H 1.0707 -0.0979 0.1210 0.028 Uiso 1 1 calc R . .
C34 C 0.7527(4) 0.0297(2) 0.0577(2) 0.0187(8) Uani 1 1 d . . .
C35 C 0.6418(4) 0.0988(2) 0.2922(2) 0.0193(8) Uani 1 1 d . . .
H35A H 0.7084 0.1318 0.2392 0.023 Uiso 1 1 calc R . .
H35B H 0.7130 0.0687 0.3310 0.023 Uiso 1 1 calc R . .
C36 C 0.8094(4) 0.2173(2) 0.0799(2) 0.0165(7) Uani 1 1 d . . .
H36A H 0.8822 0.2456 0.0973 0.020 Uiso 1 1 calc R . .
C37 C 0.3600(4) 0.5125(2) -0.3724(2) 0.0206(8) Uani 1 1 d . . .
H37A H 0.3381 0.5377 -0.4296 0.025 Uiso 1 1 calc R . .
H37B H 0.2620 0.4826 -0.3365 0.025 Uiso 1 1 calc R . .
C38 C 0.2739(4) 0.6425(2) -0.3354(2) 0.0193(8) Uani 1 1 d . . .
H38A H 0.3260 0.6935 -0.3370 0.023 Uiso 1 1 calc R . .
H38B H 0.2163 0.6571 -0.3829 0.023 Uiso 1 1 calc R . .
C39 C 0.9082(4) 0.0056(2) 0.0918(2) 0.0198(8) Uani 1 1 d . . .
C40 C 0.8353(4) 0.1354(2) 0.0819(2) 0.0170(7) Uani 1 1 d . . .
C41 C 0.6439(4) -0.0376(2) 0.2717(2) 0.0234(8) Uani 1 1 d . . .
H41A H 0.7411 -0.0170 0.2304 0.028 Uiso 1 1 calc R . .
H41B H 0.6750 -0.0696 0.3257 0.028 Uiso 1 1 calc R . .
C42 C 1.0242(4) 0.1587(2) 0.3868(2) 0.0253(9) Uani 1 1 d . . .
H42A H 0.9091 0.1619 0.3860 0.030 Uiso 1 1 calc R . .
H42B H 1.0770 0.2129 0.3517 0.030 Uiso 1 1 calc R . .
C43 C 0.0767(5) 0.6733(3) 0.3049(2) 0.0255(9) Uani 1 1 d . . .
H43A H 0.1902 0.6860 0.3022 0.031 Uiso 1 1 calc R . .
H43B H 0.0264 0.7261 0.2825 0.031 Uiso 1 1 calc R . .
C44 C 0.4087(4) 0.5782(2) -0.3439(2) 0.0217(8) Uani 1 1 d . . .
H44A H 0.5018 0.6100 -0.3830 0.026 Uiso 1 1 calc R . .
H44B H 0.4424 0.5515 -0.2894 0.026 Uiso 1 1 calc R . .
C45 C 1.0694(4) 0.1166(2) 0.2632(2) 0.0225(8) Uani 1 1 d . . .
H45A H 1.1373 0.1663 0.2284 0.027 Uiso 1 1 calc R . .
H45B H 0.9580 0.1286 0.2574 0.027 Uiso 1 1 calc R . .
C46 C 1.1148(4) 0.0662(2) 0.1438(2) 0.0232(8) Uani 1 1 d . . .
H46A H 1.1815 0.0273 0.1265 0.028 Uiso 1 1 calc R . .
H46B H 1.1702 0.1210 0.1154 0.028 Uiso 1 1 calc R . .
C47 C 0.6171(5) 0.1194(2) 0.5412(2) 0.0261(9) Uani 1 1 d . . .
H47A H 0.6575 0.0975 0.5917 0.031 Uiso 1 1 calc R . .
C48 C 0.5448(5) -0.0905(2) 0.2466(3) 0.0291(9) Uani 1 1 d . . .
H48A H 0.5239 -0.0604 0.1898 0.035 Uiso 1 1 calc R . .
H48B H 0.4422 -0.1058 0.2843 0.035 Uiso 1 1 calc R . .
C49 C 1.0911(4) 0.0910(2) 0.3550(2) 0.0226(8) Uani 1 1 d . . .
H49A H 1.2045 0.0855 0.3597 0.027 Uiso 1 1 calc R . .
H49B H 1.0338 0.0375 0.3884 0.027 Uiso 1 1 calc R . .
C50 C 0.5430(4) 0.0395(2) 0.2785(2) 0.0246(9) Uani 1 1 d . . .
H50A H 0.4994 0.0666 0.2268 0.029 Uiso 1 1 calc R . .
H50B H 0.4533 0.0191 0.3246 0.029 Uiso 1 1 calc R . .
C51 C 0.6523(4) 0.0933(2) 0.4789(2) 0.0224(8) Uani 1 1 d . . .
H51A H 0.7197 0.0506 0.4773 0.027 Uiso 1 1 calc R . .
C52 C 1.1173(4) 0.0434(2) 0.2362(2) 0.0232(8) Uani 1 1 d . . .
H52A H 1.2247 0.0280 0.2481 0.028 Uiso 1 1 calc R . .
H52B H 1.0432 -0.0046 0.2683 0.028 Uiso 1 1 calc R . .
C53 C 0.0613(5) 0.6246(3) 0.2501(2) 0.0288(9) Uani 1 1 d . . .
H53A H 0.1007 0.5696 0.2766 0.035 Uiso 1 1 calc R . .
H53B H -0.0525 0.6169 0.2491 0.035 Uiso 1 1 calc R . .
C54 C 0.5033(5) 0.4471(2) -0.3688(2) 0.0259(9) Uani 1 1 d . . .
H54A H 0.6049 0.4783 -0.3971 0.031 Uiso 1 1 calc R . .
H54B H 0.5134 0.4158 -0.3105 0.031 Uiso 1 1 calc R . .
C55 C 0.0015(5) 0.6851(3) 0.4412(2) 0.0309(10) Uani 1 1 d . . .
H55A H 0.1104 0.7025 0.4426 0.037 Uiso 1 1 calc R . .
H55B H -0.0544 0.7353 0.4155 0.037 Uiso 1 1 calc R . .
```

```
C56 C 0.6386(5) -0.1732(2) 0.2503(3) 0.0338(10) Uani 1 1 d . . .
H56A H 0.7454 -0.1581 0.2167 0.041 Uiso 1 1 calc R . .
H56B H 0.6496 -0.2067 0.3080 0.041 Uiso 1 1 calc R . .
C57 C 0.0093(5) 0.6335(3) 0.3874(3) 0.0336(10) Uani 1 1 d . . .
H57A H 0.0703 0.5850 0.4118 0.040 Uiso 1 1 calc R . .
H57B H -0.0994 0.6132 0.3894 0.040 Uiso 1 1 calc R . .
C58 C -0.0741(5) 0.6446(3) 0.5214(3) 0.0358(11) Uani 1 1 d . . .
H58A H -0.0713 0.6804 0.5530 0.054 Uiso 1 1 calc R . .
H58B H -0.0204 0.5945 0.5472 0.054 Uiso 1 1 calc R . .
H58C H -0.1842 0.6303 0.5209 0.054 Uiso 1 1 calc R . .
C59 C 0.8731(5) -0.1124(2) 0.0715(2) 0.0271(9) Uani 1 1 d . . .
H59A H 0.8871 -0.1653 0.0690 0.032 Uiso 1 1 calc R . .
C60 C 1.0590(5) 0.1325(3) 0.4779(3) 0.0341(10) Uani 1 1 d . . .
H60A H 1.0103 0.1702 0.5030 0.051 Uiso 1 1 calc R . .
H60B H 1.1734 0.1346 0.4770 0.051 Uiso 1 1 calc R . .
H60C H 1.0149 0.0765 0.5102 0.051 Uiso 1 1 calc R . .
C61 C 0.4693(5) 0.3884(3) -0.4094(3) 0.0316(10) Uani 1 1 d . . .
H61A H 0.5605 0.3551 -0.4121 0.047 Uiso 1 1 calc R . .
H61B H 0.4490 0.4193 -0.4654 0.047 Uiso 1 1 calc R . .
H61C H 0.3763 0.3525 -0.3771 0.047 Uiso 1 1 calc R . .
C100 C 0.5405(7) -0.2209(3) 0.2157(3) 0.0514(14) Uani 1 1 d . . .
H10A H 0.5971 -0.2685 0.2120 0.077 Uiso 1 1 calc R . .
H10B H 0.5224 -0.1854 0.1605 0.077 Uiso 1 1 calc R . .
H10C H 0.4388 -0.2397 0.2522 0.077 Uiso 1 1 calc R . .

loop_
 _atom_site_aniso_label
 _atom_site_aniso_U_11
 _atom_site_aniso_U_22
 _atom_site_aniso_U_33
 _atom_site_aniso_U_23
 _atom_site_aniso_U_13
 _atom_site_aniso_U_12
S1 0.0204(4) 0.0156(5) 0.0079(4) -0.0039(4) 0.0004(3) -0.0016(3)
S2 0.0223(5) 0.0113(5) 0.0160(5) -0.0054(4) -0.0010(3) -0.0025(3)
S3 0.0327(5) 0.0260(5) 0.0084(4) -0.0033(4) -0.0018(4) -0.0041(4)
S4 0.0355(5) 0.0146(5) 0.0204(5) -0.0093(4) 0.0009(4) -0.0038(4)
N3 0.0221(15) 0.0155(16) 0.0126(15) -0.0079(13) 0.0023(12) -0.0054(12)
O2 0.0200(12) 0.0194(13) 0.0138(12) -0.0054(11) 0.0014(10) -0.0094(10)
O5 0.0273(13) 0.0133(13) 0.0147(13) -0.0031(11) 0.0017(10) -0.0032(10)
C4 0.0145(16) 0.0160(18) 0.0057(16) -0.0022(14) 0.0035(12) -0.0045(13)
O1 0.0274(13) 0.0145(13) 0.0174(13) -0.0078(11) 0.0016(10) -0.0047(11)
C6 0.0133(16) 0.0151(18) 0.0082(16) -0.0036(15) 0.0036(13) -0.0051(14)
C7 0.0166(16) 0.0153(18) 0.0081(16) -0.0048(15) 0.0028(13) -0.0084(14)
C8 0.0216(17) 0.0140(18) 0.0087(17) -0.0031(15) 0.0068(13) -0.0087(14)
N4 0.0205(15) 0.0177(16) 0.0110(14) -0.0053(13) 0.0010(12) -0.0041(12)
C10 0.0135(16) 0.0167(18) 0.0062(16) -0.0014(14) 0.0034(12) -0.0036(13)
O4 0.0312(14) 0.0173(14) 0.0202(14) -0.0072(12) -0.0030(11) -0.0127(11)
N2 0.0216(15) 0.0161(16) 0.0105(14) -0.0004(13) 0.0014(12) -0.0033(12)
C13 0.0167(17) 0.0171(18) 0.0066(16) -0.0025(14) 0.0031(13) -0.0056(14)
N1 0.0220(15) 0.0165(16) 0.0154(15) -0.0076(13) 0.0061(12) -0.0045(12)
C15 0.0189(17) 0.0114(17) 0.0058(16) 0.0010(14) 0.0056(13) -0.0076(14)
C16 0.0181(17) 0.0164(18) 0.0061(16) -0.0017(15) 0.0045(13) -0.0032(14)
C2X 0.0200(17) 0.0123(17) 0.0101(17) -0.0027(15) 0.0029(13) -0.0007(14)
C18 0.0142(16) 0.0092(17) 0.0131(17) -0.0007(14) 0.0039(13) -0.0106(13)
C19 0.0194(17) 0.0132(18) 0.0135(18) -0.0033(15) 0.0029(14) -0.0086(14)
C20 0.0129(16) 0.0168(18) 0.0101(17) -0.0043(15) 0.0025(13) -0.0058(14)
C21 0.0205(18) 0.0176(19) 0.0153(18) -0.0015(16) 0.0029(14) -0.0069(15)
C22 0.0169(17) 0.0173(18) 0.0124(17) -0.0035(15) -0.0050(13) -0.0028(14)
C23 0.0180(17) 0.0135(18) 0.0128(17) -0.0034(15) 0.0065(13) -0.0061(14)
C1X 0.0141(16) 0.0184(18) 0.0093(17) -0.0048(15) 0.0064(13) -0.0033(14)
C25 0.0152(16) 0.0180(19) 0.0154(18) -0.0073(16) 0.0029(13) 0.0004(14)
C26 0.0202(17) 0.0203(19) 0.0093(17) -0.0035(15) 0.0029(13) -0.0096(15)
C27 0.0261(19) 0.0193(19) 0.0185(19) -0.0135(16) -0.0062(15) -0.0039(15)
C28 0.0244(18) 0.0155(18) 0.0121(17) -0.0047(15) 0.0058(14) -0.0050(15)
```

```
C29 0.0158(16) 0.0209(19) 0.0101(17) -0.0056(15) 0.0029(13) -0.0044(14)
C30 0.0194(17) 0.0155(18) 0.0088(16) -0.0041(15) 0.0003(13) -0.0054(14)
C31 0.0228(18) 0.0165(19) 0.0060(16) -0.0048(15) 0.0046(13) -0.0053(15)
C32 0.0144(16) 0.0133(18) 0.0165(18) -0.0041(15) 0.0041(13) -0.0105(14)
C33 0.032(2) 0.018(2) 0.0185(19) -0.0069(17) 0.0026(16) 0.0023(16)
C34 0.0259(19) 0.0161(19) 0.0118(17) -0.0062(15) 0.0067(14) -0.0082(15)
C35 0.0214(18) 0.0156(18) 0.0159(18) -0.0027(16) 0.0037(14) -0.0012(15)
C36 0.0221(18) 0.0165(18) 0.0088(16) -0.0041(15) 0.0024(13) -0.0044(14)
C37 0.0238(18) 0.021(2) 0.0144(18) -0.0049(16) 0.0017(14) -0.0086(15)
C38 0.0269(19) 0.0167(19) 0.0113(17) -0.0026(15) -0.0001(14) -0.0064(15)
C39 0.030(2) 0.0147(19) 0.0104(17) -0.0036(15) 0.0063(15) -0.0023(15)
C40 0.0192(17) 0.0174(19) 0.0123(17) -0.0050(15) 0.0031(13) -0.0025(14)
C41 0.030(2) 0.021(2) 0.0128(18) -0.0022(16) 0.0056(15) -0.0065(16)
C42 0.0250(19) 0.024(2) 0.022(2) -0.0055(18) 0.0034(15) -0.0079(16)
C43 0.027(2) 0.033(2) 0.022(2) -0.0185(19) -0.0005(16) -0.0030(17)
C44 0.0229(18) 0.024(2) 0.0168(19) -0.0081(17) 0.0025(15) -0.0055(16)
C45 0.0194(18) 0.022(2) 0.022(2) -0.0058(17) 0.0035(15) -0.0040(15)
C46 0.0202(18) 0.025(2) 0.023(2) -0.0105(18) 0.0035(15) 0.0002(16)
C47 0.032(2) 0.029(2) 0.0090(18) 0.0038(17) -0.0046(15) -0.0032(17)
C48 0.033(2) 0.030(2) 0.022(2) -0.0110(19) 0.0061(17) -0.0067(18)
C49 0.0210(18) 0.018(2) 0.021(2) -0.0013(17) 0.0037(15) -0.0078(15)
C50 0.0228(19) 0.028(2) 0.019(2) -0.0075(18) 0.0037(15) -0.0054(16)
C51 0.0271(19) 0.019(2) 0.0097(17) 0.0055(16) 0.0018(14) -0.0043(16)
C52 0.0198(18) 0.024(2) 0.022(2) -0.0064(17) 0.0000(15) -0.0029(15)
C53 0.029(2) 0.039(2) 0.025(2) -0.023(2) 0.0063(16) -0.0116(18)
C54 0.028(2) 0.026(2) 0.025(2) -0.0107(18) -0.0025(16) -0.0021(17)
C55 0.034(2) 0.038(2) 0.024(2) -0.019(2) 0.0047(17) -0.0040(19)
C56 0.048(3) 0.025(2) 0.024(2) -0.0106(19) 0.0075(19) -0.0073(19)
C57 0.034(2) 0.046(3) 0.028(2) -0.027(2) 0.0055(18) -0.011(2)
C58 0.030(2) 0.058(3) 0.025(2) -0.026(2) 0.0041(17) -0.009(2)
C59 0.040(2) 0.015(2) 0.024(2) -0.0088(18) 0.0070(17) -0.0030(17)
C60 0.044(2) 0.030(2) 0.024(2) -0.010(2) 0.0083(18) -0.0158(19)
C61 0.036(2) 0.029(2) 0.031(2) -0.014(2) 0.0012(18) -0.0039(18)
C100 0.078(4) 0.035(3) 0.037(3) -0.017(2) 0.015(3) -0.025(3)

_geom_special_details
;
 All esds (except the esd in the dihedral angle between two l.s. planes)
 are estimated using the full covariance matrix.  The cell esds are taken
 into account individually in the estimation of esds in distances, angles
 and torsion angles; correlations between esds in cell parameters are only
 used when they are defined by crystal symmetry.  An approximate (isotropic)
 treatment of cell esds is used for estimating esds involving l.s. planes.
;

loop_
 _geom_bond_atom_site_label_1
 _geom_bond_atom_site_label_2
 _geom_bond_distance
 _geom_bond_site_symmetry_2
 _geom_bond_publ_flag
S1 C7 1.718(3) . ?
S1 C32 1.942(4) . ?
S2 C31 1.722(4) . ?
S2 C28 1.939(4) . ?
S3 C26 1.758(4) . ?
S3 C47 1.931(4) . ?
S4 C34 1.677(4) . ?
S4 C59 1.970(4) . ?
N3 C27 1.480(4) . ?
N3 C15 1.535(4) . ?
N3 C30 1.581(5) . ?
O2 C15 1.357(4) . ?
O5 C25 1.298(4) . ?
C4 C15 1.473(5) . ?
```

```
C4 C10 1.507(5) . ?
C4 C6 1.606(5) . ?
O1 C30 1.322(4) . ?
C6 C6 1.413(6) 2_565 ?
C6 C20 1.526(5) . ?
C7 C29 1.505(5) . ?
C7 C10 1.658(5) . ?
C8 C13 1.477(5) . ?
C8 C23 1.607(5) . ?
N4 C25 1.391(4) . ?
N4 C19 1.474(4) . ?
N4 C22 1.638(4) . ?
C10 C2X 1.416(5) . ?
O4 C19 1.196(4) . ?
N2 C21 1.389(5) . ?
N2 C35 1.483(4) . ?
N2 C18 1.572(4) . ?
C13 C1X 1.395(5) . ?
C13 C19 1.646(5) . ?
N1 C39 1.339(5) . ?
N1 C46 1.552(5) . ?
N1 C40 1.564(4) . ?
C16 C23 1.400(5) . ?
C16 C1X 1.539(5) 2_665 ?
C16 C25 1.637(5) 2_665 ?
C2X C20 1.552(5) 2_565 ?
C18 C32 1.372(5) . ?
C18 C29 1.527(5) . ?
C20 C30 1.467(5) . ?
C20 C2X 1.553(5) 2_565 ?
C21 C26 1.480(5) . ?
C21 C51 1.606(5) . ?
C22 C38 1.355(5) . ?
C23 C31 1.580(5) . ?
C1X C16 1.539(5) 2_665 ?
C1X C1X 1.604(7) 2_665 ?
C25 C16 1.637(5) 2_665 ?
C26 C32 1.555(5) . ?
C27 C53 1.369(5) . ?
C28 C40 1.422(5) . ?
C28 C34 1.475(5) . ?
C31 C36 1.546(5) . ?
C33 C59 1.349(6) . ?
C33 C39 1.521(5) . ?
C34 C39 1.540(5) . ?
C35 C50 1.452(5) . ?
C36 C40 1.439(5) . ?
C37 C44 1.497(5) . ?
C37 C54 1.670(5) . ?
C38 C44 1.640(5) . ?
C41 C48 1.483(6) . ?
C41 C50 1.632(5) . ?
C42 C49 1.559(5) . ?
C42 C60 1.576(6) . ?
C43 C57 1.392(6) . ?
C43 C53 1.522(5) . ?
C45 C49 1.553(5) . ?
C45 C52 1.556(5) . ?
C46 C52 1.531(5) . ?
C47 C51 1.330(5) . ?
C48 C56 1.640(6) . ?
C54 C61 1.502(5) . ?
C55 C58 1.383(6) . ?
C55 C57 1.526(5) . ?
C56 C100 1.521(6) . ?
```

```
loop_
 _geom_angle_atom_site_label_1
 _geom_angle_atom_site_label_2
 _geom_angle_atom_site_label_3
 _geom_angle
 _geom_angle_site_symmetry_1
 _geom_angle_site_symmetry_3
 _geom_angle_publ_flag
C7 S1 C32 93.99(15) . . ?
C31 S2 C28 88.22(16) . . ?
C26 S3 C47 97.35(17) . . ?
C34 S4 C59 92.16(18) . . ?
C27 N3 C15 110.8(3) . . ?
C27 N3 C30 118.5(3) . . ?
C15 N3 C30 130.6(3) . . ?
C15 C4 C10 117.1(3) . . ?
C15 C4 C6 117.3(3) . . ?
C10 C4 C6 125.4(3) . . ?
C6 C6 C20 111.6(4) 2_565 . ?
C6 C6 C4 121.8(4) 2_565 . ?
C20 C6 C4 126.6(3) . . ?
C29 C7 C10 130.7(3) . . ?
C29 C7 S1 107.1(2) . . ?
C10 C7 S1 121.8(2) . . ?
C13 C8 C23 129.6(3) . . ?
C25 N4 C19 120.6(3) . . ?
C25 N4 C22 115.7(3) . . ?
C19 N4 C22 123.6(3) . . ?
C2X C10 C4 111.7(3) . . ?
C2X C10 C7 116.5(3) . . ?
C4 C10 C7 131.9(3) . . ?
C21 N2 C35 118.7(3) . . ?
C21 N2 C18 111.2(3) . . ?
C35 N2 C18 130.2(3) . . ?
C1X C13 C8 116.6(3) . . ?
C1X C13 C19 118.9(3) . . ?
C8 C13 C19 124.5(3) . . ?
C39 N1 C46 120.9(3) . . ?
C39 N1 C40 105.1(3) . . ?
C46 N1 C40 133.9(3) . . ?
O2 C15 C4 121.2(3) . . ?
O2 C15 N3 126.5(3) . . ?
C4 C15 N3 112.2(3) . . ?
C23 C16 C1X 115.2(3) . 2_665 ?
C23 C16 C25 121.1(3) . 2_665 ?
C1X C16 C25 123.5(3) 2_665 2_665 ?
C10 C2X C20 123.1(3) . 2_565 ?
C32 C18 C29 108.1(3) . . ?
C32 C18 N2 110.6(3) . . ?
C29 C18 N2 141.2(3) . . ?
O4 C19 N4 116.1(3) . . ?
O4 C19 C13 121.3(3) . . ?
N4 C19 C13 122.6(3) . . ?
C30 C20 C6 116.3(3) . . ?
C30 C20 C2X 117.6(3) . 2_565 ?
C6 C20 C2X 126.1(3) . 2_565 ?
N2 C21 C26 102.1(3) . . ?
N2 C21 C51 136.4(3) . . ?
C26 C21 C51 121.5(3) . . ?
C38 C22 N4 111.3(3) . . ?
C16 C23 C31 122.7(3) . . ?
C16 C23 C8 115.1(3) . . ?
C31 C23 C8 122.1(3) . . ?
C13 C1X C16 116.7(3) . 2_665 ?
```

```
C13 C1X C1X 115.1(4) . 2_665 ?
C16 C1X C1X 128.1(4) 2_665 2_665 ?
O5 C25 N4 114.1(3) . . ?
O5 C25 C16 129.2(3) . 2_665 ?
N4 C25 C16 116.7(3) . 2_665 ?
C21 C26 C32 114.8(3) . . ?
C21 C26 S3 102.4(2) . . ?
C32 C26 S3 142.7(3) . . ?
C53 C27 N3 115.2(3) . . ?
C40 C28 C34 98.1(3) . . ?
C40 C28 S2 116.4(3) . . ?
C34 C28 S2 145.5(3) . . ?
C7 C29 C18 118.9(3) . . ?
O1 C30 C20 117.4(3) . . ?
O1 C30 N3 127.8(3) . . ?
C20 C30 N3 114.7(3) . . ?
C36 C31 C23 136.6(3) . . ?
C36 C31 S2 111.6(2) . . ?
C23 C31 S2 111.7(2) . . ?
C18 C32 C26 101.3(3) . . ?
C18 C32 S1 111.9(3) . . ?
C26 C32 S1 146.6(2) . . ?
C59 C33 C39 103.2(3) . . ?
C28 C34 C39 114.2(3) . . ?
C28 C34 S4 138.9(3) . . ?
C39 C34 S4 106.8(2) . . ?
C50 C35 N2 114.1(3) . . ?
C40 C36 C31 117.8(3) . . ?
C44 C37 C54 110.0(3) . . ?
C22 C38 C44 111.7(3) . . ?
N1 C39 C33 131.7(3) . . ?
N1 C39 C34 106.7(3) . . ?
C33 C39 C34 121.6(3) . . ?
C28 C40 C36 106.0(3) . . ?
C28 C40 N1 115.8(3) . . ?
C36 C40 N1 138.2(3) . . ?
C48 C41 C50 109.0(3) . . ?
C49 C42 C60 105.9(3) . . ?
C57 C43 C53 114.5(4) . . ?
C37 C44 C38 116.0(3) . . ?
C49 C45 C52 107.0(3) . . ?
C52 C46 N1 123.4(3) . . ?
C51 C47 S3 111.5(3) . . ?
C41 C48 C56 108.7(3) . . ?
C45 C49 C42 108.0(3) . . ?
C35 C50 C41 110.9(3) . . ?
C47 C51 C21 107.3(3) . . ?
C46 C52 C45 110.7(3) . . ?
C27 C53 C43 117.7(3) . . ?
C61 C54 C37 111.3(3) . . ?
C58 C55 C57 113.7(4) . . ?
C100 C56 C48 106.7(4) . . ?
C43 C57 C55 115.7(4) . . ?
C33 C59 S4 116.3(3) . . ?

_diffrn_measured_fraction_theta_max    0.905
_diffrn_reflns_theta_full              25.00
_diffrn_measured_fraction_theta_full   0.905
_refine_diff_density_max    0.725
_refine_diff_density_min   -0.549
_refine_diff_density_rms    0.126
```

B.3 Chapter 4

B.3.1 Compound 4.4

NOTE: The compound **4.4** crystallizes with two independent molecules in the unit cell. The crystals were found to be twinned and refined with the *twin law* –1, 0, 0, 0, –1, 0, 0, 0, 1. The ratio of twinning component was found to be 0.34606(5)/0.65394(5). The small size of the crystal and, hence, low quality data obtained did not allow to refine the structure in the anisotropic model. The crystal identification file attached below represents an incomplete picture of the full structure, but is included for reference.

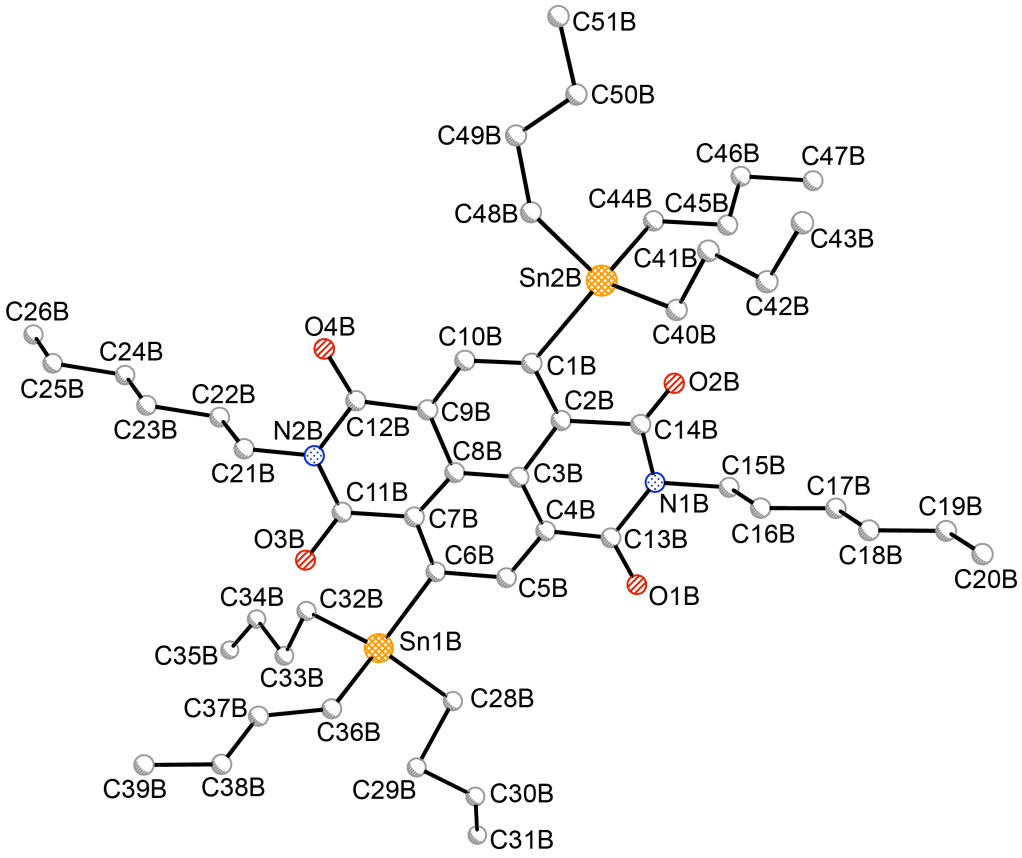

Figure B.3. Crystal structure of **4.4** for independent molecule B. Hydrogen atoms are omitted for clarity. Atoms are shown as spheres of arbitrary size.

*Crystal Identification File for Compound **4.4***

```
data_a

_audit_creation_method            SHELXL-97
_chemical_name_systematic
;
 ?
;
_chemical_name_common             ?
_chemical_melting_point           ?
_chemical_formula_moiety
 'C50 N2 O4 Sn2'
_chemical_formula_sum
 'C50 N2 O4 Sn2'
_chemical_formula_weight          929.90

loop_
 _atom_type_symbol
 _atom_type_description
 _atom_type_scat_dispersion_real
 _atom_type_scat_dispersion_imag
 _atom_type_scat_source
 'C'  'C'   0.0033   0.0016
 'International Tables Vol C Tables 4.2.6.8 and 6.1.1.4'
 'N'  'N'   0.0061   0.0033
 'International Tables Vol C Tables 4.2.6.8 and 6.1.1.4'
 'O'  'O'   0.0106   0.0060
 'International Tables Vol C Tables 4.2.6.8 and 6.1.1.4'
 'Sn'  'Sn'  -0.6537   1.4246
 'International Tables Vol C Tables 4.2.6.8 and 6.1.1.4'

_symmetry_cell_setting            Monoclinic
_symmetry_space_group_name_H-M    'P 21'
_symmetry_space_group_name_Hall   'P 2yb'


loop_
 _symmetry_equiv_pos_as_xyz
 'x, y, z'
 '-x, y+1/2, -z'

_cell_length_a                    9.444(7)
_cell_length_b                    28.244(19)
_cell_length_c                    18.659(13)
_cell_angle_alpha                 90.00
_cell_angle_beta                  90.279(12)
_cell_angle_gamma                 90.00
_cell_volume                      4977(6)
_cell_formula_units_Z             4
_cell_measurement_temperature     296(2)
_cell_measurement_reflns_used     2315
_cell_measurement_theta_min       2.18
_cell_measurement_theta_max       20.40

_exptl_crystal_description        'needle'
_exptl_crystal_colour             'yellow'
_exptl_crystal_size_max           0.10
_exptl_crystal_size_mid           0.06
_exptl_crystal_size_min           0.04
_exptl_crystal_density_meas       'not measured'
_exptl_crystal_density_diffrn     1.241
_exptl_crystal_density_method     'not measured'
_exptl_crystal_F_000              1784
```

```
_exptl_absorpt_coefficient_mu     1.042
_exptl_absorpt_correction_type    'multi-scan'
_exptl_absorpt_correction_T_min   0.9030
_exptl_absorpt_correction_T_max   0.9595
_exptl_absorpt_process_details    'SADABS (Sheldrick, 2003)'

_exptl_special_details
;
 ?
;

_diffrn_ambient_temperature       296(2)
_diffrn_radiation_wavelength      0.71073
_diffrn_radiation_type            MoK\a
_diffrn_radiation_source          'fine-focus sealed tube'
_diffrn_radiation_monochromator   graphite
_diffrn_measurement_device_type   'Bruker SMART APEX II CCD area detector'
_diffrn_measurement_method        'phi and omega scans'
_diffrn_detector_area_resol_mean  ?
_diffrn_standards_number          ?
_diffrn_standards_interval_count  ?
_diffrn_standards_interval_time   ?
_diffrn_standards_decay_%         ?
_diffrn_reflns_number             43598
_diffrn_reflns_av_R_equivalents   0.1723
_diffrn_reflns_av_sigmaI/netI     0.2386
_diffrn_reflns_limit_h_min        -11
_diffrn_reflns_limit_h_max        11
_diffrn_reflns_limit_k_min        -34
_diffrn_reflns_limit_k_max        34
_diffrn_reflns_limit_l_min        -23
_diffrn_reflns_limit_l_max        22
_diffrn_reflns_theta_min          1.81
_diffrn_reflns_theta_max          26.00
_reflns_number_total              19526
_reflns_number_gt                 13256
_reflns_threshold_expression      >2sigma(I)

_computing_data_collection        'APEX2  (Bruker, 2005)'
_computing_cell_refinement        'SAINT+ ver. 6.2 (Bruker, 2001)'
_computing_data_reduction         'SAINT+ ver. 6.2 (Bruker, 2001)'
_computing_structure_solution     'SHELXTL ver. 6.12 (Sheldrick, 2001)'
_computing_structure_refinement   'SHELXTL ver. 6.12 (Sheldrick, 2001)'
_computing_molecular_graphics     'SHELXTL ver. 6.12 (Sheldrick, 2001)'
_computing_publication_material   'SHELXTL ver. 6.12 (Sheldrick, 2001)'

_refine_special_details
;
 Refinement of F^2^ against ALL reflections.  The weighted R-factor wR and
 goodness of fit S are based on F^2^, conventional R-factors R are based
 on F, with F set to zero for negative F^2^. The threshold expression of
 F^2^ > 2sigma(F^2^) is used only for calculating R-factors(gt) etc. and is
 not relevant to the choice of reflections for refinement.  R-factors based
 on F^2^ are statistically about twice as large as those based on F, and R-
 factors based on ALL data will be even larger.
;

_refine_ls_structure_factor_coef  Fsqd
_refine_ls_matrix_type            full
_refine_ls_weighting_scheme       calc
_refine_ls_weighting_details
 'calc w=1/[\s^2^(Fo^2^)+(0.1500P)^2^+164.0000P] where P=(Fo^2^+2Fc^2^)/3'
_atom_sites_solution_primary      direct
_atom_sites_solution_secondary    difmap
_atom_sites_solution_hydrogens    none
```

```
_refine_ls_hydrogen_treatment     none
_refine_ls_extinction_method      none
_refine_ls_extinction_coef        ?
_refine_ls_abs_structure_details
 'Flack H D (1983), Acta Cryst. A39, 876-881'
_refine_ls_abs_structure_Flack    0.47(11)
_refine_ls_number_reflns          19526
_refine_ls_number_parameters      425
_refine_ls_number_restraints      122
_refine_ls_R_factor_all           0.1868
_refine_ls_R_factor_gt            0.1400
_refine_ls_wR_factor_ref          0.3628
_refine_ls_wR_factor_gt           0.3251
_refine_ls_goodness_of_fit_ref    1.040
_refine_ls_restrained_S_all       1.039
_refine_ls_shift/su_max           1.275
_refine_ls_shift/su_mean          0.048

loop_
 _atom_site_label
 _atom_site_type_symbol
 _atom_site_fract_x
 _atom_site_fract_y
 _atom_site_fract_z
 _atom_site_U_iso_or_equiv
 _atom_site_adp_type
 _atom_site_occupancy
 _atom_site_symmetry_multiplicity
 _atom_site_calc_flag
 _atom_site_refinement_flags
 _atom_site_disorder_assembly
 _atom_site_disorder_group
Sn1B Sn 1.59659(16) 0.30343(5) 0.48178(8) 0.0160(3) Uiso 1 1 d D . .
Sn1A Sn 0.92854(15) 0.15391(5) 0.48123(8) 0.0144(3) Uiso 1 1 d D . .
Sn2A Sn 1.12357(15) 0.29430(6) 0.03427(8) 0.0147(3) Uiso 1 1 d D . .
Sn2B Sn 1.45225(17) 0.14471(6) 0.03692(8) 0.0201(4) Uiso 1 1 d D . .
O4B O 1.7740(18) 0.3078(6) 0.1199(9) 0.021(4) Uiso 1 1 d . . .
O1B O 1.2771(19) 0.1443(7) 0.3950(9) 0.026(4) Uiso 1 1 d . . .
O3B O 1.751(2) 0.3341(6) 0.3634(10) 0.027(4) Uiso 1 1 d . . .
C2B C 1.430(2) 0.1835(7) 0.2039(11) 0.008(4) Uiso 1 1 d . . .
O2B O 1.2786(18) 0.1191(5) 0.1554(8) 0.013(3) Uiso 1 1 d . . .
N1B N 1.2761(17) 0.1335(5) 0.2753(8) 0.002(3) Uiso 1 1 d . . .
C11B C 1.711(3) 0.3045(9) 0.3102(14) 0.024(6) Uiso 1 1 d . . .
C12B C 1.716(2) 0.2945(7) 0.1789(9) 0.003(3) Uiso 1 1 d . . .
C28B C 1.448(2) 0.2712(6) 0.5551(9) 0.003(4) Uiso 1 1 d . . .
C10B C 1.596(2) 0.2262(7) 0.1287(10) 0.008(4) Uiso 1 1 d . . .
N2B N 1.766(3) 0.3221(10) 0.2450(16) 0.048(8) Uiso 1 1 d . . .
C32B C 1.5770(8) 0.37872(13) 0.4692(4) 0.12(2) Uiso 1 1 d D . .
C4B C 1.408(3) 0.1967(9) 0.3343(13) 0.022(5) Uiso 1 1 d . . .
C5B C 1.442(3) 0.2217(11) 0.3873(16) 0.034(7) Uiso 1 1 d . . .
C21B C 1.8609(10) 0.35804(18) 0.23479(9) 0.038(3) Uiso 1 1 d D . .
C13B C 1.313(4) 0.1612(11) 0.3412(17) 0.038(7) Uiso 1 1 d . . .
C9B C 1.626(2) 0.2540(7) 0.1899(10) 0.006(4) Uiso 1 1 d . . .
C33B C 1.5485(9) 0.4108(2) 0.5336(4) 0.019(5) Uiso 1 1 d D . .
C1B C 1.502(3) 0.1909(8) 0.1378(12) 0.012(5) Uiso 1 1 d . . .
C15B C 1.1592(11) 0.0902(2) 0.28287(7) 0.061(4) Uiso 1 1 d D . .
C14B C 1.326(2) 0.1378(7) 0.2052(10) 0.002(4) Uiso 1 1 d . . .
O1A O 0.761(2) 0.1303(6) 0.3639(10) 0.024(4) Uiso 1 1 d . . .
O2A O 0.7971(16) 0.1342(5) 0.1232(8) 0.010(3) Uiso 1 1 d . . .
N1A N 0.783(2) 0.1331(6) 0.2419(10) 0.010(2) Uiso 1 1 d . . .
C22B C 1.7832(7) 0.40418(17) 0.21704(16) 0.038(3) Uiso 1 1 d D . .
C15A C 0.6742(10) 0.0896(2) 0.23383(7) 0.051(4) Uiso 1 1 d D . .
C6A C 1.089(3) 0.2529(8) 0.1269(12) 0.014(5) Uiso 1 1 d . . .
C16B C 1.2515(8) 0.04570(18) 0.28162(14) 0.061(4) Uiso 1 1 d D . .
C23B C 1.8973(7) 0.44222(14) 0.20943(10) 0.038(3) Uiso 1 1 d D . .
```

```
C13A C 0.802(2) 0.1479(8) 0.3152(11) 0.012(4) Uiso 1 1 d . . .
C14A C 0.823(2) 0.1491(8) 0.1743(11) 0.011(4) Uiso 1 1 d . . .
C12A C 1.228(2) 0.3049(7) 0.2066(9) 0.001(4) Uiso 1 1 d . . .
C10A C 1.068(2) 0.2354(6) 0.3907(10) 0.005(4) Uiso 1 1 d . . .
C5A C 0.976(2) 0.2176(7) 0.1198(10) 0.0042(15) Uiso 1 1 d . . .
C36A C 0.7188(3) 0.1584(3) 0.5230(5) 0.011(4) Uiso 1 1 d D . .
C8A C 1.073(3) 0.2452(7) 0.2596(11) 0.012(4) Uiso 1 1 d . . .
C37A C 0.630(2) 0.1168(6) 0.5218(10) 0.003(3) Uiso 1 1 d . . .
C2A C 0.925(2) 0.1840(7) 0.3173(10) 0.0042(15) Uiso 1 1 d . . .
C9A C 1.123(2) 0.2557(7) 0.3263(11) 0.007(4) Uiso 1 1 d . . .
C49A C 1.0650(4) 0.3990(3) -0.0254(9) 0.058(9) Uiso 1 1 d D . .
C7A C 1.132(2) 0.2660(7) 0.1965(10) 0.0042(15) Uiso 1 1 d . . .
C38A C 0.487(2) 0.1262(7) 0.5522(11) 0.010(4) Uiso 1 1 d . . .
C4A C 0.935(2) 0.1887(7) 0.1792(10) 0.0042(15) Uiso 1 1 d . . .
C48A C 1.0791(5) 0.36870(12) 0.0414(5) 0.098(16) Uiso 1 1 d D . .
C3A C 0.973(2) 0.2079(7) 0.2504(10) 0.0042(15) Uiso 1 1 d . . .
O3A O 1.2447(19) 0.3150(6) 0.4072(9) 0.021(4) Uiso 1 1 d . . .
C39A C 0.391(2) 0.0795(7) 0.5516(11) 0.012(4) Uiso 1 1 d . . .
N2A N 1.276(2) 0.3192(6) 0.2756(10) 0.010(2) Uiso 1 1 d . . .
O4A O 1.2811(19) 0.3229(6) 0.1534(9) 0.020(4) Uiso 1 1 d . . .
C34B C 1.4593(11) 0.4521(2) 0.5054(5) 0.20(4) Uiso 1 1 d D . .
C16A C 0.7665(8) 0.04533(18) 0.24072(14) 0.051(4) Uiso 1 1 d D . .
C1A C 0.990(2) 0.1963(7) 0.3853(10) 0.0042(15) Uiso 1 1 d . . .
C3B C 1.477(2) 0.2059(7) 0.2684(10) 0.005(4) Uiso 1 1 d . . .
C23A C 1.3791(7) 0.44704(12) 0.30099(6) 0.043(3) Uiso 1 1 d D . .
C35B C 1.460(2) 0.4898(3) 0.5643(7) 0.038(7) Uiso 1 1 d D . .
C33A C 0.9920(3) 0.04652(12) 0.5307(3) 0.023(5) Uiso 1 1 d D . .
C21A C 1.3627(11) 0.3612(2) 0.27887(11) 0.043(3) Uiso 1 1 d D . .
C25A C 1.3866(7) 0.53298(16) 0.32316(15) 0.043(3) Uiso 1 1 d D . .
C34A C 1.0510(6) 0.00011(13) 0.5009(3) 0.013(4) Uiso 1 1 d D . .
C26A C 1.2909(13) 0.5761(2) 0.3344(2) 0.043(3) Uiso 1 1 d D . .
C24A C 1.2869(8) 0.49094(15) 0.31243(17) 0.043(3) Uiso 1 1 d D . .
C22A C 1.2751(8) 0.40600(18) 0.2905(2) 0.043(3) Uiso 1 1 d D . .
C40A C 1.3283(3) 0.28822(12) -0.0142(4) 0.114(10) Uiso 1 1 d D . .
C41A C 1.4280(5) 0.32785(15) 0.0101(3) 0.114(10) Uiso 1 1 d D . .
C42A C 1.4737(6) 0.35392(18) -0.0578(4) 0.114(10) Uiso 1 1 d D . .
C43A C 1.5734(6) 0.39355(18) -0.0334(7) 0.114(10) Uiso 1 1 d D . .
C29B C 1.498(3) 0.2804(10) 0.6315(16) 0.035(7) Uiso 1 1 d . . .
C30B C 1.378(4) 0.2623(11) 0.6800(17) 0.041(7) Uiso 1 1 d . . .
C25B C 1.9383(7) 0.52599(16) 0.1844(2) 0.038(3) Uiso 1 1 d D . .
C41B C 1.5241(4) 0.0442(4) -0.0207(8) 0.029(6) Uiso 1 1 d D . .
C40B C 1.5017(5) 0.07104(12) 0.0492(4) 0.013(5) Uiso 1 1 d D . .
C24B C 1.8215(8) 0.48869(15) 0.19163(17) 0.038(3) Uiso 1 1 d D . .
C32A C 0.9755(6) 0.08027(10) 0.4672(3) 0.024(5) Uiso 1 1 d D . .
C37B C 1.908(2) 0.3358(6) 0.5275(11) 0.009(2) Uiso 1 1 d . . .
C36B C 1.8102(6) 0.2909(3) 0.5172(8) 0.009(2) Uiso 1 1 d D . .
C39B C 2.134(2) 0.3730(7) 0.5683(11) 0.009(2) Uiso 1 1 d . . .
C38B C 2.049(2) 0.3293(7) 0.5638(11) 0.009(2) Uiso 1 1 d . . .
C6B C 1.557(3) 0.2618(7) 0.3853(11) 0.009(4) Uiso 1 1 d . . .
C7B C 1.605(2) 0.2708(7) 0.3208(11) 0.007(4) Uiso 1 1 d . . .
C8B C 1.573(2) 0.2417(6) 0.2631(10) 0.003(4) Uiso 1 1 d . . .
C11A C 1.207(2) 0.2996(8) 0.3365(11) 0.009(4) Uiso 1 1 d . . .
C42B C 1.5553(8) -0.0074(4) -0.0002(9) 0.025(6) Uiso 1 1 d D . .
C31B C 1.297(3) 0.2843(10) 0.7498(15) 0.031(6) Uiso 1 1 d . . .
C27A C 1.0683(5) 0.1789(2) 0.56414(18) 0.012(4) Uiso 1 1 d D . .
C28A C 1.0217(8) 0.1661(7) 0.6403(2) 0.080(14) Uiso 1 1 d D . .
C30A C 1.1462(9) 0.1787(9) 0.6896(2) 0.054(9) Uiso 1 1 d D . .
C17B C 1.1511(8) 0.00315(16) 0.27957(8) 0.061(4) Uiso 1 1 d D . .
C43B C 1.5779(9) -0.0350(6) -0.0675(12) 0.051(9) Uiso 1 1 d D . .
C26B C 1.8646(14) 0.5728(2) 0.1666(2) 0.038(3) Uiso 1 1 d D . .
C48B C 1.5968(4) 0.17152(10) -0.0419(3) 0.080(7) Uiso 1 1 d D . .
C44B C 1.2459(3) 0.14810(17) -0.01083(18) 0.071(6) Uiso 1 1 d D . .
C18A C 0.7605(7) -0.04097(14) 0.24968(15) 0.051(4) Uiso 1 1 d D . .
C19A C 0.6630(8) -0.08409(17) 0.25185(16) 0.051(4) Uiso 1 1 d D . .
C19B C 1.1485(7) -0.08396(16) 0.27628(17) 0.061(4) Uiso 1 1 d D . .
```

```
C18B C 1.2460(8) -0.04078(16) 0.27834(15) 0.061(4) Uiso 1 1 d D . .
C17A C 0.6660(8) 0.00283(16) 0.24277(9) 0.051(4) Uiso 1 1 d D . .
C20B C 1.2455(13) -0.1274(3) 0.2751(2) 0.061(4) Uiso 1 1 d D . .
C51A C 0.9876(10) 0.4765(5) -0.0707(10) 0.025(6) Uiso 1 1 d D . .
C46B C 1.0020(4) 0.1262(2) -0.0414(3) 0.071(6) Uiso 1 1 d D . .
C50A C 1.0012(13) 0.4463(4) -0.0030(10) 0.039(7) Uiso 1 1 d D . .
C45B C 1.1416(4) 0.1067(2) -0.0114(4) 0.071(6) Uiso 1 1 d D . .
C47B C 0.8978(6) 0.0847(3) -0.0419(5) 0.071(6) Uiso 1 1 d D . .
C31A C 1.0950(17) 0.1706(11) 0.7663(2) 0.054(9) Uiso 1 1 d D . .
C49B C 1.5979(17) 0.16360(19) -0.1223(8) 0.080(7) Uiso 1 1 d D . .
C20A C 0.7600(14) -0.1273(3) 0.2587(2) 0.051(4) Uiso 1 1 d D . .
C50B C 1.4476(18) 0.1536(3) -0.1454(8) 0.080(7) Uiso 1 1 d D . .
C35A C 1.0671(8) -0.0334(2) 0.5648(5) 0.089(15) Uiso 1 1 d D . .
C51B C 1.455(3) 0.1458(3) -0.2274(9) 0.080(7) Uiso 1 1 d D . .
C44A C 0.9744(4) 0.26576(11) -0.04089(18) 0.052(5) Uiso 1 1 d D . .
C45A C 1.0312(6) 0.28364(19) -0.1127(2) 0.052(5) Uiso 1 1 d D . .
C46A C 0.9085(7) 0.2787(3) -0.1663(2) 0.052(5) Uiso 1 1 d D . .
C47A C 0.9640(13) 0.2965(3) -0.2383(2) 0.078(5) Uiso 1 1 d D . .

_geom_special_details
;
 All esds (except the esd in the dihedral angle between two l.s. planes)
 are estimated using the full covariance matrix.  The cell esds are taken
 into account individually in the estimation of esds in distances, angles
 and torsion angles; correlations between esds in cell parameters are only
 used when they are defined by crystal symmetry.  An approximate (isotropic)
 treatment of cell esds is used for estimating esds involving l.s. planes.
;

loop_
 _geom_bond_atom_site_label_1
 _geom_bond_atom_site_label_2
 _geom_bond_distance
 _geom_bond_site_symmetry_2
 _geom_bond_publ_flag
Sn1B C32B 2.148(4) . ?
Sn1B C36B 2.149(4) . ?
Sn1B C28B 2.168(19) . ?
Sn1B C6B 2.18(2) . ?
Sn1A C36A 2.136(4) . ?
Sn1A C32A 2.143(3) . ?
Sn1A C27A 2.147(3) . ?
Sn1A C1A 2.23(2) . ?
Sn2A C6A 2.11(2) . ?
Sn2A C40A 2.145(4) . ?
Sn2A C44A 2.140(3) . ?
Sn2A C48A 2.147(3) . ?
Sn2B C44B 2.141(3) . ?
Sn2B C40B 2.145(3) . ?
Sn2B C48B 2.149(4) . ?
Sn2B C1B 2.33(2) . ?
O4B C12B 1.29(2) . ?
O1B C13B 1.16(4) . ?
O3B C11B 1.35(3) . ?
C2B C3B 1.43(3) . ?
C2B C1B 1.43(3) . ?
C2B C14B 1.62(3) . ?
O2B C14B 1.16(2) . ?
N1B C14B 1.40(2) . ?
N1B C13B 1.49(4) . ?
N1B C15B 1.655(18) . ?
C11B C7B 1.39(3) . ?
C11B N2B 1.42(4) . ?
C12B C9B 1.45(3) . ?
C12B N2B 1.53(3) . ?
```

```
C28B C29B 1.52(3) . ?
C10B C1B 1.35(3) . ?
C10B C9B 1.41(3) . ?
N2B C21B 1.37(3) . ?
C32B C33B 1.531(5) . ?
C4B C5B 1.26(4) . ?
C4B C13B 1.36(4) . ?
C4B C3B 1.42(3) . ?
C5B C6B 1.57(4) . ?
C21B C22B 1.531(5) . ?
C9B C8B 1.50(3) . ?
C33B C34B 1.530(5) . ?
C15B C16B 1.529(5) . ?
O1A C13A 1.11(3) . ?
O2A C14A 1.07(3) . ?
N1A C14A 1.40(3) . ?
N1A C13A 1.44(3) . ?
N1A C15A 1.61(2) . ?
C22B C23B 1.529(5) . ?
C15A C16A 1.529(5) . ?
C6A C7A 1.41(3) . ?
C6A C5A 1.47(3) . ?
C16B C17B 1.531(5) . ?
C23B C24B 1.531(5) . ?
C13A C2A 1.55(3) . ?
C14A C4A 1.54(3) . ?
C12A O4A 1.23(3) . ?
C12A N2A 1.42(3) . ?
C12A C7A 1.44(3) . ?
C10A C1A 1.33(3) . ?
C10A C9A 1.43(3) . ?
C5A C4A 1.43(3) . ?
C36A C37A 1.443(18) . ?
C8A C9A 1.36(3) . ?
C8A C7A 1.43(3) . ?
C8A C3A 1.43(3) . ?
C37A C38A 1.50(3) . ?
C2A C1A 1.45(3) . ?
C2A C3A 1.49(3) . ?
C9A C11A 1.49(3) . ?
C49A C48A 1.516(14) . ?
C49A C50A 1.525(14) . ?
C38A C39A 1.60(3) . ?
C4A C3A 1.48(3) . ?
O3A C11A 1.43(3) . ?
N2A C11A 1.42(3) . ?
N2A C21A 1.45(2) . ?
C34B C35B 1.529(5) . ?
C16A C17A 1.531(5) . ?
C3B C8B 1.36(3) . ?
C23A C24A 1.531(5) . ?
C23A C22A 1.531(5) . ?
C33A C32A 1.529(4) . ?
C33A C34A 1.530(4) . ?
C21A C22A 1.527(5) . ?
C25A C24A 1.528(5) . ?
C25A C26A 1.532(5) . ?
C34A C35A 1.530(5) . ?
C40A C41A 1.530(4) . ?
C41A C42A 1.530(5) . ?
C42A C43A 1.530(5) . ?
C29B C30B 1.54(5) . ?
C30B C31B 1.64(4) . ?
C25B C26B 1.529(5) . ?
C25B C24B 1.531(5) . ?
```

```
C41B C40B 1.525(14) . ?
C41B C42B 1.534(14) . ?
C37B C38B 1.50(3) . ?
C37B C36B 1.58(2) . ?
C39B C38B 1.47(3) . ?
C6B C7B 1.31(3) . ?
C7B C8B 1.39(3) . ?
C42B C43B 1.494(16) . ?
C27A C28A 1.532(5) . ?
C28A C30A 1.531(5) . ?
C30A C31A 1.530(5) . ?
C17B C18B 1.531(5) . ?
C48B C49B 1.517(14) . ?
C44B C45B 1.530(4) . ?
C18A C19A 1.527(5) . ?
C18A C17A 1.530(5) . ?
C19A C20A 1.530(5) . ?
C19B C18B 1.528(5) . ?
C19B C20B 1.531(5) . ?
C51A C50A 1.530(16) . ?
C46B C47B 1.530(5) . ?
C46B C45B 1.531(4) . ?
C49B C50B 1.508(16) . ?
C50B C51B 1.546(16) . ?
C44A C45A 1.531(4) . ?
C45A C46A 1.533(5) . ?
C46A C47A 1.529(5) . ?

loop_
 _geom_angle_atom_site_label_1
 _geom_angle_atom_site_label_2
 _geom_angle_atom_site_label_3
 _geom_angle
 _geom_angle_site_symmetry_1
 _geom_angle_site_symmetry_3
 _geom_angle_publ_flag
C32B Sn1B C36B 106.1(2) . . ?
C32B Sn1B C28B 115.4(5) . . ?
C36B Sn1B C28B 110.4(6) . . ?
C32B Sn1B C6B 115.4(6) . . ?
C36B Sn1B C6B 108.8(7) . . ?
C28B Sn1B C6B 100.7(7) . . ?
C36A Sn1A C32A 107.1(2) . . ?
C36A Sn1A C27A 106.6(2) . . ?
C32A Sn1A C27A 106.25(19) . . ?
C36A Sn1A C1A 120.5(6) . . ?
C32A Sn1A C1A 111.5(5) . . ?
C27A Sn1A C1A 103.9(5) . . ?
C6A Sn2A C40A 116.4(7) . . ?
C6A Sn2A C44A 102.9(6) . . ?
C40A Sn2A C44A 106.58(19) . . ?
C6A Sn2A C48A 117.3(6) . . ?
C40A Sn2A C48A 106.33(18) . . ?
C44A Sn2A C48A 106.3(2) . . ?
C44B Sn2B C40B 106.58(18) . . ?
C44B Sn2B C48B 106.21(19) . . ?
C40B Sn2B C48B 106.05(19) . . ?
C44B Sn2B C1B 119.2(6) . . ?
C40B Sn2B C1B 114.4(6) . . ?
C48B Sn2B C1B 103.3(6) . . ?
C3B C2B C1B 121(2) . . ?
C3B C2B C14B 121.8(17) . . ?
C1B C2B C14B 114.8(17) . . ?
C14B N1B C13B 130.3(19) . . ?
C14B N1B C15B 111.9(13) . . ?
```

```
C13B N1B C15B 117.8(16) . . ?
O3B C11B C7B 121(2) . . ?
O3B C11B N2B 108(2) . . ?
C7B C11B N2B 129(2) . . ?
O4B C12B C9B 127.3(17) . . ?
O4B C12B N2B 114.4(19) . . ?
C9B C12B N2B 117.9(18) . . ?
C29B C28B Sn1B 108.6(16) . . ?
C1B C10B C9B 115.8(19) . . ?
C21B N2B C11B 129(3) . . ?
C21B N2B C12B 118(2) . . ?
C11B N2B C12B 114(2) . . ?
C33B C32B Sn1B 121.1(4) . . ?
C5B C4B C13B 121(3) . . ?
C5B C4B C3B 118(3) . . ?
C13B C4B C3B 122(2) . . ?
C4B C5B C6B 124(3) . . ?
N2B C21B C22B 110.3(14) . . ?
O1B C13B C4B 125(3) . . ?
O1B C13B N1B 116(3) . . ?
C4B C13B N1B 117(3) . . ?
C10B C9B C12B 116.0(17) . . ?
C10B C9B C8B 123.1(18) . . ?
C12B C9B C8B 120.9(17) . . ?
C34B C33B C32B 106.3(4) . . ?
C10B C1B C2B 122(2) . . ?
C10B C1B Sn2B 116.1(15) . . ?
C2B C1B Sn2B 121.5(16) . . ?
C16B C15B N1B 103.1(8) . . ?
O2B C14B N1B 125.5(19) . . ?
O2B C14B C2B 125.7(18) . . ?
N1B C14B C2B 106.8(15) . . ?
C14A N1A C13A 136.8(19) . . ?
C14A N1A C15A 109.9(15) . . ?
C13A N1A C15A 112.9(15) . . ?
C23B C22B C21B 106.3(4) . . ?
C16A C15A N1A 104.8(8) . . ?
C7A C6A C5A 118.0(19) . . ?
C7A C6A Sn2A 124.3(16) . . ?
C5A C6A Sn2A 114.7(15) . . ?
C15B C16B C17B 107.0(5) . . ?
C22B C23B C24B 107.1(4) . . ?
O1A C13A N1A 127(2) . . ?
O1A C13A C2A 122(2) . . ?
N1A C13A C2A 107.9(17) . . ?
O2A C14A N1A 128(2) . . ?
O2A C14A C4A 120(2) . . ?
N1A C14A C4A 111.9(17) . . ?
O4A C12A N2A 119.1(18) . . ?
O4A C12A C7A 118.2(18) . . ?
N2A C12A C7A 122.3(17) . . ?
C1A C10A C9A 118.1(18) . . ?
C4A C5A C6A 121.0(18) . . ?
C37A C36A Sn1A 119.0(8) . . ?
C9A C8A C7A 122(2) . . ?
C9A C8A C3A 119.8(18) . . ?
C7A C8A C3A 117.7(17) . . ?
C36A C37A C38A 112.0(13) . . ?
C1A C2A C3A 119.7(18) . . ?
C1A C2A C13A 119.8(17) . . ?
C3A C2A C13A 120.5(17) . . ?
C8A C9A C10A 124(2) . . ?
C8A C9A C11A 118.8(18) . . ?
C10A C9A C11A 114.9(17) . . ?
C48A C49A C50A 107.6(11) . . ?
```

```
C6A C7A C8A 122.7(19) . . ?
C6A C7A C12A 120.1(18) . . ?
C8A C7A C12A 117.0(17) . . ?
C37A C38A C39A 111.2(16) . . ?
C5A C4A C3A 115.1(17) . . ?
C5A C4A C14A 123.6(17) . . ?
C3A C4A C14A 118.8(17) . . ?
C49A C48A Sn2A 121.2(6) . . ?
C8A C3A C4A 122.4(17) . . ?
C8A C3A C2A 115.9(16) . . ?
C4A C3A C2A 121.0(17) . . ?
C11A N2A C12A 118.0(17) . . ?
C11A N2A C21A 123.1(16) . . ?
C12A N2A C21A 116.7(15) . . ?
C35B C34B C33B 106.5(4) . . ?
C15A C16A C17A 106.9(5) . . ?
C10A C1A C2A 119.8(18) . . ?
C10A C1A Sn1A 122.1(14) . . ?
C2A C1A Sn1A 117.5(14) . . ?
C8B C3B C4B 120.5(18) . . ?
C8B C3B C2B 118.3(17) . . ?
C4B C3B C2B 120(2) . . ?
C24A C23A C22A 105.4(4) . . ?
C32A C33A C34A 106.7(3) . . ?
N2A C21A C22A 112.3(10) . . ?
C24A C25A C26A 105.8(5) . . ?
C33A C34A C35A 106.4(4) . . ?
C25A C24A C23A 107.3(4) . . ?
C21A C22A C23A 107.3(5) . . ?
C41A C40A Sn2A 111.8(3) . . ?
C40A C41A C42A 106.4(4) . . ?
C41A C42A C43A 106.4(4) . . ?
C28B C29B C30B 105(2) . . ?
C29B C30B C31B 134(3) . . ?
C26B C25B C24B 106.7(5) . . ?
C40B C41B C42B 106.7(11) . . ?
C41B C40B Sn2B 115.0(6) . . ?
C23B C24B C25B 105.9(4) . . ?
C33A C32A Sn1A 122.1(3) . . ?
C38B C37B C36B 118.2(14) . . ?
C37B C36B Sn1B 117.0(8) . . ?
C39B C38B C37B 113.8(17) . . ?
C7B C6B C5B 114(2) . . ?
C7B C6B Sn1B 126.4(16) . . ?
C5B C6B Sn1B 119.0(16) . . ?
C6B C7B C8B 121(2) . . ?
C6B C7B C11B 121(2) . . ?
C8B C7B C11B 117(2) . . ?
C3B C8B C7B 121.8(18) . . ?
C3B C8B C9B 117.6(17) . . ?
C7B C8B C9B 119.9(17) . . ?
O3A C11A N2A 120.5(18) . . ?
O3A C11A C9A 120.1(17) . . ?
N2A C11A C9A 117.9(17) . . ?
C43B C42B C41B 108.3(12) . . ?
C28A C27A Sn1A 114.4(4) . . ?
C30A C28A C27A 106.2(4) . . ?
C31A C30A C28A 106.4(4) . . ?
C18B C17B C16B 105.9(5) . . ?
C49B C48B Sn2B 129.2(6) . . ?
C45B C44B Sn2B 123.6(3) . . ?
C19A C18A C17A 107.2(4) . . ?
C18A C19A C20A 106.1(5) . . ?
C18B C19B C20B 106.2(5) . . ?
C19B C18B C17B 107.1(5) . . ?
```

```
C18A C17A C16A 105.9(5) . . ?
C47B C46B C45B 106.3(4) . . ?
C49A C50A C51A 107.1(12) . . ?
C44B C45B C46B 106.3(4) . . ?
C50B C49B C48B 107.4(11) . . ?
C49B C50B C51B 105.3(14) . . ?
C45A C44A Sn2A 102.6(3) . . ?
C44A C45A C46A 105.9(3) . . ?
C47A C46A C45A 106.4(4) . . ?

_diffrn_measured_fraction_theta_max    0.999
_diffrn_reflns_theta_full              26.00
_diffrn_measured_fraction_theta_full   0.999
_refine_diff_density_max    3.118
_refine_diff_density_min   -3.930
_refine_diff_density_rms    0.344
```

B.4 Chapter 5

B.4.1 Compound 5.2

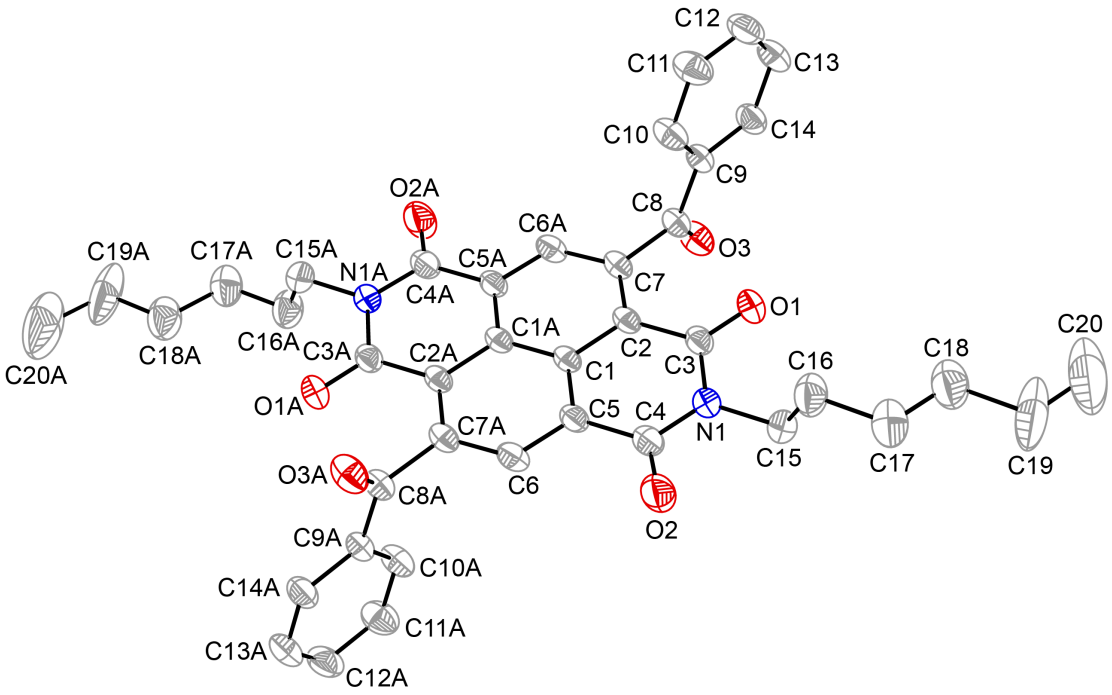

Figure B.4. The structure of compound **5.2**. Ellipsoids are shown at the 30% level. Hydrogen atoms are omitted for clarity.

*Crystal Identification File for Compound **5.2***

```
data_15

_audit_creation_method            SHELXL-97
_chemical_name_systematic
;
 ?
;
_chemical_name_common             ?
_chemical_melting_point           ?
_chemical_formula_moiety          ?
_chemical_formula_sum
 'C40 H38 N2 O6'
_chemical_formula_weight          642.72

loop_
 _atom_type_symbol
 _atom_type_description
 _atom_type_scat_dispersion_real
 _atom_type_scat_dispersion_imag
 _atom_type_scat_source
 'C'  'C'   0.0033   0.0016
 'International Tables Vol C Tables 4.2.6.8 and 6.1.1.4'
 'H'  'H'   0.0000   0.0000
 'International Tables Vol C Tables 4.2.6.8 and 6.1.1.4'
 'N'  'N'   0.0061   0.0033
 'International Tables Vol C Tables 4.2.6.8 and 6.1.1.4'
 'O'  'O'   0.0106   0.0060
 'International Tables Vol C Tables 4.2.6.8 and 6.1.1.4'

_symmetry_cell_setting            ?
_symmetry_space_group_name_H-M    ?

loop_
 _symmetry_equiv_pos_as_xyz
 'x, y, z'
 '-x, y, -z+1/2'
 'x+1/2, y+1/2, z'
 '-x+1/2, y+1/2, -z+1/2'
 '-x, -y, -z'
 'x, -y, z-1/2'
 '-x+1/2, -y+1/2, -z'
 'x+1/2, -y+1/2, z-1/2'

_cell_length_a                    27.241(10)
_cell_length_b                    5.734(2)
_cell_length_c                    23.284(8)
_cell_angle_alpha                 90.00
_cell_angle_beta                  112.558(7)
_cell_angle_gamma                 90.00
_cell_volume                      3358(2)
_cell_formula_units_Z             4
_cell_measurement_temperature     100(2)
_cell_measurement_reflns_used     ?
_cell_measurement_theta_min       ?
_cell_measurement_theta_max       ?

_exptl_crystal_description        ?
_exptl_crystal_colour             ?
_exptl_crystal_size_max           ?
_exptl_crystal_size_mid           ?
_exptl_crystal_size_min           ?
_exptl_crystal_density_meas       ?
```

```
_exptl_crystal_density_diffrn     1.271
_exptl_crystal_density_method     'not measured'
_exptl_crystal_F_000              1360
_exptl_absorpt_coefficient_mu     0.086
_exptl_absorpt_correction_type    ?
_exptl_absorpt_correction_T_min   ?
_exptl_absorpt_correction_T_max   ?
_exptl_absorpt_process_details    ?

_exptl_special_details
;
 ?
;

_diffrn_ambient_temperature       100(2)
_diffrn_radiation_wavelength      0.71073
_diffrn_radiation_type            MoK\a
_diffrn_radiation_source          'fine-focus sealed tube'
_diffrn_radiation_monochromator   graphite
_diffrn_measurement_device_type   ?
_diffrn_measurement_method        ?
_diffrn_detector_area_resol_mean  ?
_diffrn_standards_number          ?
_diffrn_standards_interval_count  ?
_diffrn_standards_interval_time   ?
_diffrn_standards_decay_%         ?
_diffrn_reflns_number             18860
_diffrn_reflns_av_R_equivalents   0.0495
_diffrn_reflns_av_sigmaI/netI     0.0302
_diffrn_reflns_limit_h_min        -32
_diffrn_reflns_limit_h_max        32
_diffrn_reflns_limit_k_min        -6
_diffrn_reflns_limit_k_max        6
_diffrn_reflns_limit_l_min        -27
_diffrn_reflns_limit_l_max        27
_diffrn_reflns_theta_min          1.89
_diffrn_reflns_theta_max          25.00
_reflns_number_total              2958
_reflns_number_gt                 1882
_reflns_threshold_expression      >2sigma(I)

_computing_data_collection        ?
_computing_cell_refinement        ?
_computing_data_reduction         ?
_computing_structure_solution     'SHELXS-97 (Sheldrick, 1990)'
_computing_structure_refinement   'SHELXL-97 (Sheldrick, 1997)'
_computing_molecular_graphics     ?
_computing_publication_material   ?

_refine_special_details
;
 Refinement of F^2^ against ALL reflections.  The weighted R-factor wR and
 goodness of fit S are based on F^2^, conventional R-factors R are based
 on F, with F set to zero for negative F^2^. The threshold expression of
 F^2^ > 2sigma(F^2^) is used only for calculating R-factors(gt) etc. and is
 not relevant to the choice of reflections for refinement.  R-factors based
 on F^2^ are statistically about twice as large as those based on F, and R-
 factors based on ALL data will be even larger.
;

_refine_ls_structure_factor_coef  Fsqd
_refine_ls_matrix_type            full
_refine_ls_weighting_scheme       calc
_refine_ls_weighting_details
 'calc w=1/[\s^2^(Fo^2^)+(0.0662P)^2^+2.7983P] where P=(Fo^2^+2Fc^2^)/3'
```

```
_atom_sites_solution_primary      direct
_atom_sites_solution_secondary    difmap
_atom_sites_solution_hydrogens    geom
_refine_ls_hydrogen_treatment     mixed
_refine_ls_extinction_method      none
_refine_ls_extinction_coef        ?
_refine_ls_number_reflns          2958
_refine_ls_number_parameters      230
_refine_ls_number_restraints      5
_refine_ls_R_factor_all           0.0865
_refine_ls_R_factor_gt            0.0516
_refine_ls_wR_factor_ref          0.1549
_refine_ls_wR_factor_gt           0.1279
_refine_ls_goodness_of_fit_ref    1.013
_refine_ls_restrained_S_all       1.024
_refine_ls_shift/su_max           0.000
_refine_ls_shift/su_mean          0.000

loop_
 _atom_site_label
 _atom_site_type_symbol
 _atom_site_fract_x
 _atom_site_fract_y
 _atom_site_fract_z
 _atom_site_U_iso_or_equiv
 _atom_site_adp_type
 _atom_site_occupancy
 _atom_site_symmetry_multiplicity
 _atom_site_calc_flag
 _atom_site_refinement_flags
 _atom_site_disorder_assembly
 _atom_site_disorder_group
N1 N 0.21615(8) 0.6639(4) 0.13023(9) 0.0557(6) Uani 1 1 d . . .
O1 O 0.15029(7) 0.9320(3) 0.09216(8) 0.0651(5) Uani 1 1 d . . .
O2 O 0.27313(9) 0.3582(5) 0.15973(11) 0.1006(8) Uani 1 1 d . . .
O3 O 0.14538(7) 1.3901(3) 0.01483(10) 0.0730(6) Uani 1 1 d . . .
C1 C 0.24257(8) 0.7315(4) 0.02561(10) 0.0459(6) Uani 1 1 d . . .
C2 C 0.20194(8) 0.8683(4) 0.03227(11) 0.0462(6) Uani 1 1 d . . .
C3 C 0.18666(9) 0.8265(4) 0.08599(11) 0.0511(6) Uani 1 1 d . . .
C4 C 0.25316(10) 0.5140(5) 0.12253(13) 0.0643(7) Uani 1 1 d . . .
C5 C 0.26821(9) 0.5552(4) 0.06866(11) 0.0513(6) Uani 1 1 d . . .
C6 C 0.30728(9) 0.4235(4) 0.06073(12) 0.0565(7) Uani 1 1 d . . .
H6A H 0.3240 0.3034 0.0898 0.068 Uiso 1 1 calc R . .
C7 C 0.17678(8) 1.0384(4) -0.01081(12) 0.0496(6) Uani 1 1 d . . .
C8 C 0.13337(9) 1.1967(4) -0.00730(12) 0.0517(6) Uani 1 1 d . . .
C9 C 0.07745(9) 1.1189(4) -0.03752(11) 0.0495(6) Uani 1 1 d . . .
C10 C 0.06369(10) 0.9089(5) -0.06831(14) 0.0661(8) Uani 1 1 d . . .
H10A H 0.0907 0.8053 -0.0689 0.079 Uiso 1 1 calc R . .
C11 C 0.01065(11) 0.8474(6) -0.09845(15) 0.0790(9) Uani 1 1 d . . .
H11A H 0.0014 0.7032 -0.1200 0.095 Uiso 1 1 calc R . .
C12 C -0.02848(11) 0.9956(6) -0.09706(15) 0.0785(9) Uani 1 1 d . . .
H12A H -0.0648 0.9540 -0.1177 0.094 Uiso 1 1 calc R . .
C13 C -0.01524(11) 1.2018(6) -0.06611(15) 0.0767(9) Uani 1 1 d . . .
H13A H -0.0424 1.3030 -0.0649 0.092 Uiso 1 1 calc R . .
C14 C 0.03732(10) 1.2653(5) -0.03640(13) 0.0635(7) Uani 1 1 d . . .
H14A H 0.0461 1.4102 -0.0151 0.076 Uiso 1 1 calc R . .
C15 C 0.20241(11) 0.6284(5) 0.18531(12) 0.0666(8) Uani 1 1 d . B .
H15A H 0.1887 0.7766 0.1952 0.080 Uiso 1 1 calc R . .
H15B H 0.2350 0.5864 0.2214 0.080 Uiso 1 1 calc R . .
C16 C 0.16158(13) 0.4413(6) 0.17556(15) 0.0851(10) Uani 1 1 d . . .
H16A H 0.1740 0.2983 0.1614 0.102 Uiso 1 1 calc R A 1
H16B H 0.1283 0.4911 0.1416 0.102 Uiso 1 1 calc R A 1
C17 C 0.1490(3) 0.3800(11) 0.2318(3) 0.0948(18) Uani 0.736(5) 1 d PD B 1
H17A H 0.1324 0.2237 0.2258 0.114 Uiso 0.736(5) 1 calc PR B 1
H17B H 0.1824 0.3740 0.2692 0.114 Uiso 0.736(5) 1 calc PR B 1
```

```
C18 C 0.1127(2) 0.5530(11) 0.2415(3) 0.1117(18) Uani 0.736(5) 1 d PD B 1
H18A H 0.0797 0.5651 0.2037 0.134 Uiso 0.736(5) 1 calc PR B 1
H18B H 0.1299 0.7083 0.2503 0.134 Uiso 0.736(5) 1 calc PR B 1
C19 C 0.0996(5) 0.468(2) 0.2983(4) 0.187(4) Uani 0.736(5) 1 d PD B 1
H19A H 0.0807 0.3168 0.2890 0.224 Uiso 0.736(5) 1 calc PR B 1
H19B H 0.1326 0.4504 0.3359 0.224 Uiso 0.736(5) 1 calc PR B 1
C20 C 0.0652(4) 0.653(3) 0.3079(6) 0.284(9) Uani 0.736(5) 1 d PD B 1
H20A H 0.0555 0.6102 0.3429 0.425 Uiso 0.736(5) 1 calc PR B 1
H20B H 0.0329 0.6686 0.2702 0.425 Uiso 0.736(5) 1 calc PR B 1
H20C H 0.0844 0.8014 0.3168 0.425 Uiso 0.736(5) 1 calc PR B 1
C17' C 0.1511(9) 0.487(3) 0.2429(12) 0.0948(18) Uani 0.264(5) 1 d PD B 2
H17C H 0.1841 0.4589 0.2797 0.114 Uiso 0.264(5) 1 calc PR B 2
H17D H 0.1393 0.6496 0.2446 0.114 Uiso 0.264(5) 1 calc PR B 2
C18' C 0.1095(6) 0.321(3) 0.2410(7) 0.1117(18) Uani 0.264(5) 1 d PD B 2
H18C H 0.1238 0.1661 0.2369 0.134 Uiso 0.264(5) 1 calc PR B 2
H18D H 0.0798 0.3509 0.2008 0.134 Uiso 0.264(5) 1 calc PR B 2
C19' C 0.0828(10) 0.285(5) 0.2885(10) 0.187(4) Uani 0.264(5) 1 d PD B 2
H19C H 0.0443 0.2505 0.2683 0.224 Uiso 0.264(5) 1 calc PR B 2
H19D H 0.1008 0.1649 0.3201 0.224 Uiso 0.264(5) 1 calc PR B 2
C20' C 0.0935(19) 0.526(7) 0.314(2) 0.284(9) Uani 0.264(5) 1 d PD B 2
H20D H 0.1249 0.5258 0.3528 0.425 Uiso 0.264(5) 1 calc PR B 2
H20E H 0.0628 0.5839 0.3216 0.425 Uiso 0.264(5) 1 calc PR B 2
H20F H 0.1000 0.6282 0.2836 0.425 Uiso 0.264(5) 1 calc PR B 2

loop_
 _atom_site_aniso_label
 _atom_site_aniso_U_11
 _atom_site_aniso_U_22
 _atom_site_aniso_U_33
 _atom_site_aniso_U_23
 _atom_site_aniso_U_13
 _atom_site_aniso_U_12
N1 0.0468(11) 0.0696(15) 0.0533(12) 0.0007(11) 0.0221(10) 0.0042(10)
O1 0.0561(10) 0.0738(12) 0.0745(12) -0.0035(10) 0.0353(9) 0.0117(9)
O2 0.0954(16) 0.130(2) 0.0944(16) 0.0546(16) 0.0561(13) 0.0546(15)
O3 0.0591(11) 0.0541(11) 0.1060(15) -0.0178(11) 0.0318(11) -0.0033(9)
C1 0.0313(10) 0.0498(13) 0.0556(14) -0.0023(12) 0.0156(10) -0.0012(10)
C2 0.0322(11) 0.0477(13) 0.0581(14) -0.0047(11) 0.0165(10) -0.0025(10)
C3 0.0401(13) 0.0563(15) 0.0578(15) -0.0089(12) 0.0196(11) -0.0030(11)
C4 0.0495(14) 0.0798(19) 0.0656(17) 0.0132(16) 0.0241(13) 0.0134(14)
C5 0.0365(11) 0.0601(15) 0.0579(15) 0.0040(12) 0.0188(11) 0.0042(11)
C6 0.0419(13) 0.0574(16) 0.0691(17) 0.0095(13) 0.0201(12) 0.0093(12)
C7 0.0369(12) 0.0472(14) 0.0657(15) -0.0025(12) 0.0207(11) -0.0008(11)
C8 0.0441(13) 0.0468(14) 0.0660(16) -0.0009(12) 0.0231(12) 0.0042(11)
C9 0.0415(12) 0.0484(14) 0.0612(15) 0.0026(12) 0.0226(11) 0.0073(11)
C10 0.0459(14) 0.0587(17) 0.091(2) -0.0078(15) 0.0236(14) 0.0053(12)
C11 0.0540(16) 0.074(2) 0.100(2) -0.0134(17) 0.0195(16) -0.0071(15)
C12 0.0406(14) 0.098(2) 0.090(2) 0.0033(19) 0.0182(14) 0.0023(16)
C13 0.0476(15) 0.091(2) 0.092(2) 0.0017(19) 0.0277(15) 0.0200(16)
C14 0.0498(15) 0.0667(18) 0.0746(17) -0.0027(14) 0.0248(13) 0.0132(13)
C15 0.0634(16) 0.086(2) 0.0546(15) -0.0031(14) 0.0266(13) 0.0019(15)
C16 0.088(2) 0.101(2) 0.083(2) -0.0060(19) 0.0503(18) -0.0137(19)
C17 0.103(3) 0.097(5) 0.103(4) -0.013(4) 0.060(3) -0.012(4)
C18 0.097(3) 0.142(5) 0.114(4) -0.033(4) 0.060(3) -0.029(4)
C19 0.216(9) 0.269(12) 0.139(6) -0.092(7) 0.139(6) -0.115(8)
C20 0.183(11) 0.52(2) 0.210(9) -0.166(14) 0.149(10) -0.137(14)
C17' 0.103(3) 0.097(5) 0.103(4) -0.013(4) 0.060(3) -0.012(4)
C18' 0.097(3) 0.142(5) 0.114(4) -0.033(4) 0.060(3) -0.029(4)
C19' 0.216(9) 0.269(12) 0.139(6) -0.092(7) 0.139(6) -0.115(8)
C20' 0.183(11) 0.52(2) 0.210(9) -0.166(14) 0.149(10) -0.137(14)

_geom_special_details
;
 All esds (except the esd in the dihedral angle between two l.s. planes)
 are estimated using the full covariance matrix.  The cell esds are taken
```

```
 into account individually in the estimation of esds in distances, angles
 and torsion angles; correlations between esds in cell parameters are only
 used when they are defined by crystal symmetry.  An approximate (isotropic)
 treatment of cell esds is used for estimating esds involving l.s. planes.
;

loop_
 _geom_bond_atom_site_label_1
 _geom_bond_atom_site_label_2
 _geom_bond_distance
 _geom_bond_site_symmetry_2
 _geom_bond_publ_flag
N1 C4 1.387(3) . ?
N1 C3 1.393(3) . ?
N1 C15 1.481(3) . ?
O1 C3 1.216(3) . ?
O2 C4 1.218(3) . ?
O3 C8 1.214(3) . ?
C1 C5 1.406(3) . ?
C1 C2 1.413(3) . ?
C1 C1 1.415(4) 7_565 ?
C2 C7 1.378(3) . ?
C2 C3 1.482(3) . ?
C4 C5 1.481(4) . ?
C5 C6 1.374(3) . ?
C6 C7 1.405(3) 7_565 ?
C6 H6A 0.9500 . ?
C7 C6 1.405(3) 7_565 ?
C7 C8 1.517(3) . ?
C8 C9 1.481(3) . ?
C9 C10 1.378(4) . ?
C9 C14 1.386(3) . ?
C10 C11 1.388(4) . ?
C10 H10A 0.9500 . ?
C11 C12 1.373(4) . ?
C11 H11A 0.9500 . ?
C12 C13 1.359(4) . ?
C12 H12A 0.9500 . ?
C13 C14 1.379(4) . ?
C13 H13A 0.9500 . ?
C14 H14A 0.9500 . ?
C15 C16 1.498(4) . ?
C15 H15A 0.9900 . ?
C15 H15B 0.9900 . ?
C16 C17 1.516(7) . ?
C16 C17' 1.72(2) . ?
C16 H16A 0.9900 . ?
C16 H16B 0.9900 . ?
C17 C18 1.477(7) . ?
C17 H17A 0.9900 . ?
C17 H17B 0.9900 . ?
C18 C19 1.574(8) . ?
C18 H18A 0.9900 . ?
C18 H18B 0.9900 . ?
C19 C20 1.486(14) . ?
C19 H19A 0.9900 . ?
C19 H19B 0.9900 . ?
C20 H20A 0.9800 . ?
C20 H20B 0.9800 . ?
C20 H20C 0.9800 . ?
C17' C18' 1.468(15) . ?
C17' H17C 0.9900 . ?
C17' H17D 0.9900 . ?
C18' C19' 1.554(14) . ?
C18' H18C 0.9900 . ?
```

```
C18' H18D 0.9900 . ?
C19' C20' 1.49(2) . ?
C19' H19C 0.9900 . ?
C19' H19D 0.9900 . ?
C20' H20D 0.9800 . ?
C20' H20E 0.9800 . ?
C20' H20F 0.9800 . ?

loop_
 _geom_angle_atom_site_label_1
 _geom_angle_atom_site_label_2
 _geom_angle_atom_site_label_3
 _geom_angle
 _geom_angle_site_symmetry_1
 _geom_angle_site_symmetry_3
 _geom_angle_publ_flag
C4 N1 C3 124.1(2) . . ?
C4 N1 C15 117.7(2) . . ?
C3 N1 C15 117.8(2) . . ?
C5 C1 C2 121.1(2) . . ?
C5 C1 C1 119.0(3) . 7_565 ?
C2 C1 C1 119.9(3) . 7_565 ?
C7 C2 C1 120.3(2) . . ?
C7 C2 C3 120.5(2) . . ?
C1 C2 C3 119.2(2) . . ?
O1 C3 N1 120.7(2) . . ?
O1 C3 C2 121.6(2) . . ?
N1 C3 C2 117.6(2) . . ?
O2 C4 N1 120.7(2) . . ?
O2 C4 C5 121.8(2) . . ?
N1 C4 C5 117.5(2) . . ?
C6 C5 C1 119.9(2) . . ?
C6 C5 C4 120.4(2) . . ?
C1 C5 C4 119.7(2) . . ?
C5 C6 C7 121.8(2) . 7_565 ?
C5 C6 H6A 119.1 . . ?
C7 C6 H6A 119.1 7_565 . ?
C2 C7 C6 119.1(2) . 7_565 ?
C2 C7 C8 124.3(2) . . ?
C6 C7 C8 116.5(2) 7_565 . ?
O3 C8 C9 122.5(2) . . ?
O3 C8 C7 118.7(2) . . ?
C9 C8 C7 118.4(2) . . ?
C10 C9 C14 118.7(2) . . ?
C10 C9 C8 122.4(2) . . ?
C14 C9 C8 118.9(2) . . ?
C9 C10 C11 120.5(2) . . ?
C9 C10 H10A 119.8 . . ?
C11 C10 H10A 119.8 . . ?
C12 C11 C10 119.9(3) . . ?
C12 C11 H11A 120.1 . . ?
C10 C11 H11A 120.1 . . ?
C13 C12 C11 120.0(3) . . ?
C13 C12 H12A 120.0 . . ?
C11 C12 H12A 120.0 . . ?
C12 C13 C14 120.6(3) . . ?
C12 C13 H13A 119.7 . . ?
C14 C13 H13A 119.7 . . ?
C13 C14 C9 120.3(3) . . ?
C13 C14 H14A 119.8 . . ?
C9 C14 H14A 119.8 . . ?
N1 C15 C16 112.7(2) . . ?
N1 C15 H15A 109.0 . . ?
C16 C15 H15A 109.0 . . ?
N1 C15 H15B 109.0 . . ?
```

```
C16 C15 H15B 109.0 . . ?
H15A C15 H15B 107.8 . . ?
C15 C16 C17 115.8(3) . . ?
C15 C16 C17' 97.2(5) . . ?
C17 C16 C17' 22.5(6) . . ?
C15 C16 H16A 108.3 . . ?
C17 C16 H16A 108.3 . . ?
C17' C16 H16A 128.9 . . ?
C15 C16 H16B 108.3 . . ?
C17 C16 H16B 108.3 . . ?
C17' C16 H16B 105.1 . . ?
H16A C16 H16B 107.4 . . ?
C18 C17 C16 111.2(5) . . ?
C18 C17 H17A 109.4 . . ?
C16 C17 H17A 109.4 . . ?
C18 C17 H17B 109.4 . . ?
C16 C17 H17B 109.4 . . ?
H17A C17 H17B 108.0 . . ?
C17 C18 C19 107.6(6) . . ?
C17 C18 H18A 110.2 . . ?
C19 C18 H18A 110.2 . . ?
C17 C18 H18B 110.2 . . ?
C19 C18 H18B 110.2 . . ?
H18A C18 H18B 108.5 . . ?
C20 C19 C18 105.4(9) . . ?
C20 C19 H19A 110.7 . . ?
C18 C19 H19A 110.7 . . ?
C20 C19 H19B 110.7 . . ?
C18 C19 H19B 110.7 . . ?
H19A C19 H19B 108.8 . . ?
C19 C20 H20A 109.5 . . ?
C19 C20 H20B 109.5 . . ?
H20A C20 H20B 109.5 . . ?
C19 C20 H20C 109.5 . . ?
H20A C20 H20C 109.5 . . ?
H20B C20 H20C 109.5 . . ?
C18' C17' C16 105.7(12) . . ?
C18' C17' H17C 110.6 . . ?
C16 C17' H17C 110.6 . . ?
C18' C17' H17D 110.6 . . ?
C16 C17' H17D 110.6 . . ?
H17C C17' H17D 108.7 . . ?
C17' C18' C19' 129.2(14) . . ?
C17' C18' H18C 105.0 . . ?
C19' C18' H18C 105.0 . . ?
C17' C18' H18D 105.0 . . ?
C19' C18' H18D 105.0 . . ?
H18C C18' H18D 105.8 . . ?
C20' C19' C18' 94.7(17) . . ?
C20' C19' H19C 112.8 . . ?
C18' C19' H19C 112.8 . . ?
C20' C19' H19D 112.8 . . ?
C18' C19' H19D 112.8 . . ?
H19C C19' H19D 110.2 . . ?
C19' C20' H20D 109.5 . . ?
C19' C20' H20E 109.5 . . ?
H20D C20' H20E 109.5 . . ?
C19' C20' H20F 109.5 . . ?
H20D C20' H20F 109.5 . . ?
H20E C20' H20F 109.5 . . ?

_diffrn_measured_fraction_theta_max    1.000
_diffrn_reflns_theta_full              25.00
_diffrn_measured_fraction_theta_full   1.000
_refine_diff_density_max    0.233
```

```
_refine_diff_density_min   -0.167
_refine_diff_density_rms    0.034
```

B.4.2 Compound 5.6

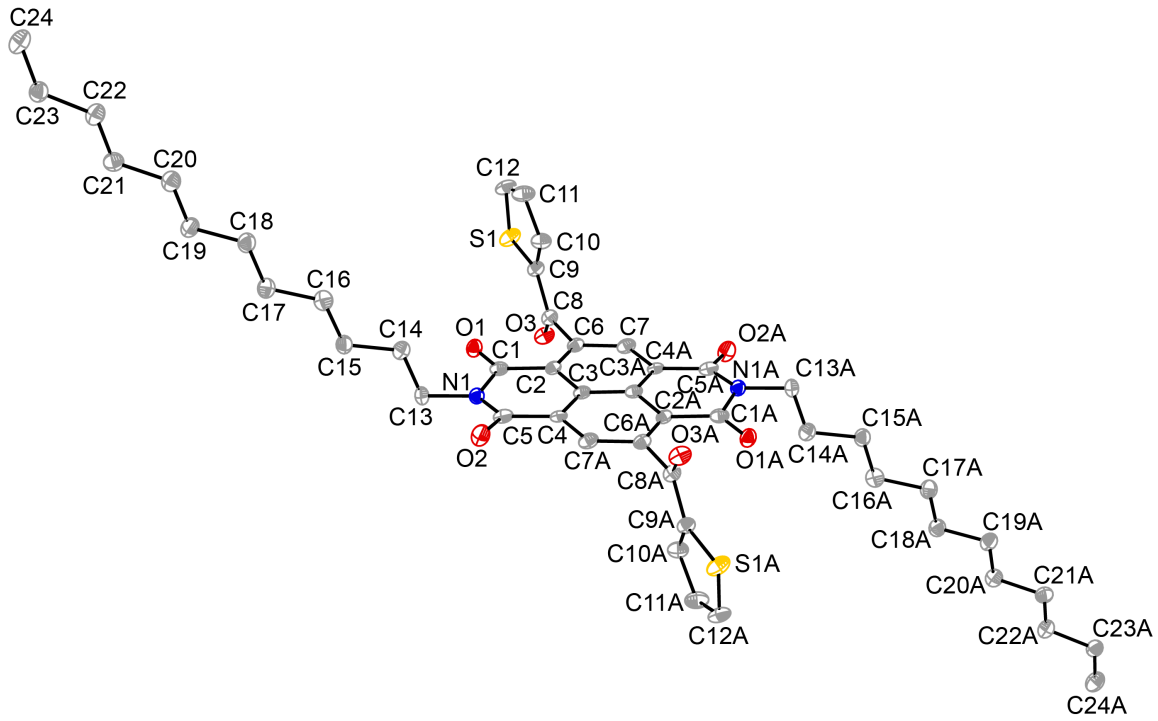

Figure B.5. The structure of compound **5.6**. Ellipsoids are shown at the 50% level. Hydrogen atoms are omitted for clarity.

*Crystal Identification File for **5.6***

```
data_a

_audit_creation_method            SHELXL-97
_chemical_name_systematic
;
 ?
;
_chemical_name_common             ?
_chemical_melting_point           ?
_chemical_formula_moiety
 'C48 H58 N2 O6 S2'
_chemical_formula_sum
 'C48 H58 N2 O6 S2'
_chemical_formula_weight          823.08

loop_
 _atom_type_symbol
 _atom_type_description
 _atom_type_scat_dispersion_real
 _atom_type_scat_dispersion_imag
 _atom_type_scat_source
 'C'  'C'   0.0033   0.0016
 'International Tables Vol C Tables 4.2.6.8 and 6.1.1.4'
 'H'  'H'   0.0000   0.0000
 'International Tables Vol C Tables 4.2.6.8 and 6.1.1.4'
 'N'  'N'   0.0061   0.0033
 'International Tables Vol C Tables 4.2.6.8 and 6.1.1.4'
 'O'  'O'   0.0106   0.0060
 'International Tables Vol C Tables 4.2.6.8 and 6.1.1.4'
 'S'  'S'   0.1246   0.1234
 'International Tables Vol C Tables 4.2.6.8 and 6.1.1.4'

_symmetry_cell_setting            Triclinic
_symmetry_space_group_name_H-M    'P - 1'
_symmetry_space_group_name_Hall   '-P 1'

loop_
 _symmetry_equiv_pos_as_xyz
 'x, y, z'
 '-x, -y, -z'

_cell_length_a                    5.714(3)
_cell_length_b                    9.811(4)
_cell_length_c                    19.638(9)
_cell_angle_alpha                 100.270(8)
_cell_angle_beta                  97.424(9)
_cell_angle_gamma                 94.807(9)
_cell_volume                      1067.8(8)
_cell_formula_units_Z             1
_cell_measurement_temperature     100(2)
_cell_measurement_reflns_used     869
_cell_measurement_theta_min       2.55
_cell_measurement_theta_max       27.70

_exptl_crystal_description        'needle'
_exptl_crystal_colour             'colorless'
_exptl_crystal_size_max           0.59
_exptl_crystal_size_mid           0.05
_exptl_crystal_size_min           0.05
_exptl_crystal_density_meas       'not measured'
_exptl_crystal_density_diffrn     1.280
_exptl_crystal_density_method     'not measured'
```

```
_exptl_crystal_F_000              440
_exptl_absorpt_coefficient_mu     0.177
_exptl_absorpt_correction_type    'multi-scan'
_exptl_absorpt_correction_T_min   0.8999
_exptl_absorpt_correction_T_max   0.9912
_exptl_absorpt_process_details    'SADABS (Sheldrick, 2003)'

_exptl_special_details
;
 ?
;

_diffrn_ambient_temperature       100(2)
_diffrn_radiation_wavelength      0.71073
_diffrn_radiation_type            MoK\a
_diffrn_radiation_source          'fine-focus sealed tube'
_diffrn_radiation_monochromator   graphite
_diffrn_measurement_device_type   'Bruker SMART APEX II CCD area detector'
_diffrn_measurement_method        'phi and omega scans'
_diffrn_detector_area_resol_mean  ?
_diffrn_standards_number          ?
_diffrn_standards_interval_count  ?
_diffrn_standards_interval_time   ?
_diffrn_standards_decay_%         ?
_diffrn_reflns_number             13255
_diffrn_reflns_av_R_equivalents   0.0756
_diffrn_reflns_av_sigmaI/netI     0.0807
_diffrn_reflns_limit_h_min        -7
_diffrn_reflns_limit_h_max        7
_diffrn_reflns_limit_k_min        -12
_diffrn_reflns_limit_k_max        12
_diffrn_reflns_limit_l_min        -24
_diffrn_reflns_limit_l_max        24
_diffrn_reflns_theta_min          2.12
_diffrn_reflns_theta_max          26.00
_reflns_number_total              4164
_reflns_number_gt                 2821
_reflns_threshold_expression      >2sigma(I)

_computing_data_collection        'APEX2  (Bruker, 2005)'
_computing_cell_refinement        'SAINT+ ver. 6.2 (Bruker, 2001)'
_computing_data_reduction         'SAINT+ ver. 6.2 (Bruker, 2001)'
_computing_structure_solution     'SHELXTL ver. 6.12 (Sheldrick, 2001)'
_computing_structure_refinement   'SHELXTL ver. 6.12 (Sheldrick, 2001)'
_computing_molecular_graphics     'SHELXTL ver. 6.12 (Sheldrick, 2001)'
_computing_publication_material   'SHELXTL ver. 6.12 (Sheldrick, 2001)'

_refine_special_details
;
 Refinement of F^2^ against ALL reflections.  The weighted R-factor wR and
 goodness of fit S are based on F^2^, conventional R-factors R are based
 on F, with F set to zero for negative F^2^. The threshold expression of
 F^2^ > 2sigma(F^2^) is used only for calculating R-factors(gt) etc. and is
 not relevant to the choice of reflections for refinement.  R-factors based
 on F^2^ are statistically about twice as large as those based on F, and R-
 factors based on ALL data will be even larger.
;

_refine_ls_structure_factor_coef  Fsqd
_refine_ls_matrix_type            full
_refine_ls_weighting_scheme       calc
_refine_ls_weighting_details
 'calc w=1/[\s^2^(Fo^2^)+(0.0500P)^2^+3.5000P] where P=(Fo^2^+2Fc^2^)/3'
_atom_sites_solution_primary      direct
_atom_sites_solution_secondary    difmap
```

```
_atom_sites_solution_hydrogens    geom
_refine_ls_hydrogen_treatment     constr
_refine_ls_extinction_method      none
_refine_ls_extinction_coef        ?
_refine_ls_number_reflns          4164
_refine_ls_number_parameters      262
_refine_ls_number_restraints      0
_refine_ls_R_factor_all           0.1155
_refine_ls_R_factor_gt            0.0760
_refine_ls_wR_factor_ref          0.1894
_refine_ls_wR_factor_gt           0.1744
_refine_ls_goodness_of_fit_ref    1.057
_refine_ls_restrained_S_all       1.057
_refine_ls_shift/su_max           0.000
_refine_ls_shift/su_mean          0.000

loop_
 _atom_site_label
 _atom_site_type_symbol
 _atom_site_fract_x
 _atom_site_fract_y
 _atom_site_fract_z
 _atom_site_U_iso_or_equiv
 _atom_site_adp_type
 _atom_site_occupancy
 _atom_site_symmetry_multiplicity
 _atom_site_calc_flag
 _atom_site_refinement_flags
 _atom_site_disorder_assembly
 _atom_site_disorder_group
S1 S 1.06142(19) 0.04177(12) 0.13735(6) 0.0254(3) Uani 1 1 d . . .
O1 O 0.7941(5) 0.4089(3) 0.19085(15) 0.0216(7) Uani 1 1 d . . .
O3 O 1.1880(5) 0.3131(3) 0.09625(16) 0.0237(7) Uani 1 1 d . . .
C6 C 0.8080(7) 0.3565(4) 0.0455(2) 0.0171(9) Uani 1 1 d . . .
N1 N 0.5207(6) 0.5625(3) 0.18356(17) 0.0178(7) Uani 1 1 d . . .
C3 C 0.5037(7) 0.5115(4) 0.0363(2) 0.0157(8) Uani 1 1 d . . .
C4 C 0.3458(7) 0.5974(4) 0.0684(2) 0.0160(8) Uani 1 1 d . . .
O2 O 0.2056(5) 0.6872(3) 0.17295(16) 0.0266(7) Uani 1 1 d . . .
C2 C 0.6595(7) 0.4426(4) 0.0771(2) 0.0153(8) Uani 1 1 d . . .
C7 C 0.8079(7) 0.3383(4) -0.0275(2) 0.0200(9) Uani 1 1 d . . .
H7A H 0.9150 0.2811 -0.0487 0.024 Uiso 1 1 calc R . .
C5 C 0.3465(7) 0.6186(4) 0.1444(2) 0.0194(9) Uani 1 1 d . . .
C1 C 0.6670(7) 0.4667(4) 0.1541(2) 0.0181(9) Uani 1 1 d . . .
C8 C 0.9744(7) 0.2738(4) 0.0837(2) 0.0180(9) Uani 1 1 d . . .
C9 C 0.8738(7) 0.1428(4) 0.0982(2) 0.0190(9) Uani 1 1 d . . .
C13 C 0.5269(7) 0.5835(4) 0.2597(2) 0.0200(9) Uani 1 1 d . . .
H13A H 0.4849 0.6780 0.2772 0.024 Uiso 1 1 calc R . .
H13B H 0.6899 0.5768 0.2822 0.024 Uiso 1 1 calc R . .
C15 C 0.3782(8) 0.4803(5) 0.3581(2) 0.0226(9) Uani 1 1 d . . .
H15A H 0.3643 0.5763 0.3822 0.027 Uiso 1 1 calc R . .
H15B H 0.5370 0.4557 0.3750 0.027 Uiso 1 1 calc R . .
C10 C 0.6449(7) 0.0811(4) 0.0845(2) 0.0213(9) Uani 1 1 d . . .
H10A H 0.5158 0.1209 0.0630 0.026 Uiso 1 1 calc R . .
C14 C 0.3548(8) 0.4755(5) 0.2796(2) 0.0222(9) Uani 1 1 d . . .
H14A H 0.1905 0.4909 0.2622 0.027 Uiso 1 1 calc R . .
H14B H 0.3828 0.3816 0.2561 0.027 Uiso 1 1 calc R . .
C22 C -0.3982(8) 0.0240(5) 0.6328(2) 0.0258(10) Uani 1 1 d . . .
H22A H -0.5428 0.0703 0.6229 0.031 Uiso 1 1 calc R . .
H22B H -0.4104 -0.0625 0.5972 0.031 Uiso 1 1 calc R . .
C16 C 0.1884(8) 0.3803(5) 0.3758(2) 0.0241(10) Uani 1 1 d . . .
H16A H 0.1924 0.2869 0.3471 0.029 Uiso 1 1 calc R . .
H16B H 0.0313 0.4111 0.3623 0.029 Uiso 1 1 calc R . .
C21 C -0.1830(8) 0.1196(5) 0.6255(2) 0.0240(10) Uani 1 1 d . . .
H21A H -0.0374 0.0761 0.6382 0.029 Uiso 1 1 calc R . .
H21B H -0.1765 0.2088 0.6588 0.029 Uiso 1 1 calc R . .
```

```
C17 C 0.2114(8) 0.3671(5) 0.4528(2) 0.0243(10) Uani 1 1 d . . .
H17A H 0.3655 0.3330 0.4665 0.029 Uiso 1 1 calc R . .
H17B H 0.2097 0.4601 0.4821 0.029 Uiso 1 1 calc R . .
C18 C 0.0107(8) 0.2674(5) 0.4666(2) 0.0248(10) Uani 1 1 d . . .
H18A H -0.1423 0.3026 0.4528 0.030 Uiso 1 1 calc R . .
H18B H 0.0117 0.1754 0.4362 0.030 Uiso 1 1 calc R . .
C12 C 0.8332(8) -0.0832(4) 0.1351(2) 0.0245(10) Uani 1 1 d . . .
H12A H 0.8508 -0.1671 0.1522 0.029 Uiso 1 1 calc R . .
C23 C -0.3912(8) -0.0145(5) 0.7044(2) 0.0247(10) Uani 1 1 d . . .
H23A H -0.3827 0.0717 0.7400 0.030 Uiso 1 1 calc R . .
H23B H -0.2452 -0.0593 0.7149 0.030 Uiso 1 1 calc R . .
C20 C -0.1862(8) 0.1496(5) 0.5518(2) 0.0246(10) Uani 1 1 d . . .
H20A H -0.1908 0.0600 0.5189 0.030 Uiso 1 1 calc R . .
H20B H -0.3346 0.1904 0.5390 0.030 Uiso 1 1 calc R . .
C19 C 0.0222(8) 0.2471(5) 0.5414(2) 0.0247(10) Uani 1 1 d . . .
H19A H 0.0240 0.3387 0.5723 0.030 Uiso 1 1 calc R . .
H19B H 0.1720 0.2086 0.5551 0.030 Uiso 1 1 calc R . .
C11 C 0.6223(8) -0.0483(4) 0.1059(2) 0.0268(10) Uani 1 1 d . . .
H11A H 0.4757 -0.1053 0.1006 0.032 Uiso 1 1 calc R . .
C24 C -0.6054(8) -0.1126(5) 0.7105(3) 0.0313(11) Uani 1 1 d . . .
H24A H -0.5908 -0.1331 0.7578 0.047 Uiso 1 1 calc R . .
H24B H -0.6127 -0.1994 0.6763 0.047 Uiso 1 1 calc R . .
H24C H -0.7507 -0.0683 0.7012 0.047 Uiso 1 1 calc R . .

loop_
 _atom_site_aniso_label
 _atom_site_aniso_U_11
 _atom_site_aniso_U_22
 _atom_site_aniso_U_33
 _atom_site_aniso_U_23
 _atom_site_aniso_U_13
 _atom_site_aniso_U_12
S1 0.0171(5) 0.0283(6) 0.0368(7) 0.0182(5) 0.0056(5) 0.0086(4)
O1 0.0233(16) 0.0244(16) 0.0188(15) 0.0071(13) 0.0019(12) 0.0081(13)
O3 0.0161(16) 0.0251(16) 0.0326(18) 0.0107(13) 0.0060(13) 0.0033(12)
C6 0.013(2) 0.017(2) 0.022(2) 0.0070(17) 0.0009(17) -0.0013(16)
N1 0.0194(18) 0.0183(17) 0.0165(17) 0.0037(14) 0.0044(14) 0.0032(14)
C3 0.0130(19) 0.0132(19) 0.022(2) 0.0056(16) 0.0050(16) 0.0011(15)
C4 0.018(2) 0.0097(18) 0.021(2) 0.0057(16) 0.0037(17) 0.0024(16)
O2 0.0292(17) 0.0311(17) 0.0251(17) 0.0097(14) 0.0103(14) 0.0157(14)
C2 0.0132(19) 0.0149(19) 0.019(2) 0.0063(16) 0.0027(16) 0.0001(16)
C7 0.018(2) 0.017(2) 0.028(2) 0.0088(18) 0.0066(18) 0.0068(17)
C5 0.018(2) 0.015(2) 0.029(2) 0.0078(18) 0.0078(18) 0.0031(17)
C1 0.015(2) 0.0148(19) 0.026(2) 0.0053(17) 0.0058(17) 0.0014(16)
C8 0.016(2) 0.020(2) 0.021(2) 0.0065(17) 0.0077(17) 0.0067(17)
C9 0.019(2) 0.018(2) 0.023(2) 0.0067(17) 0.0079(18) 0.0072(17)
C13 0.022(2) 0.024(2) 0.014(2) 0.0025(17) 0.0017(17) 0.0034(18)
C15 0.025(2) 0.024(2) 0.019(2) 0.0043(18) 0.0047(18) 0.0053(18)
C10 0.016(2) 0.018(2) 0.031(2) 0.0056(18) 0.0047(18) 0.0054(17)
C14 0.022(2) 0.024(2) 0.022(2) 0.0067(18) 0.0048(18) 0.0035(18)
C22 0.026(2) 0.030(2) 0.024(2) 0.0097(19) 0.0055(19) 0.006(2)
C16 0.019(2) 0.028(2) 0.026(2) 0.0045(19) 0.0060(18) 0.0038(18)
C21 0.024(2) 0.022(2) 0.027(2) 0.0062(19) 0.0035(19) 0.0055(18)
C17 0.023(2) 0.028(2) 0.022(2) 0.0052(19) 0.0056(18) 0.0033(19)
C18 0.029(2) 0.025(2) 0.022(2) 0.0052(18) 0.0079(19) 0.0067(19)
C12 0.025(2) 0.018(2) 0.037(3) 0.0124(19) 0.014(2) 0.0076(18)
C23 0.027(2) 0.025(2) 0.024(2) 0.0067(19) 0.0070(19) 0.0066(19)
C20 0.024(2) 0.027(2) 0.025(2) 0.0060(19) 0.0068(19) 0.0066(19)
C19 0.027(2) 0.026(2) 0.024(2) 0.0087(19) 0.0075(19) 0.0059(19)
C11 0.019(2) 0.021(2) 0.041(3) 0.008(2) 0.006(2) -0.0013(18)
C24 0.030(3) 0.037(3) 0.032(3) 0.015(2) 0.011(2) 0.005(2)

_geom_special_details
;
 All esds (except the esd in the dihedral angle between two l.s. planes)
```

```
 are estimated using the full covariance matrix.  The cell esds are taken
 into account individually in the estimation of esds in distances, angles
 and torsion angles; correlations between esds in cell parameters are only
 used when they are defined by crystal symmetry.  An approximate (isotropic)
 treatment of cell esds is used for estimating esds involving l.s. planes.
;

loop_
 _geom_bond_atom_site_label_1
 _geom_bond_atom_site_label_2
 _geom_bond_distance
 _geom_bond_site_symmetry_2
 _geom_bond_publ_flag
S1 C12 1.705(4) . ?
S1 C9 1.720(4) . ?
O1 C1 1.204(5) . ?
O3 C8 1.228(5) . ?
C6 C2 1.374(5) . ?
C6 C7 1.412(6) . ?
C6 C8 1.513(6) . ?
N1 C5 1.389(5) . ?
N1 C1 1.407(5) . ?
N1 C13 1.469(5) . ?
C3 C3 1.399(8) 2_665 ?
C3 C2 1.414(5) . ?
C3 C4 1.416(5) . ?
C4 C7 1.381(5) 2_665 ?
C4 C5 1.470(6) . ?
O2 C5 1.220(5) . ?
C2 C1 1.482(6) . ?
C7 C4 1.381(5) 2_665 ?
C7 H7A 0.9500 . ?
C8 C9 1.454(6) . ?
C9 C10 1.367(6) . ?
C13 C14 1.521(6) . ?
C13 H13A 0.9900 . ?
C13 H13B 0.9900 . ?
C15 C14 1.522(6) . ?
C15 C16 1.518(6) . ?
C15 H15A 0.9900 . ?
C15 H15B 0.9900 . ?
C10 C11 1.408(6) . ?
C10 H10A 0.9500 . ?
C14 H14A 0.9900 . ?
C14 H14B 0.9900 . ?
C22 C23 1.517(6) . ?
C22 C21 1.521(6) . ?
C22 H22A 0.9900 . ?
C22 H22B 0.9900 . ?
C16 C17 1.530(6) . ?
C16 H16A 0.9900 . ?
C16 H16B 0.9900 . ?
C21 C20 1.526(6) . ?
C21 H21A 0.9900 . ?
C21 H21B 0.9900 . ?
C17 C18 1.527(6) . ?
C17 H17A 0.9900 . ?
C17 H17B 0.9900 . ?
C18 C19 1.510(6) . ?
C18 H18A 0.9900 . ?
C18 H18B 0.9900 . ?
C12 C11 1.363(6) . ?
C12 H12A 0.9500 . ?
C23 C24 1.523(6) . ?
C23 H23A 0.9900 . ?
```

```
C23 H23B 0.9900 . ?
C20 C19 1.522(6) . ?
C20 H20A 0.9900 . ?
C20 H20B 0.9900 . ?
C19 H19A 0.9900 . ?
C19 H19B 0.9900 . ?
C11 H11A 0.9500 . ?
C24 H24A 0.9800 . ?
C24 H24B 0.9800 . ?
C24 H24C 0.9800 . ?

loop_
 _geom_angle_atom_site_label_1
 _geom_angle_atom_site_label_2
 _geom_angle_atom_site_label_3
 _geom_angle
 _geom_angle_site_symmetry_1
 _geom_angle_site_symmetry_3
 _geom_angle_publ_flag
C12 S1 C9 91.6(2) . . ?
C2 C6 C7 120.2(4) . . ?
C2 C6 C8 124.2(4) . . ?
C7 C6 C8 115.6(4) . . ?
C5 N1 C1 123.7(3) . . ?
C5 N1 C13 118.7(3) . . ?
C1 N1 C13 116.7(3) . . ?
C3 C3 C2 119.8(4) 2_665 . ?
C3 C3 C4 119.9(4) 2_665 . ?
C2 C3 C4 120.2(4) . . ?
C7 C4 C3 119.3(4) 2_665 . ?
C7 C4 C5 120.3(4) 2_665 . ?
C3 C4 C5 120.4(3) . . ?
C6 C2 C3 119.9(4) . . ?
C6 C2 C1 120.2(3) . . ?
C3 C2 C1 119.9(4) . . ?
C4 C7 C6 120.8(4) 2_665 . ?
C4 C7 H7A 119.6 2_665 . ?
C6 C7 H7A 119.6 . . ?
O2 C5 N1 120.6(4) . . ?
O2 C5 C4 121.7(4) . . ?
N1 C5 C4 117.6(3) . . ?
O1 C1 N1 120.4(4) . . ?
O1 C1 C2 122.3(4) . . ?
N1 C1 C2 117.3(3) . . ?
O3 C8 C9 122.8(4) . . ?
O3 C8 C6 119.7(4) . . ?
C9 C8 C6 117.3(3) . . ?
C10 C9 C8 130.2(4) . . ?
C10 C9 S1 111.4(3) . . ?
C8 C9 S1 118.4(3) . . ?
N1 C13 C14 111.1(3) . . ?
N1 C13 H13A 109.4 . . ?
C14 C13 H13A 109.4 . . ?
N1 C13 H13B 109.4 . . ?
C14 C13 H13B 109.4 . . ?
H13A C13 H13B 108.0 . . ?
C14 C15 C16 111.3(4) . . ?
C14 C15 H15A 109.4 . . ?
C16 C15 H15A 109.4 . . ?
C14 C15 H15B 109.4 . . ?
C16 C15 H15B 109.4 . . ?
H15A C15 H15B 108.0 . . ?
C9 C10 C11 112.3(4) . . ?
C9 C10 H10A 123.8 . . ?
C11 C10 H10A 123.8 . . ?
```

```
C15 C14 C13 113.2(4) . . ?
C15 C14 H14A 108.9 . . ?
C13 C14 H14A 108.9 . . ?
C15 C14 H14B 108.9 . . ?
C13 C14 H14B 108.9 . . ?
H14A C14 H14B 107.8 . . ?
C23 C22 C21 114.0(4) . . ?
C23 C22 H22A 108.7 . . ?
C21 C22 H22A 108.7 . . ?
C23 C22 H22B 108.7 . . ?
C21 C22 H22B 108.7 . . ?
H22A C22 H22B 107.6 . . ?
C15 C16 C17 115.2(4) . . ?
C15 C16 H16A 108.5 . . ?
C17 C16 H16A 108.5 . . ?
C15 C16 H16B 108.5 . . ?
C17 C16 H16B 108.5 . . ?
H16A C16 H16B 107.5 . . ?
C22 C21 C20 113.1(4) . . ?
C22 C21 H21A 109.0 . . ?
C20 C21 H21A 109.0 . . ?
C22 C21 H21B 109.0 . . ?
C20 C21 H21B 109.0 . . ?
H21A C21 H21B 107.8 . . ?
C18 C17 C16 112.0(4) . . ?
C18 C17 H17A 109.2 . . ?
C16 C17 H17A 109.2 . . ?
C18 C17 H17B 109.2 . . ?
C16 C17 H17B 109.2 . . ?
H17A C17 H17B 107.9 . . ?
C19 C18 C17 115.3(4) . . ?
C19 C18 H18A 108.5 . . ?
C17 C18 H18A 108.5 . . ?
C19 C18 H18B 108.5 . . ?
C17 C18 H18B 108.5 . . ?
H18A C18 H18B 107.5 . . ?
C11 C12 S1 111.8(3) . . ?
C11 C12 H12A 124.1 . . ?
S1 C12 H12A 124.1 . . ?
C22 C23 C24 113.4(4) . . ?
C22 C23 H23A 108.9 . . ?
C24 C23 H23A 108.9 . . ?
C22 C23 H23B 108.9 . . ?
C24 C23 H23B 108.9 . . ?
H23A C23 H23B 107.7 . . ?
C19 C20 C21 115.7(4) . . ?
C19 C20 H20A 108.3 . . ?
C21 C20 H20A 108.3 . . ?
C19 C20 H20B 108.3 . . ?
C21 C20 H20B 108.3 . . ?
H20A C20 H20B 107.4 . . ?
C18 C19 C20 112.5(4) . . ?
C18 C19 H19A 109.1 . . ?
C20 C19 H19A 109.1 . . ?
C18 C19 H19B 109.1 . . ?
C20 C19 H19B 109.1 . . ?
H19A C19 H19B 107.8 . . ?
C12 C11 C10 112.8(4) . . ?
C12 C11 H11A 123.6 . . ?
C10 C11 H11A 123.6 . . ?
C23 C24 H24A 109.5 . . ?
C23 C24 H24B 109.5 . . ?
H24A C24 H24B 109.5 . . ?
C23 C24 H24C 109.5 . . ?
H24A C24 H24C 109.5 . . ?
```

```
H24B C24 H24C 109.5 . . ?

loop_
 _geom_torsion_atom_site_label_1
 _geom_torsion_atom_site_label_2
 _geom_torsion_atom_site_label_3
 _geom_torsion_atom_site_label_4
 _geom_torsion
 _geom_torsion_site_symmetry_1
 _geom_torsion_site_symmetry_2
 _geom_torsion_site_symmetry_3
 _geom_torsion_site_symmetry_4
 _geom_torsion_publ_flag
C3 C3 C4 C7 -2.4(7) 2_665 . . 2_665 ?
C2 C3 C4 C7 -178.8(4) . . . 2_665 ?
C3 C3 C4 C5 177.9(4) 2_665 . . . ?
C2 C3 C4 C5 1.6(6) . . . . ?
C7 C6 C2 C3 0.9(6) . . . . ?
C8 C6 C2 C3 -177.6(4) . . . . ?
C7 C6 C2 C1 -177.3(4) . . . . ?
C8 C6 C2 C1 4.2(6) . . . . ?
C3 C3 C2 C6 1.9(7) 2_665 . . . ?
C4 C3 C2 C6 178.3(4) . . . . ?
C3 C3 C2 C1 -179.8(4) 2_665 . . . ?
C4 C3 C2 C1 -3.5(5) . . . . ?
C2 C6 C7 C4 -2.1(6) . . . 2_665 ?
C8 C6 C7 C4 176.5(4) . . . 2_665 ?
C1 N1 C5 O2 170.7(4) . . . . ?
C13 N1 C5 O2 2.0(6) . . . . ?
C1 N1 C5 C4 -11.9(6) . . . . ?
C13 N1 C5 C4 179.3(3) . . . . ?
C7 C4 C5 O2 3.5(6) 2_665 . . . ?
C3 C4 C5 O2 -176.8(4) . . . . ?
C7 C4 C5 N1 -173.8(4) 2_665 . . . ?
C3 C4 C5 N1 5.8(5) . . . . ?
C5 N1 C1 O1 -170.8(4) . . . . ?
C13 N1 C1 O1 -1.9(5) . . . . ?
C5 N1 C1 C2 10.0(5) . . . . ?
C13 N1 C1 C2 179.0(3) . . . . ?
C6 C2 C1 O1 -2.9(6) . . . . ?
C3 C2 C1 O1 178.9(4) . . . . ?
C6 C2 C1 N1 176.3(4) . . . . ?
C3 C2 C1 N1 -2.0(5) . . . . ?
C2 C6 C8 O3 -104.1(5) . . . . ?
C7 C6 C8 O3 77.4(5) . . . . ?
C2 C6 C8 C9 81.3(5) . . . . ?
C7 C6 C8 C9 -97.3(4) . . . . ?
O3 C8 C9 C10 -176.5(4) . . . . ?
C6 C8 C9 C10 -2.1(7) . . . . ?
O3 C8 C9 S1 2.1(6) . . . . ?
C6 C8 C9 S1 176.6(3) . . . . ?
C12 S1 C9 C10 0.1(3) . . . . ?
C12 S1 C9 C8 -178.7(3) . . . . ?
C5 N1 C13 C14 83.8(4) . . . . ?
C1 N1 C13 C14 -85.8(4) . . . . ?
C8 C9 C10 C11 178.7(4) . . . . ?
S1 C9 C10 C11 0.0(5) . . . . ?
C16 C15 C14 C13 174.7(4) . . . . ?
N1 C13 C14 C15 172.2(3) . . . . ?
C14 C15 C16 C17 174.4(4) . . . . ?
C23 C22 C21 C20 176.4(4) . . . . ?
C15 C16 C17 C18 178.6(4) . . . . ?
C16 C17 C18 C19 179.3(4) . . . . ?
C9 S1 C12 C11 -0.3(4) . . . . ?
C21 C22 C23 C24 -178.8(4) . . . . ?
```

```
C22 C21 C20 C19 178.8(4) . . . . ?
C17 C18 C19 C20 178.5(4) . . . . ?
C21 C20 C19 C18 177.9(4) . . . . ?
S1 C12 C11 C10 0.4(5) . . . . ?
C9 C10 C11 C12 -0.3(6) . . . . ?

_diffrn_measured_fraction_theta_max    0.996
_diffrn_reflns_theta_full              26.00
_diffrn_measured_fraction_theta_full   0.996
_refine_diff_density_max    0.388
_refine_diff_density_min   -0.310
_refine_diff_density_rms    0.076
```

B.4.3 Compound 5.7

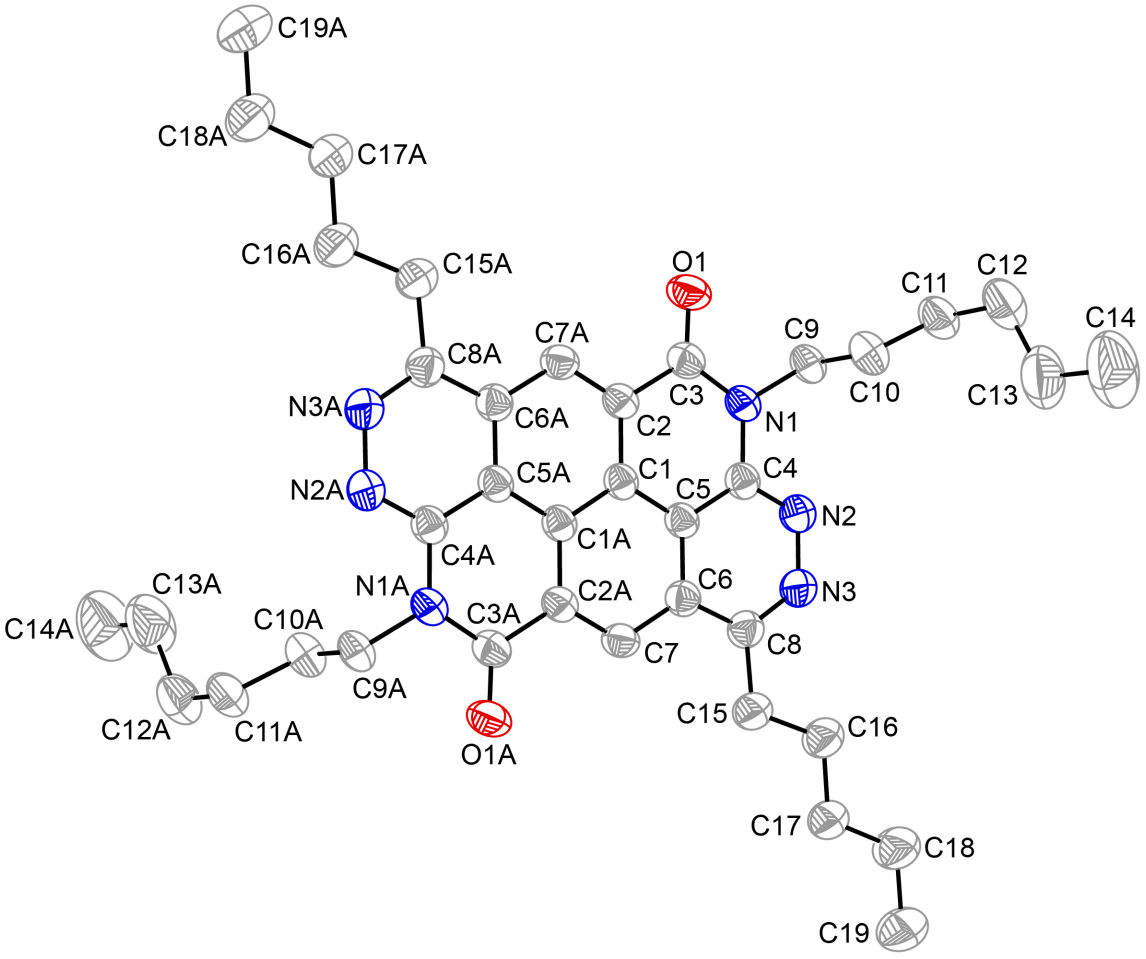

Figure B.6. The structure of compound **5.7**. Ellipsoids are shown at the 30% level. Hydrogen atoms are omitted for clarity.

*Crystal Identification File for Compound **5.7***

```
data_2

_audit_creation_method            SHELXL-97
_chemical_name_systematic
;
 ?
;
_chemical_name_common             ?
_chemical_melting_point           ?
_chemical_formula_moiety          ?
_chemical_formula_sum
 'C38 H50 N6 O2'
_chemical_formula_weight          622.84

loop_
 _atom_type_symbol
 _atom_type_description
 _atom_type_scat_dispersion_real
 _atom_type_scat_dispersion_imag
 _atom_type_scat_source
 'C'  'C'   0.0033   0.0016
 'International Tables Vol C Tables 4.2.6.8 and 6.1.1.4'
 'H'  'H'   0.0000   0.0000
 'International Tables Vol C Tables 4.2.6.8 and 6.1.1.4'
 'N'  'N'   0.0061   0.0033
 'International Tables Vol C Tables 4.2.6.8 and 6.1.1.4'
 'O'  'O'   0.0106   0.0060
 'International Tables Vol C Tables 4.2.6.8 and 6.1.1.4'

_symmetry_cell_setting            ?
_symmetry_space_group_name_H-M    ?

loop_
 _symmetry_equiv_pos_as_xyz
 'x, y, z'
 '-x, -y, -z'

_cell_length_a                    4.8953(10)
_cell_length_b                    12.709(3)
_cell_length_c                    14.175(3)
_cell_angle_alpha                 88.727(4)
_cell_angle_beta                  83.038(4)
_cell_angle_gamma                 79.127(4)
_cell_volume                      859.7(3)
_cell_formula_units_Z             1
_cell_measurement_temperature     100(2)
_cell_measurement_reflns_used     ?
_cell_measurement_theta_min       ?
_cell_measurement_theta_max       ?

_exptl_crystal_description        ?
_exptl_crystal_colour             ?
_exptl_crystal_size_max           ?
_exptl_crystal_size_mid           ?
_exptl_crystal_size_min           ?
_exptl_crystal_density_meas       ?
_exptl_crystal_density_diffrn     1.203
_exptl_crystal_density_method     'not measured'
_exptl_crystal_F_000              336
_exptl_absorpt_coefficient_mu     0.076
_exptl_absorpt_correction_type    ?
_exptl_absorpt_correction_T_min   ?
```

```
_exptl_absorpt_correction_T_max   ?
_exptl_absorpt_process_details    ?

_exptl_special_details
;
 ?
;

_diffrn_ambient_temperature       100(2)
_diffrn_radiation_wavelength      0.71073
_diffrn_radiation_type            MoK\a
_diffrn_radiation_source          'fine-focus sealed tube'
_diffrn_radiation_monochromator   graphite
_diffrn_measurement_device_type   ?
_diffrn_measurement_method        ?
_diffrn_detector_area_resol_mean  ?
_diffrn_standards_number          ?
_diffrn_standards_interval_count  ?
_diffrn_standards_interval_time   ?
_diffrn_standards_decay_%         ?
_diffrn_reflns_number             10272
_diffrn_reflns_av_R_equivalents   0.0264
_diffrn_reflns_av_sigmaI/netI     0.0237
_diffrn_reflns_limit_h_min        -5
_diffrn_reflns_limit_h_max        5
_diffrn_reflns_limit_k_min        -15
_diffrn_reflns_limit_k_max        15
_diffrn_reflns_limit_l_min        -16
_diffrn_reflns_limit_l_max        16
_diffrn_reflns_theta_min          2.18
_diffrn_reflns_theta_max          25.00
_reflns_number_total              3022
_reflns_number_gt                 2123
_reflns_threshold_expression      >2sigma(I)

_computing_data_collection        ?
_computing_cell_refinement        ?
_computing_data_reduction         ?
_computing_structure_solution     'SHELXS-97 (Sheldrick, 1990)'
_computing_structure_refinement   'SHELXL-97 (Sheldrick, 1997)'
_computing_molecular_graphics     ?
_computing_publication_material   ?

_refine_special_details
;
 Refinement of F^2^ against ALL reflections.  The weighted R-factor wR and
 goodness of fit S are based on F^2^, conventional R-factors R are based
 on F, with F set to zero for negative F^2^. The threshold expression of
 F^2^ > 2sigma(F^2^) is used only for calculating R-factors(gt) etc. and is
 not relevant to the choice of reflections for refinement.  R-factors based
 on F^2^ are statistically about twice as large as those based on F, and R-
 factors based on ALL data will be even larger.
;

_refine_ls_structure_factor_coef  Fsqd
_refine_ls_matrix_type            full
_refine_ls_weighting_scheme       calc
_refine_ls_weighting_details
 'calc w=1/[\s^2^(Fo^2^)+(0.0796P)^2^+0.3139P] where P=(Fo^2^+2Fc^2^)/3'
_atom_sites_solution_primary      direct
_atom_sites_solution_secondary    difmap
_atom_sites_solution_hydrogens    geom
_refine_ls_hydrogen_treatment     mixed
_refine_ls_extinction_method      none
_refine_ls_extinction_coef        ?
```

```
_refine_ls_number_reflns          3022
_refine_ls_number_parameters      215
_refine_ls_number_restraints      1
_refine_ls_R_factor_all           0.0703
_refine_ls_R_factor_gt            0.0485
_refine_ls_wR_factor_ref          0.1562
_refine_ls_wR_factor_gt           0.1340
_refine_ls_goodness_of_fit_ref    0.929
_refine_ls_restrained_S_all       0.929
_refine_ls_shift/su_max           0.000
_refine_ls_shift/su_mean          0.000

loop_
 _atom_site_label
 _atom_site_type_symbol
 _atom_site_fract_x
 _atom_site_fract_y
 _atom_site_fract_z
 _atom_site_U_iso_or_equiv
 _atom_site_adp_type
 _atom_site_occupancy
 _atom_site_symmetry_multiplicity
 _atom_site_calc_flag
 _atom_site_refinement_flags
 _atom_site_disorder_assembly
 _atom_site_disorder_group
N1 N 0.0868(3) 0.80268(11) 0.04226(11) 0.0448(4) Uani 1 1 d . . .
N2 N -0.1172(3) 0.88461(13) 0.18525(11) 0.0520(4) Uani 1 1 d . . .
N3 N -0.1452(4) 0.96395(13) 0.25136(11) 0.0540(4) Uani 1 1 d . . .
O1 O 0.2796(3) 0.72205(11) -0.09783(10) 0.0621(4) Uani 1 1 d . . .
C1 C 0.4187(4) 0.96033(13) 0.00762(12) 0.0396(4) Uani 1 1 d . . .
C2 C 0.4415(4) 0.87813(14) -0.06079(12) 0.0413(4) Uani 1 1 d . . .
C3 C 0.2668(4) 0.79445(15) -0.04197(14) 0.0464(5) Uani 1 1 d . . .
C4 C 0.0644(4) 0.88449(14) 0.10898(13) 0.0425(4) Uani 1 1 d . . .
C5 C 0.2332(4) 0.96336(14) 0.09141(12) 0.0403(4) Uani 1 1 d . . .
C6 C 0.2058(4) 1.04428(14) 0.15917(12) 0.0428(4) Uani 1 1 d . . .
C7 C 0.3748(4) 1.12445(14) 0.14194(13) 0.0442(5) Uani 1 1 d . . .
H7A H 0.3596 1.1800 0.1871 0.053 Uiso 1 1 calc R . .
C8 C 0.0070(4) 1.03951(15) 0.24060(13) 0.0480(5) Uani 1 1 d . . .
C9 C -0.0718(4) 0.71532(14) 0.06442(14) 0.0494(5) Uani 1 1 d . . .
H9A H -0.1104 0.6856 0.0045 0.059 Uiso 1 1 calc R . .
H9B H -0.2536 0.7444 0.1018 0.059 Uiso 1 1 calc R . .
C10 C 0.0899(5) 0.62685(16) 0.12022(16) 0.0576(5) Uani 1 1 d . . .
H10A H 0.1411 0.6580 0.1775 0.069 Uiso 1 1 calc R . .
H10B H 0.2655 0.5946 0.0808 0.069 Uiso 1 1 calc R . .
C11 C -0.0766(5) 0.53971(16) 0.15034(17) 0.0631(6) Uani 1 1 d . B .
H11A H -0.2514 0.5724 0.1899 0.076 Uiso 1 1 calc R . .
H11B H -0.1298 0.5097 0.0929 0.076 Uiso 1 1 calc R . .
C12 C 0.0786(6) 0.44946(19) 0.20537(19) 0.0782(7) Uani 1 1 d . . .
H12A H 0.2627 0.4219 0.1688 0.094 Uiso 1 1 calc R A 1
H12B H -0.0285 0.3904 0.2117 0.094 Uiso 1 1 calc R A 1
C13 C 0.1252(10) 0.4815(3) 0.3034(2) 0.1177(19) Uani 0.820(6) 1 d PD B 1
H13A H 0.2361 0.5394 0.2962 0.141 Uiso 0.820(6) 1 calc PR B 1
H13B H -0.0594 0.5119 0.3384 0.141 Uiso 0.820(6) 1 calc PR B 1
C14 C 0.2654(10) 0.3979(3) 0.3614(2) 0.135(2) Uani 0.820(6) 1 d PRD B 1
H14A H 0.2828 0.4277 0.4231 0.202 Uiso 0.820(6) 1 calc PR B 1
H14B H 0.4523 0.3687 0.3292 0.202 Uiso 0.820(6) 1 calc PR B 1
H14C H 0.1559 0.3406 0.3710 0.202 Uiso 0.820(6) 1 calc PR B 1
C13' C 0.177(7) 0.477(2) 0.275(2) 0.1177(19) Uani 0.180(6) 1 d PD B 2
H13C H 0.2165 0.5496 0.2609 0.141 Uiso 0.180(6) 1 calc PR B 2
H13D H 0.3614 0.4290 0.2766 0.141 Uiso 0.180(6) 1 calc PR B 2
C14' C 0.039(6) 0.4806(19) 0.3698(19) 0.135(2) Uani 0.180(6) 1 d PD B 2
H14E H -0.0393 0.5553 0.3877 0.202 Uiso 0.180(6) 1 calc PR B 2
H14F H 0.1735 0.4496 0.4134 0.202 Uiso 0.180(6) 1 calc PR B 2
H14G H -0.1125 0.4396 0.3734 0.202 Uiso 0.180(6) 1 calc PR B 2
```

```
C15 C -0.0400(5) 1.12242(17) 0.31815(14) 0.0596(6) Uani 1 1 d . . .
H15A H 0.1449 1.1289 0.3366 0.072 Uiso 1 1 calc R . .
H15B H -0.1214 1.1923 0.2914 0.072 Uiso 1 1 calc R . .
C16 C -0.2252(5) 1.10288(19) 0.40656(15) 0.0639(6) Uani 1 1 d . . .
H16A H -0.1558 1.0303 0.4308 0.077 Uiso 1 1 calc R . .
H16B H -0.4170 1.1047 0.3902 0.077 Uiso 1 1 calc R . .
C17 C -0.2381(5) 1.18331(18) 0.48423(15) 0.0637(6) Uani 1 1 d . . .
H17A H -0.0450 1.1822 0.4990 0.076 Uiso 1 1 calc R . .
H17B H -0.3088 1.2555 0.4596 0.076 Uiso 1 1 calc R . .
C18 C -0.4153(6) 1.1669(2) 0.57415(17) 0.0838(8) Uani 1 1 d . . .
H18A H -0.3486 1.0938 0.5978 0.101 Uiso 1 1 calc R . .
H18B H -0.6099 1.1705 0.5598 0.101 Uiso 1 1 calc R . .
C19 C -0.4195(8) 1.2451(3) 0.65194(19) 0.1036(10) Uani 1 1 d . . .
H19A H -0.5368 1.2266 0.7086 0.155 Uiso 1 1 calc R . .
H19B H -0.4961 1.3176 0.6310 0.155 Uiso 1 1 calc R . .
H19C H -0.2283 1.2425 0.6671 0.155 Uiso 1 1 calc R . .

loop_
 _atom_site_aniso_label
 _atom_site_aniso_U_11
 _atom_site_aniso_U_22
 _atom_site_aniso_U_33
 _atom_site_aniso_U_23
 _atom_site_aniso_U_13
 _atom_site_aniso_U_12
N1 0.0463(9) 0.0415(8) 0.0497(9) -0.0005(7) -0.0049(7) -0.0169(7)
N2 0.0554(10) 0.0533(10) 0.0498(9) -0.0009(7) 0.0004(8) -0.0212(8)
N3 0.0598(11) 0.0576(10) 0.0475(9) -0.0021(8) 0.0010(8) -0.0227(8)
O1 0.0684(10) 0.0555(9) 0.0668(9) -0.0182(7) 0.0046(7) -0.0287(7)
C1 0.0380(9) 0.0392(9) 0.0432(10) 0.0029(8) -0.0076(8) -0.0102(7)
C2 0.0414(10) 0.0389(10) 0.0453(10) 0.0000(8) -0.0081(8) -0.0101(8)
C3 0.0461(11) 0.0437(10) 0.0515(11) -0.0021(9) -0.0065(9) -0.0134(8)
C4 0.0413(10) 0.0424(10) 0.0457(10) 0.0030(8) -0.0081(8) -0.0106(8)
C5 0.0404(10) 0.0399(10) 0.0431(10) 0.0024(8) -0.0085(8) -0.0118(8)
C6 0.0434(10) 0.0433(10) 0.0430(10) 0.0012(8) -0.0070(8) -0.0104(8)
C7 0.0472(11) 0.0427(10) 0.0448(10) -0.0048(8) -0.0074(8) -0.0116(8)
C8 0.0476(11) 0.0521(11) 0.0452(10) 0.0000(8) -0.0037(8) -0.0132(9)
C9 0.0482(11) 0.0464(11) 0.0587(12) 0.0019(9) -0.0052(9) -0.0229(9)
C10 0.0567(12) 0.0482(11) 0.0708(14) 0.0050(10) -0.0078(10) -0.0178(9)
C11 0.0701(14) 0.0497(12) 0.0743(14) 0.0022(10) -0.0071(11) -0.0248(11)
C12 0.0906(19) 0.0558(14) 0.0934(19) 0.0130(13) -0.0158(15) -0.0253(13)
C13 0.179(5) 0.104(3) 0.095(5) 0.042(3) -0.058(4) -0.070(3)
C14 0.160(5) 0.122(4) 0.142(4) 0.060(3) -0.070(3) -0.048(3)
C13' 0.179(5) 0.104(3) 0.095(5) 0.042(3) -0.058(4) -0.070(3)
C14' 0.160(5) 0.122(4) 0.142(4) 0.060(3) -0.070(3) -0.048(3)
C15 0.0681(14) 0.0636(13) 0.0492(12) -0.0082(10) 0.0034(10) -0.0231(11)
C16 0.0678(14) 0.0730(14) 0.0523(12) -0.0067(10) 0.0027(10) -0.0224(12)
C17 0.0732(15) 0.0671(14) 0.0523(12) -0.0071(10) 0.0028(11) -0.0222(11)
C18 0.0928(19) 0.098(2) 0.0639(15) -0.0178(14) 0.0139(14) -0.0383(16)
C19 0.137(3) 0.106(2) 0.0669(17) -0.0272(16) 0.0221(17) -0.039(2)

_geom_special_details
;
 All esds (except the esd in the dihedral angle between two l.s. planes)
 are estimated using the full covariance matrix.  The cell esds are taken
 into account individually in the estimation of esds in distances, angles
 and torsion angles; correlations between esds in cell parameters are only
 used when they are defined by crystal symmetry.  An approximate (isotropic)
 treatment of cell esds is used for estimating esds involving l.s. planes.
;

loop_
 _geom_bond_atom_site_label_1
 _geom_bond_atom_site_label_2
 _geom_bond_distance
```

```
 _geom_bond_site_symmetry_2
 _geom_bond_publ_flag
N1 C3 1.389(2) . ?
N1 C4 1.401(2) . ?
N1 C9 1.478(2) . ?
N2 C4 1.314(2) . ?
N2 N3 1.368(2) . ?
N3 C8 1.318(2) . ?
O1 C3 1.215(2) . ?
C1 C1 1.396(3) 2_675 ?
C1 C5 1.401(2) . ?
C1 C2 1.421(2) . ?
C2 C7 1.368(3) 2_675 ?
C2 C3 1.486(2) . ?
C4 C5 1.415(2) . ?
C5 C6 1.400(2) . ?
C6 C8 1.425(3) . ?
C6 C7 1.428(3) . ?
C7 C2 1.368(3) 2_675 ?
C7 H7A 0.9500 . ?
C8 C15 1.507(3) . ?
C9 C10 1.514(3) . ?
C9 H9A 0.9900 . ?
C9 H9B 0.9900 . ?
C10 C11 1.519(3) . ?
C10 H10A 0.9900 . ?
C10 H10B 0.9900 . ?
C11 C12 1.509(3) . ?
C11 H11A 0.9900 . ?
C11 H11B 0.9900 . ?
C12 C13' 1.24(3) . ?
C12 C13 1.513(5) . ?
C12 H12A 0.9900 . ?
C12 H12B 0.9900 . ?
C13 C14 1.4486 . ?
C13 H13A 0.9900 . ?
C13 H13B 0.9900 . ?
C14 H14A 0.9800 . ?
C14 H14B 0.9800 . ?
C14 H14C 0.9800 . ?
C13' C14' 1.427(19) . ?
C13' H13C 0.9900 . ?
C13' H13D 0.9900 . ?
C14' H14E 0.9800 . ?
C14' H14F 0.9800 . ?
C14' H14G 0.9800 . ?
C15 C16 1.500(3) . ?
C15 H15A 0.9900 . ?
C15 H15B 0.9900 . ?
C16 C17 1.506(3) . ?
C16 H16A 0.9900 . ?
C16 H16B 0.9900 . ?
C17 C18 1.486(3) . ?
C17 H17A 0.9900 . ?
C17 H17B 0.9900 . ?
C18 C19 1.497(3) . ?
C18 H18A 0.9900 . ?
C18 H18B 0.9900 . ?
C19 H19A 0.9800 . ?
C19 H19B 0.9800 . ?
C19 H19C 0.9800 . ?

loop_
 _geom_angle_atom_site_label_1
 _geom_angle_atom_site_label_2
```

```
 _geom_angle_atom_site_label_3
 _geom_angle
 _geom_angle_site_symmetry_1
 _geom_angle_site_symmetry_3
 _geom_angle_publ_flag
C3 N1 C4 123.44(15) . . ?
C3 N1 C9 117.18(15) . . ?
C4 N1 C9 119.22(15) . . ?
C4 N2 N3 119.03(15) . . ?
C8 N3 N2 121.57(16) . . ?
C1 C1 C5 118.8(2) 2_675 . ?
C1 C1 C2 120.4(2) 2_675 . ?
C5 C1 C2 120.79(16) . . ?
C7 C2 C1 120.21(16) 2_675 . ?
C7 C2 C3 120.78(16) 2_675 . ?
C1 C2 C3 119.00(16) . . ?
O1 C3 N1 121.24(17) . . ?
O1 C3 C2 121.64(17) . . ?
N1 C3 C2 117.12(16) . . ?
N2 C4 N1 117.70(16) . . ?
N2 C4 C5 122.96(17) . . ?
N1 C4 C5 119.33(16) . . ?
C6 C5 C1 121.61(16) . . ?
C6 C5 C4 118.08(17) . . ?
C1 C5 C4 120.31(16) . . ?
C5 C6 C8 116.27(17) . . ?
C5 C6 C7 118.49(17) . . ?
C8 C6 C7 125.25(17) . . ?
C2 C7 C6 120.47(17) 2_675 . ?
C2 C7 H7A 119.8 2_675 . ?
C6 C7 H7A 119.8 . . ?
N3 C8 C6 122.09(17) . . ?
N3 C8 C15 117.03(17) . . ?
C6 C8 C15 120.88(17) . . ?
N1 C9 C10 111.21(15) . . ?
N1 C9 H9A 109.4 . . ?
C10 C9 H9A 109.4 . . ?
N1 C9 H9B 109.4 . . ?
C10 C9 H9B 109.4 . . ?
H9A C9 H9B 108.0 . . ?
C9 C10 C11 112.45(17) . . ?
C9 C10 H10A 109.1 . . ?
C11 C10 H10A 109.1 . . ?
C9 C10 H10B 109.1 . . ?
C11 C10 H10B 109.1 . . ?
H10A C10 H10B 107.8 . . ?
C12 C11 C10 114.06(19) . . ?
C12 C11 H11A 108.7 . . ?
C10 C11 H11A 108.7 . . ?
C12 C11 H11B 108.7 . . ?
C10 C11 H11B 108.7 . . ?
H11A C11 H11B 107.6 . . ?
C13' C12 C11 115.4(14) . . ?
C13' C12 C13 14.8(16) . . ?
C11 C12 C13 113.8(2) . . ?
C13' C12 H12A 95.0 . . ?
C11 C12 H12A 108.8 . . ?
C13 C12 H12A 108.8 . . ?
C13' C12 H12B 119.6 . . ?
C11 C12 H12B 108.8 . . ?
C13 C12 H12B 108.8 . . ?
H12A C12 H12B 107.7 . . ?
C14 C13 C12 116.71(18) . . ?
C14 C13 H13A 108.1 . . ?
C12 C13 H13A 108.1 . . ?
```

```
C14 C13 H13B 108.1 . . ?
C12 C13 H13B 108.1 . . ?
H13A C13 H13B 107.3 . . ?
C12 C13' C14' 124(3) . . ?
C12 C13' H13C 106.3 . . ?
C14' C13' H13C 106.3 . . ?
C12 C13' H13D 106.3 . . ?
C14' C13' H13D 106.3 . . ?
H13C C13' H13D 106.4 . . ?
C13' C14' H14E 109.5 . . ?
C13' C14' H14F 109.5 . . ?
H14E C14' H14F 109.5 . . ?
C13' C14' H14G 109.5 . . ?
H14E C14' H14G 109.5 . . ?
H14F C14' H14G 109.5 . . ?
C16 C15 C8 116.91(18) . . ?
C16 C15 H15A 108.1 . . ?
C8 C15 H15A 108.1 . . ?
C16 C15 H15B 108.1 . . ?
C8 C15 H15B 108.1 . . ?
H15A C15 H15B 107.3 . . ?
C15 C16 C17 113.56(19) . . ?
C15 C16 H16A 108.9 . . ?
C17 C16 H16A 108.9 . . ?
C15 C16 H16B 108.9 . . ?
C17 C16 H16B 108.9 . . ?
H16A C16 H16B 107.7 . . ?
C18 C17 C16 115.9(2) . . ?
C18 C17 H17A 108.3 . . ?
C16 C17 H17A 108.3 . . ?
C18 C17 H17B 108.3 . . ?
C16 C17 H17B 108.3 . . ?
H17A C17 H17B 107.4 . . ?
C17 C18 C19 115.5(2) . . ?
C17 C18 H18A 108.4 . . ?
C19 C18 H18A 108.4 . . ?
C17 C18 H18B 108.4 . . ?
C19 C18 H18B 108.4 . . ?
H18A C18 H18B 107.5 . . ?
C18 C19 H19A 109.5 . . ?
C18 C19 H19B 109.5 . . ?
H19A C19 H19B 109.5 . . ?
C18 C19 H19C 109.5 . . ?
H19A C19 H19C 109.5 . . ?
H19B C19 H19C 109.5 . . ?

_diffrn_measured_fraction_theta_max    0.999
_diffrn_reflns_theta_full              25.00
_diffrn_measured_fraction_theta_full   0.999
_refine_diff_density_max    0.176
_refine_diff_density_min   -0.142
_refine_diff_density_rms    0.031
```

B.4.4 Compound 5.8

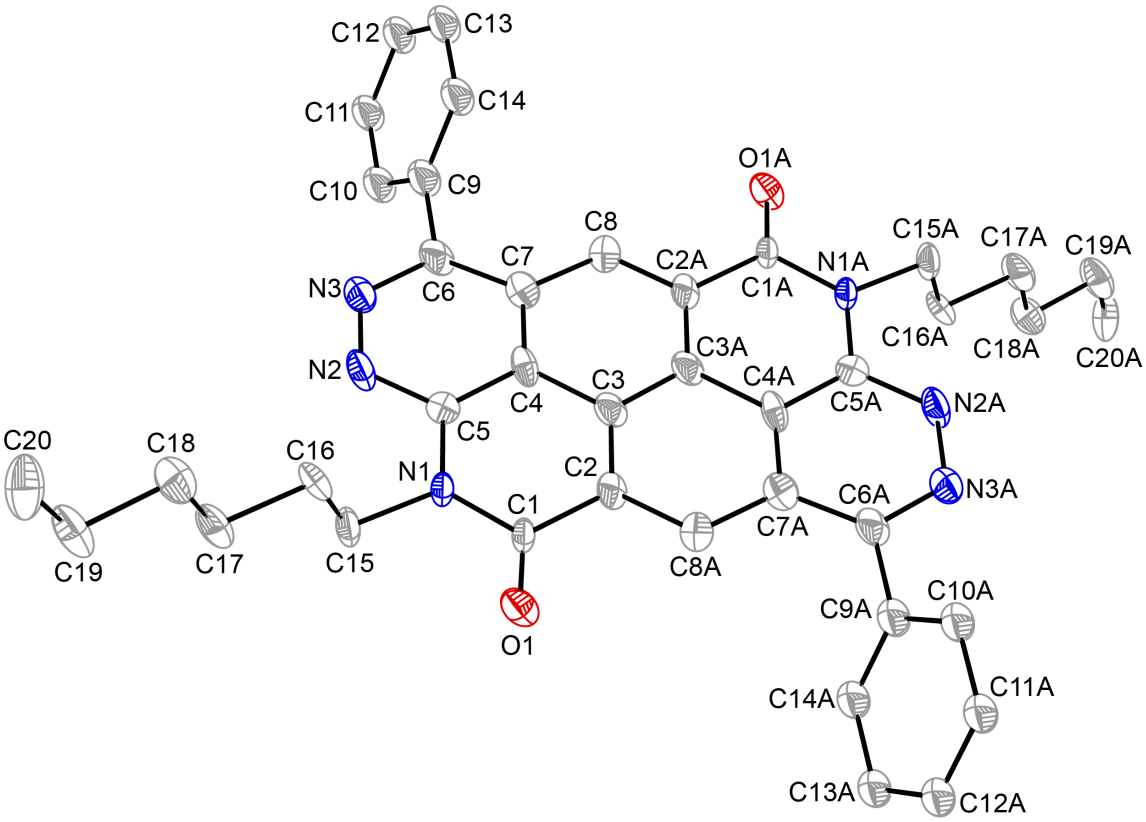

Figure B.7. The structure of compound **5.8**. Ellipsoids are shown at the 50% level. Hydrogen atoms are omitted for clarity.

*Crystal Identification File for Compound **5.8***

```
data_b

_audit_creation_method            SHELXL-97
_chemical_name_systematic
;
 ?
;
_chemical_name_common             ?
_chemical_melting_point           ?
_chemical_formula_moiety
 'C40 H38 N6 O2'
_chemical_formula_sum
 'C40 H38 N6 O2'
_chemical_formula_weight          634.76

loop_
 _atom_type_symbol
 _atom_type_description
 _atom_type_scat_dispersion_real
 _atom_type_scat_dispersion_imag
 _atom_type_scat_source
 'C'  'C'   0.0033   0.0016
 'International Tables Vol C Tables 4.2.6.8 and 6.1.1.4'
 'H'  'H'   0.0000   0.0000
 'International Tables Vol C Tables 4.2.6.8 and 6.1.1.4'
 'N'  'N'   0.0061   0.0033
 'International Tables Vol C Tables 4.2.6.8 and 6.1.1.4'
 'O'  'O'   0.0106   0.0060
 'International Tables Vol C Tables 4.2.6.8 and 6.1.1.4'

_symmetry_cell_setting            Triclinic
_symmetry_space_group_name_H-M    'P - 1'
_symmetry_space_group_name_Hall   '-P 1'

loop_
 _symmetry_equiv_pos_as_xyz
 'x, y, z'
 '-x, -y, -z'

_cell_length_a                    4.806(6)
_cell_length_b                    14.85(2)
_cell_length_c                    14.93(2)
_cell_angle_alpha                 60.43(2)
_cell_angle_beta                  85.26(2)
_cell_angle_gamma                 89.20(2)
_cell_volume                      923(2)
_cell_formula_units_Z             1
_cell_measurement_temperature     100(2)
_cell_measurement_reflns_used     717
_cell_measurement_theta_min       2.75
_cell_measurement_theta_max       25.64

_exptl_crystal_description        'needle'
_exptl_crystal_colour             'yellow'
_exptl_crystal_size_max           0.23
_exptl_crystal_size_mid           0.07
_exptl_crystal_size_min           0.05
_exptl_crystal_density_meas       'not measured'
_exptl_crystal_density_diffrn     1.142
_exptl_crystal_density_method     'not measured'
_exptl_crystal_F_000              336
_exptl_absorpt_coefficient_mu     0.072
```

```
_exptl_absorpt_correction_type    'multi-scan'
_exptl_absorpt_correction_T_min   0.9836
_exptl_absorpt_correction_T_max   0.9964
_exptl_absorpt_process_details    'SADABS (Sheldrick, 2003)'

_exptl_special_details
;
 ?
;

_diffrn_ambient_temperature       100(2)
_diffrn_radiation_wavelength      0.71073
_diffrn_radiation_type            MoK\a
_diffrn_radiation_source          'fine-focus sealed tube'
_diffrn_radiation_monochromator   graphite
_diffrn_measurement_device_type   'Bruker SMART APEX II CCD area detector'
_diffrn_measurement_method        'phi and omega scans'
_diffrn_detector_area_resol_mean  ?
_diffrn_standards_number          ?
_diffrn_standards_interval_count  ?
_diffrn_standards_interval_time   ?
_diffrn_standards_decay_%         ?
_diffrn_reflns_number             3546
_diffrn_reflns_av_R_equivalents   0.0000
_diffrn_reflns_av_sigmaI/netI     0.2156
_diffrn_reflns_limit_h_min        -5
_diffrn_reflns_limit_h_max        5
_diffrn_reflns_limit_k_min        -15
_diffrn_reflns_limit_k_max        18
_diffrn_reflns_limit_l_min        0
_diffrn_reflns_limit_l_max        18
_diffrn_reflns_theta_min          1.58
_diffrn_reflns_theta_max          26.00
_reflns_number_total              3546
_reflns_number_gt                 1257
_reflns_threshold_expression      >2sigma(I)

_computing_data_collection        'APEX2  (Bruker, 2005)'
_computing_cell_refinement        'SAINT+ ver. 6.2 (Bruker, 2001)'
_computing_data_reduction         'SAINT+ ver. 6.2 (Bruker, 2001)'
_computing_structure_solution     'SHELXTL ver. 6.12 (Sheldrick, 2001)'
_computing_structure_refinement   'SHELXTL ver. 6.12 (Sheldrick, 2001)'
_computing_molecular_graphics     'SHELXTL ver. 6.12 (Sheldrick, 2001)'
_computing_publication_material   'SHELXTL ver. 6.12 (Sheldrick, 2001)'

_refine_special_details
;
 Refinement of F^2^ against ALL reflections.  The weighted R-factor wR and
 goodness of fit S are based on F^2^, conventional R-factors R are based
 on F, with F set to zero for negative F^2^. The threshold expression of
 F^2^ > 2sigma(F^2^) is used only for calculating R-factors(gt) etc. and is
 not relevant to the choice of reflections for refinement.  R-factors based
 on F^2^ are statistically about twice as large as those based on F, and R-
 factors based on ALL data will be even larger.
;

_refine_ls_structure_factor_coef  Fsqd
_refine_ls_matrix_type            full
_refine_ls_weighting_scheme       calc
_refine_ls_weighting_details
 'calc w=1/[\s^2^(Fo^2^)+(0.0700P)^2^+0.0000P] where P=(Fo^2^+2Fc^2^)/3'
_atom_sites_solution_primary      direct
_atom_sites_solution_secondary    difmap
_atom_sites_solution_hydrogens    geom
_refine_ls_hydrogen_treatment     constr
```

```
_refine_ls_extinction_method      SHELXL
_refine_ls_extinction_coef        0.010(3)
_refine_ls_extinction_expression
 'Fc^*^=kFc[1+0.001xFc^2^\l^3^/sin(2\q)]^-1/4^'
_refine_ls_number_reflns          3546
_refine_ls_number_parameters      194
_refine_ls_number_restraints      31
_refine_ls_R_factor_all           0.2011
_refine_ls_R_factor_gt            0.1000
_refine_ls_wR_factor_ref          0.2218
_refine_ls_wR_factor_gt           0.1992
_refine_ls_goodness_of_fit_ref    0.998
_refine_ls_restrained_S_all       0.997
_refine_ls_shift/su_max           0.000
_refine_ls_shift/su_mean          0.000

loop_
 _atom_site_label
 _atom_site_type_symbol
 _atom_site_fract_x
 _atom_site_fract_y
 _atom_site_fract_z
 _atom_site_U_iso_or_equiv
 _atom_site_adp_type
 _atom_site_occupancy
 _atom_site_symmetry_multiplicity
 _atom_site_calc_flag
 _atom_site_refinement_flags
 _atom_site_disorder_assembly
 _atom_site_disorder_group
C5 C 0.5142(9) 0.8819(3) 0.1581(4) 0.0206(11) Uani 1 1 d . . .
O1 O 0.5605(6) 0.7508(3) 0.0138(3) 0.0295(9) Uani 1 1 d . . .
N1 N 0.4609(8) 0.8126(3) 0.1226(3) 0.0230(8) Uani 1 1 d . . .
N3 N 0.4050(8) 0.9336(3) 0.2806(3) 0.0304(11) Uani 1 1 d . . .
C4 C 0.7344(9) 0.9540(4) 0.1125(4) 0.0228(12) Uani 1 1 d . . .
C3 C 0.8948(9) 0.9629(4) 0.0223(4) 0.0262(12) Uani 1 1 d . . .
C6 C 0.6065(9) 1.0084(4) 0.2350(4) 0.0303(13) Uani 1 1 d . . .
C7 C 0.7855(10) 1.0206(4) 0.1493(4) 0.0286(13) Uani 1 1 d . . .
N2 N 0.3570(8) 0.8701(3) 0.2427(3) 0.0300(11) Uani 1 1 d . . .
C8 C 1.0031(10) 1.0989(4) 0.0966(4) 0.0252(12) Uani 1 1 d . . .
H8A H 1.0367 1.1469 0.1195 0.030 Uiso 1 1 calc R . .
C1 C 0.6129(9) 0.8122(4) 0.0397(3) 0.0230(8) Uani 1 1 d . . .
C2 C 0.8369(9) 0.8953(4) -0.0131(4) 0.0226(11) Uani 1 1 d . . .
C15 C 0.2430(10) 0.7275(4) 0.1835(4) 0.0264(12) Uani 1 1 d . . .
H15A H 0.0901 0.7534 0.2125 0.032 Uiso 1 1 calc R . .
H15B H 0.1629 0.7071 0.1368 0.032 Uiso 1 1 calc R . .
C18 C 0.2647(10) 0.4489(4) 0.4155(4) 0.0330(13) Uani 1 1 d . . .
H18A H 0.4277 0.4274 0.3862 0.040 Uiso 1 1 calc R . .
H18B H 0.3299 0.4655 0.4670 0.040 Uiso 1 1 calc R . .
C20 C 0.1634(11) 0.2628(4) 0.5539(4) 0.0418(15) Uani 1 1 d . . .
H20A H 0.0158 0.2085 0.5855 0.063 Uiso 1 1 calc R . .
H20B H 0.2270 0.2771 0.6064 0.063 Uiso 1 1 calc R . .
H20C H 0.3205 0.2395 0.5251 0.063 Uiso 1 1 calc R . .
C19 C 0.0498(10) 0.3609(4) 0.4680(4) 0.0397(15) Uani 1 1 d . . .
H19A H -0.1122 0.3827 0.4973 0.048 Uiso 1 1 calc R . .
H19B H -0.0169 0.3455 0.4158 0.048 Uiso 1 1 calc R . .
C17 C 0.1416(10) 0.5463(4) 0.3283(4) 0.0324(13) Uani 1 1 d . . .
H17A H 0.0657 0.5286 0.2790 0.039 Uiso 1 1 calc R . .
H17B H -0.0141 0.5702 0.3582 0.039 Uiso 1 1 calc R . .
C16 C 0.3649(9) 0.6341(4) 0.2702(4) 0.0257(12) Uani 1 1 d . . .
H16A H 0.4371 0.6534 0.3188 0.031 Uiso 1 1 calc R . .
H16B H 0.5230 0.6097 0.2416 0.031 Uiso 1 1 calc R . .
C12 C 0.6974(8) 1.1835(3) 0.3861(3) 0.0387(7) Uani 1 1 d D . .
H12A H 0.7178 1.2226 0.4208 0.046 Uiso 1 1 d R A .
C9 C 0.6387(8) 1.0700(3) 0.2864(3) 0.0387(7) Uani 1 1 d D . .
```

```
C11 C 0.4509(10) 1.1851(5) 0.3446(5) 0.0387(7) Uani 0.51 1 d PD A 1
H11A H 0.3013 1.2250 0.3502 0.046 Uiso 0.51 1 calc PR A 1
C13 C 0.9169(10) 1.1249(5) 0.3784(5) 0.0387(7) Uani 0.51 1 d PD A 1
H13A H 1.0866 1.1237 0.4073 0.046 Uiso 0.51 1 calc PR A 1
C14 C 0.8879(11) 1.0684(5) 0.3285(5) 0.0387(7) Uani 0.51 1 d PD A 1
H14A H 1.0378 1.0285 0.3231 0.046 Uiso 0.51 1 calc PR A 1
C10 C 0.4202(11) 1.1285(5) 0.2946(5) 0.0387(7) Uani 0.51 1 d PD A 1
H10A H 0.2499 1.1298 0.2660 0.046 Uiso 0.51 1 calc PR A 1
C13' C 0.6989(13) 1.0765(4) 0.4412(3) 0.0387(7) Uani 0.49 1 d PD A 2
H13B H 0.7199 1.0420 0.5133 0.046 Uiso 0.49 1 calc PR A 2
C14' C 0.6700(12) 1.0194(4) 0.3917(4) 0.0387(7) Uani 0.49 1 d PD A 2
H14B H 0.6715 0.9459 0.4297 0.046 Uiso 0.49 1 calc PR A 2
C11' C 0.6652(12) 1.2341(3) 0.2806(4) 0.0387(7) Uani 0.49 1 d PD A 2
H11B H 0.6630 1.3076 0.2427 0.046 Uiso 0.49 1 calc PR A 2
C10' C 0.6361(11) 1.1772(4) 0.2308(4) 0.0387(7) Uani 0.49 1 d PD A 2
H10B H 0.6145 1.2116 0.1588 0.046 Uiso 0.49 1 calc PR A 2

loop_
 _atom_site_aniso_label
 _atom_site_aniso_U_11
 _atom_site_aniso_U_22
 _atom_site_aniso_U_33
 _atom_site_aniso_U_23
 _atom_site_aniso_U_13
 _atom_site_aniso_U_12
C5 0.021(3) 0.017(3) 0.023(3) -0.009(2) -0.005(2) 0.004(2)
O1 0.0211(17) 0.031(2) 0.047(2) -0.028(2) 0.0017(17) -0.0012(15)
N1 0.0168(16) 0.0304(19) 0.0162(17) -0.0080(16) 0.0047(14) -0.0054(15)
N3 0.025(2) 0.034(3) 0.034(3) -0.019(2) 0.004(2) -0.008(2)
C4 0.013(2) 0.017(3) 0.027(3) -0.002(2) 0.001(2) 0.003(2)
C3 0.015(2) 0.033(3) 0.036(3) -0.022(3) -0.001(2) 0.002(2)
C6 0.014(2) 0.042(3) 0.044(3) -0.028(3) -0.002(2) 0.005(2)
C7 0.023(3) 0.029(3) 0.033(3) -0.015(3) -0.002(3) 0.000(2)
N2 0.021(2) 0.029(2) 0.040(3) -0.018(2) 0.009(2) -0.010(2)
C8 0.026(3) 0.021(3) 0.026(3) -0.009(2) 0.001(2) 0.002(2)
C1 0.0168(16) 0.0304(19) 0.0162(17) -0.0080(16) 0.0047(14) -0.0054(15)
C2 0.012(2) 0.027(3) 0.028(3) -0.013(3) -0.001(2) 0.008(2)
C15 0.024(3) 0.026(3) 0.029(3) -0.014(3) 0.012(2) -0.011(2)
C18 0.028(3) 0.026(3) 0.040(3) -0.012(3) -0.002(3) -0.003(2)
C20 0.033(3) 0.037(4) 0.045(4) -0.016(3) 0.016(3) 0.002(3)
C19 0.028(3) 0.032(3) 0.057(4) -0.021(3) 0.005(3) -0.013(3)
C17 0.026(3) 0.024(3) 0.046(3) -0.018(3) 0.003(3) -0.010(2)
C16 0.013(2) 0.025(3) 0.037(3) -0.015(3) 0.000(2) -0.006(2)
C12 0.0243(11) 0.0595(18) 0.0476(17) -0.0396(16) 0.0091(12) -0.0103(12)
C9 0.0243(11) 0.0595(18) 0.0476(17) -0.0396(16) 0.0091(12) -0.0103(12)
C11 0.0243(11) 0.0595(18) 0.0476(17) -0.0396(16) 0.0091(12) -0.0103(12)
C13 0.0243(11) 0.0595(18) 0.0476(17) -0.0396(16) 0.0091(12) -0.0103(12)
C14 0.0243(11) 0.0595(18) 0.0476(17) -0.0396(16) 0.0091(12) -0.0103(12)
C10 0.0243(11) 0.0595(18) 0.0476(17) -0.0396(16) 0.0091(12) -0.0103(12)
C13' 0.0243(11) 0.0595(18) 0.0476(17) -0.0396(16) 0.0091(12) -0.0103(12)
C14' 0.0243(11) 0.0595(18) 0.0476(17) -0.0396(16) 0.0091(12) -0.0103(12)
C11' 0.0243(11) 0.0595(18) 0.0476(17) -0.0396(16) 0.0091(12) -0.0103(12)
C10' 0.0243(11) 0.0595(18) 0.0476(17) -0.0396(16) 0.0091(12) -0.0103(12)

_geom_special_details
;
 All esds (except the esd in the dihedral angle between two l.s. planes)
 are estimated using the full covariance matrix.  The cell esds are taken
 into account individually in the estimation of esds in distances, angles
 and torsion angles; correlations between esds in cell parameters are only
 used when they are defined by crystal symmetry.  An approximate (isotropic)
 treatment of cell esds is used for estimating esds involving l.s. planes.
;

loop_
```

```
 _geom_bond_atom_site_label_1
 _geom_bond_atom_site_label_2
 _geom_bond_distance
 _geom_bond_site_symmetry_2
 _geom_bond_publ_flag
C5 N2 1.351(6) . ?
C5 C4 1.387(6) . ?
C5 N1 1.405(6) . ?
O1 C1 1.190(5) . ?
N1 C1 1.386(6) . ?
N1 C15 1.505(6) . ?
N3 N2 1.347(5) . ?
N3 C6 1.345(6) . ?
C4 C7 1.381(7) . ?
C4 C3 1.442(7) . ?
C3 C3 1.370(9) 2_775 ?
C3 C2 1.385(7) . ?
C6 C7 1.415(7) . ?
C6 C9 1.472(6) . ?
C7 C8 1.435(7) . ?
C8 C2 1.375(6) 2_775 ?
C8 H8A 0.9500 . ?
C1 C2 1.497(7) . ?
C2 C8 1.375(6) 2_775 ?
C15 C16 1.507(7) . ?
C15 H15A 0.9900 . ?
C15 H15B 0.9900 . ?
C18 C19 1.511(7) . ?
C18 C17 1.543(7) . ?
C18 H18A 0.9900 . ?
C18 H18B 0.9900 . ?
C20 C19 1.521(8) . ?
C20 H20A 0.9800 . ?
C20 H20B 0.9800 . ?
C20 H20C 0.9800 . ?
C19 H19A 0.9900 . ?
C19 H19B 0.9900 . ?
C17 C16 1.540(6) . ?
C17 H17A 0.9900 . ?
C17 H17B 0.9900 . ?
C16 H16A 0.9900 . ?
C16 H16B 0.9900 . ?
C12 C11 1.377(4) . ?
C12 C13' 1.382(4) . ?
C12 C13 1.391(4) . ?
C12 C11' 1.392(4) . ?
C12 H12A 0.9599 . ?
C9 C14' 1.388(5) . ?
C9 C10' 1.386(5) . ?
C9 C10 1.390(5) . ?
C9 C14 1.393(5) . ?
C11 C10 1.386(4) . ?
C11 H11A 0.9500 . ?
C13 C14 1.384(4) . ?
C13 H13A 0.9500 . ?
C14 H14A 0.9500 . ?
C10 H10A 0.9500 . ?
C13' C14' 1.388(4) . ?
C13' H13B 0.9500 . ?
C14' H14B 0.9500 . ?
C11' C10' 1.388(4) . ?
C11' H11B 0.9500 . ?
C10' H10B 0.9500 . ?

loop_
```

```
 _geom_angle_atom_site_label_1
 _geom_angle_atom_site_label_2
 _geom_angle_atom_site_label_3
 _geom_angle
 _geom_angle_site_symmetry_1
 _geom_angle_site_symmetry_3
 _geom_angle_publ_flag
N2 C5 C4 121.6(4) . . ?
N2 C5 N1 117.4(4) . . ?
C4 C5 N1 120.8(4) . . ?
C1 N1 C5 123.9(4) . . ?
C1 N1 C15 117.5(4) . . ?
C5 N1 C15 118.3(4) . . ?
N2 N3 C6 120.8(4) . . ?
C7 C4 C5 119.9(4) . . ?
C7 C4 C3 120.9(4) . . ?
C5 C4 C3 119.0(4) . . ?
C3 C3 C2 123.3(6) 2_775 . ?
C3 C3 C4 117.2(5) 2_775 . ?
C2 C3 C4 119.5(4) . . ?
N3 C6 C7 122.0(4) . . ?
N3 C6 C9 114.6(4) . . ?
C7 C6 C9 123.2(4) . . ?
C4 C7 C6 116.2(4) . . ?
C4 C7 C8 118.8(4) . . ?
C6 C7 C8 124.9(4) . . ?
N3 N2 C5 119.3(4) . . ?
C2 C8 C7 120.2(4) 2_775 . ?
C2 C8 H8A 119.9 2_775 . ?
C7 C8 H8A 119.9 . . ?
O1 C1 N1 121.1(4) . . ?
O1 C1 C2 124.5(4) . . ?
N1 C1 C2 114.5(4) . . ?
C8 C2 C3 119.5(4) 2_775 . ?
C8 C2 C1 118.4(4) 2_775 . ?
C3 C2 C1 122.1(4) . . ?
C16 C15 N1 111.4(4) . . ?
C16 C15 H15A 109.4 . . ?
N1 C15 H15A 109.4 . . ?
C16 C15 H15B 109.4 . . ?
N1 C15 H15B 109.4 . . ?
H15A C15 H15B 108.0 . . ?
C19 C18 C17 111.1(4) . . ?
C19 C18 H18A 109.4 . . ?
C17 C18 H18A 109.4 . . ?
C19 C18 H18B 109.4 . . ?
C17 C18 H18B 109.4 . . ?
H18A C18 H18B 108.0 . . ?
C19 C20 H20A 109.5 . . ?
C19 C20 H20B 109.5 . . ?
H20A C20 H20B 109.5 . . ?
C19 C20 H20C 109.5 . . ?
H20A C20 H20C 109.5 . . ?
H20B C20 H20C 109.5 . . ?
C20 C19 C18 112.8(4) . . ?
C20 C19 H19A 109.0 . . ?
C18 C19 H19A 109.0 . . ?
C20 C19 H19B 109.0 . . ?
C18 C19 H19B 109.0 . . ?
H19A C19 H19B 107.8 . . ?
C16 C17 C18 111.2(4) . . ?
C16 C17 H17A 109.4 . . ?
C18 C17 H17A 109.4 . . ?
C16 C17 H17B 109.4 . . ?
C18 C17 H17B 109.4 . . ?
```

```
H17A C17 H17B 108.0 . . ?
C15 C16 C17 110.5(4) . . ?
C15 C16 H16A 109.6 . . ?
C17 C16 H16A 109.6 . . ?
C15 C16 H16B 109.6 . . ?
C17 C16 H16B 109.6 . . ?
H16A C16 H16B 108.1 . . ?
C11 C12 C13' 93.5(3) . . ?
C11 C12 C13 120.2(3) . . ?
C13' C12 C13 55.8(3) . . ?
C11 C12 C11' 55.8(3) . . ?
C13' C12 C11' 119.9(2) . . ?
C13 C12 C11' 93.7(3) . . ?
C11 C12 H12A 120.0 . . ?
C13' C12 H12A 119.8 . . ?
C13 C12 H12A 119.9 . . ?
C11' C12 H12A 120.2 . . ?
C14' C9 C10' 120.3(3) . . ?
C14' C9 C10 93.3(3) . . ?
C10' C9 C10 55.8(3) . . ?
C14' C9 C14 55.9(3) . . ?
C10' C9 C14 93.8(3) . . ?
C10 C9 C14 119.8(3) . . ?
C14' C9 C6 119.2(4) . . ?
C10' C9 C6 120.5(4) . . ?
C10 C9 C6 120.4(4) . . ?
C14 C9 C6 119.8(4) . . ?
C12 C11 C10 120.2(3) . . ?
C12 C11 H11A 119.9 . . ?
C10 C11 H11A 119.9 . . ?
C14 C13 C12 120.0(3) . . ?
C14 C13 H13A 120.0 . . ?
C12 C13 H13A 120.0 . . ?
C13 C14 C9 119.9(4) . . ?
C13 C14 H14A 120.0 . . ?
C9 C14 H14A 120.0 . . ?
C11 C10 C9 120.0(4) . . ?
C11 C10 H10A 120.0 . . ?
C9 C10 H10A 120.0 . . ?
C12 C13' C14' 120.2(3) . . ?
C12 C13' H13B 119.9 . . ?
C14' C13' H13B 119.9 . . ?
C9 C14' C13' 119.8(3) . . ?
C9 C14' H14B 120.1 . . ?
C13' C14' H14B 120.1 . . ?
C10' C11' C12 120.0(3) . . ?
C10' C11' H11B 120.0 . . ?
C12 C11' H11B 120.0 . . ?
C9 C10' C11' 119.8(3) . . ?
C9 C10' H10B 120.1 . . ?
C11' C10' H10B 120.1 . . ?

loop_
 _geom_torsion_atom_site_label_1
 _geom_torsion_atom_site_label_2
 _geom_torsion_atom_site_label_3
 _geom_torsion_atom_site_label_4
 _geom_torsion
 _geom_torsion_site_symmetry_1
 _geom_torsion_site_symmetry_2
 _geom_torsion_site_symmetry_3
 _geom_torsion_site_symmetry_4
 _geom_torsion_publ_flag
N2 C5 N1 C1 -177.1(5) . . . . ?
C4 C5 N1 C1 -2.0(7) . . . . ?
```

```
N2 C5 N1 C15 -2.7(6) . . . . ?
C4 C5 N1 C15 172.4(4) . . . . ?
N2 C5 C4 C7 -4.3(7) . . . . ?
N1 C5 C4 C7 -179.2(5) . . . . ?
N2 C5 C4 C3 180.0(5) . . . . ?
N1 C5 C4 C3 5.1(6) . . . . ?
C7 C4 C3 C3 2.5(8) . . . 2_775 ?
C5 C4 C3 C3 178.1(6) . . . 2_775 ?
C7 C4 C3 C2 -179.5(5) . . . . ?
C5 C4 C3 C2 -3.9(6) . . . . ?
N2 N3 C6 C7 -3.3(8) . . . . ?
N2 N3 C6 C9 -178.7(4) . . . . ?
C5 C4 C7 C6 1.2(7) . . . . ?
C3 C4 C7 C6 176.9(5) . . . . ?
C5 C4 C7 C8 -176.0(4) . . . . ?
C3 C4 C7 C8 -0.4(7) . . . . ?
N3 C6 C7 C4 2.5(7) . . . . ?
C9 C6 C7 C4 177.5(5) . . . . ?
N3 C6 C7 C8 179.6(5) . . . . ?
C9 C6 C7 C8 -5.4(8) . . . . ?
C6 N3 N2 C5 0.2(7) . . . . ?
C4 C5 N2 N3 3.6(7) . . . . ?
N1 C5 N2 N3 178.6(4) . . . . ?
C4 C7 C8 C2 -2.2(7) . . . 2_775 ?
C6 C7 C8 C2 -179.2(5) . . . 2_775 ?
C5 N1 C1 O1 179.1(5) . . . . ?
C15 N1 C1 O1 4.7(7) . . . . ?
C5 N1 C1 C2 -2.1(6) . . . . ?
C15 N1 C1 C2 -176.6(4) . . . . ?
C3 C3 C2 C8 0.4(9) 2_775 . . 2_775 ?
C4 C3 C2 C8 -177.5(5) . . . 2_775 ?
C3 C3 C2 C1 177.5(6) 2_775 . . . ?
C4 C3 C2 C1 -0.4(7) . . . . ?
O1 C1 C2 C8 -0.9(7) . . . 2_775 ?
N1 C1 C2 C8 -179.6(4) . . . 2_775 ?
O1 C1 C2 C3 -178.0(5) . . . . ?
N1 C1 C2 C3 3.3(7) . . . . ?
C1 N1 C15 C16 88.9(5) . . . . ?
C5 N1 C15 C16 -85.9(5) . . . . ?
C17 C18 C19 C20 179.4(5) . . . . ?
C19 C18 C17 C16 -176.5(5) . . . . ?
N1 C15 C16 C17 -177.5(4) . . . . ?
C18 C17 C16 C15 178.5(4) . . . . ?
N3 C6 C9 C14' 51.9(6) . . . . ?
C7 C6 C9 C14' -123.4(5) . . . . ?
N3 C6 C9 C10' -127.7(5) . . . . ?
C7 C6 C9 C10' 57.0(6) . . . . ?
N3 C6 C9 C10 -62.0(6) . . . . ?
C7 C6 C9 C10 122.7(5) . . . . ?
N3 C6 C9 C14 117.0(5) . . . . ?
C7 C6 C9 C14 -58.3(7) . . . . ?
C13' C12 C11 C10 -52.2(3) . . . . ?
C13 C12 C11 C10 -0.2(3) . . . . ?
C11' C12 C11 C10 72.1(3) . . . . ?
C11 C12 C13 C14 0.3(4) . . . . ?
C13' C12 C13 C14 72.2(4) . . . . ?
C11' C12 C13 C14 -51.8(4) . . . . ?
C12 C13 C14 C9 -0.2(4) . . . . ?
C14' C9 C14 C13 -72.1(3) . . . . ?
C10' C9 C14 C13 52.3(3) . . . . ?
C10 C9 C14 C13 0.1(3) . . . . ?
C6 C9 C14 C13 -179.0(5) . . . . ?
C12 C11 C10 C9 0.06(14) . . . . ?
C14' C9 C10 C11 52.1(2) . . . . ?
C10' C9 C10 C11 -72.7(3) . . . . ?
```

```
C14 C9 C10 C11 0.01(14) . . . . ?
C6 C9 C10 C11 179.0(4) . . . . ?
C11 C12 C13' C14' 52.4(4) . . . . ?
C13 C12 C13' C14' -72.2(3) . . . . ?
C11' C12 C13' C14' 0.4(4) . . . . ?
C10' C9 C14' C13' 0.0(3) . . . . ?
C10 C9 C14' C13' -51.8(3) . . . . ?
C14 C9 C14' C13' 72.3(3) . . . . ?
C6 C9 C14' C13' -179.6(4) . . . . ?
C12 C13' C14' C9 -0.2(4) . . . . ?
C11 C12 C11' C10' -72.5(3) . . . . ?
C13' C12 C11' C10' -0.4(3) . . . . ?
C13 C12 C11' C10' 51.9(3) . . . . ?
C14' C9 C10' C11' 0.05(14) . . . . ?
C10 C9 C10' C11' 71.7(3) . . . . ?
C14 C9 C10' C11' -52.2(2) . . . . ?
C6 C9 C10' C11' 179.6(4) . . . . ?
C12 C11' C10' C9 0.15(14) . . . . ?

_diffrn_measured_fraction_theta_max    0.982
_diffrn_reflns_theta_full              26.00
_diffrn_measured_fraction_theta_full   0.982
_refine_diff_density_max    0.407
_refine_diff_density_min   -0.329
_refine_diff_density_rms    0.078

# SQUEEZE RESULTS (APPEND TO CIF)
# Note: Data are Listed for all Voids in the P1 Unit Cell
# i.e. Centre of Gravity, Solvent Accessible Volume,
# Recovered number of Electrons in the Void and
# Details about the Squeezed Material
loop_
  _platon_squeeze_void_nr
  _platon_squeeze_void_average_x
  _platon_squeeze_void_average_y
  _platon_squeeze_void_average_z
  _platon_squeeze_void_volume
  _platon_squeeze_void_count_electrons
  _platon_squeeze_void_content
   1 -0.031  0.500  0.000       160       103 ' '
_platon_squeeze_details
;
;
```

B.5 References

(1) Bruker (2005), APEX2 software package, Bruker AXS Inc., 5465, East Cheryl Parkway, Madison, WI 5317.

(2) Spek, A. L. *Acta Cryst. D* **2009**, *65*, 148–155.

(3) Sluis, P.; Spek, A. L. *Acta Cryst. A*, **1990**, *46*, 194.

(4) Sheldrick, G. *Acta Cryst. A* **1990**, *46*, 467.

(5) Sheldrick, G. M.; Schneider, T. R. (1997) [16] SHELXL: High-resolution refinement. In Methods in Enzymology, vol. 277. Edited by Carter, C. W. Jr. Academic Press, pp. 319.

(6) Sheldrick, G. M.; Hauptman, H. A.; Weeks, C. M.; Miller, R.; and Usón, I. (2001) Direct methods. In International Tables for Crystallography, vol. F. Edited by Rossmann, M.; and Arnold, E. Dordrecht/Boston/London: Kluwer Academic, pp. 333-345.

APPENDIX C

COMPUTATIONAL METHODOLOGY

The quantum-chemical calculations presented in this thesis were performed by Laxman Pandey and Dr. Chad Risko while working in Prof. Jean-Luc Brédas' research group in the School of Chemistry and Biochemistry at Georgia Institute of Technology.

C.1 Experimental Details

Calculations for the isolated (neutral, radical-cation and radical-anion) molecules in their electronic ground state were carried with density functional theory (DFT), using the generalized gradient approximation B3LYP functional,[1-3] in conjunction with a 6-31G**[4-6] basis set. Due to the tendency of DFT methods to overestimate the extent of wavefunction delocalization,[7,8] geometries were also optimized at the Hartree-Fock (HF/6-31G**) level. All alkyl side chains were replaced with methyl groups to reduce the computational cost. Low-lying singlet excited states were evaluated at the neutral ground-state geometries using time-dependent density functional theory (TDDFT) at the B3LYP/6-31G** level of theory. Since TD-DFT-B3LYP is known to have problems giving the correct description of charge-transfer excitations[9,10], long-range-corrected CAM-B3LYP[11] and ωB97X[9] functionals (with ω-values of 0.33 $bohr^{-1}$ and 0.30 $bohr^{-1}$, respectively for the long-range correction parameters) were also used to investigate the $S_0 \rightarrow S_n$ transitions. Additionally, TD-UB3LYP/6-31G** was also employed to evaluate the vertical transition energies of the radical-cation structures in Chapter 2. Also in Chapter 2, solvation effects on the IPs and EAs were evaluated with the polarization continuum model[12] taking into account the dielectric constant of dichloromethane, ε = 8.93. All

calculations were performed using the Gaussian (03 Revision E.01[13] and 09 Revision A.02[14]) suite of programs.

C.2 References

(1) Becke, A. D. *Phys. Rev. A* **1988**, *38*, 3098.

(2) Becke, A. *J. Chem. Phys.* **1993**, *98*, 5648.

(3) Lee, C.; Yang, W.; Parr, R. G. *Phys. Rev. B* **1988**, *37*, 785.

(4) Hariharan, P. C.; Pople, J. A. *Theor. Chim. Acta* **1973**, *28*, 213.

(5) Francl, M. M.; Pietro, W. J.; Hehre, W. J.; Binkley, J. S.; Gordon, M. S.; DeFrees, D. J.; Pople, J. A. *J. Chem. Phys.* **1982**, *77*, 3654.

(6) Rassolov, V. A.; Pople, J. A.; Ratner, M. A.; Windus, T. L. *J. Chem. Phys.* **1998**, *109*, 1223.

(7) Mori-Sánchez, P.; Cohen, A. J.; Yang, W. *Phys. Rev. Lett.* **2008**, *100*, 146401.

(8) Pacchioni, G.; Frigoli, F.; Ricci, D.; Weil, J. A. *Phys. Rev. B* **2000**, *63*, 054102.

(9) Chai, J.; Head-Gordon, M. *J. Chem. Phys.* **2008**, *128*, 084106.

(10) Dreuw, A.; Head-Gordon, M. *J. Am. Chem. Soc.* **2004**, *126*, 4007.

(11) Yanai, T.; Tew, D. P.; Handy, N. C. *Chem. Phys. Lett.* **2004**, *393*, 51.

(12) Scalmani, G.; Frisch, M. J. *J. Chem. Phys.* **2010**, *132*, 114110.

(13) Frisch, M. J. T., G. W.; Schlegel, H. B.; Scuseria, G. E.; Robb, M. A.; Cheeseman, J. R.; Montgomery, Jr., J. A.; Vreven, T.; Kudin, K. N.; Burant, J. C.; Millam, J. M.; Iyengar, S. S.; Tomasi, J.; Barone, V.; Mennucci, B.; Cossi, M.; Scalmani, G.; Rega, N.; Petersson, G. A.; Nakatsuji, H.; Hada, M.; Ehara, M.; Toyota, K.; Fukuda, R.; Hasegawa, J.; Ishida, M.; Nakajima, T.; Honda, Y.; Kitao, O.; Nakai, H.; Klene, M.; Li, X.; Knox, J. E.; Hratchian, H. P.; Cross, J. B.; Bakken, V.; Adamo, C.; Jaramillo, J.; Gomperts, R.; Stratmann, R. E.; Yazyev, O.; Austin, A. J.; Cammi, R.; Pomelli, C.; Ochterski, J. W.; Ayala, P. Y.; Morokuma, K.; Voth, G. A.; Salvador, P.; Dannenberg, J. J.; Zakrzewski, V. G.; Dapprich, S.; Daniels, A. D.; Strain, M. C.; Farkas, O.; Malick, D. K.; Rabuck, A. D.; Raghavachari, K.; Foresman, J. B.; Ortiz, J. V.; Cui, Q.; Baboul, A. G.; Clifford, S.; Cioslowski, J.; Stefanov, B. B.; Liu, G.; Liashenko, A.; Piskorz, P.; Komaromi, I.; Martin, R. L.; Fox, D. J.; Keith, T.; Al-Laham, M. A.; Peng, C. Y.; Nanayakkara, A.; Challacombe, M.; Gill, P. M. W.; Johnson, B.; Chen, W.; Wong, M. W.; Gonzalez, C.; and Pople, J. A. Gaussian, Inc., Wallingford CT **2004**.

(14) Frisch, M. J. T., G. W.; Schlegel, H. B.; Scuseria, G. E.; Robb, M. A.; Cheeseman, J. R.; Scalmani, G.; Barone, V.; Mennucci, B.; Petersson, G. A.; Nakatsuji, H.; Caricato, M.; Li, X.; Hratchian, H. P.; Izmaylov, A. F.; Bloino, J.; Zheng, G.; Sonnenberg, J. L.; Hada, M.; Ehara, M.; Toyota, K.; Fukuda, R.; Hasegawa, J.; Ishida, M.; Nakajima, T.; Honda, Y.; Kitao, O.; Nakai, H.; Vreven, T.; Montgomery, Jr., J. A.; Peralta, J. E.; Ogliaro, F.; Bearpark, M.; Heyd, J. J.; Brothers, E.; Kudin, K. N.; Staroverov, V. N.; Kobayashi, R.; Normand, J.; Raghavachari, K.; Rendell, A.; Burant, J. C.; Iyengar, S. S.; Tomasi, J.; Cossi, M.; Rega, N.; Millam, N. J.; Klene, M.; Knox, J. E.; Cross, J. B.; Bakken, V.; Adamo, C.; Jaramillo, J.; Gomperts, R.; Stratmann, R. E.; Yazyev, O.; Austin, A. J.; Cammi, R.; Pomelli, C.; Ochterski, J. W.; Martin, R. L.; Morokuma, K.; Zakrzewski, V. G.; Voth, G. A.; Salvador, P.; Dannenberg, J. J.; Dapprich, S.; Daniels, A. D.; Farkas, Ö.; Foresman, J. B.; Ortiz, J. V.; Cioslowski, J.; Fox, D. J. Gaussian Inc., Wallingford CT **2009**.

APPENDIX D

FABRICATION OF THIN-FILM TRANSISTORS

The fabrication and measurement of the field-effect transistor device characteristics presented in this thesis was performed by either Dr. Shree Prakash Tiwari or Dr. Do Kyung Hwang, as specified, while working in Prof. Bernard Kippelen's research group in the School of Electrical and Computer Engineering at Georgia Institute of Technology.

D.1 Chapter 2 (Shree Tiwari)

D.1.1 Experimental Details

Device measurements were performed on bottom-gate OFETs were fabricated on heavily doped n-type silicon substrate (also serves as gate electrodes) with 200 nm thick thermally grown SiO_2 as the gate dielectric. Ti / Au (10 nm/100 nm) metallization on the backside of the substrate was done to enhance the gate electrical contact. First, the substrates were cleaned by O_2 plasma for 3 min, to improve film formation by increasing the hydrophilicity of the SiO_2 surface. The capacitance density of the SiO_2 layer was 16.2 $nFcm^{-2}$. A thin layer of organic semiconductor was formed on the substrates by spin coating with a solution (12 mg / mL) in chloroform. Au (ca. 75 nm) was deposited through a shadow mask to act as top source / drain electrode. The devices were annealed at 130 °C for 30 min before device characterization.

D.1.2 Device Characteristics

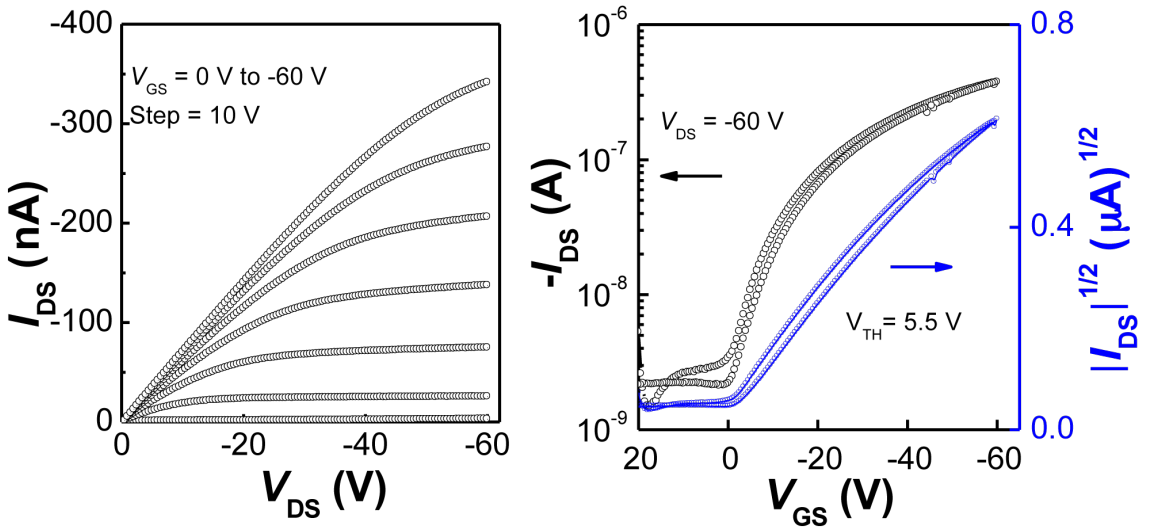

Figure D.1. Output (left) and transfer (right) characteristics of a particular p-channel bottom-gate OFET with **2.7a** as semiconductor and SiO_2 gate dielectric layer with Au source / drain electrodes (*W/L*= 1200 μm/100 μm).

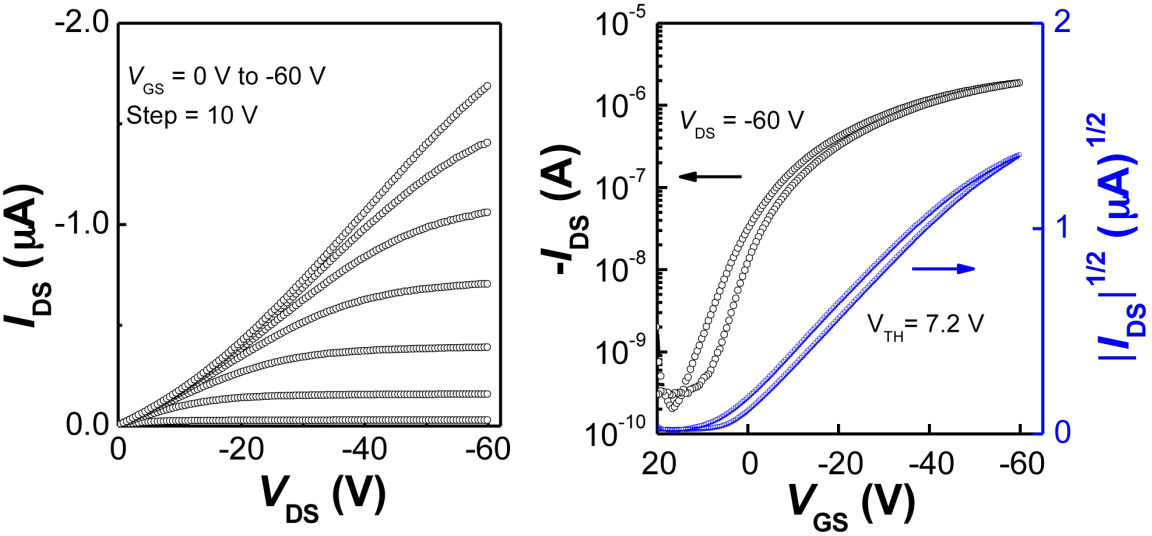

Figure D.2. Output (left) and transfer (right) characteristics of a particular p-channel bottom-gate OFET with **2.7b** as semiconductor and SiO_2 gate dielectric layer with Au source / drain electrodes (*W/L*= 1200 μm/100 μm).

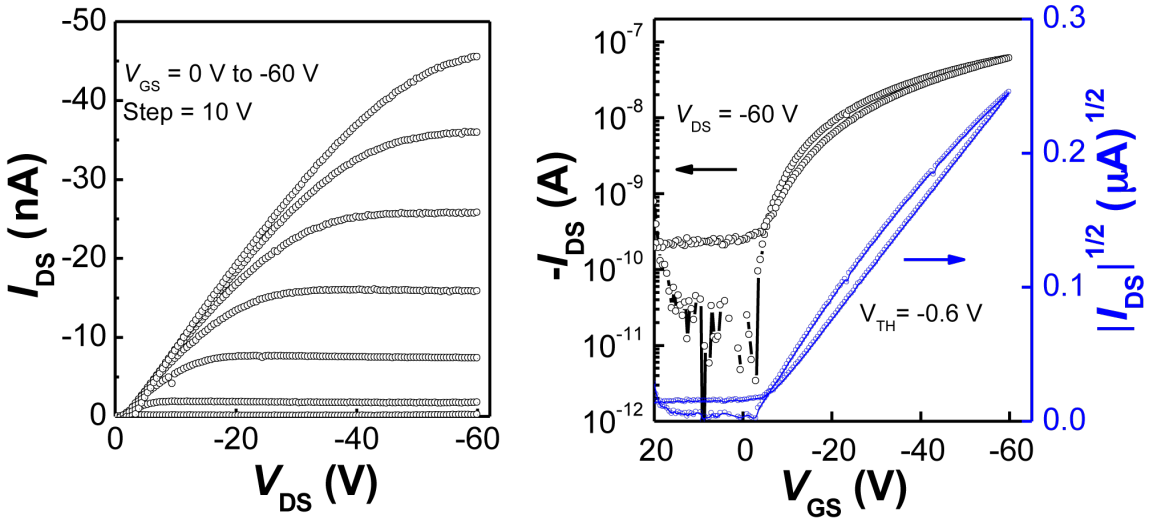

Figure D.3. Output (left) and transfer (right) characteristics of a particular p-channel bottom-gate OFET with **2.7c** as semiconductor and SiO_2 gate dielectric layer with Au source / drain electrodes (*W/L*= 1200 μm/100 μm).

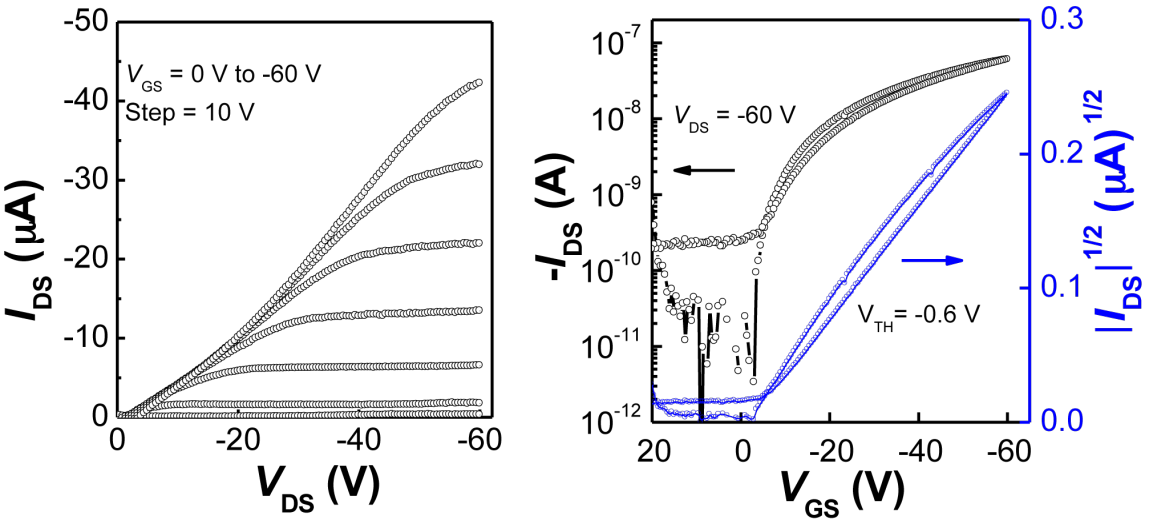

Figure D.4. Output (left) and transfer (right) characteristics of a particular p-channel bottom-gate OFET with **2.7d** as semiconductor and SiO_2 gate dielectric layer with Au source / drain electrodes (*W/L*= 1200 μm/100 μm).

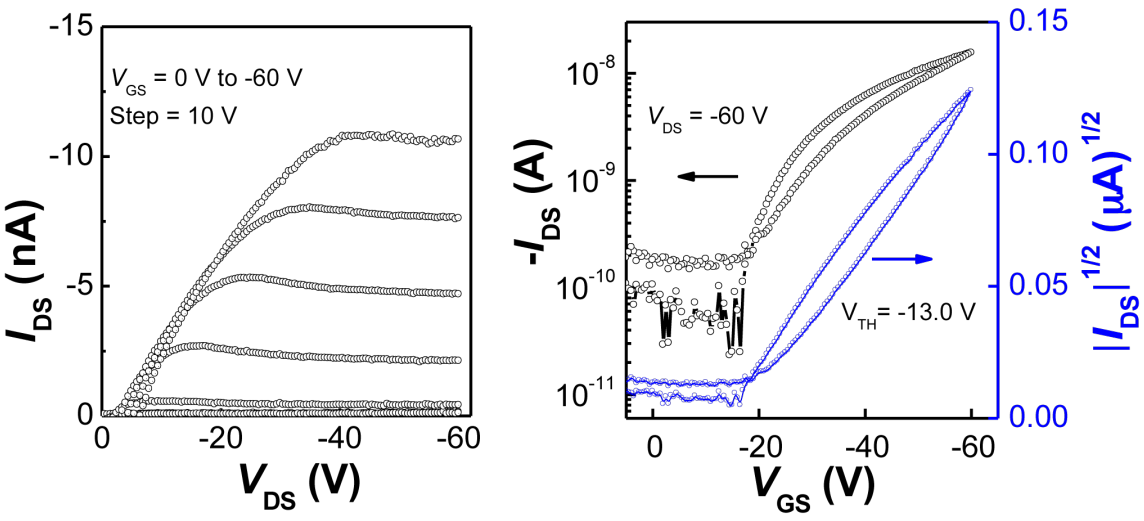

Figure D.5. Output (left) and transfer (right) characteristics of a particular p-channel bottom-gate OFET with **2.8b** as semiconductor and SiO_2 gate dielectric layer with Au source / drain electrodes (*W/L*= 1200 μm/100 μm).

D.2 Chapter 3 (Shree Tiwari)

D.2.1 Experimental Details (Top-Gate, Bottom-Contact Geometry)

Top-gate OFET devices were fabricated with CYTOP/Al_2O_3 bi-layer gate dielectric to study the n-channel (and ambipolar) performance of this series of compounds. This bilayer dielectric has been recently shown to produce very stable devices.[1] Gold (50 nm) source and drain electrodes were deposited by thermal evaporation through a shadow mask onto Corning glass substrates (roughness <2 nm). Thin-films of **3.4c** were deposited by spin coating a 30 mg / mL solution in dichlorobenzene. Uniform films were not obtained from spin-casting **3.4a** and **3.4b** due to reduced solubility of these materials in dichlorobenzene, and so films of these materials were prepared by drop casting. The thin-films were then annealed at 100 °C for 15 min. CYTOP solution (CTL-809M, ca. 9 wt%) was diluted with solvent (CT-solv.180) to make 2 wt% solution and spin casted at 3000 rpm for 60 s to form a 40 nm

thick CYTOP layer. The CYTOP film was annealed at 100 °C for 20 min before Al_2O_3 (50 nm) films were deposited by atomic layer deposition at 110 °C using a Savannah 100 system from Cambridge Nanotech. Finally, Al (ca. 150 nm) gate electrodes were deposited by thermal evaporation through a shadow mask. All current-voltage (I−V) characteristics of OFETs were measured in a N_2-filled glove box (O_2, H_2O < 0.1 ppm). Average values of mobility, threshold and voltage, and current on/off rato were calculated based on 3 to 6 devices fabricated with W = 2550 or 6050 μm, and L = 180 μm from a single substrate. The capacitance density of the gate dielectric was measured in parallel plate capacitors fabricated using the same procedures as described above on independent substrates with the following geometry glass/Au/CYTOP (40 nm)/Al_2O_3 (50 nm)/Al (measured at a frequency of 1 kHz) with areas ranging from 1 mm^2 to 4 mm^2. A capacitance density of 34.5(±1.0) nF/cm^2 was obtained from 4 different batches of samples.

D.2.2 Experimental Details (Top-Contact, Bottom-Gate Geometry)

Device measurements performed on top-contact, bottom-gate OFETs were fabricated on heavily doped n-type silicon substrate (also serves as gate electrodes) with 200 nm thick thermally grown SiO_2 as the gate dielectric. Ti / Au (10 nm/100 nm) metallization on the backside of the substrate was done to enhance the gate electrical contact. First, the substrates were cleaned by O_2 plasma for 3 min, to improve film formation by increasing the hydrophilicity of the SiO_2 surface. The SiO_2 dielectric surface was then passivated with a thin buffer layer of BCB (Cyclotene™, Dow Chemicals, Product# XU71918.30), to provide a high-quality hydroxyl-free interface. The BCB was diluted in trimethylbenzene with the ratio 1:20, and spin-coated at 3000 rpm for 60 s to provide a very thin uniform layer (thickness was not measured). The samples were annealed at 250°C for 1 h inside N_2 glove box for crosslinking. The total capacitance

density measured from parallel-plate capacitors was ~13.86 nFcm^{-2}. A thin layer of organic semiconductor was formed on the substrates by spin coating with a solution (20 mg / mL) in 1,2-dichlorobenzene at 1000 rpm for 60 s. Devices were not exposed to air during the fabrication process. Ca covered by Au (Ca/Au ~ 40 nm/60 nm) electrodes were deposited in Spectros system through a shadow mask to act as top source / drain electrode.

D.2.3 Device Characteristics

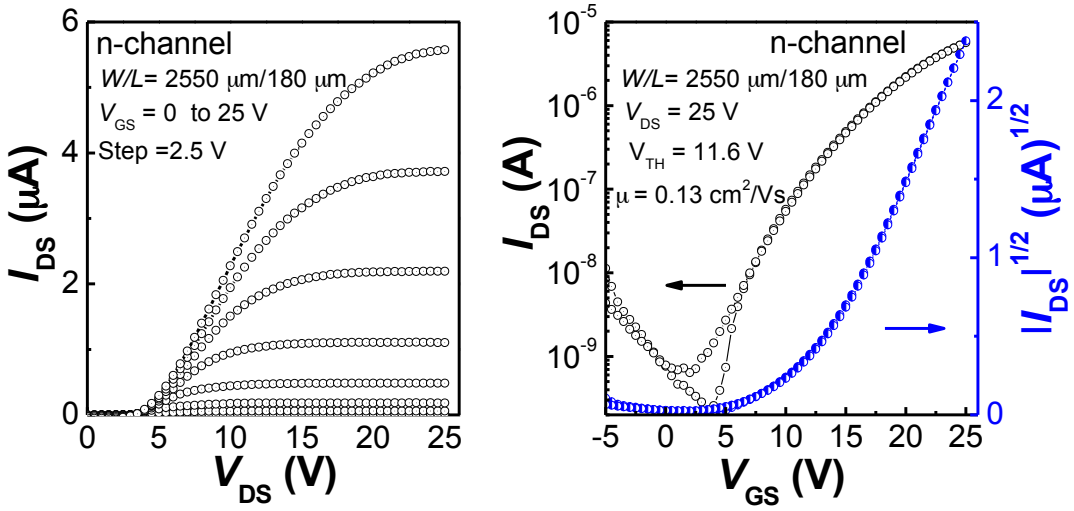

Figure D.6. Output (left) and transfer (right) characteristics of a particular n-channel top-gate OFET with **3.4a** as semiconductor and CYTOP/Al_2O_3 gate dielectric layer with Au source / drain electrodes (*W/L*= 2550 μm/180 μm).

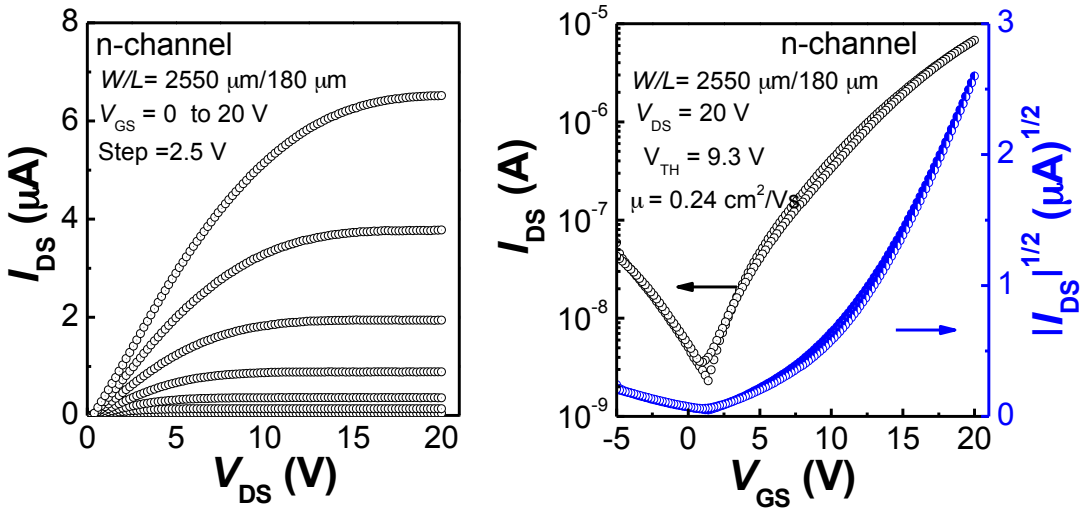

Figure D.7. Output (left) and transfer (right) characteristics of a particular n-channel top-gate OFET with **3.4b** as semiconductor and CYTOP/Al_2O_3 gate dielectric layer with Au source / drain electrodes (*W/L*= 2550 μm/180 μm).

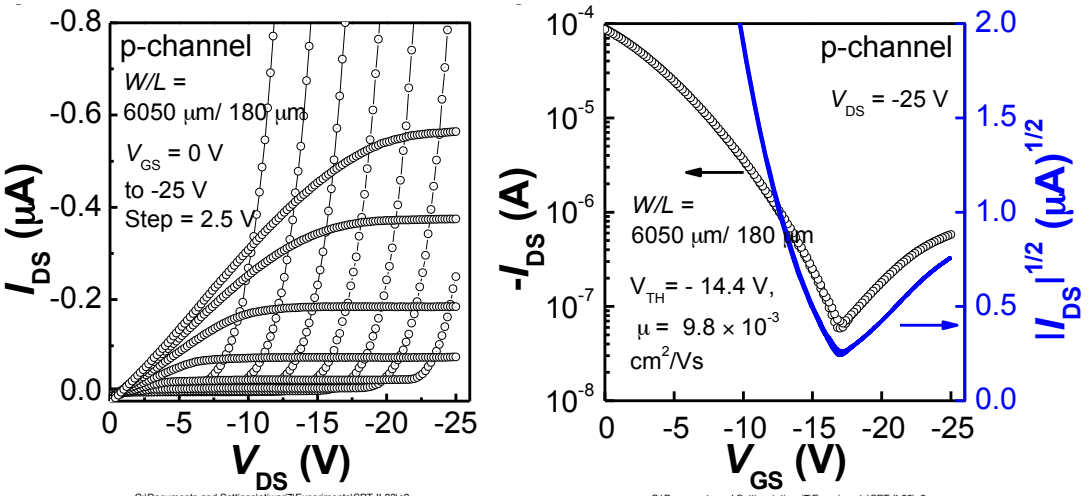

Figure D.8. Output (left) and transfer (right) characteristics of a particular p-channel top-gate OFET with **3.4c** as semiconductor and CYTOP/Al_2O_3 gate dielectric layer with Au source / drain electrodes (*W/L*= 6050 μm/180 μm).

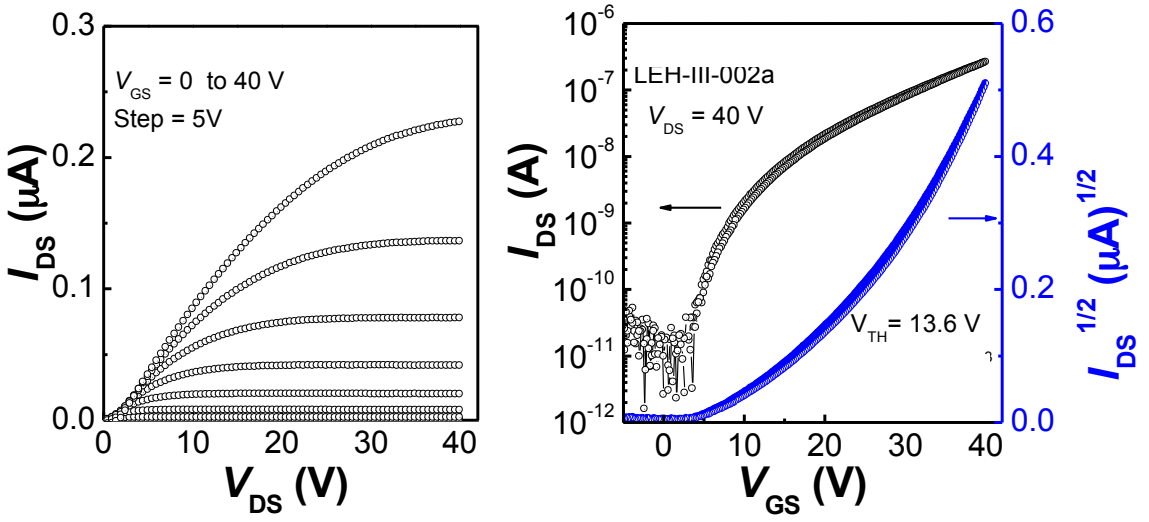

Figure D.9. Output (left) and transfer (right) characteristics of a particular n-channel bottom-gate, top-contact OFET with **3.4c** as semiconductor and SiO_2 / BCB gate dielectric layer with Ca / Au source / drain electrodes (*W/L*= 1200 μm/25 μm).

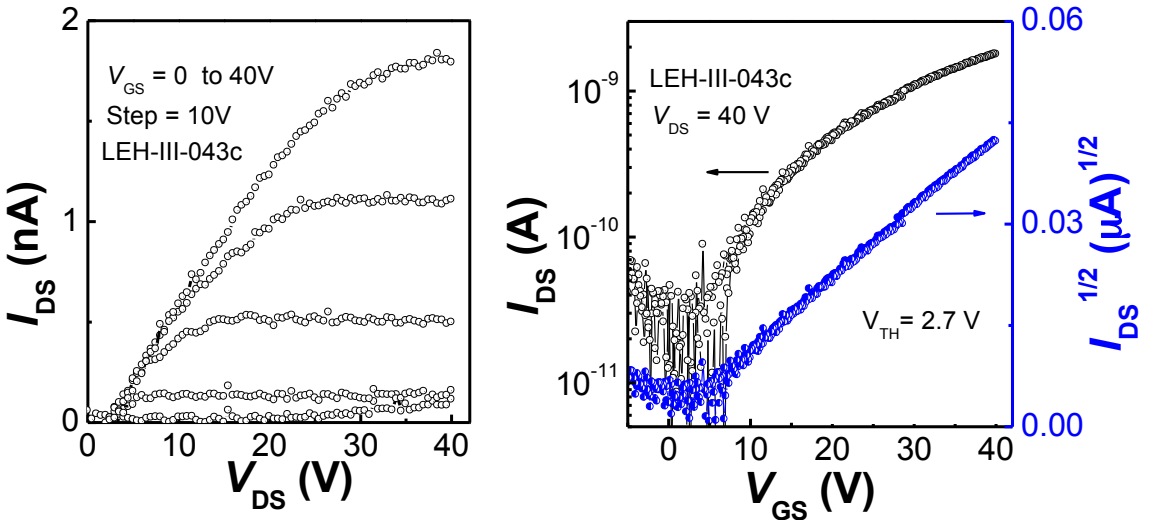

Figure D.10. Output (left) and transfer (right) characteristics of a particular n-channel bottom-gate, top-contact OFET with **3.6** as semiconductor and SiO_2 / BCB gate dielectric layer with Ca / Au source / drain electrodes (*W/L*= 1200 μm/50 μm).

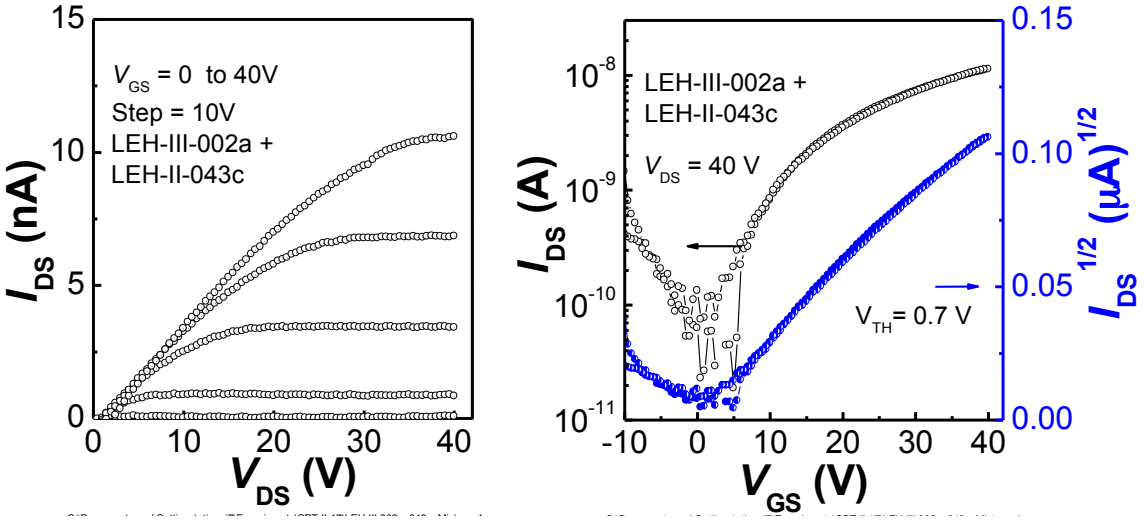

Figure D.11. Output (left) and transfer (right) characteristics of a particular n-channel bottom-gate, top-contact OFET with a mixture (1:1 by weight) of **3.4c** and **3.6** as semiconductor and SiO_2 / BCB gate dielectric layer with Ca / Au source / drain electrodes (*W/L*= 1200 μm/50 μm).

D.3 Chapter 4 (Shree Tiwari and Do Kyung Hwang)

D.3.1 Experimental Details (Shree Tiwari)

OFETs with bottom contact and top gate structure were fabricated on glass substrates for compound **4.16**. Au (~ 50 nm) or Al (~ 50 nm) bottom contact source / drain electrodes were deposited by thermal evaporation through a shadow mask. Thin films of the organic semiconductor were deposited by spin coating with a 30 mg / mL solution prepared from 1,2-dichlorobenzene at 500 rpm for 10 s followed by 2000 rpm for 20 s. The films were annealed at 100 °C for 15 min. A CYTOP (40 nm) / Al_2O_3 (50 nm) bilayer was used as top gate dielectric. CYTOP solution (CTL-809M, ~ 9 wt%) was purchased from Asahi Glass, which was diluted with solvent (CT-solv.180) to make 2 wt% solution. The solution was spin cast at 3000 rpm for 60 sec and the CYTOP film was annealed at 100 °C for 20 min. Al_2O_3 (50 nm) films were deposited on the CYTOP layer by atomic layer deposition at 110 °C using alternating exposures of trimethyl aluminum

and H_2O vapor at a deposition rate of approximately 0.1 nm per cycle. The capacitance density in devices with CYTOP / Al_2O_3 devices was found to be 34.5 $nFcm^{-2}$ (obtained from capacitance values of capacitors with varying area). Finally, Al (~ 150 nm) gate electrodes were deposited by thermal evaporation through a shadow mask. All current-voltage (I−V) characteristics of OFETs were measured in a N_2-filled glove box (O_2, H_2O < 0.1 ppm) with an Agilent E5272A source / monitor unit.

D.3.2 Experimental Details (Do Kyung Hwang)

OFETs with bottom contact and top gate structure were fabricated on glass substrates (Eagle 2000 Corning) for compounds **4.7**, **4.8** and **4.15**. Au (50 nm) bottom contact source / drain electrodes were deposited by thermal evaporation through a shadow mask. The organic semiconductor layer was formed on the substrates by spin coating a solution prepared from 1,1',2,2'-tetrachloroethane (15 mg / mL) at 500 rpm for 10 sec and at 2000 rpm for 20 sec. A CYTOP (45 nm) / Al_2O_3 (50 nm) bi-layer was used as top gate dielectric.[1] The CYTOP solution (CTL-809M) was purchased from Asahi Glass with a concentration of 9 wt.%. To deposit the 45-nm-thick fluoropolymer layer, the original solution was diluted with solvent (CT-solv.180) to have solution:solvent ratios of 1:3.5. The CYTOP layers were then deposited by spin coating at 3000 rpm for 60 sec. Al_2O_3 (50 nm) films were deposited on CYTOP layers by atomic layer deposition (ALD) at 110 °C using alternating exposures of trimethyl aluminum and H_2O vapor at a deposition rate of approximately 0.1 nm per cycle. All spin coating and annealing processes were carried out in a N_2-filled dry box. Finally, Al (150 nm) gate electrodes were deposited by thermal evaporation through a shadow mask. All current-voltage (I-V) characteristics were measured with an Agilent E5272A source/monitor unit in a N_2-filled glove box (O_2, H_2O < 0.1 ppm).

D.3.3 Device Characteristics

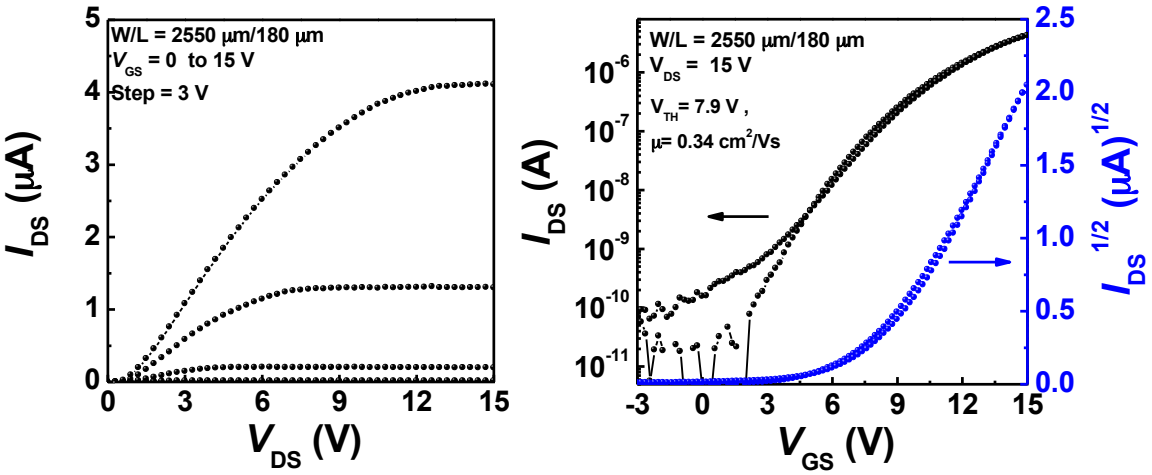

Figure D.12. Output (left) and transfer (right) characteristics of a particular p-channel top-gate OFET with **4.7** as semiconductor and CYTOP/Al_2O_3 gate dielectric layer with Au source / drain electrodes (*W/L*= 2550 µm/180 µm).

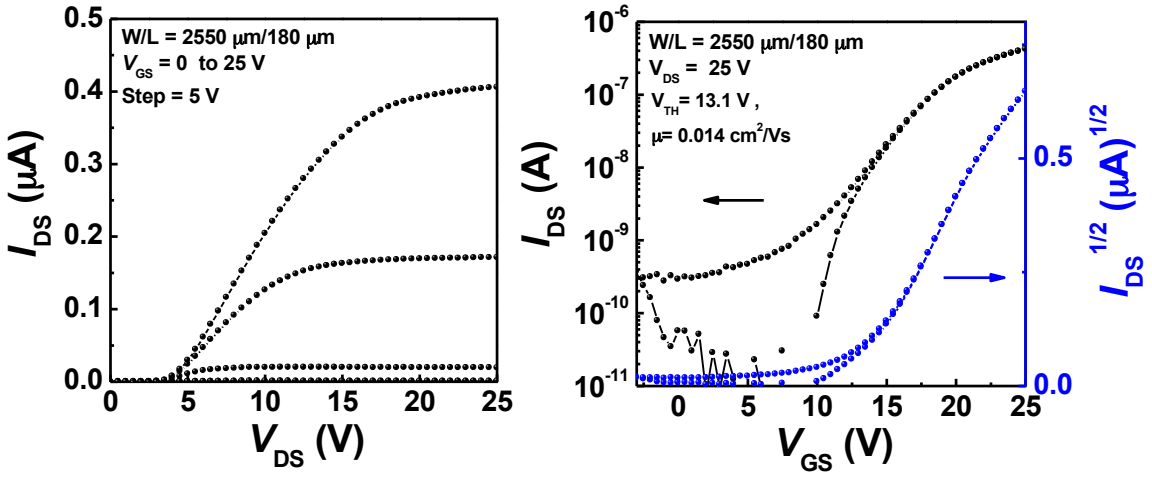

Figure D.13. Output (left) and transfer (right) characteristics of a particular p-channel top-gate OFET with **4.8** as semiconductor and CYTOP/Al_2O_3 gate dielectric layer with Au source / drain electrodes (*W/L*= 2550 µm/180 µm).

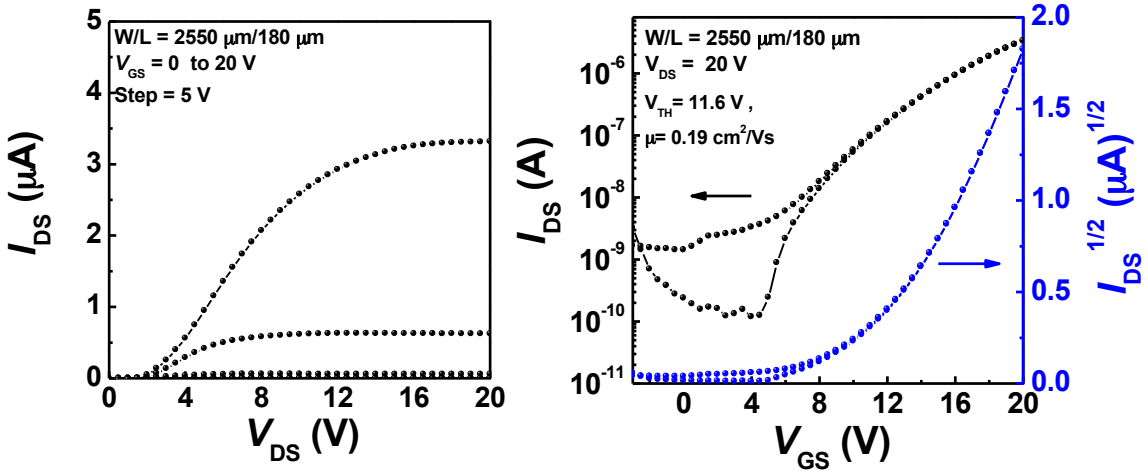

Figure D.14. Output (left) and transfer (right) characteristics of a particular p-channel top-gate OFET with **4.15** as semiconductor and CYTOP/Al_2O_3 gate dielectric layer with Au source / drain electrodes (*W/L*= 2550 μm/180 μm).

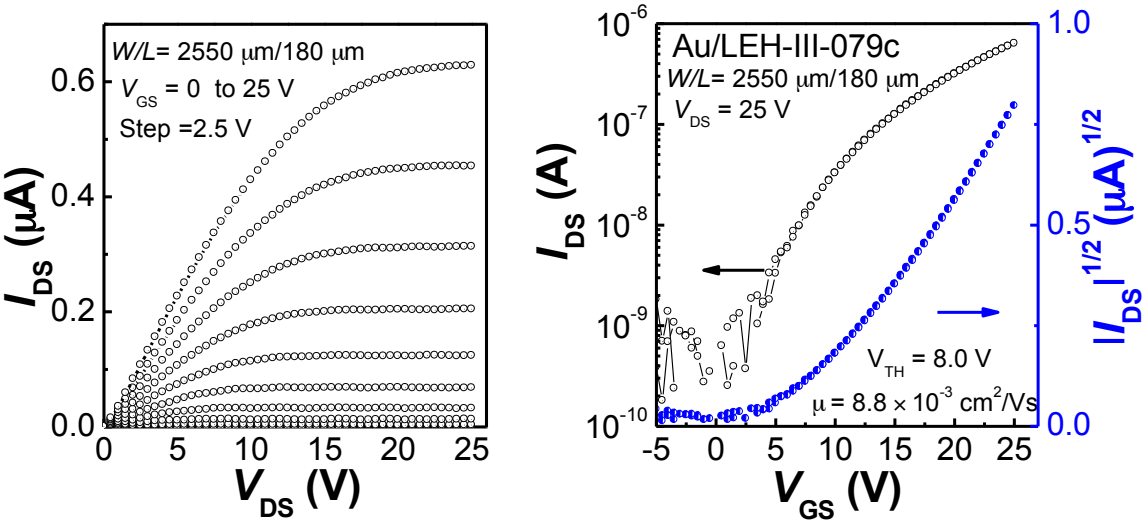

Figure D.15. Output (left) and transfer (right) characteristics of a particular p-channel top-gate OFET with **4.16** as semiconductor and CYTOP/Al_2O_3 gate dielectric layer with Au source / drain electrodes (*W/L*= 2550 μm/180 μm).

D.4 Chapter 5 (Shree Tiwari and Do Kyung Hwang)

D.4.1 Experimental Details (Shree Tiwari)

OFETs with top-gate, bottom-contact structure were fabricated on glass substrates for compound **5.1** and **5.2**. Au (~ 50 nm) or Al (~ 50 nm) bottom contact source / drain electrodes were deposited by thermal evaporation through a shadow mask. Thin films of the organic semiconductor were deposited by spin coating with a 30 mg / mL solution prepared from 1,2-dichlorobenzene at 500 rpm for 10 s followed by 2000 rpm for 20 s. The films were annealed at 100 °C for 15 min. A CYTOP (40 nm) / Al_2O_3 (50 nm) bilayer was used as top gate dielectric. CYTOP solution (CTL-809M, ~ 9 wt%) was purchased from Asahi Glass, which was diluted with solvent (CT-solv.180) to make 2 wt% solution. The solution was spin cast at 3000 rpm for 60 sec and the CYTOP film was annealed at 100 °C for 20 min. Al_2O_3 (50 nm) films were deposited on the CYTOP layer by atomic layer deposition at 110 °C using alternating exposures of trimethyl aluminum and H_2O vapor at a deposition rate of approximately 0.1 nm per cycle. The capacitance density in devices with CYTOP / Al_2O_3 devices was found to be 34.5 $nFcm^{-2}$ (obtained from capacitance values of capacitors with varying area). Finally, Al (~ 150 nm) gate electrodes were deposited by thermal evaporation through a shadow mask. All current-voltage (I−V) characteristics of OFETs were measured in a N_2-filled glove box (O_2, H_2O < 0.1 ppm) with an Agilent E5272A source / monitor unit.

D.4.2 Experimental Details (Do Kyung Hwang)

OFETs with top-gate, bottom-contact structure were fabricated on glass substrates (Eagle 2000 Corning) for compounds **5.6**, **5.7** and **5.9**. Au (50 nm) bottom contact source / drain electrodes were deposited by thermal evaporation through a shadow mask. The organic semiconductor layer was formed on the substrates by spin

coating a solution prepared from 1,1',2,2'-tetrachloroethane (15 mg / mL) at 500 rpm for 10 sec and at 2000 rpm for 20 sec. A CYTOP (45 nm) / Al_2O_3 (50 nm) bi-layer was used as top gate dielectric.[1] The CYTOP solution (CTL-809M) was purchased from Asahi Glass with a concentration of 9 wt.%. To deposit the 45-nm-thick fluoropolymer layer, the original solution was diluted with solvent (CT-solv.180) to have solution:solvent ratios of 1:3.5. The CYTOP layers were then deposited by spin coating at 3000 rpm for 60 sec. Al_2O_3 (50 nm) films were deposited on CYTOP layers by atomic layer deposition (ALD) at 110 °C using alternating exposures of trimethyl aluminum and H_2O vapor at a deposition rate of approximately 0.1 nm per cycle. All spin coating and annealing processes were carried out in a N_2-filled dry box. Finally, Al (150 nm) gate electrodes were deposited by thermal evaporation through a shadow mask. All current-voltage (I-V) characteristics were measured with an Agilent E5272A source/monitor unit in a N_2-filled glove box (O_2, H_2O < 0.1 ppm).

D.4.3 Device Characteristics

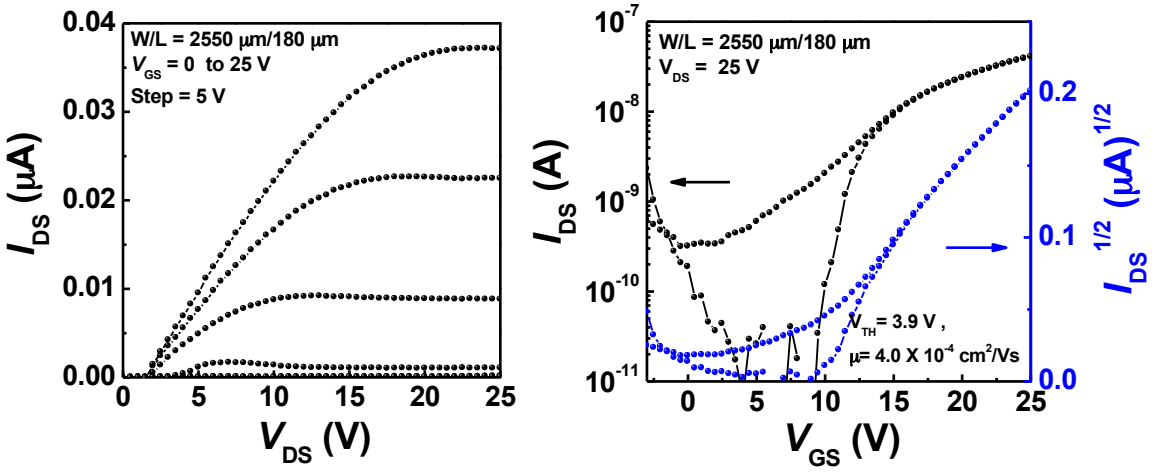

Figure D.16. Output (left) and transfer (right) characteristics of a particular p-channel top-gate OFET with **5.6** as semiconductor and CYTOP/Al_2O_3 gate dielectric layer with Au source / drain electrodes (*W/L*= 2550 µm/180 µm).

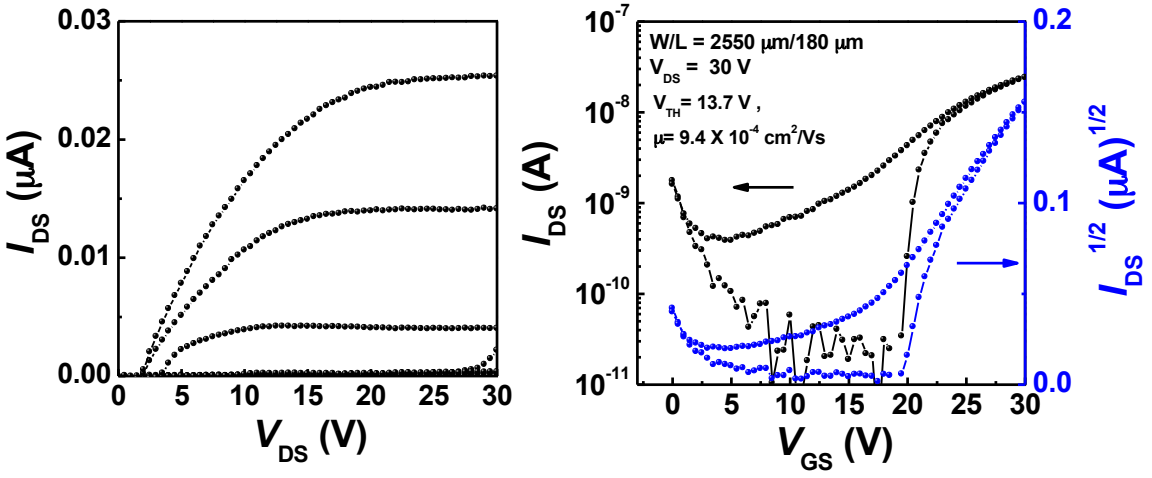

Figure D.17. Output (left) and transfer (right) characteristics of a particular p-channel top-gate OFET with **5.9** as semiconductor and CYTOP/Al_2O_3 gate dielectric layer with Au source / drain electrodes (*W/L*= 2550 μm/180 μm).

D.5 References

(1) Hwang, D. K.; Fuentes-Hernandez, C.; Kim, J.; Potscavage, W. J.; Kim, S.-J.; Kippelen, B. *Adv. Mater.* **2011**, *23*, 1293.

VITA

Lauren Polander (Hayden) was born on December 10, 1984 in Reston, Virginia and grew up primarily in Englewood, Colorado. After graduating from Cherry Creek High School in 2003, she attended Georgia Institute of Technology for her undergraduate studies. Lauren graduated in 2007 with a major in Chemistry and began her graduate work the following Fall, also at Georgia Tech. She has co-authored 4 articles in peer-reviewed scientific journals and has several more in preparation as a result of her undergraduate and graduate research. Following graduation, Lauren plans to move to Lausanne, Switzerland to work with Prof. Michael Grätzel at École Polytechnique Fédérale de Lausanne. When Lauren is not in the lab, she enjoys spending time at home with her husband, Brandon, and her two cats, Lily and Tucker.

lauren.polander@gmail.com